

EFFECTS OF SEVERAL FACTORS ON THEORETICAL
PREDICTIONS OF AIRPLANE SPIN CHARACTERISTICS

AUGUST 1974

by

William Bihrle, Jr.

and

Billy Barnhart

Prepared Under Contract NAS 1-12519

for

Langley Research Center

National Aeronautics and Space Administration

by

Grumman Aerospace Corporation

Bethpage, New York

SUMMARY

An analytical investigation has been made to establish the influence that different mathematical and aerodynamic models have on the computed spin motion and to determine the importance of some of the aerodynamic and non-aerodynamic quantities defined in these models. Because of the knowledge acquired in this investigation, it should be possible to identify the reason for any discrepancy that may be noted in the future between predicted and flight recorded spin motions.

The conventional analytical technique used in spin investigations does not include the aerodynamic forces and moments acting on a spinning aircraft due to steady rotational flow nor does it limit the contribution of the rotary derivatives to the oscillatory component of the total angular rates. Whereas, an analytical technique employing rotation-balance data investigated herein does both. It was shown that a spin cannot be computed using the conventional analytical technique when a rotary derivative is unstable over some portion of the angle-of-attack region. This was not the case when the analytical technique based on rotation-balance data was used. Some of the conclusions arrived at in the past using the conventional analytical technique, therefore, are incorrect relative to the significance of rotary derivatives on the spinning motion. Also the spin computed with rotation-balance data duplicated the developed spin obtained in the spin tunnel whereas, an appreciably less severe spin was realized with the conventional technique. It was indicated, therefore, that the aerodynamic moments generated in a spin due to rotational flow, as measured by a rotation-balance, are indeed significant. The analytical technique used to date is, therefore, a pseudo-technique which cannot be used to predict aircraft spins.

A preliminary study indicated that static aerodynamic derivatives can be extracted from rotation-balance data. It may be possible, therefore, to simply add the aerodynamics associated with steady rotation flow to the conventional aerodynamic model.

It was also shown that during experimental-analytical correlation studies the flight recorded control time histories must be faithfully duplicated since the spinning motion can be acutely sensitive to a small change in the application of the spin entry controls. However, an error in the assumed inertias, yawing moments at high angle of attack and initial spin entry bank angle do not influence the developed spin significantly. The damping in pitch derivative and center of gravity location were shown to play a significant role in the spinning motion.

It was also concluded that the experimental spin investigations conducted in a constant atmospheric density environment duplicate the Froude number only at the initial full-scale spin altitude since the full-scale airplane at high altitudes experiences large density changes during the spin. Therefore, the full-scale rate of sink and spin rate predicted from a constant density environment model test will be greater (conservative) than the actual airplane values.

CONTENTS

	Page
SUMMARY	1
INTRODUCTION	1
TECHNICAL APPROACH	2
Required Studies	2
Analytical Technique	4
Aerodynamic, Inertia and Mass Data	5
Initial Spin Entry Conditions	9
RESULTS AND DISCUSSION	11
Validity of Computational and Model Testing Technique.....	11
Importance of Duplicating Control Time Histories	14
Importance of Duplicating Initial Bank Angle	16
Significance of Errors in Assumed Physical Characteristics	16
Significance of Errors in Assumed Aerodynamic Characteristics....	18
Significance of Selecting a Different Type of Analytical Model...	21
Simple Aerodynamic Model Based on Rotation-Balance Data	23
CONCLUSIONS	25
REFERENCES	28
LIST OF FIGURES	29
APPENDICES	91
Appendix A: Equations of Motion and Associated Formulas	91
Appendix B: Symbols	93
Appendix C: Aerodynamic Data Employed in Investigation	102

INTRODUCTION

The Langley Research Center has a broad research program designed to advance the state-of-the art in the area of stall/spin technology. One major requirement existing in this area is the development and validation of reliable theoretical methods for prediction and analysis of stall/spin characteristics. Although theoretical studies have been made in the past, no concentrated nor continuing effort has been made to rigorously validate the analytical techniques employed in these studies. In view of the urgent need for valid theoretical techniques, this study was performed as a step toward advances in this area.

The analytical technique most commonly employed relative to the study of the stall/spin phenomenon involves the simultaneous solution of the equations of motion and associated formulas. However, little confidence is placed in the technique and this attitude will persist until the incipient, developed and recovery phases of the spinning motion recorded in flight with the full-scale airplane are truly matched by a computer solution.

The inability to satisfactorily demonstrate this "motion matching" in the past might be attributed to the use of an incomplete or a poor representation of the stalled aerodynamics that exist in a spin. For instance, the aerodynamic model employed analytically may be based on low Reynolds number wind tunnel tests when it is known that Reynolds number has a significant effect on the aerodynamic characteristics obtained at spinning conditions

2

for some current configurations. Also, the technique employed to represent the aerodynamic forces and moments may very well be a pseudo-technique which must be abandoned when attempting to compute spins in which the aircraft rapidly rotates about a vertical axis located near the center of gravity. For these spins, the sideslip angle varies along the length of the aircraft; being of opposite sign forward and aft of the axis of rotation. It may be necessary, therefore, that a rotation-balance rig be employed to obtain a set of aerodynamic data while the model is under the same local flow conditions that exist during the actual spin.

The investigation reported herein is the first phase of a two part effort. The objective of the final phase is to determine how well analytically determined motions correlate with those measured in flight when the theoretically and experimentally determined motions are based on the same Reynolds number. This is to be accomplished by using $\frac{1}{10}$ - scale radio-control model time histories. To be able to quickly identify the cause for any discrepancy that may be noted during this forthcoming correlation study, it is necessary that the importance various factors play in the computed motion be known. Therefore, the objective of the first phase of the investigation is to establish the required background of knowledge.

TECHNICAL APPROACH

Required Studies

As indicated in the Introduction, the principal objective of

this investigation is to establish a background of knowledge relative to

- 1) computational procedures and analytical models (both mathematical and aerodynamic) and
- 2) the influence that various non-aerodynamic and aerodynamic quantities have on the computed spin motion

to aid in identifying the reasons for a discrepancy between predicted and flight spin motions. Also, by achieving the objective one can select an analytical model which appears to give solutions more representative of the "real world". The following four distinct studies were required to achieve the objective.

The first study attempts to verify that the computational procedures employed would not in themselves be the source of a discrepancy between computed and measured motions. The concern is that an undetected error may have inadvertently been incorporated into the large, complex computer program required for calculating spin motions or that the integration routine employed would be lacking relative to the rapid motions experienced with a scaled model.

The second study determines the significance of not duplicating the attitude of the aircraft in space at the beginning of the spin entry maneuver or the control time histories. The first item is of concern since attitude gyros are not included in the instrumentation package placed aboard Langley radio-control models. The latter item is to be studied since instrumentation errors, aero-elastic effects, engineering approximations of complex recorded flight control time histories, etc., may preclude simulating the

exact control time histories experienced by the aircraft.

The third study determines the influence that possible errors in the physical (i.e., moments of inertia, center-of-gravity location) and aerodynamic characteristics selected to represent the aircraft have on the computed motion.

These three studies used the conventional analytical technique where the aerodynamics are represented by static data and dynamic derivatives. The aerodynamic model used for these studies is referred to as model 1 which is described under the appropriate heading. The study concerned with the influence of aerodynamic characteristics also investigated a set of aerodynamic data referred to as model 2.

The fourth study conducted herein investigates the significance of employing a different type of mathematical and aerodynamic model which is described in reference 1. In this instance, the models are based on available rotation-balance data.

This technique is investigated since the conventional technique does not include the aerodynamic forces and moments acting on the spinning aircraft due to steady rotational flow nor does it restrict the dynamic derivatives to the oscillatory component of the total angular rates. Whereas, the technique of this latter study does both (see Appendix A). The aerodynamic models employed during this study are referred to as models 3 and 4 which are also described in this section.

Analytical Technique

The influence that a mathematical or aerodynamic model, or

some individual non-aerodynamic or aerodynamic quantity has on the computed motion was determined by examining the path of the center of gravity and the motion about the center of gravity during the incipient and developed spin phases. All of the studies referred to herein, therefore, required the computation of large angle motions using a large angle, six-degree-of-freedom, plotted output digital computer program with nonlinear, multifunctioned aerodynamics coefficients. This program solved the equations of motion and associated formulas presented in Appendix A.

Forty second time histories, deemed of interest to the reader, are presented herein. One 120 second time history is also included for calculation made to simulate the full-scale aircraft. Each time history is presented in a figure consisting of two 11" x 17" pages and each page contains the following variables plotted versus time.

Page 1

γ

α

β

v_R

Page 2

p

q

r

Ω

It was felt that the spinning motion was sufficiently illustrated by describing the relative wind vector at the center of gravity on the first page and the angular velocities about the axes having their origin at the center of gravity on the second page.

Aerodynamic, Inertia and Mass Data

The aerodynamic data which represented the clean, 22 degree

leading edge wing-sweep configuration of a $\frac{1}{10}$ - scale radio-control model are presented in Appendix C. All the data in this appendix were reduced to standard coefficient form on the basis of the following geometric characteristics:

$$S = 5.65 \text{ ft}^2 \quad \bar{c} = 11.76 \text{ in} \quad b = 6.41 \text{ ft}$$

and were transferred during the computations to a 14 percent \bar{c} moment reference center to correspond with the flight model center-of-gravity location.

The Appendix C data were employed to construct four basic aerodynamic models which, as previously mentioned, represent two different type of models i.e., the conventional aerodynamic model and one based on rotation-balance data.

The conventional models are identified in Appendix C as models 1 and 2. Model 1 has been used in a previous investigation (reference 2) and includes static data, experimentally obtained over a wide range of Reynolds numbers in various test facilities, as well as estimated rotary derivatives. These data are referred to a moment reference center located longitudinally at 9 percent \bar{c} unless otherwise noted. Model 2 consists of static data (some of which is presented in reference 3) and rotary derivatives (reference 4) which were experimentally obtained in the Langley Full-Scale Tunnel facility with a $\frac{1}{10}$ - scale model. As shown, rotary derivatives were measured at two forced frequencies. However, for this investigation, the rotary derivatives were assumed to be invariant with frequency and the values obtained at the high frequency were selected as the base for model 2. The model 2 data are referred to a moment

center located longitudinally at 16.25 and 31.55 percent \bar{c} for the static and dynamic data, respectively. All of these data were measured at a Reynolds number based on \bar{c} between .4 and $.5 \times 10^6$ which is equivalent to the flight Reynolds number of the radio-control model.

Models 3 and 4 both use the same rotation-balance data but different rotary derivatives. Model 3 employs the estimated rotary derivatives from model 1 whereas model 4 used the experimentally derived derivatives from model 2. The rotation-balance data were obtained at a Reynolds number based on \bar{c} of $.47 \times 10^6$ in both the clockwise and counterclockwise direction on the rig shown in figure 1 for the following control configurations.

all neutral controls $(i_s, \delta_a, \delta_R = 0^\circ)$

stick full aft $(i_s = -30^\circ; \delta_a, \delta_R = 0^\circ)$

right pro-spin controls $(i_s = -30^\circ, \delta_a = + 5^\circ, \delta_R = -30^\circ)$

left pro-spin controls $(i_s = -30^\circ, -\delta_a = - 5^\circ, \delta_R = 30^\circ)$

Data were recorded at $\theta = 55, 60, 65, 70, 75, 80, 85$ and 90 degrees for ϕ values of 0 and 5 degrees at $\frac{\Omega b}{2V}$ values of $0, .0493, .1030, .1523, .2015, .2553$ and $.3045$ and were measured about a moment reference center located longitudinally at $31.55 \bar{c}$. These data are presented in Appendix C and were inputed "as is" into the computer in tabular form i.e., tables of aerodynamic data as a function of θ and Ω exist for each control configuration at $\phi = 0$ and 5 degrees. The test attitude angles θ and ϕ were assumed to be equal to α and β , respectively when these tables were used. However,

since $\alpha = \tan^{-1} (\tan \theta_e \cos \phi_e)$ and $\beta = \tan^{-1} (\sin \theta_e \sin \phi_e)$, this assumption results in some small errors when the $\theta = 5$ degree tables were used as shown below:

θ	$\phi = 5$	
	α	β
55	54.90	4.09
60	59.91	4.33
65	64.92	4.53
70	69.93	4.70
75	74.95	4.83
80	79.96	4.92
85	84.95	4.98
90	90.00	5.00

If an angle of attack and/or sideslip angle were computed momentarily which was greater or less than those available in the tables (overflow condition) the last value used would be maintained until the computed angle fell within the confines of the available data.

A weight of 149 pounds, a center-of-gravity location of 14 percent \bar{c} and inertias of 2.205, 8.074, 10.096 and 0 slug-ft² for I_x , I_y , I_z and I_{xz} , respectively were experimentally determined for the $\frac{1}{10}$ - scale radio-control model. (The corresponding full-scale values for the weight and inertias are 46,000 pounds, 72,700, 266,000 and 333,000 slug-ft²). These model values were used, therefore, to compute the spinning motion for a model whose mass is distributed slightly more in the fuselage than in the wings as indicated by the values of the inertia parameters, i.e.,

$(I_x - I_y)/mb^2$, $(I_y - I_z)/mb^2$ and $(I_z - I_x)/mb^2$ equal -309, -106 and 415×10^{-4} , respectively.

Initial Spin Entry Conditions

All the studies conducted with the classical aerodynamic models used the following entry conditions unless otherwise noted. Motions were initiated at an altitude and speed of 4000 ft and 173 ft/sec, respectively in a trimmed lg wings level attitude. The trim values for models 1 and 2 were as follows:

	Model 1	Model 2
i_s	-1.9°	-0.29°
α	6.1°	7.8°
T	17.5#	19.6#

An accelerated stall entry was then performed. The entry maneuver involved applying a stabilizer deflection of -30 degrees and a differential horizontal tail deflection of +12 degrees at a rate of 94.8 deg/sec starting at time equal to zero and 0.5 seconds, respectively. These maximum control deflections were then held constant during the ensuing motions. The rudder was left undeflected. A slight variation in this spin entry maneuver was employed in the aerodynamic study. In this instance, upon reaching a -30 degree stabilizer deflection the stabilizer was immediately reduced to -23 degrees at the 94.8 deg/sec rate; and the differential horizontal tail movement began at a time equal to 0.316 seconds rather than 0.5 seconds. (It should be noted that a control rate of 94.8 deg/sec and a time of 0.316 seconds is equivalent to 30 deg/sec and 1 second,

respectively for the full-scale aircraft.) The thrust was arbitrarily reduced to zero above 20 degrees angle of attack.

The studies conducted for aerodynamic models 3 and 4, which are based on rotation-balance data, employed initial conditions which would be realized during the incipient spin phase. This approach was necessary since rotation-balance data were not available below an angle of attack of 55 degrees or for a side-slip angle greater than 5 degrees. The initial values at time equal zero seconds employed for these studies when spinning to the right were as follows:

	Model 3	Model 4
T	0	0
V_R	93.4	92.4
H	3939	3912
γ	-61.6	-63.9
α	69.6	72.6
β	0	0
p	0.7314	1.1064
q	-0.00045	0.0345
r	2.0452	2.4011
ϕ	0	0
ψ	-44.5	-64.0
δ_a	+5	+5
δ_s	-30	-30
δ_R	-30	-30

These initial conditions for models 3 and 4 were based on the values realized at $t = 6$ seconds during a 60 degree banked spin entry maneuver that had been computed with models 1 and 2, respectively. In retrospect, it appears that assumed initial values would have sufficed for this study. The time histories associated with this study are terminated before 40 seconds have elapsed. The reason being that computations were terminated upon reaching sea level. The control deflections at $t = 0$ seconds were predicated on the pro-spin control configuration for which rotation-balance data were available. Because of adverse yaw due to the lateral control, crossed controls are considered to be pro-spin for this model.

RESULTS AND DISCUSSION

Validity of Computational and Model Testing Technique

As stated previously, the first objective of this investigation was to eliminate the possibility that an improperly programmed computer would be the source of some discrepancy that might be noted between computed and measured spins. A check case was selected, therefore, which would thoroughly exercise a large-angle six-degree-of-freedom computer program. This check case was then solved using different programs and computers that were available in-house at Grumman and Langley. The solution from these facilities were compared and the studies presented herein were not initiated until perfect agreement was noted.

Although the final objective of this investigation is limited to determining the degree of correlation obtained between computed

and measured model motions, there is always the underlying interest in how well the model motions simulate the full-scale aircraft. The time was taken, therefore, to briefly investigate the importance on the spin of a factor that is not simulated during experimental Langley spin studies.

Dimensionally scaled Langley radio-controlled drop models and models tested in the free-spinning tunnel facility are dynamically ballasted for some full-scale altitude (usually 35,000 to 40,000 ft) so that the models and full-scale airplane have similar geometrical paths; even though the radio-controlled models are tested near an altitude of 3,000 ft and the free-spinning models at sea level conditions. This is accomplished by making the weight of the model equal to $\frac{\rho_M}{\rho_A} w_A (N)^{-3}$ and the model moments of inertia equal to $\frac{\rho_M}{\rho_A} I_A (N)^{-5}$. (N in the formulas represents the scale i.e., $\frac{1}{10}$, $\frac{1}{20}$ etc.) In this manner the Froude number of the full-scale airplane is duplicated i.e., similarity between inertia and gravitational forces is maintained. Consequently, the attitude angles (θ_e , ϕ_e , ψ_e), α , β , and turns required for recovery of the airplane and model are the same, the linear velocities of the airplane center of gravity (c.g.) equals $v_M (N)^{-1/2}$ and the airplane angular velocities about the c.g. equals $\omega_M (N)^{1/2}$. It should be noted, however, that the Froude number is only duplicated at the initial full-scale spin altitude since the experimental spin investigation are conducted in a constant density environment whereas the full-scale airplane at high altitude experiences large density changes during the spin. The role that the rate of change in atmospheric density with altitude plays in the spinning motion of the aircraft, therefore,

is of interest. .

The effect of density can be determined from figure 2 which presents the time histories ensuing when the same control manipulations are applied to a full-scale aircraft at 35,000 ft and a $\frac{1}{10}$ - scale model at 4,000 ft. It can be seen that the overall incipient and developed phases of the full-scale spins are predicted rather well by the model. If one applies the previously discussed scaling factors, it will be found that V_R , α , β , p , q , r , and ω vs time are faithfully duplicated up to approximately 40 seconds (full-scale value).

Beyond 40 seconds the velocity traces between the model and full-scale aircraft depart. Since an aircraft descends through the atmosphere at a constant value of dynamic pressure, the resultant velocity (rate of descent) continuously changes and is an inverse function of rate of change of density with altitude. Consequently, the altitude loss and ratio of altitude loss per turn obtained with the scaled models becomes correspondingly inflated with decreasing altitude relative to the full-scale value.

The rate of change in atmospheric density experienced by the full-scale aircraft at high altitude influences the α and β values in the developed spin only slightly. However, the angular velocities are significantly affected. Since a flat spin is computed, this effect is most obvious in the yaw rate which shows the full-scale aircraft reaching an equilibrium value sooner and of a lower magnitude than that realized with the model. The importance of not duplicating the Froude number during the developed spin phase is illustrated by taking the model values at $t = 31.6$ sec (model time) and

scaling them up to the full-scale values which are then compared with the values computed at 100 sec for the full-scale aircraft.

At $t = 100$ sec	α	β	V_R	p	q	r	Ω
Scaled-model values	83	-0.7	303	.300	-.024	2.69	2.70
Full-scale values	81	-1.6	208	.320	-.003	2.16	2.20

As shown, the V_R and Ω of the developed spin measured in a constant density environment will be greater than the values realized with the full-scale aircraft and, therefore, are conservative.

Importance of Duplicating Control Time Histories

The sensitivity of the spinning motion to simple variations in the spin entry control time history was investigated by systematically changing the time of control application (t_0), the control rate or control deflection of the stabilizer and differential horizontal tail. It was found that although the incipient spin motion reflected these control changes, as would be expected, the developed spin remained unaffected until some small additional control change triggered a radically different type of spinning motion. This extreme control sensitivity is illustrated by the time histories presented in figure 3 and summarized for various control manipulations on the next page.

Fig.	Control Manipulation						Ensuing Motion
	t_o	i_s	i_s	t_o	δ_a	$\dot{\delta}_a$	
	sec	deg	deg/sec	sec	deg	deg/sec	
3a	0	-23	94.8	1.0	+12	94.8	post stall gyration
3b	0	-23	94.8	.316	+12	94.8	steady flat spin
3c	0	-30	30	.316	+12	94.8	moderate osc. spin
3d	0	-30	30	.500	+12	94.8	steady flat spin
3e	0	-30	94.8	.500	+ 5	94.8	steep osc. spin
3f	0	-30	94.8	.750	+ 5	94.8	steady flat spin

It can be seen from the time histories and the above table that an apparently insignificant change in the control time history can alter radically the nature of the ensuing motion. The reader is reminded that this set of data was specifically selected to illustrate this point and that actually broad bands of control manipulation exist for which the developed spin remains unaltered. The boundaries separating these broad bands (and correspondingly different motions) are extremely narrow. The boundaries being defined by some critical control phasing. Unfortunately, the control phasing required to trigger a radical change in the behavior of the airplane cannot be predicted at this time. For example, the steep oscillatory spin obtained after the application of $+ 5^\circ$ of differential horizontal tail was not surprising. The encounter of a flat spin by delaying the application of this small control deflection by 0.25 seconds obviously was unanticipated.

In light of these results, it is recommended that analytical-experimental correlation studies employ flight time histories which are specifically obtained for such studies and that considerable

thought be given to the type of control manipulation used for spin entry. Also, if the nature of the analytical spin is appreciably different from that obtained in flight, the effect of control perturbations about the flight measured control manipulation should be investigated analytically.

Importance of Duplicating Initial Bank Angles

The influence on the spinning motion of having the aircraft banked at the time spin entry controls are applied was determined for initial bank angles of 0, ± 10 , ± 40 , and ± 60 degrees. It was found that the developed spin characteristics are unaffected by the initial bank angle, but that a noticeable influence on the incipient spin motion is realized for bank angles 40 degrees and greater. The effect on the incipient spin motion can be seen by comparing the time histories presented in figures 4a and b ($\phi_0 = 60^\circ$ and -60° respectively) with figure 3d ($\phi_0 = 0^\circ$). The $\phi_0 = -60^\circ$ does not differ significantly from the $\phi_0 = 0^\circ$ spin entry whereas the $\phi_0 = 60^\circ$ exhibits a more rapid decay in the α , β , p , q , and r oscillations. Entry into the developed steady flat spin, therefore, is achieved more smoothly by having the aircraft initially banked in the direction of the spin. It is interesting to note that this is exactly the situation that is experienced by a pilot when he picks up a wing with a lateral control that generates adverse yaw.

Significance of Errors in Assumed Physical Characteristics

Sensitivity of the spinning motion to center-of-gravity location can be determined by comparing the time histories presented

in figures 5a, b and 3d for a c.g. location of 6, 26 and 14 percent \bar{c} , respectively. It is shown that an aircraft capable of entering a flat spin will do so regardless of the magnitude of the spring constant. Of course, as would be expected, there is a small decrease and increase in the spin rate of rotation and angle of attack, respectively as the c.g. moves aft. The most significant effect, however, is on the incipient spin phase of the motion. As shown in figure 5, the effect of c.g. location on the time required and the type of motion experienced before the equilibrium spin condition is reached is appreciable. Moving the c.g. forward increases appreciably the amplitude and the required decay time of the initial spin entry oscillation. This effect is so great that for the 6 percent \bar{c} case the steady-state values have yet to be attained at the end of 40 seconds (126.4 sec full-scale); whereas, for the aft c.g. location the steady state flat spin is achieved rapidly and smoothly.

It has been demonstrated experimentally and analytically many times that inertia changes which significantly alter the gyroscopic moments will appreciably modify the spin and recovery characteristics to be realized with a given aerodynamic configuration. The error in measuring the inertia about one axis that would be required to produce this effect, however, would not go undetected. The errors to be incurred in measuring or estimating the inertias would in fact be even considerably less than the differences incurred in attempting to dynamically simulate a set of full-scale values on a dimensionally scaled model. Since the weight and inertia must be reduced to the third and fifth power of the scale, respectively it is indeed difficult not to exceed the required

(desired) values. For example, the I_x , I_y and I_z values for the subject model would have to be reduced by 10.6, 16.7 and 18.0 percent, respectively, to simulate the full-scale airplane. Even though these representative scaling errors greatly exceed experimental measuring errors, their influence on the spinning motion is presented in figure 6. There is a detectable difference between the motions. These differences, however, would be considered acceptable if obtained during an analytical-experimental correlation study. It is interesting to note that since slightly higher rotation rates are realized for the lower (desired) inertia, the model results are a shade unconservative.

Significance of Errors in Assumed Aerodynamic Characteristics

The influence of the static and the dynamic aerodynamic characteristics on the spinning motion of an aircraft presented in reference 5 were verified during this study. However, besides investigating the effect of an individual aerodynamic quantity it was also the intent of this study to determine the significance on the spinning motion employing two conventional aerodynamic models which differed in many respects. Both models were assumed to represent the same aircraft. Figure 7 presents time histories which illustrate results deemed to be significant and of interest.

It was found that an equilibrium spin could not be computed with model 2 since the solutions "blow-up". That is, as shown in figure 7a, an ever increasing yaw rate results in a divergence in α and β . The peak α value increasingly exceeds 90 degrees for which there was no aerodynamic data. Consequently, the time

histories computed become invalid and meaningless. As shown in figure 7b, the same type of problem is experienced when the rotary derivatives based on the low-frequency forced oscillation tests are substituted for the model 2 values (high-frequency values).

A steady flat spin was obtained when model 1 was used (see figure 7c). However, when the model 1 rotary derivatives were replaced with the model 2 values (figure 7d) it was again impossible to compute a spin. The same was true when the low frequency rotary derivatives (figure 7e) were employed in model 1.

In Appendix C the rotary derivatives used in model 1 are compared with the model 2 values in figures C-19 thru C-22. Although the derivatives for model 1 and 2 are referred to different moment centers they still are representative of the values to be realized when they are all transferred to 14 percent \bar{c} during the spin computation. It can be seen that the values of C_{nr} and $C_{\alpha r}$ (figure C-21c and C-22b, respectively) are appreciably different for models 1 and 2 in that the model 2 values are unstable at some angles of attack. The importance of each derivative on the motion was therefore determined.

When the model 2 C_{nr} value was employed in model 1, the previously computed steady flat spin (figure 7c) was replaced with an extremely high frequency oscillatory motion in which the value of r is ever increasing with time (figure 7f). This computed motion obviously does not represent the "real world". The steady flat spin obtained with model 1 was also radically changed when the model 2 value of $C_{\alpha r}$ was used in model 1. As shown in figure 7g, a low frequency divergent oscillation in α and β is realized which eventually kicks out of the spinning motion. The inability to compute

a spin with model 2 was due, therefore, to both C_{n_r} and C_{α_r} assuming unstable values over small ranges of angle of attack.

As shown in figure C-21a, the C_{m_q} value for model 2 assumed a near zero value above $\alpha = 75^\circ$. When this value was used in model 1, the motion presented in figure 7h was obtained. It can be seen that this derivative had a significant effect in that the steady flat spin became oscillatory and assumed a lower spin rate.

The $C_n(\alpha, \beta)$ data of model 1 and 2 (see figures C-8 and C-18, respectively) are radically different above an angle of attack of 40 degrees. (Both sets of data are presented for a moment reference center of 14 percent \bar{c} .) For model 1, the highest level of instability (pro-spin yawing moment) attained in the vicinity of 40 degrees angle of attack is maintained up to 90 degrees. Whereas, the pro-spin yawing moment of model 2 rapidly falls off above an angle of attack of 40 degrees to a near zero (either slightly pro- or anti-spin) value. The spin obtained when the model 2 C_n data is used in model 1 is shown in figure 7i. The influence these different C_n characteristics have on the spin can be seen by comparing figure 7i with figure 7c. By effectively removing the large pro-spin yawing moment above $\alpha = 40^\circ$ the initial spin entry oscillation is more rapidly damped but the developed steady flat spin rate is only slightly reduced from 8.7 to 8.2 radians/sec. The reason the steady flat spin characteristics were not significantly affected by this large aerodynamic change is because the aerodynamic yawing moment approaches a value close to zero when spin equilibrium is achieved.

It was concluded from this study that the same type of spin could be obtained with the conventional aerodynamic models 1 and 2 if the stable C_{n_r} , C_{l_r} and C_{m_q} derivatives of model 1 were used in model 2.

Significance of Selecting a Different Type of Analytical Model

As stated previously, the conventional technique does not include the aerodynamic forces and moments acting on a spinning aircraft due to steady rotational flow nor does it limit the contribution of the rotary derivatives to the oscillatory component of the total angular rates. Whereas, the analytical technique employing rotation-balance data does both. It was desired, therefore, to enter a spin using the same controls employing both techniques. Because of the limited rotation-balance data available, this desire was achieved using the procedure previously discussed and by limiting the correlation to the developed spin and recovery characteristics.

Since the available rotation-balance data was limited to a positive sideslip angle, the initial attempt was to calculate left spins which would assume small positive values of sideslip. Equilibrium spins, however, could not be obtained with aerodynamic model 3 or 4. When only the $\beta = 0^\circ$ data was employed with model 4, a flat spin was attained, but this spin also could not be maintained. An analysis of the rotation-balance data indicated anomalies in the counter-clockwise data (left spin) for both $\beta = 0$ and 5 degrees which could not be explained. It was decided, therefore, to compute right spins using only

$\beta = 0^\circ$ rotation-balance data.

Figures 8a and b present the time histories for the motions attained using the conventional technique (model 1) and the technique based on rotation-balance data (model 3), respectively. (Model 3 consists of the rotation-balance data and the rotary derivatives of model 1.) In both cases, a steady flat spin is obtained. However, a more severe flat spin is obtained with the rotation-balance set-up. The angle of attack being increased from 76.7 to 85.4 degrees and the spin rate from 5.4 to 9.7 radians/sec.

Figure 8c presents the time history computed with the rotation-balance data and the rotary derivatives from model 2; this data package being referred to as model 4. With model 4, the flat spin obtained became oscillatory and spun at a lower angular rate. However, as discussed in the previous section, it was impossible to compute a spin with this set of rotary data when the conventional analytical technique was used. It should also be noted that in this instance, substituting the model 3 C_{n_r} or C_{λ_r} value in model 4 had absolutely no effect on the motion. The effect of using the C_{m_q} value of model 3 in model 4 can be seen by comparing figure 8d with 8c. With this one change, the spins obtained with models 3 and 4 are almost the same. The angle of attack and spin rate are 84.8 deg and 9.14 radians/sec, respectively. The full-scale values would correspondingly be 84.8 deg and .46 revolutions/sec which compares very favorably with the 87 deg and .47 revolutions/sec values obtained with the $\frac{1}{36}$ - scale spin model. These results were obtained for almost the same i_s , δ_a , δ_R control configuration. The only difference being that the spin model was tested with $\delta_a = +7^\circ$ and

the rotation-balance data was obtained for $\delta_a = + 5^\circ$. When both the C_{Lp} and C_{np} values were replaced in model 4 with those from model 3, an insignificant effect was noted (compare figure 8d with 8e).

These results

- 1) strongly support the belief that the conventional analytical technique employed to date is a pseudo-technique which cannot be used to predict full-scale spins and,
- 2) indicate that past conclusions (reference 5) analytically arrived at relative to the significance of rotary derivatives on the spinning motion are in many instances wrong.

A direct comparison between the recovery characteristics using the conventional and rotation-balance data technique is not possible since a more severe (higher α and α) flat spin was obtained with the rotation-balance data. However, from figure 9 it does not appear that any significant difference is realized relative to the effectiveness of the recovery controls. In both cases, the recovery controls were introduced at $t = 20$ seconds and it took six seconds to stop the spin using the conventional technique. An additional two seconds was required to terminate the more severe rotation-balance data spin.

A Simple Aerodynamic Model Based on Rotation-Balance Data

A preliminary investigation indicated that it is possible to extract static aerodynamic derivatives (i.e., C_{m_α} , C_{L_β} , C_{n_β} , $C_{n_{\delta_a}}$, $C_{m_{\delta_s}}$, etc.) from rotation-balance data. If this is indeed

the case for all aircraft configurations, then

- 1) rotation-balance tests eliminate the need for corresponding static wind tunnel tests and
- 2) a simple aerodynamic model can be constructed which is more valid than the conventional aerodynamic model since it includes the aerodynamics associated with rotational flow and, as discussed previously, permits one to apply the rotary derivatives in a more proper manner.

With a simple model one can employ all of the unstalled and stalled static ($\frac{\alpha_b}{2V} = 0$) aerodynamic data that may be available and removes the issue of how to smoothly transition from one type of aerodynamic model to another during the incipient spin calculation. Also, the model can easily be incorporated into existing large-angle six-degree-of-freedom computer programs.

The following simple model would adequately represent the vehicle investigated herein.

C_m, C_c, C_N as a function of α

C_L, C_n, C_y as a function of α, β

C_L, C_n, C_y as a function of $\frac{\alpha_b}{2V}, \alpha, i_s$

$C_{m_{is}}, C_{c_{is}}, C_{N_{is}}$ as a function of α

$C_{L_{\delta_a, \delta_R}}, C_{n_{\delta_a, \delta_R}}, C_{y_{\delta_a, \delta_R}}$ as a function of $\alpha, \frac{\alpha_b}{2V}$

CONCLUSIONS

The following major conclusions are based on the results of the analytical studies reported herein. With the exception of the first, all of the conclusions pertain to factors which can influence the outcome of an experimental-theoretical correlation study. Although these studies were made for one configuration, the conclusions should be applicable to other aircraft.

1. Experimental spin investigations conducted in a constant density environment duplicate the Froude number only at the initial full-scale spin altitude since the full-scale airplane at high altitude experiences large atmospheric density changes during the spin. Therefore, the full-scale rate of sink and spin rate predicted from a constant density environment test will be greater (conservative) than the actual airplane values.

2. The spinning motion can be acutely sensitive to a small change in the application of the spin entry controls. Since the critical control phasing required to trigger a radical change in the spin behavior of the aircraft cannot be predicted at this time, flight recorded control time histories must be faithfully duplicated during an experimental-analytical correlation study.

3. The spinning motion, both the incipient and developed phases, are sensitive to the location of the center of gravity but are not significantly effected by errors incurred in measuring airplane inertias.

4. The presence of a bank angle at the time spin entry controls are applied does not influence the developed spin. The incipient spin motion, however, is affected by bank angles 40 degrees and greater in that entry into the developed spin is achieved more

smoothly if the aircraft is initially banked in the direction of the spin.

5. The damping in pitch derivative, C_{m_q} , has a significant influence on all phases of the spinning motion. The magnitude of the static yawing moment in the 50 to 90 degree angle-of-attack range appreciably affects the incipient spin but only slightly affects the developed spin.

6. A spin may not be computed using the conventional analytical technique when the rotary derivative C_{m_q} , C_{n_r} or C_{ℓ_r} is unstable over some portion of the angle-of-attack region. This is not the case, when the contribution of the rotary derivatives are limited to the oscillatory component of the total angular rates which is the proper procedure. Some of the conclusions arrived at in the past using the conventional analytical technique, therefore, are incorrect relative to the significance of rotary derivatives on the spinning motion.

7. The spin computed with rotation-balance data duplicated the developed spin obtained in the spin tunnel. The spin computed in the conventional manner with static aerodynamic data was of the same type (flat) but was considerably less severe. It is indicated, therefore, that the aerodynamic moments generated in the spin due to steady rotational flow, as measured by a rotation-balance, are indeed significant. The analytical technique used to date is, therefore, a pseudo-technique which cannot be used to predict full-scale spin motions.

8. It appears that static aerodynamic derivatives can be extracted from rotation-balance data. It is possible, therefore, to simply add the aerodynamics associated with steady rotation flow to the conventional aerodynamic model. In this manner, not only is the aerodynamic model more valid, but it also permits one to modify the mathematical model to more properly apply the rotary derivatives.

REFERENCES

1. Anglin, Ernie L.; and Scher, Stanley H.: Analytical Study of Aircraft Developed Spins and Determination of Moments Required for Satisfactory Spin Recovery. NASA TN D-2181, 1964.
2. Bahrle, William Jr.; and Heyman, Arthur C.: F-14 Spin Avoidance/Prevention Program. NASC GAC A51-335-R-72-1, 1972.
3. Boisseau, Peter C. and Chambers, Joseph R.: Lateral-Directional Characteristics of a $\frac{1}{10}$ - scale Free-Flight Model of a Variable Sweep Fighter Airplane at High Angles of Attack. NASA TM SX-2649, 1972 (Confidential).
4. Grafton, Sue B.; and Anglin, Ernie L.: Dynamic Stability Derivatives at Angles of Attack from -5° to 90° for a Variable-Sweep Fighter Configuration with Twin Vertical Tails. NASA TN D-6909, 1972.
5. Bahrle, William Jr.; and Heyman, Arthur C.: The Spin Behavior of Aircraft. NASC GAEC 394-68-1, 1967.
6. Mechty, E.A.: The International System of Units-Physical Constants and Conversion Factors (Revised). NASA SP-7012, 1969.

LIST OF FIGURES

Fig.No.	Title	Page
1	Sketch of rotation rig showing location of some rig components.	32
2	Influence of rate of change in atmospheric density with altitude during full-scale spin.	
a)	Full scale, $H_0 = 35,000$ ft.	33
b)	$\frac{1}{10}$ - scale, $H_0 = 4,000$ ft.	35
3	Sensitivity of spinning motion to simple variations in the spin entry control time histories.	
a)	$i_s = -23^\circ$ applied at $94.8^\circ/\text{sec.}$ starting at $t = 0$ sec.	37
	$\delta_a = +12^\circ$ " " $94.8^\circ/\text{sec.}$ " " $t = 1.0$ sec.	
b)	$i_s = -23^\circ$ applied at $94.8^\circ/\text{sec.}$ starting at $t = 0$ sec.	39
	$\delta_a = +12^\circ$ " " $94.8^\circ/\text{sec.}$ " " $t = .316$ sec.	
c)	$i_s = -30^\circ$ applied at $30^\circ/\text{sec.}$ starting at $t = 0$ sec.	41
	$\delta_a = +12^\circ$ " " $94.8^\circ/\text{sec.}$ " " $t = .316$ sec.	
d)	$i_s = -30^\circ$ applied at $30^\circ/\text{sec.}$ starting at $t = 0$ sec.	43
	$\delta_a = +12^\circ$ " " $94.8^\circ/\text{sec.}$ " " $t = .500$ sec.	
e)	$i_s = -30^\circ$ applied at $94.8^\circ/\text{sec.}$ starting at $t = 0$ sec.	45
	$\delta_a = +5^\circ$ " " $94.8^\circ/\text{sec.}$ " " $t = .500$ sec.	
f)	$i_s = -30^\circ$ applied at $94.8^\circ/\text{sec.}$ starting at $t = 0$ sec.	47
	$\delta_a = +5^\circ$ " " $94.8^\circ/\text{sec.}$ " " $t = .750$ sec.	
4	Sensitivity of spinning motion to initial Euler angles.	
a)	$\phi_0 = 60^\circ$, right spin	49
b)	$\phi_0 = -60^\circ$, right spin	51

LIST OF FIGURES (Cont'd.)

Fig. No.	Title	Page
5	Sensitivity of spinning motion to center-of-gravity location.	
a)	6 percent \bar{c}	53
b)	26 percent \bar{c}	55
6	Influence of errors incurred in ballasting model for some full-scale test altitude.	57
7	Influence of some aerodynamic characteristics on spinning motion.	
a)	Model # 2	59
b)	Model # 2 with low frequency dynamic derivatives	61
c)	Model # 1	63
d)	Model # 1 with high frequency dynamic derivatives	65
e)	Model # 1 with low frequency dynamic derivatives	67
f)	Model # 1 with high frequency (Model # 2) C_{n_r}	69
g)	Model # 1 with high frequency (Model # 2) C_{l_r}	71
h)	Model # 1 with high frequency (Model # 2) C_{m_q}	73
i)	Model # 1 with Model # 2 C_n (α, β)	75
8	Influence of rotation-balance data on computed spinning motion.	
a)	Classical aerodynamic Model # 1	77
b)	Rotation-balance Model # 3	79
c)	Rotation-balance Model # 4	81
d)	Rotation-balance Model # 4 with estimated C_{m_q} (Model #3)	83
e)	Rotation-balance Model # 4 with estimated C_{m_q} , C_{l_p} , C_{n_p} (Model # 3)	85

LIST OF FIGURES (Cont'd.)

Fig.No.	Title	Page
9	Influence of rotation-balance data on computed recovery characteristics.	
a)	Full opposite spin controls at $t = 20$ sec., classical Model # 1	87
b)	Full opposite spin controls at $t = 20$ sec., rotation-balance Model # 3	89

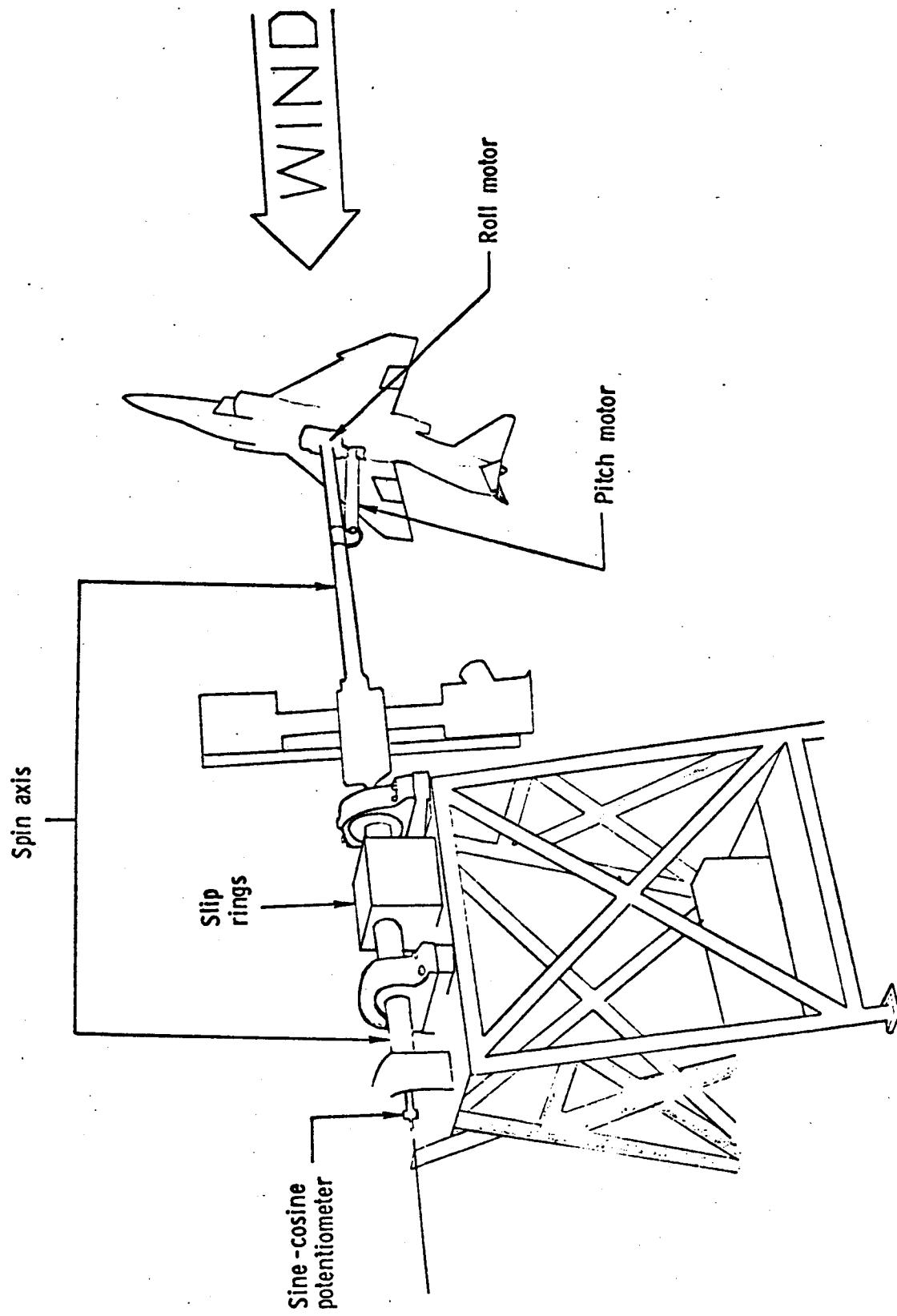
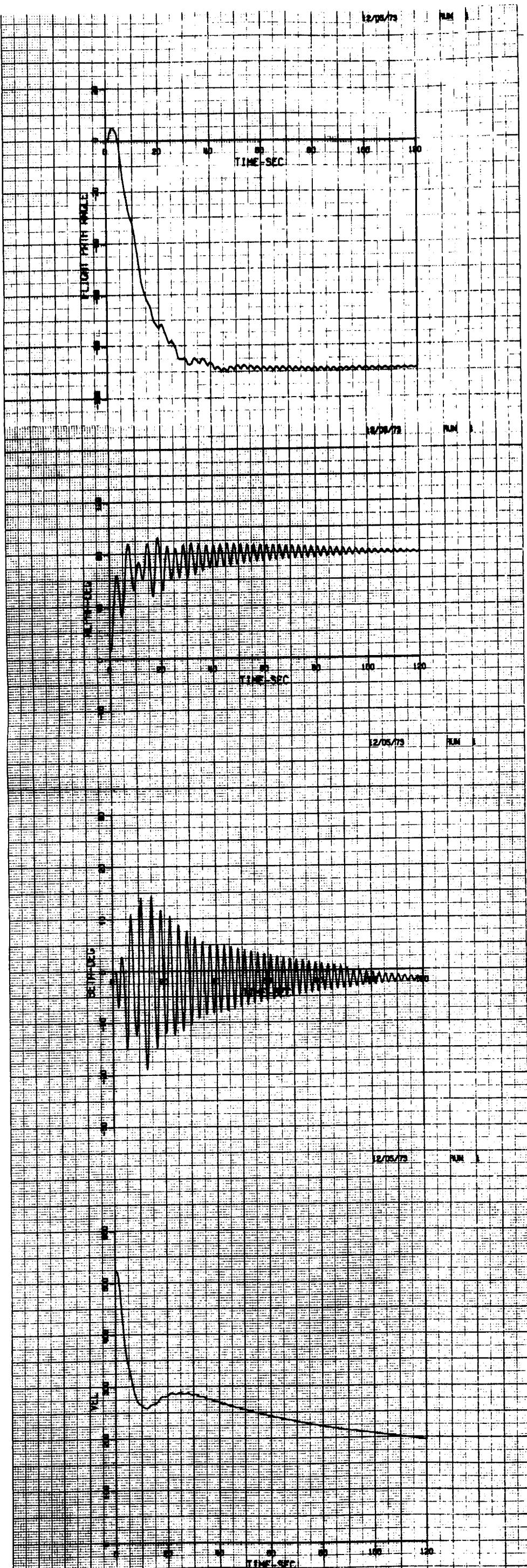
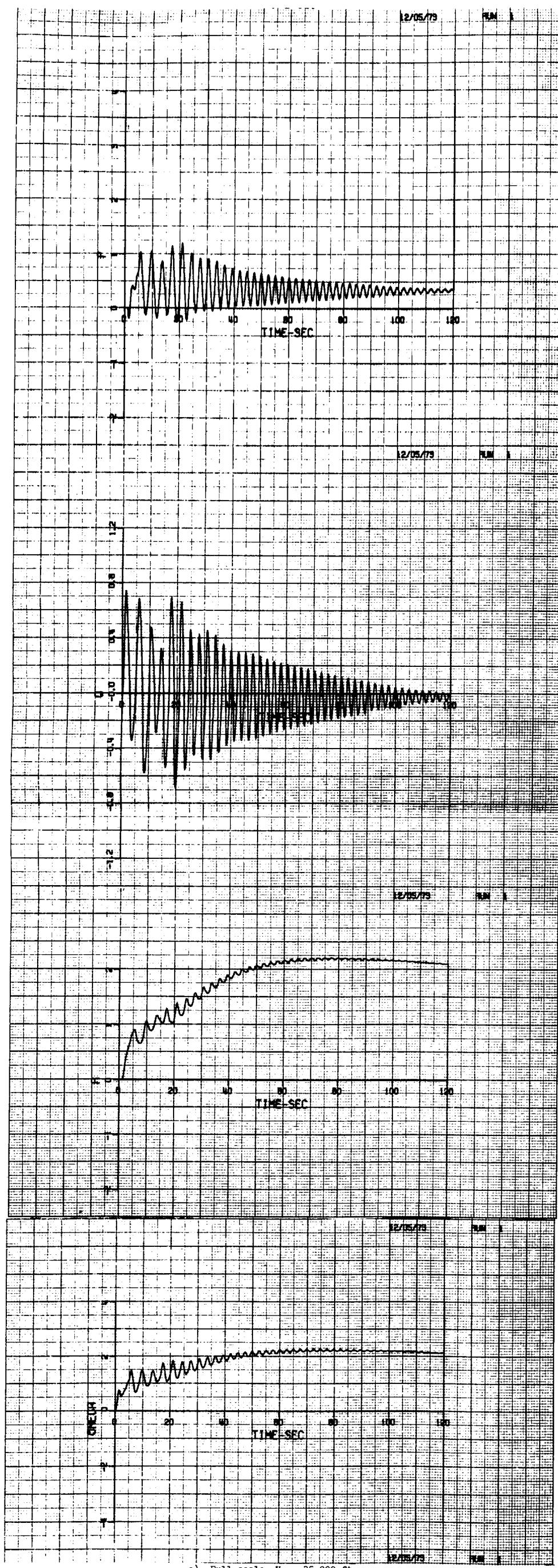


Figure 1.- Sketch of rotation rig showing location of some rig components.



a) Full scale, $H_0 = 35,000$ ft.

Figure 2.- Influence of rate of change in atmospheric density with altitude during full-scale spin.



a) Full scale, $H_0 = 35,000$ ft.

Figure 2.- Continued.

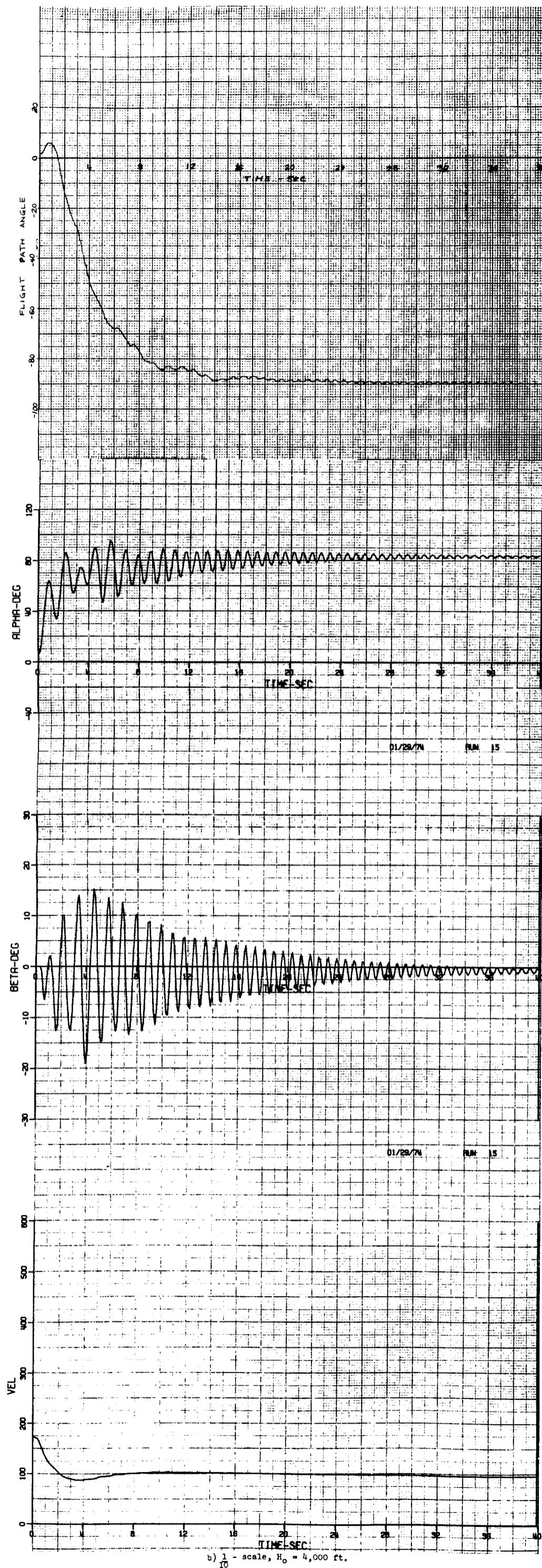
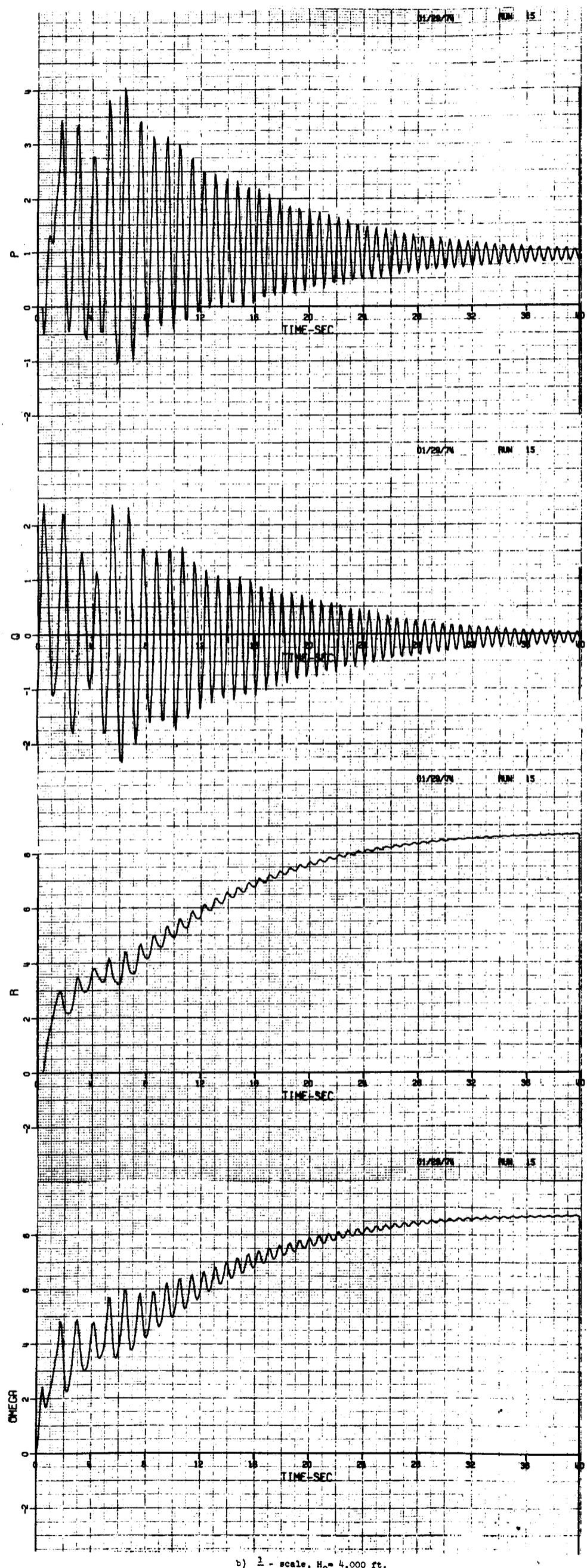
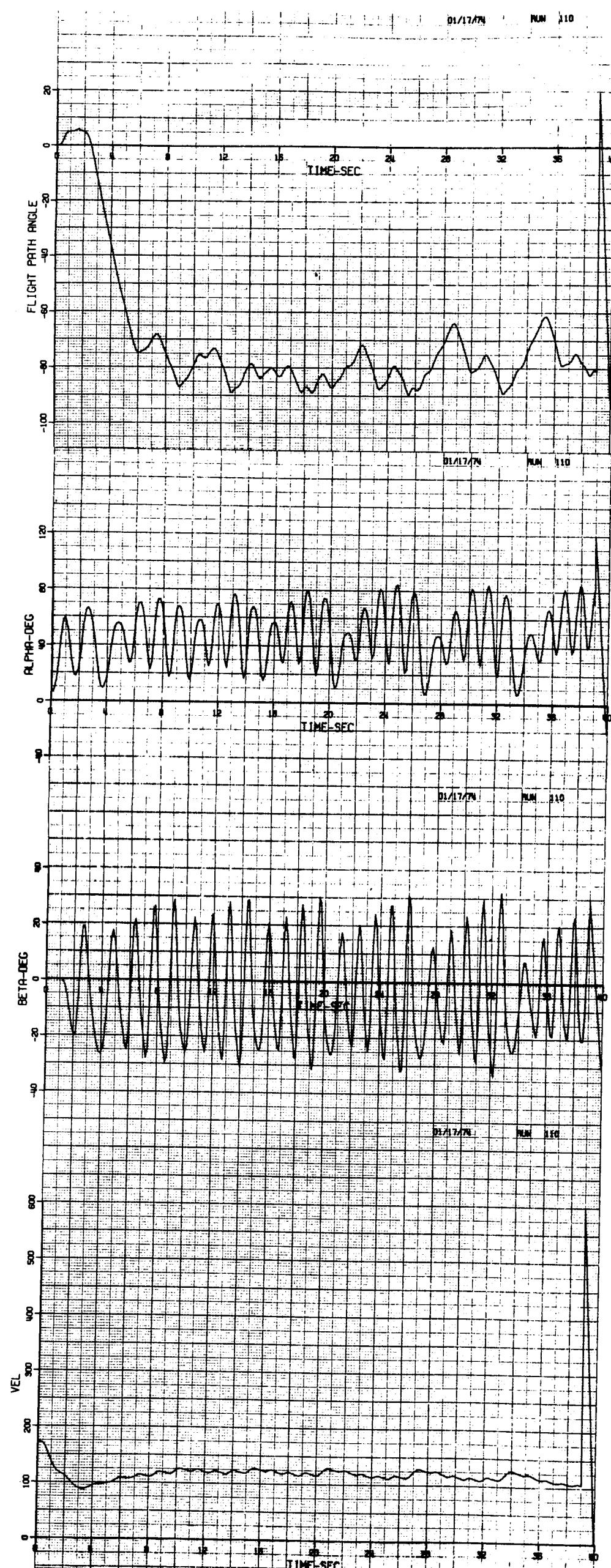


Figure 2. - Continued.



b) $\frac{1}{10}$ - scale, $H_0 = 4,000$ ft.

Figure 2.- Concluded.



$t_s = -23^\circ$ applied at 94.8°/sec. starting at $t = 0$ sec.

a) $\delta_a = +12^\circ$ " 94.8°/sec. " " $t = 1.0$ sec.

Figure 3.- Sensitivity of spinning motion to simple variations in the spin entry control time.

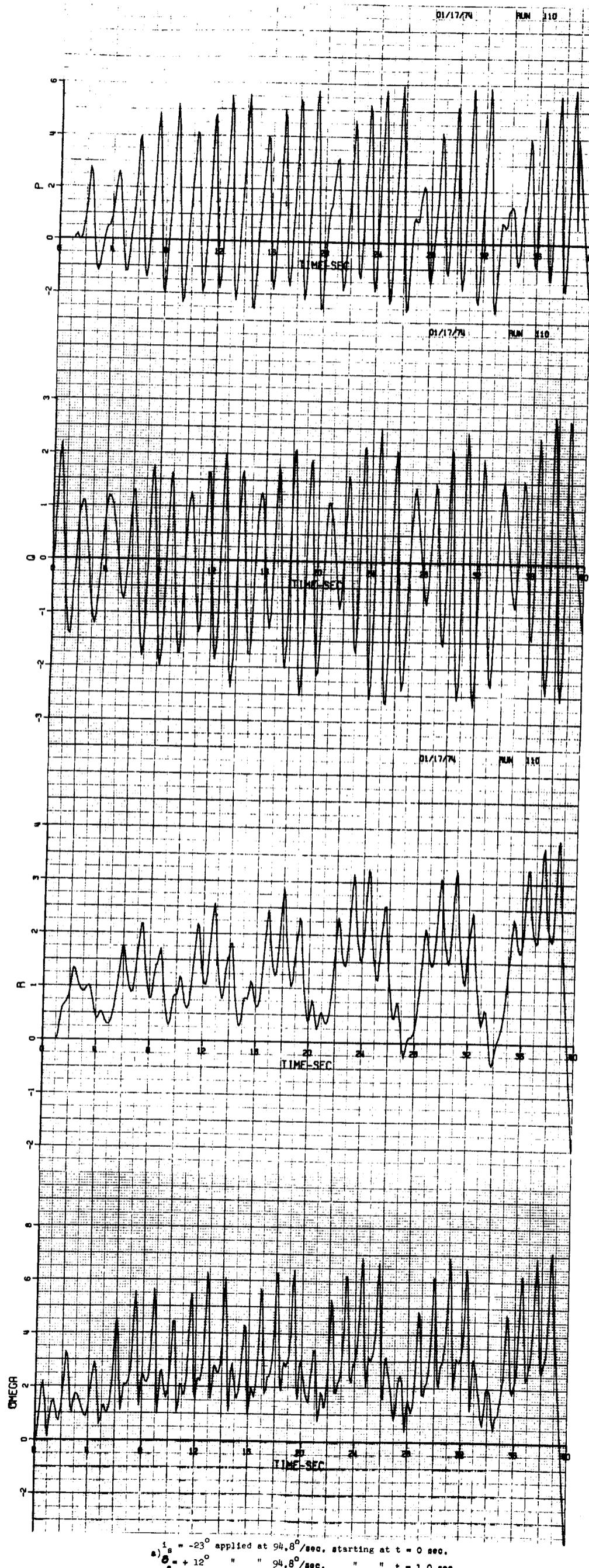


Figure 3.- Continued.

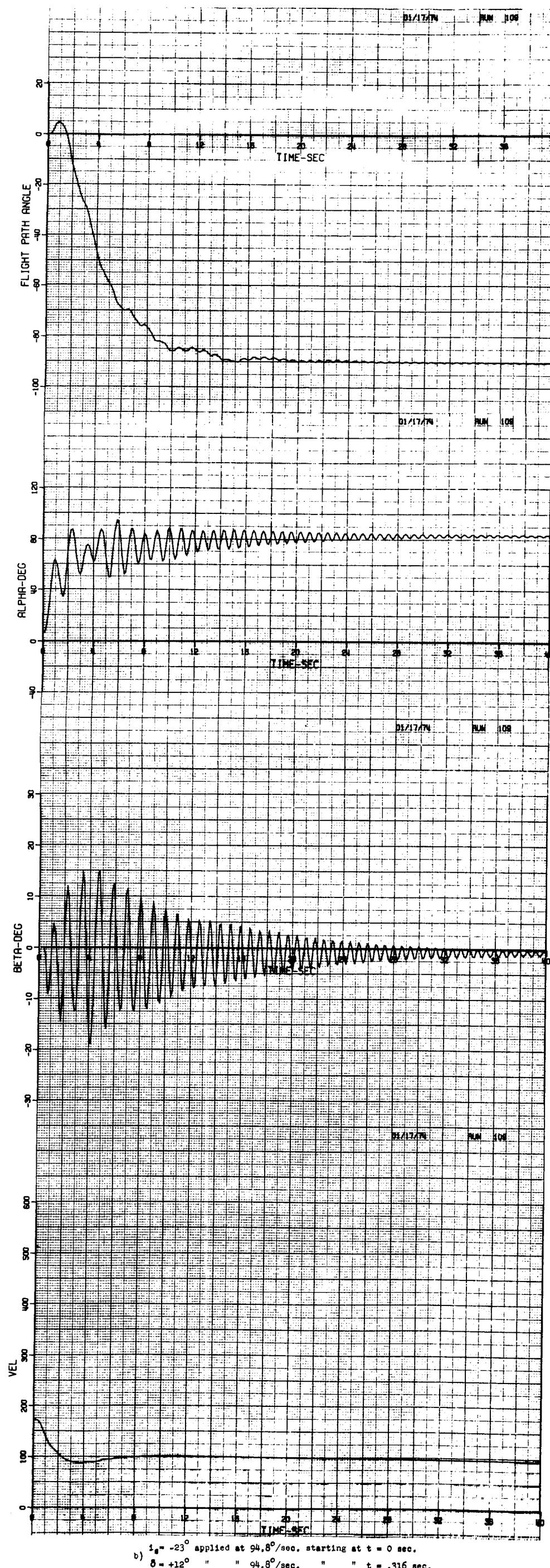


Figure 3.- Continued.

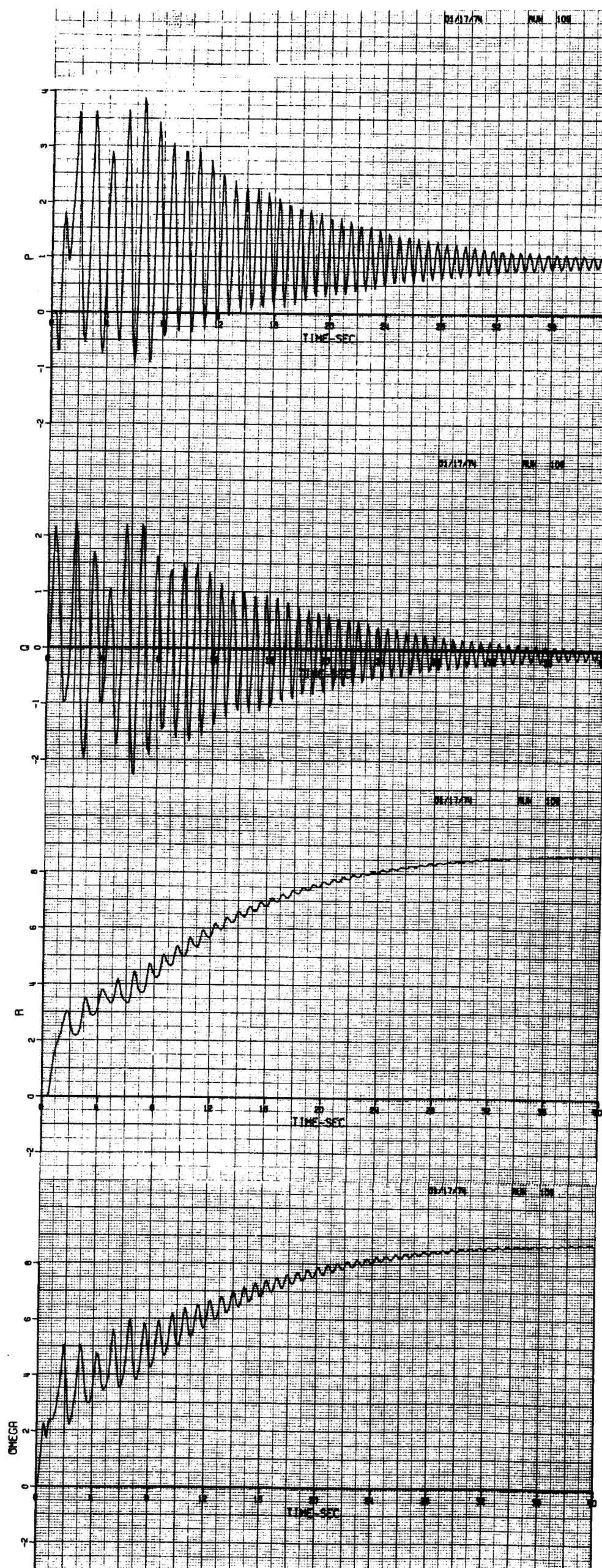
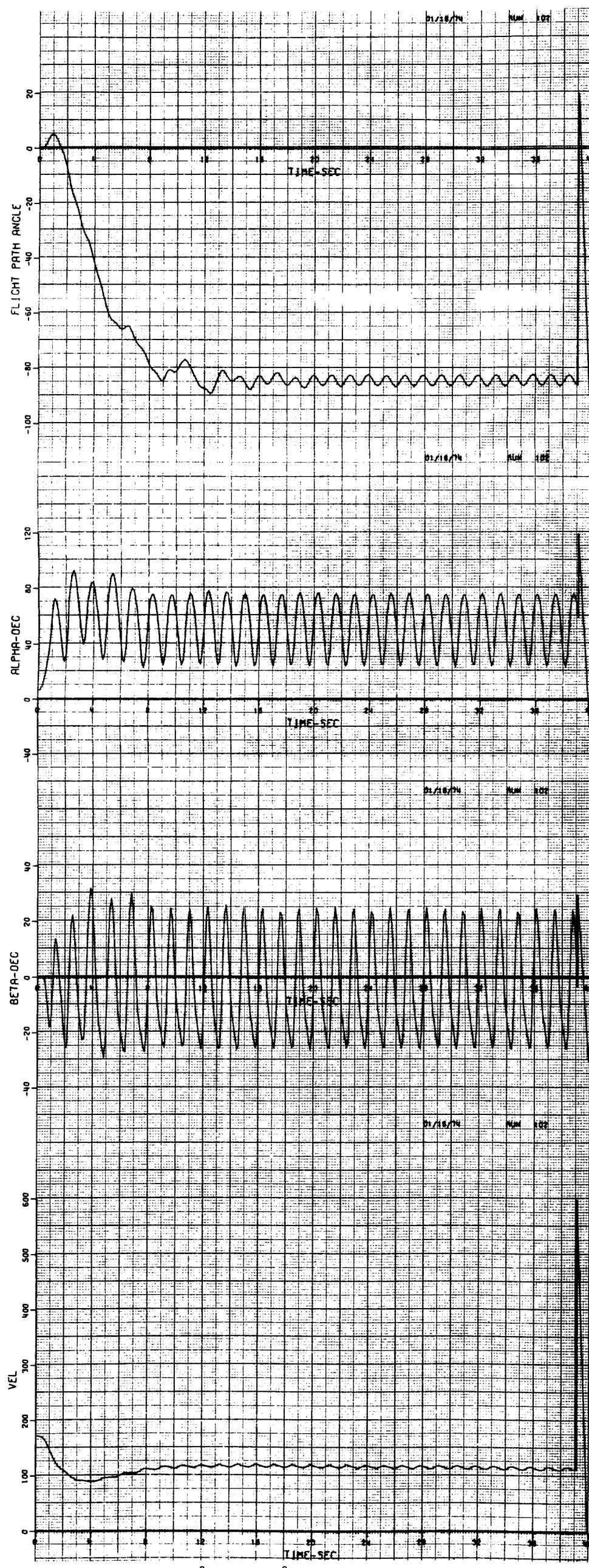
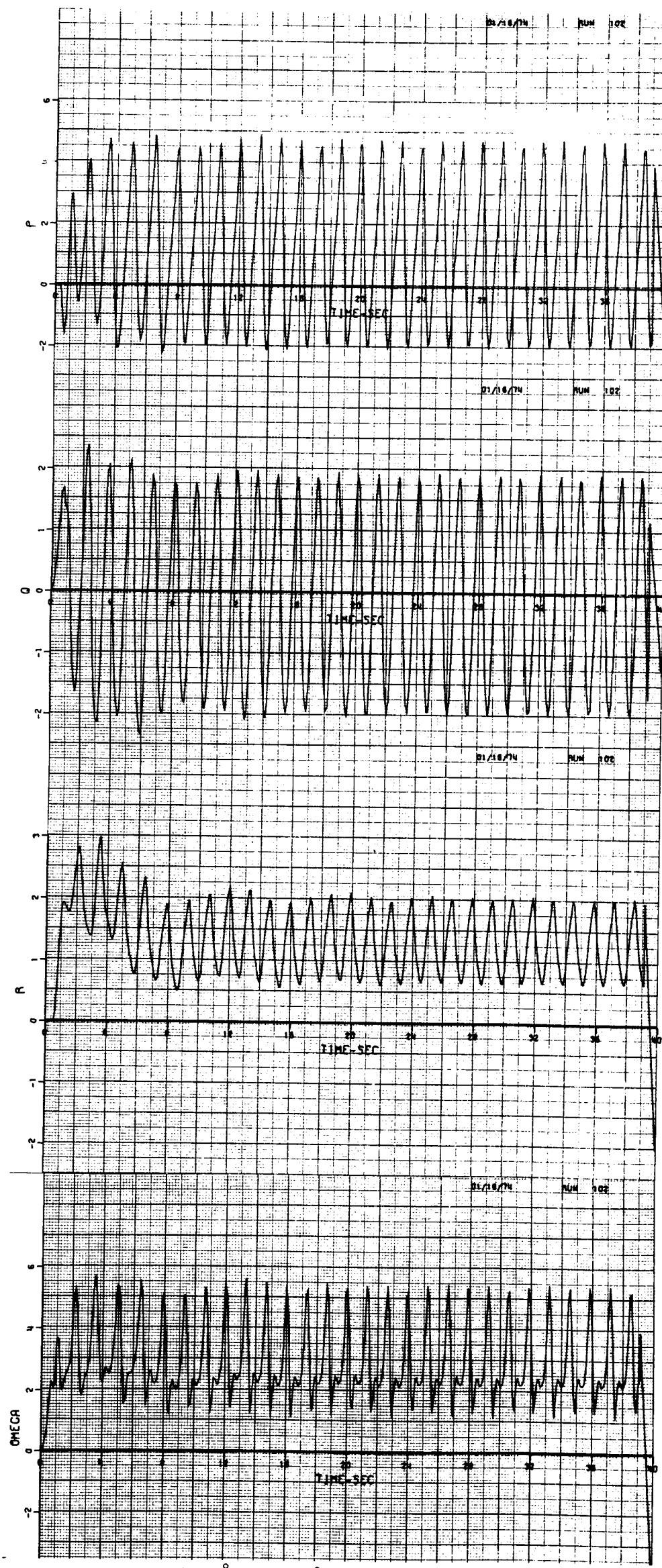


Figure 3.- Continued.



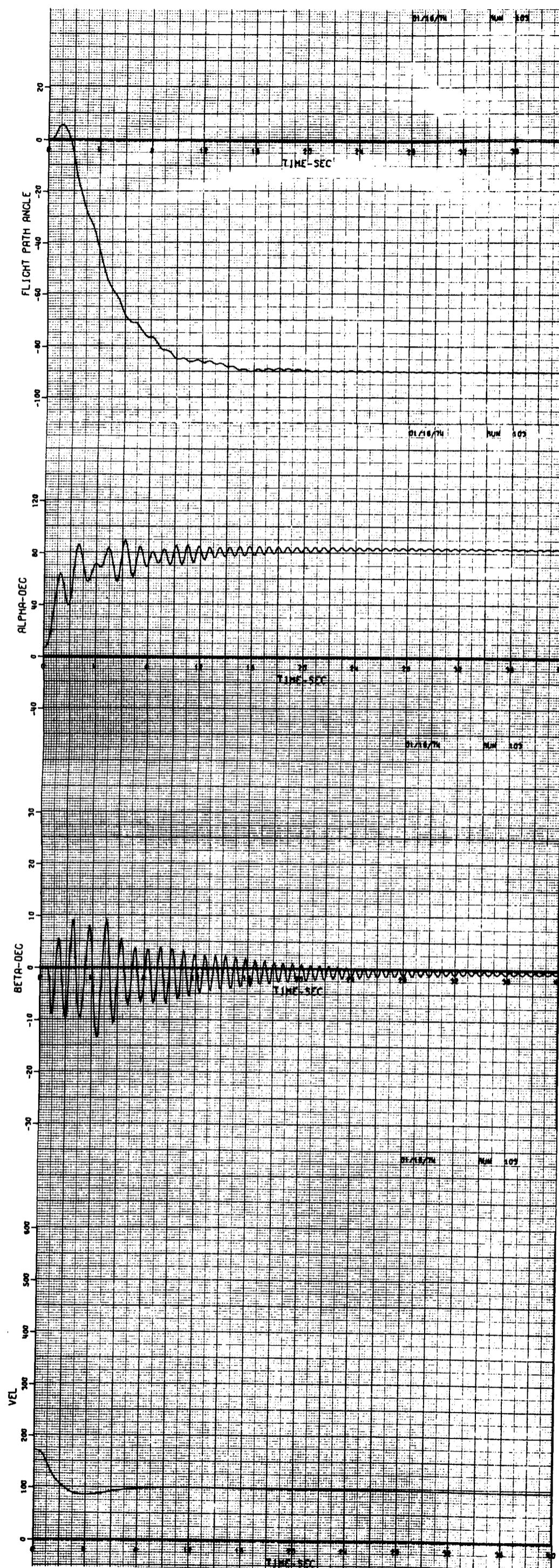
c) $i_s = -30^\circ$ applied at $30^\circ/\text{sec.}$ starting at $t = 0 \text{ sec.}$
 $\delta_a = +12^\circ$ " " $94.8^\circ/\text{sec.}$ " " $t = .316 \text{ sec.}$

Figure 3.- Continued.



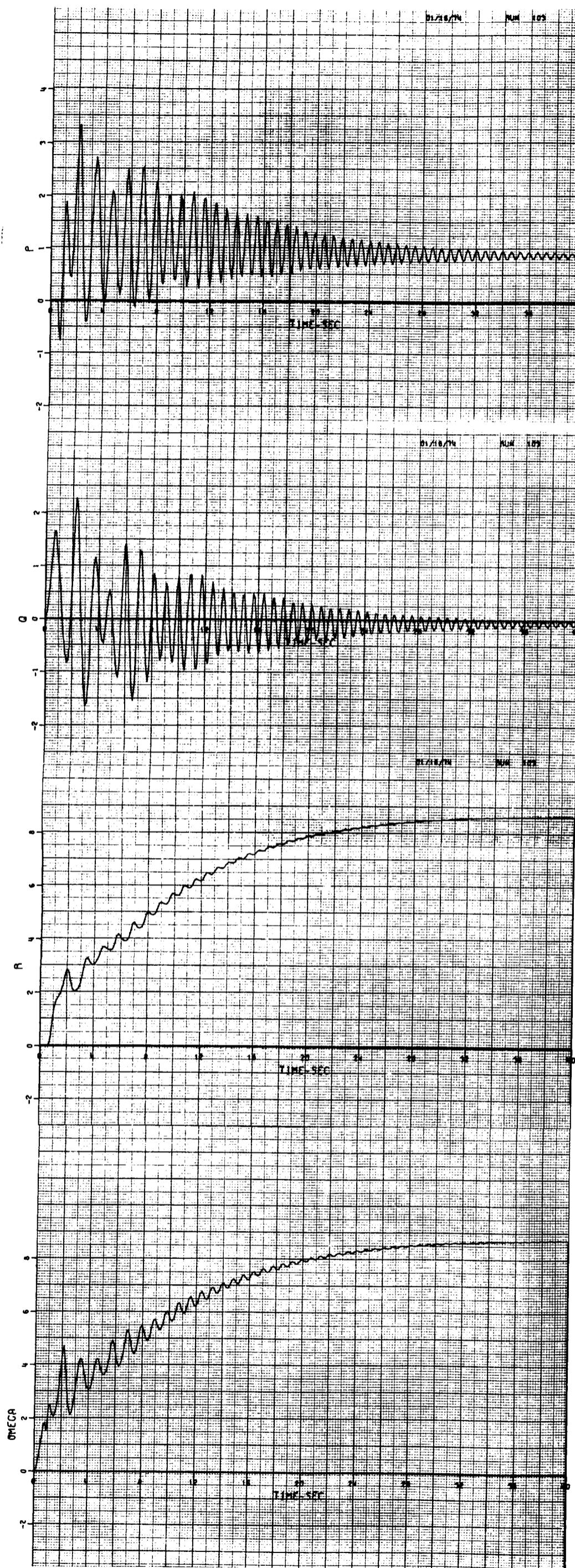
$i_a = -30^\circ$ applied at $30^\circ/\text{sec.}$ starting at $t = 0 \text{ sec.}$
 $c) \theta_a = +12^\circ$ " " $94.8^\circ/\text{sec.}$ " " $t = .316 \text{ sec.}$

Figure 3.- Continued.



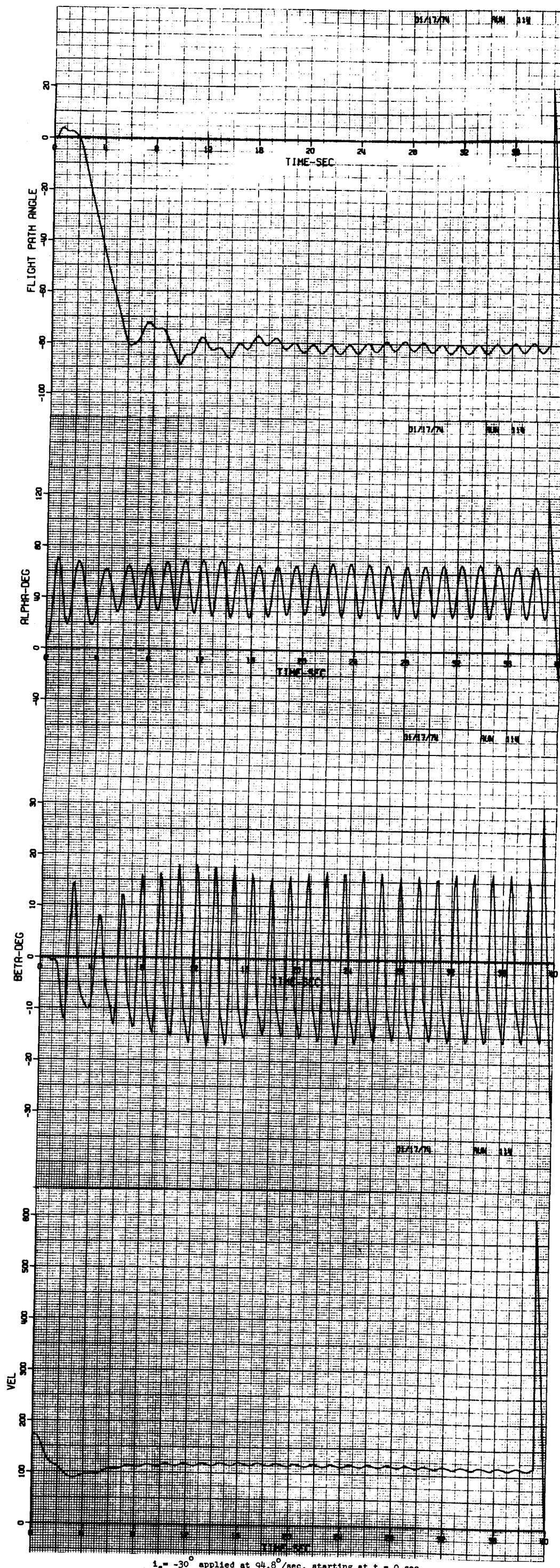
d) $i_s = -30^\circ$ applied at $30^\circ/\text{sec}$, starting at $t = 0$ sec.
 $\delta = +12^\circ$ " " $94.8^\circ/\text{sec}$. " " $t = .500$ sec.
a

Figure 3.- Continued.



d) $\dot{\theta}_s = -30^\circ$ applied at $30^\circ/\text{sec.}$ starting at $t = 0$ sec.
 $\dot{\theta}_s = +12^\circ$ " " $94.8^\circ/\text{sec.}$ " " $t = .500$ sec.

Figure 3.- Continued.



e) $i_s = -30^\circ$ applied at $94.8^\circ/\text{sec.}$ starting at $t = 0 \text{ sec.}$
 $\delta = +5^\circ$ " " $94.8^\circ/\text{sec.}$ " " $t = .500 \text{ sec.}$

Figure 3.- Continued.

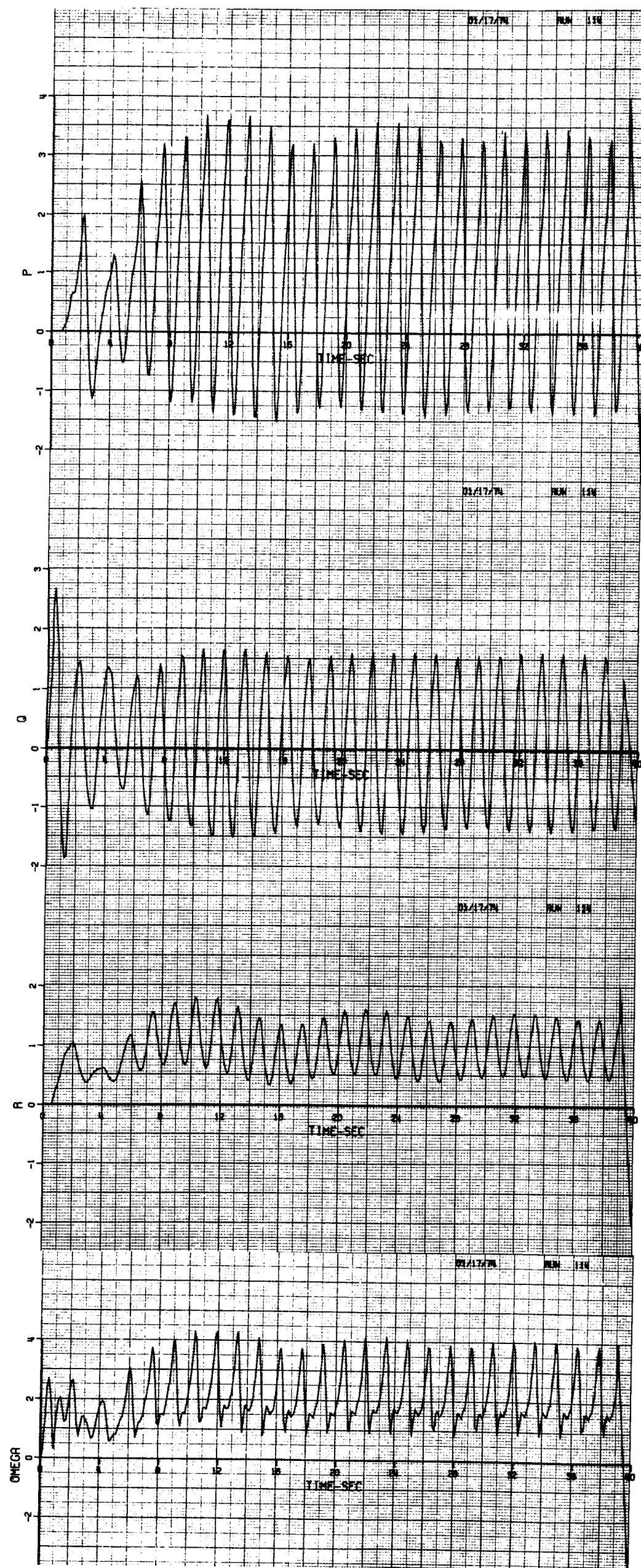


Figure 3.- Continued.

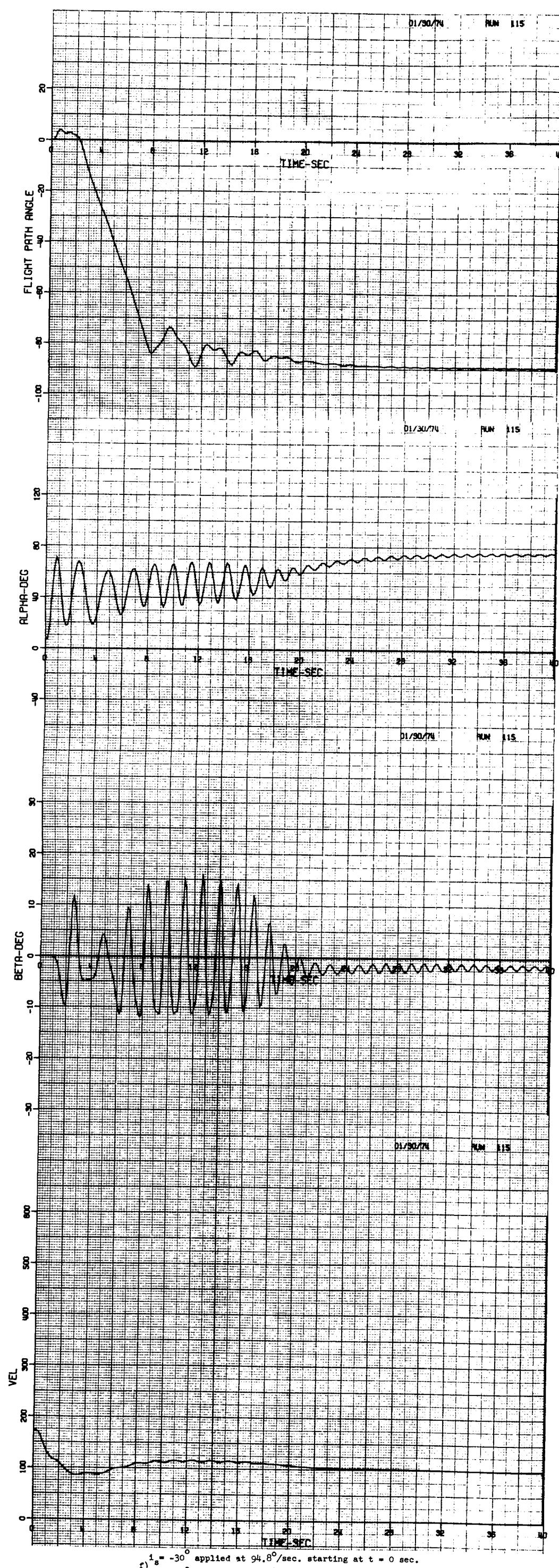
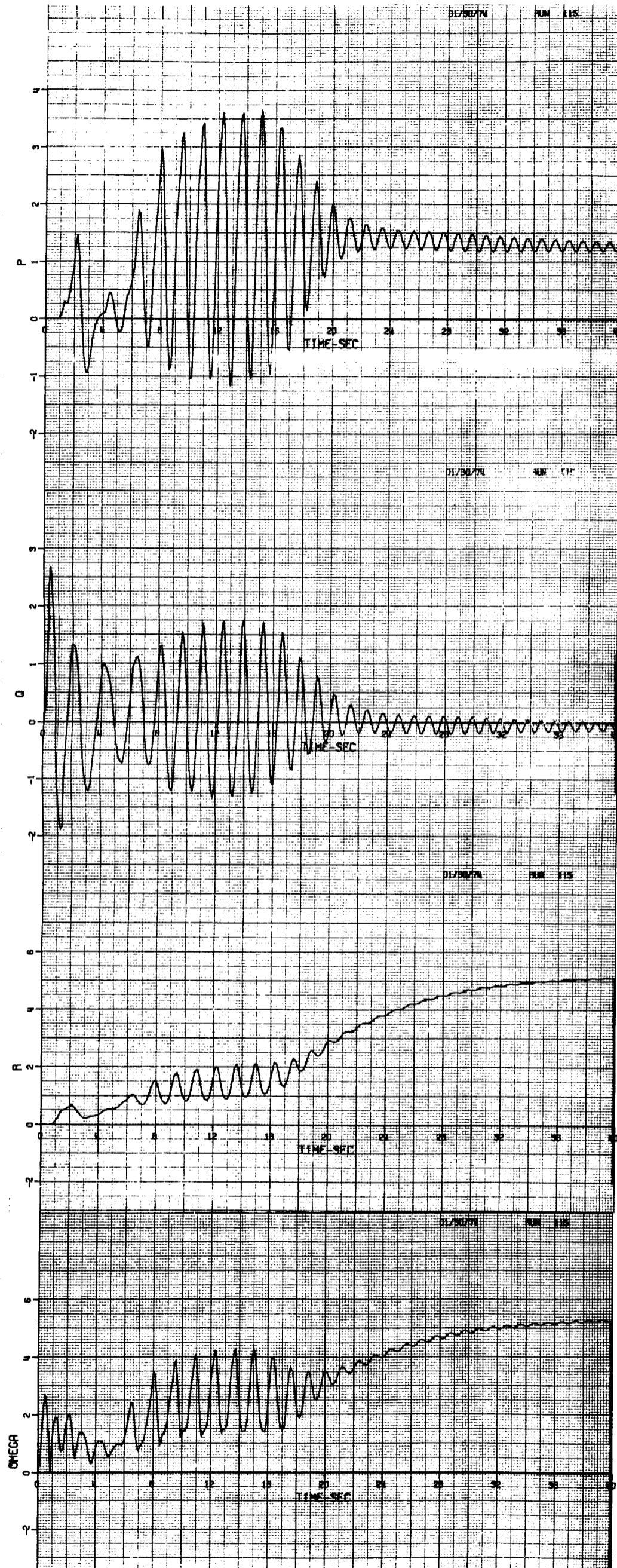
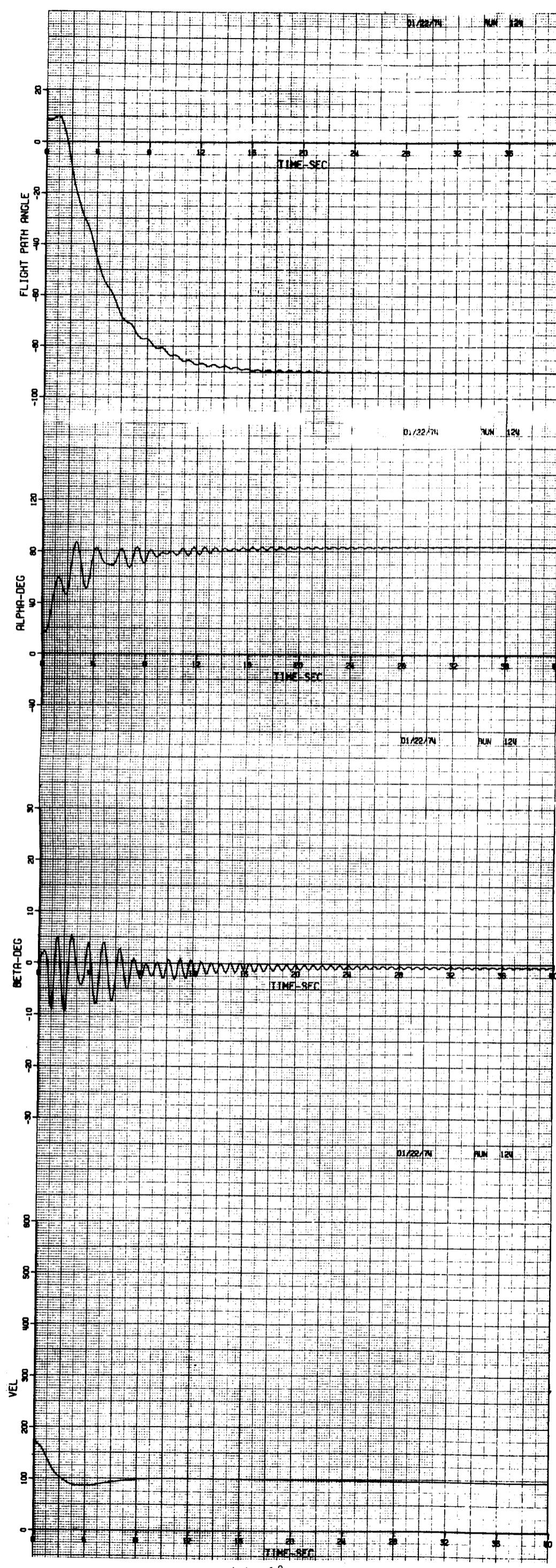


Figure 3.- Continued.



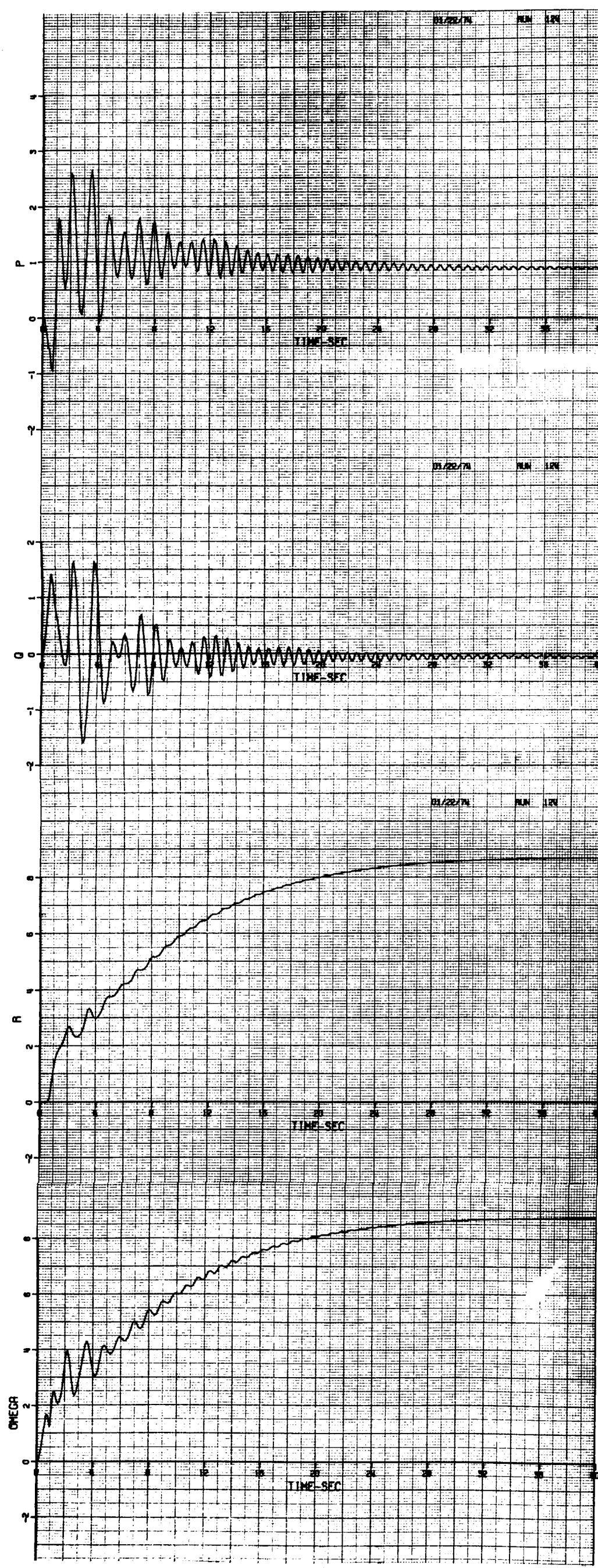
f) $i_s = -30^\circ$ applied at $94.8^\circ/\text{sec.}$ starting at $t = 0 \text{ sec.}$
 f) $\delta_a = +5^\circ$ " " $94.8^\circ/\text{sec.}$ " " $t = .750 \text{ sec.}$

Figure 3.- Concluded.



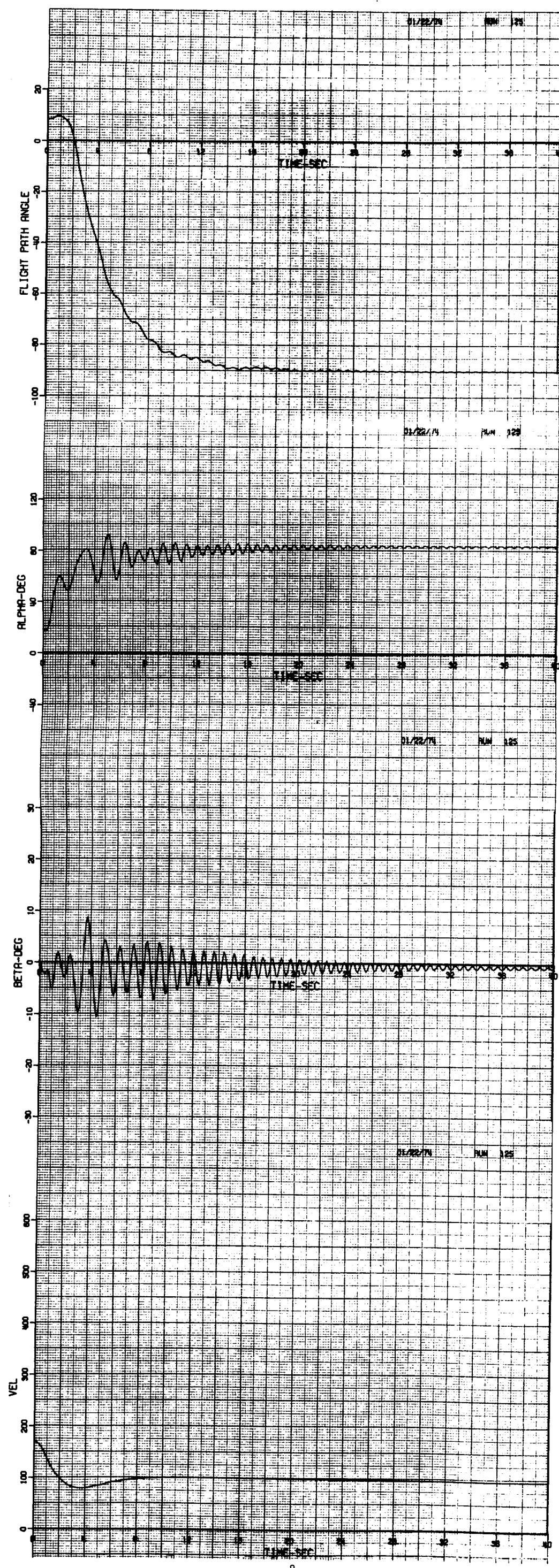
a) $\phi_0 = 60^\circ$, right spin

Figure 4.- Sensitivity of spinning motion to initial Euler angles.



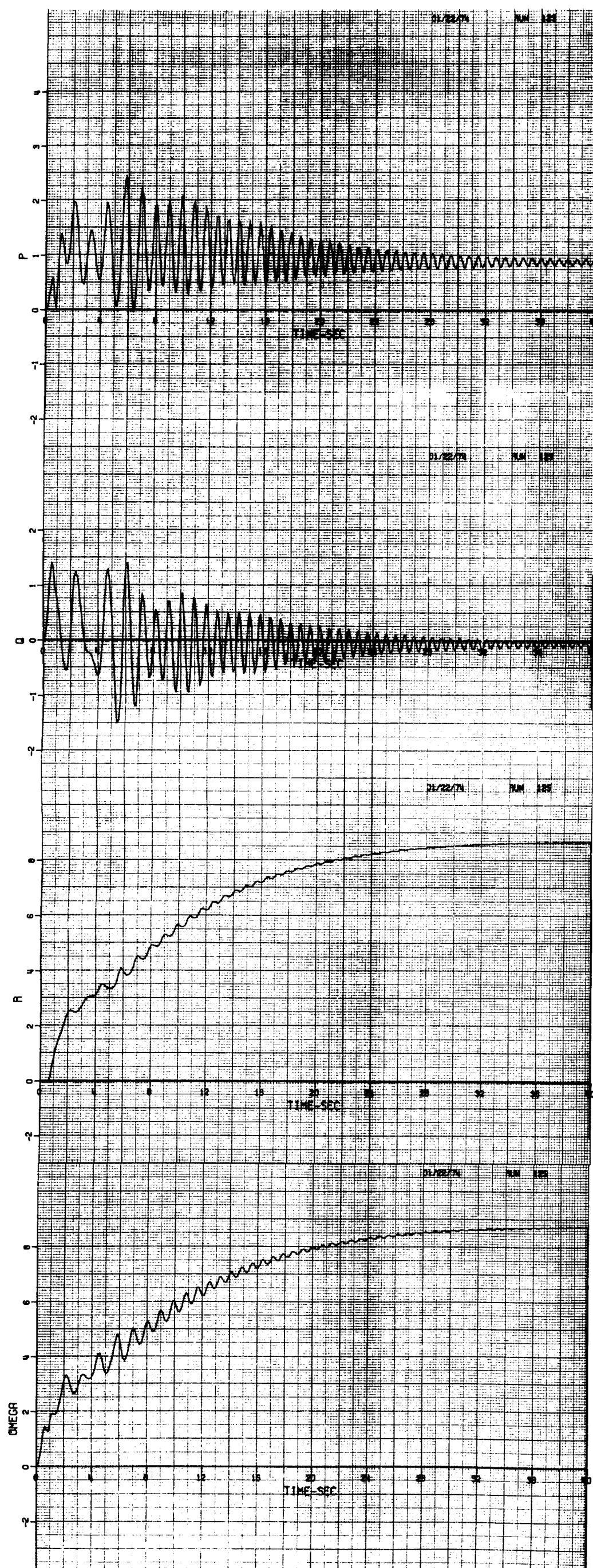
a) $\phi_0 = 60^\circ$, right spin

Figure 4.- Continued.



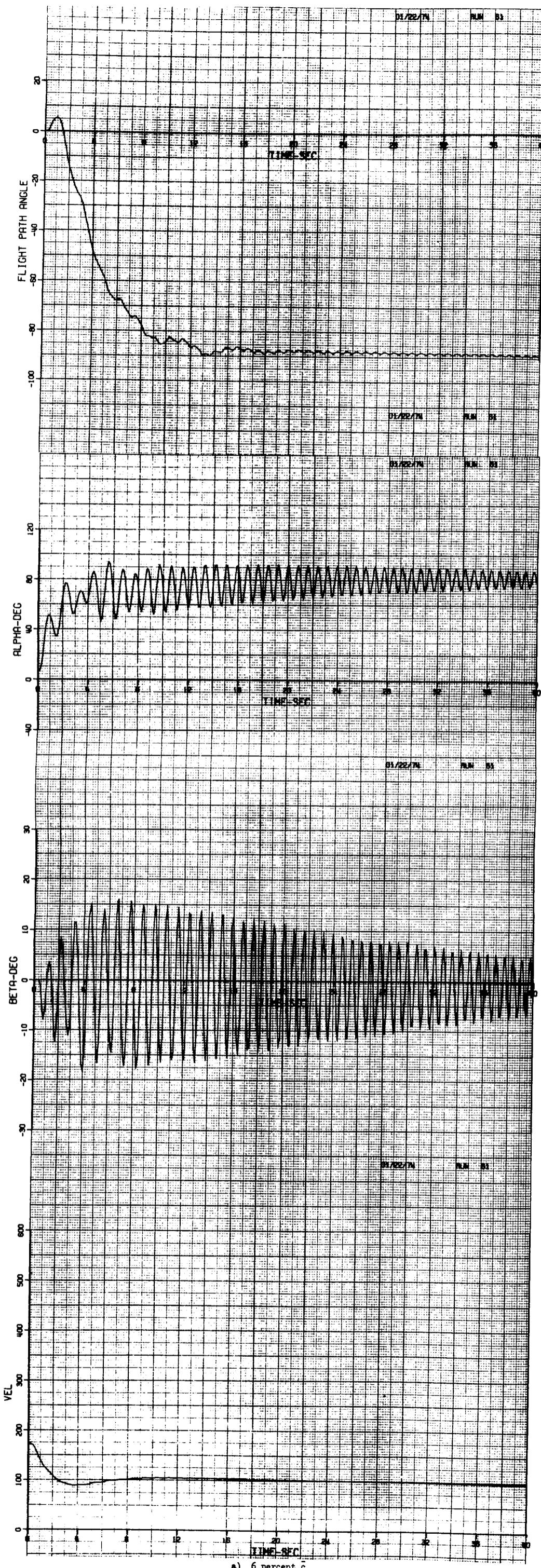
b) $\beta_0 = -60^\circ$, right spin

Figure 4.- Continued.



b) $\phi_0 = -60^\circ$, right spin

Figure 4.- Concluded.



a) 6 percent c

Figure 5.- Sensitivity of spinning motion to center-of-gravity location.

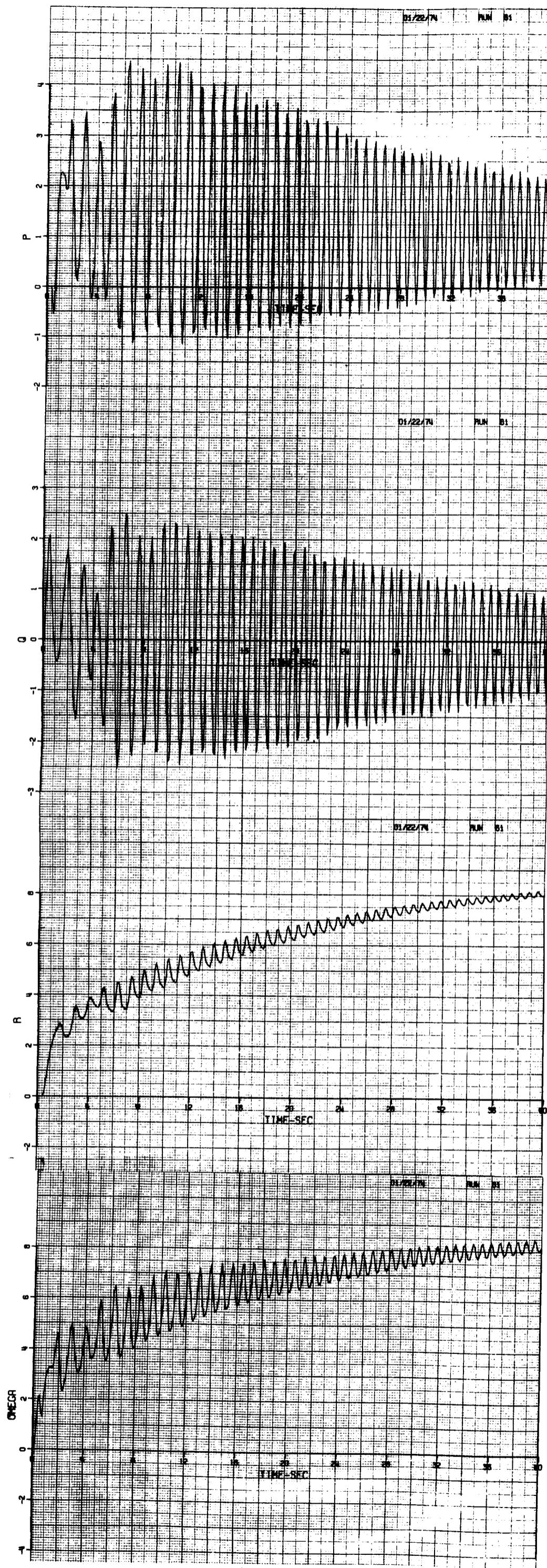
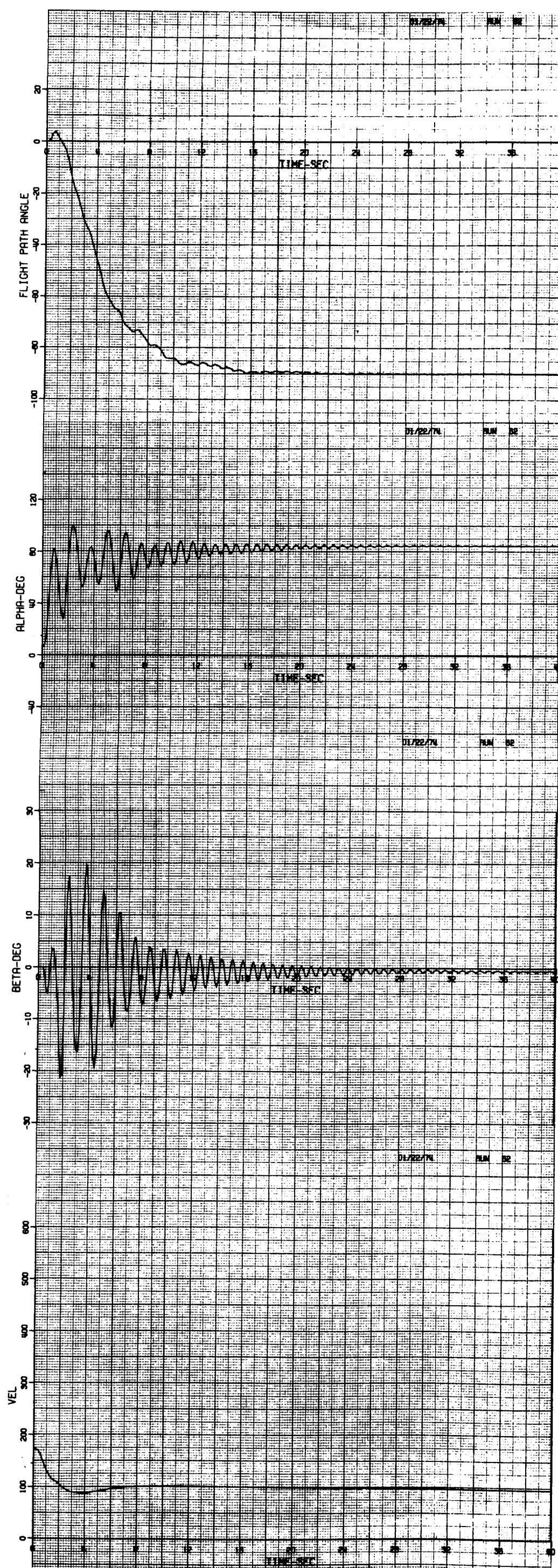


Figure 5.- Continued.



b) 26 percent c

Figure 5.- Continued.

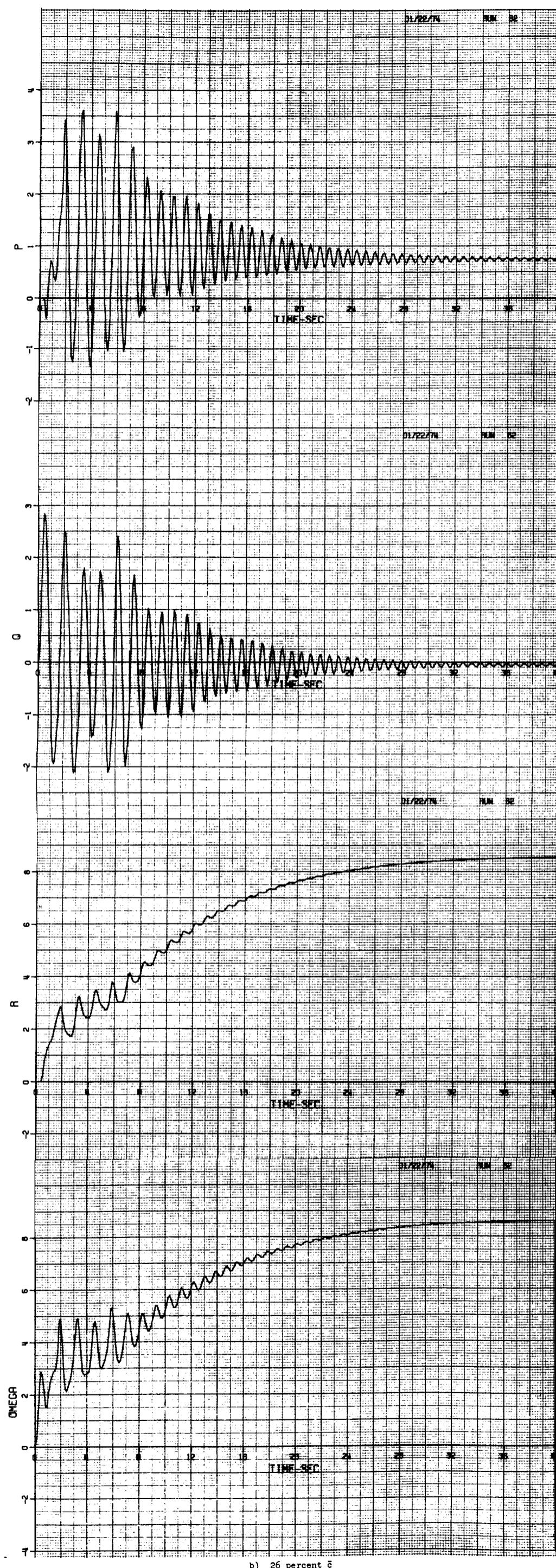


Figure 5.- Concluded.

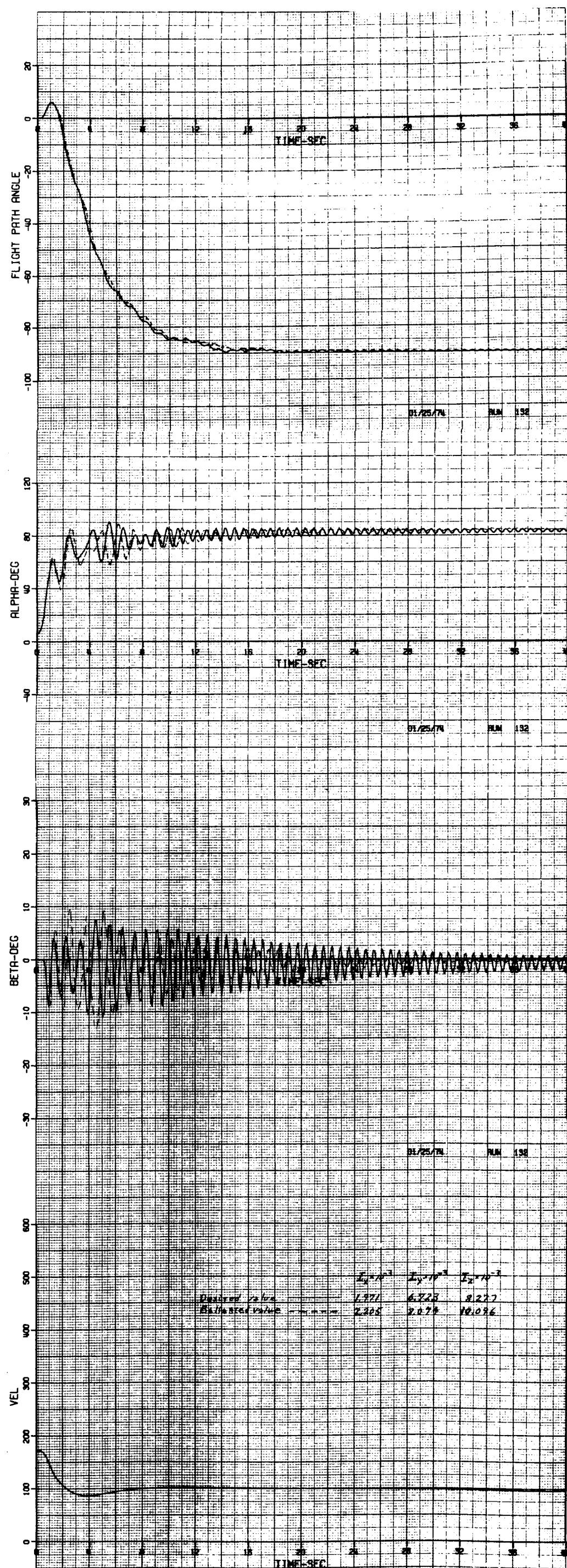


Figure 6.- Influence of errors incurred in ballasting model for some full-scale test altitude.

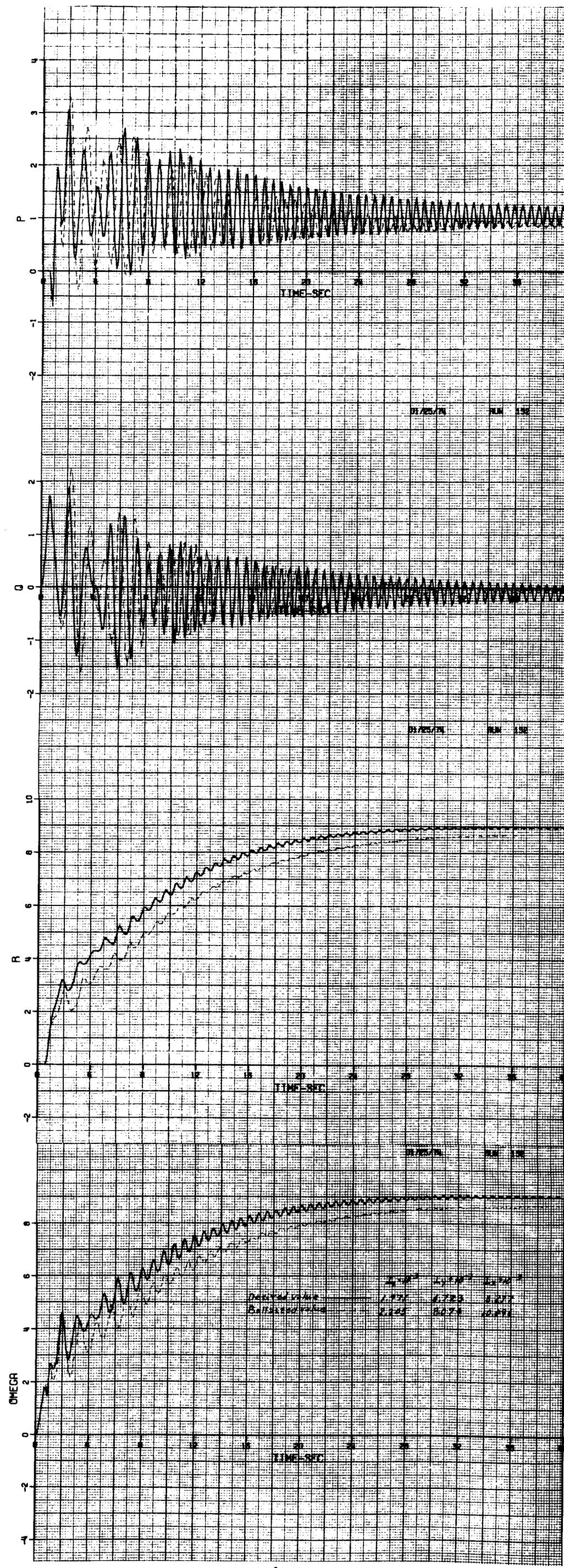
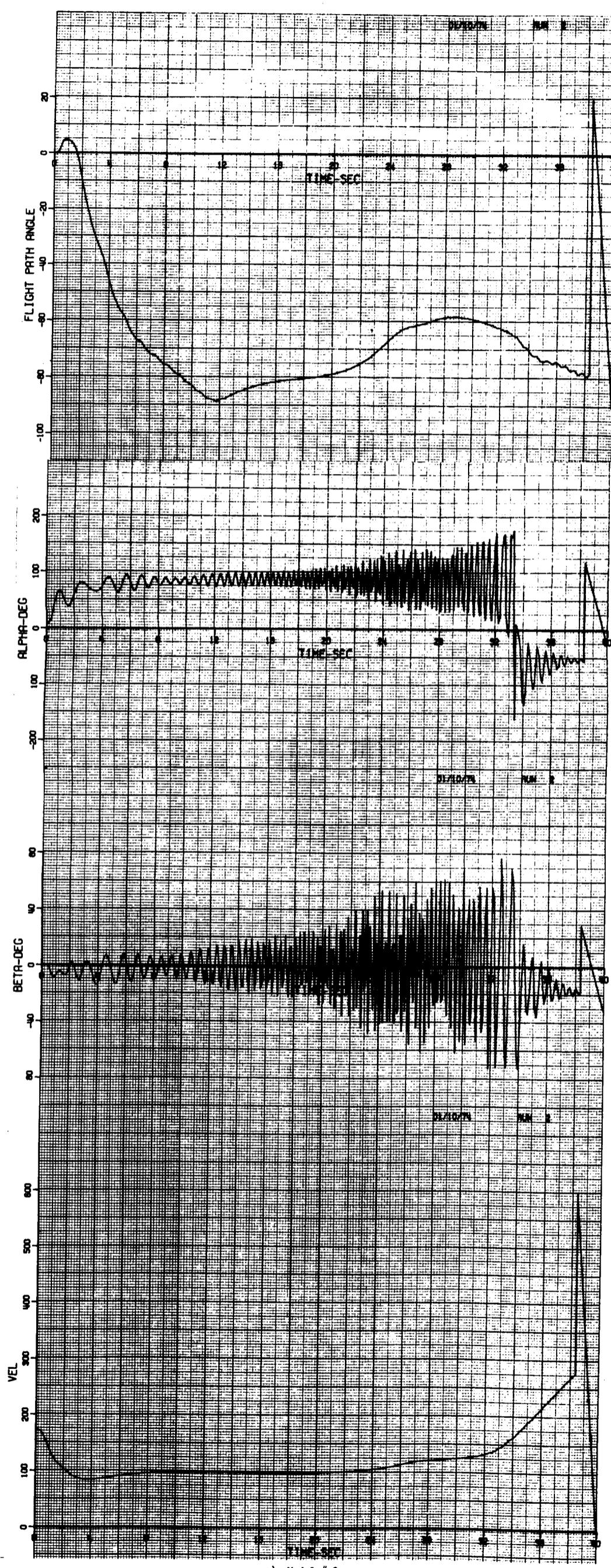
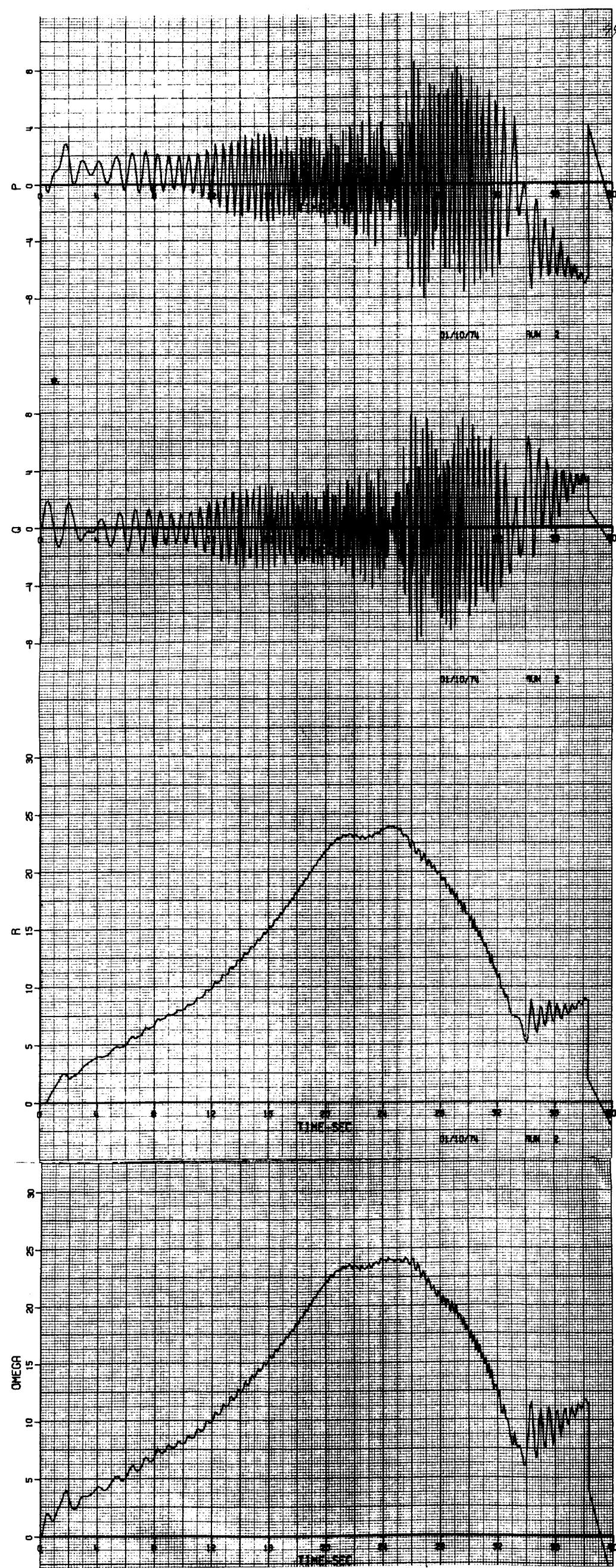


Figure 6.- Concluded.



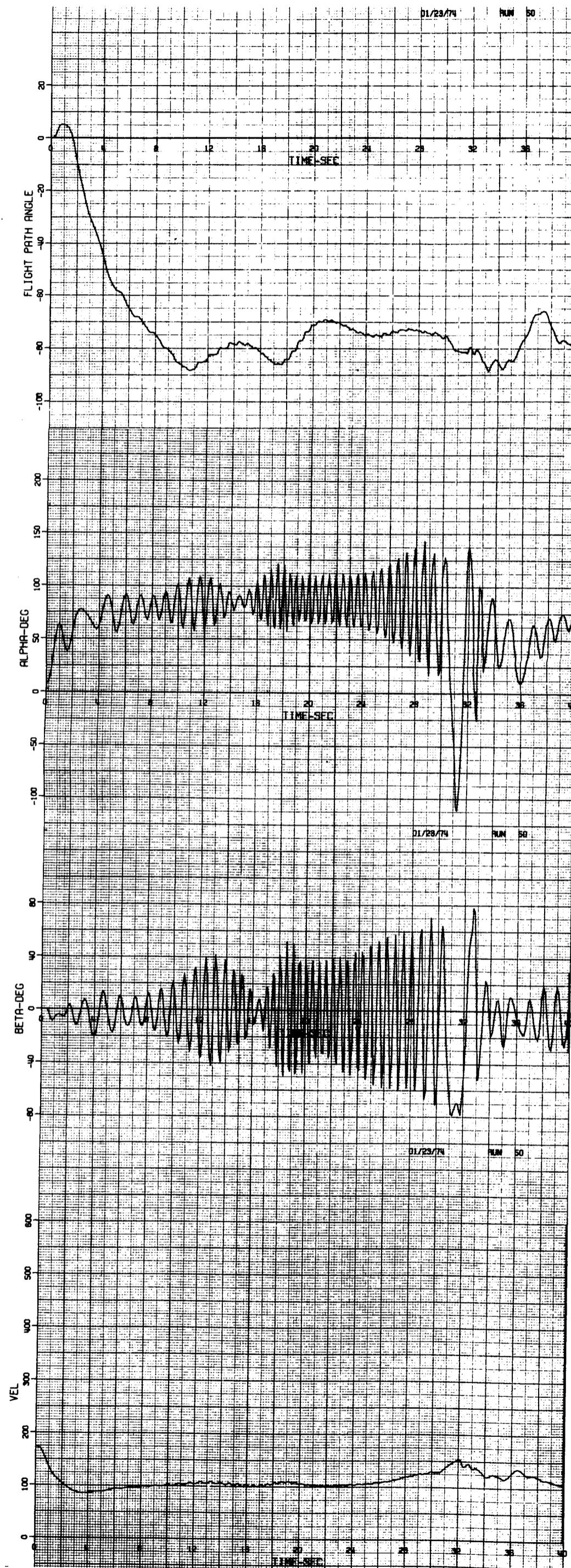
a) Model # 2

Figure 7.- Influence of some aerodynamic characteristics on spinning motion.



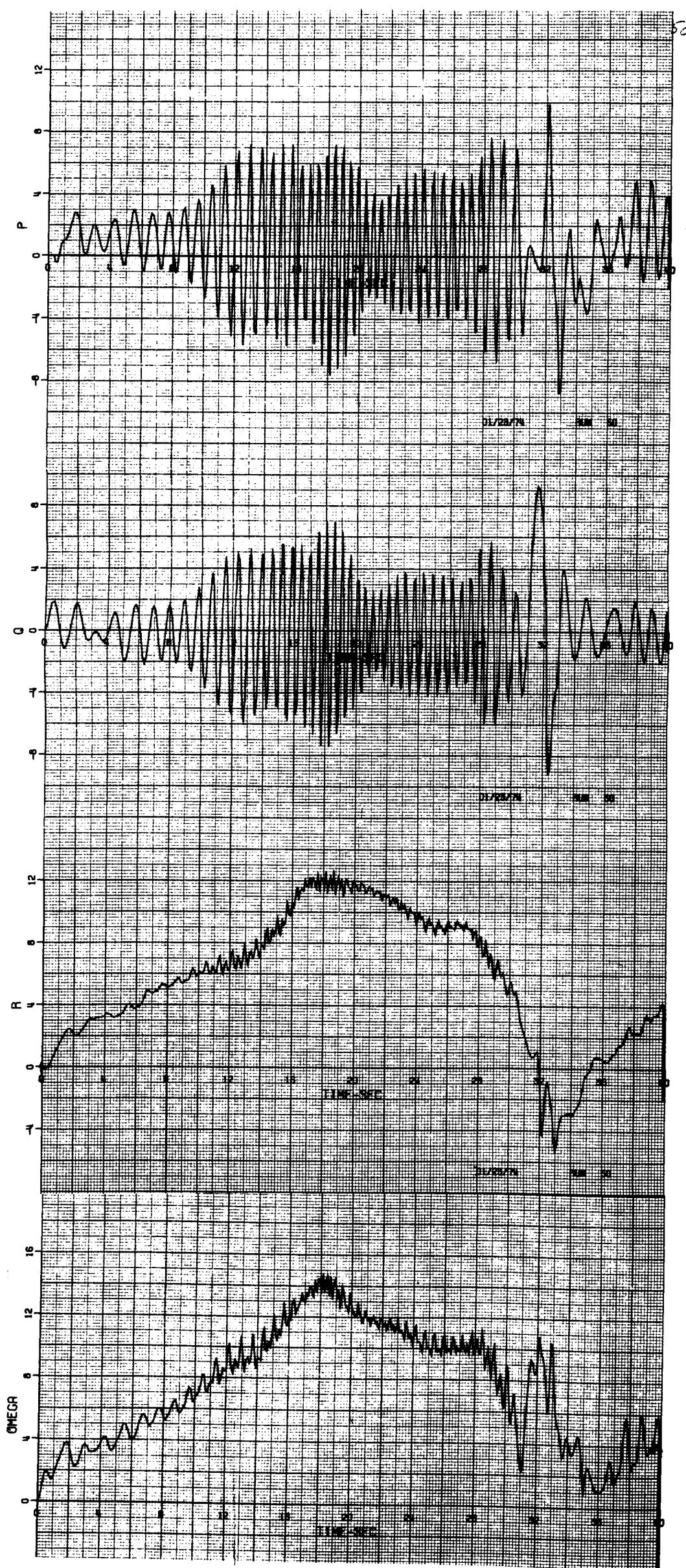
a) Model # 2

Figure 7.- Continued.



b) Model # 2 with low frequency dynamic derivatives.

Figure 7.- Continued.



b) Model #2 with low frequency dynamic derivatives.

Figure 7.- Continued.

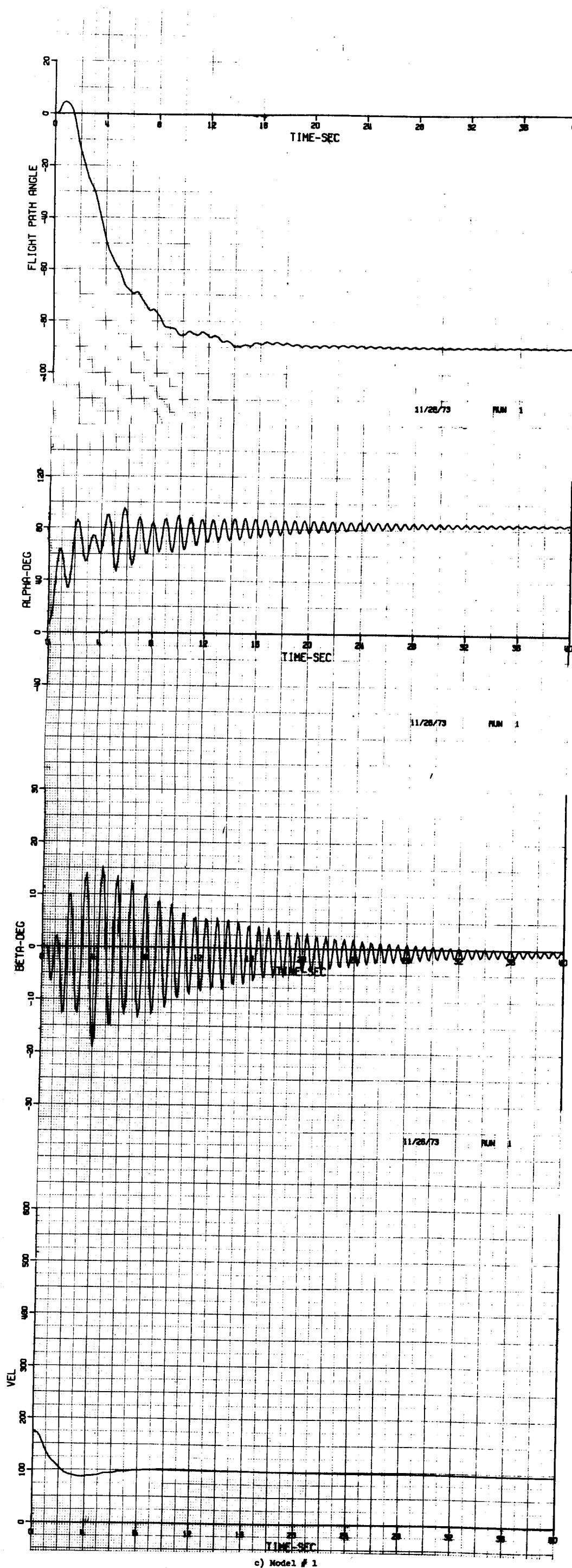
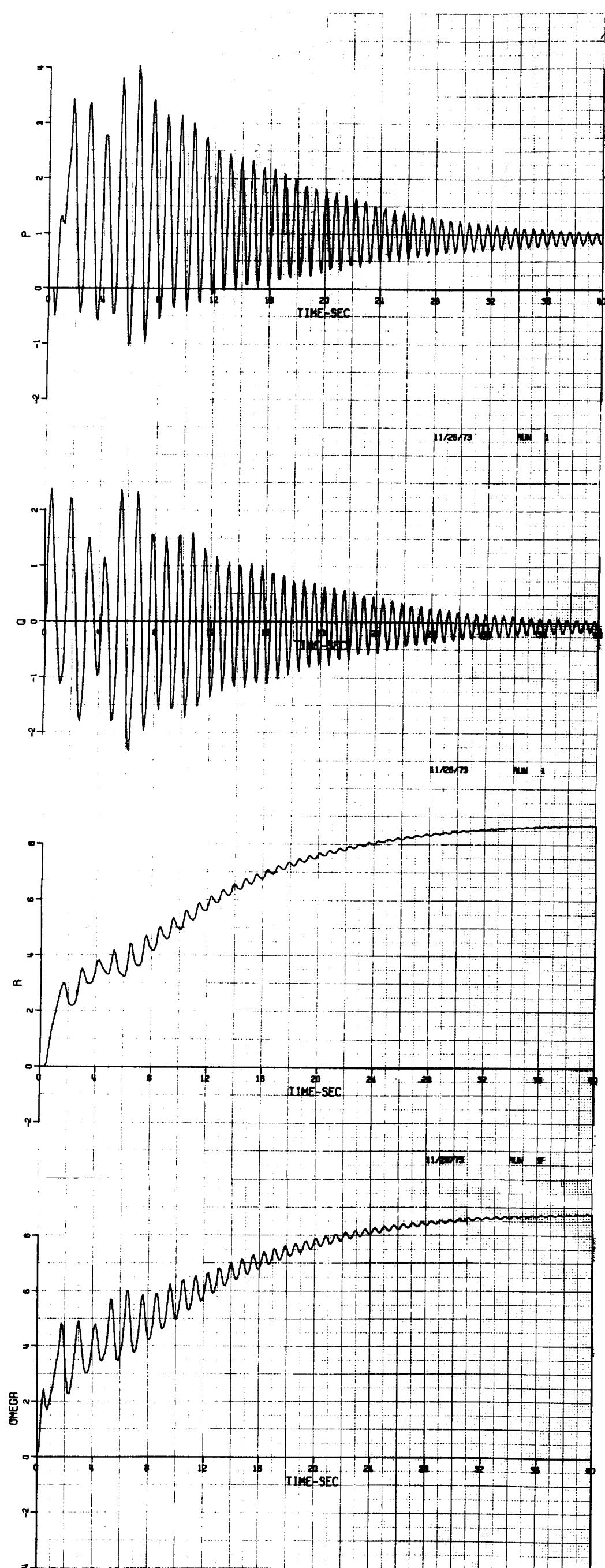
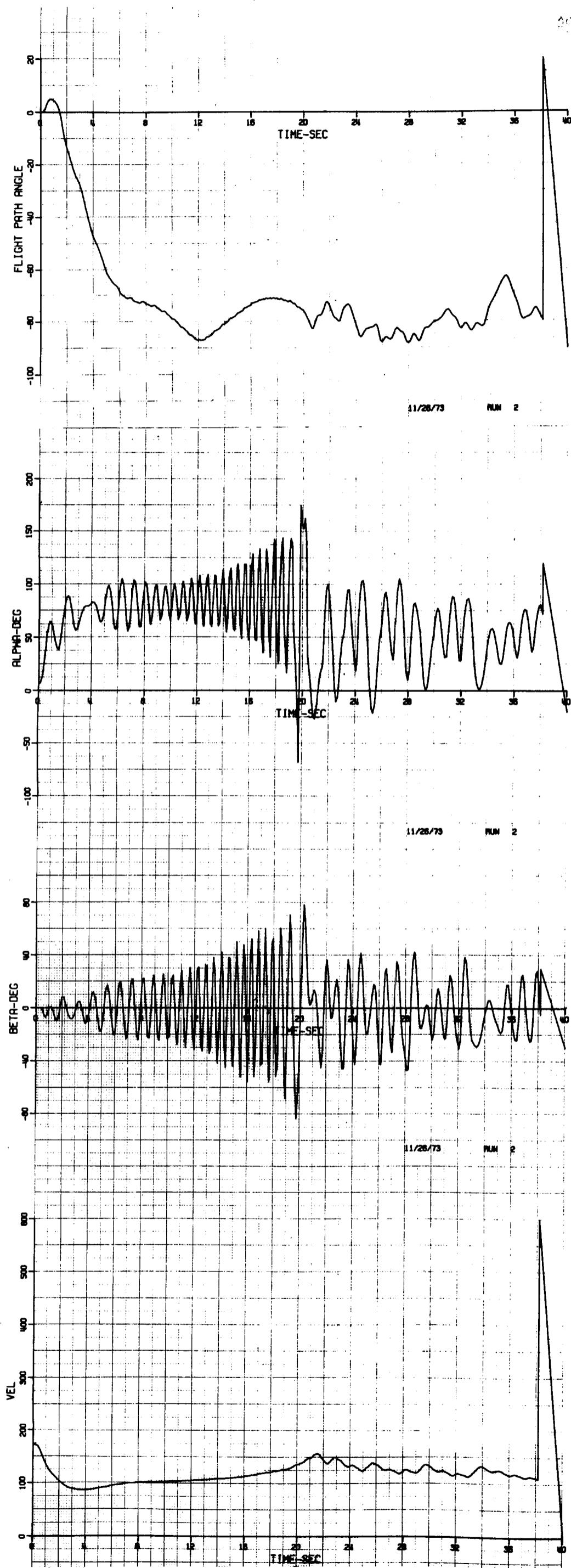


Figure 7.- Continued.

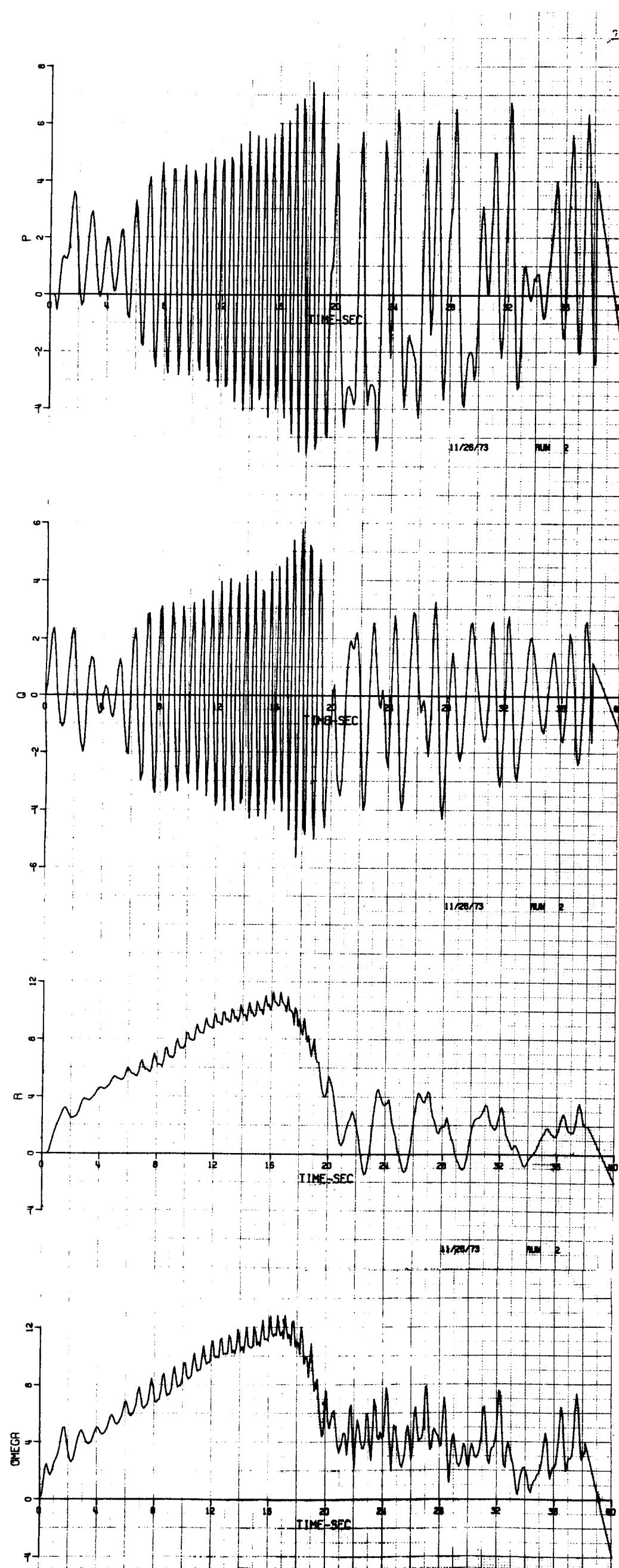


c) Model # 1
Figure 7.- Continued.



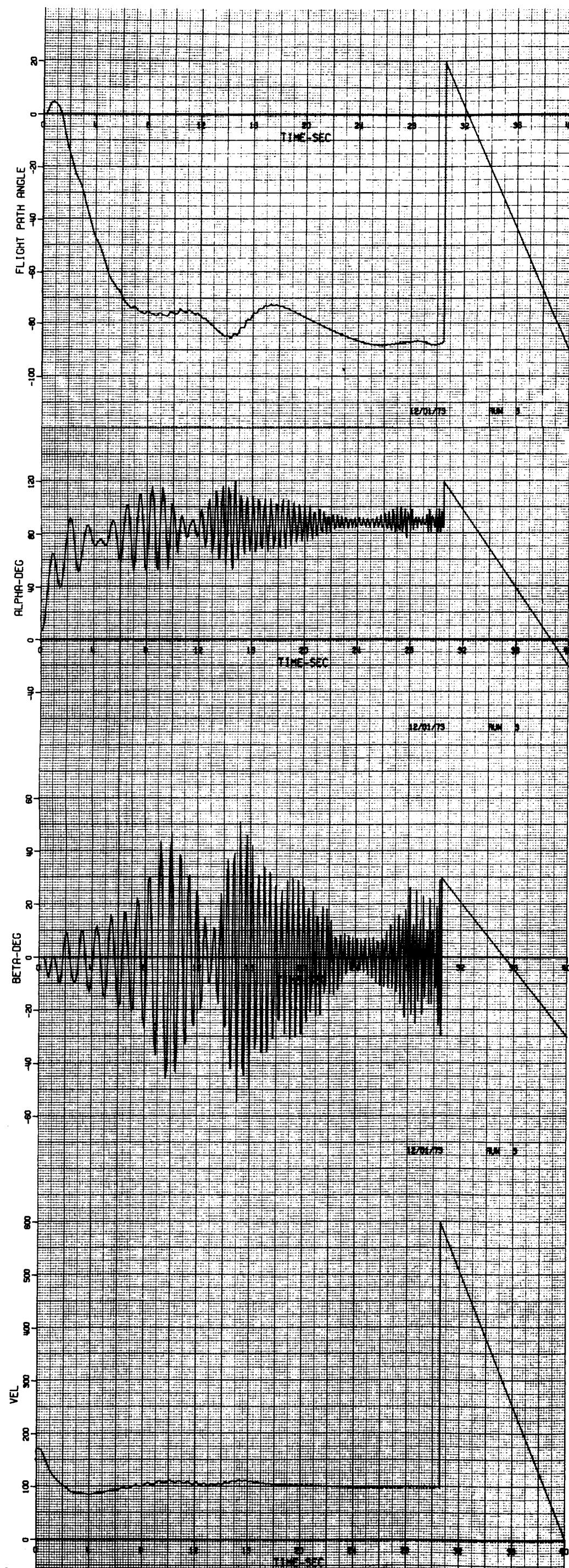
d) Model # 1 with high frequency dynamic derivatives.

Figure 7.- Continued.



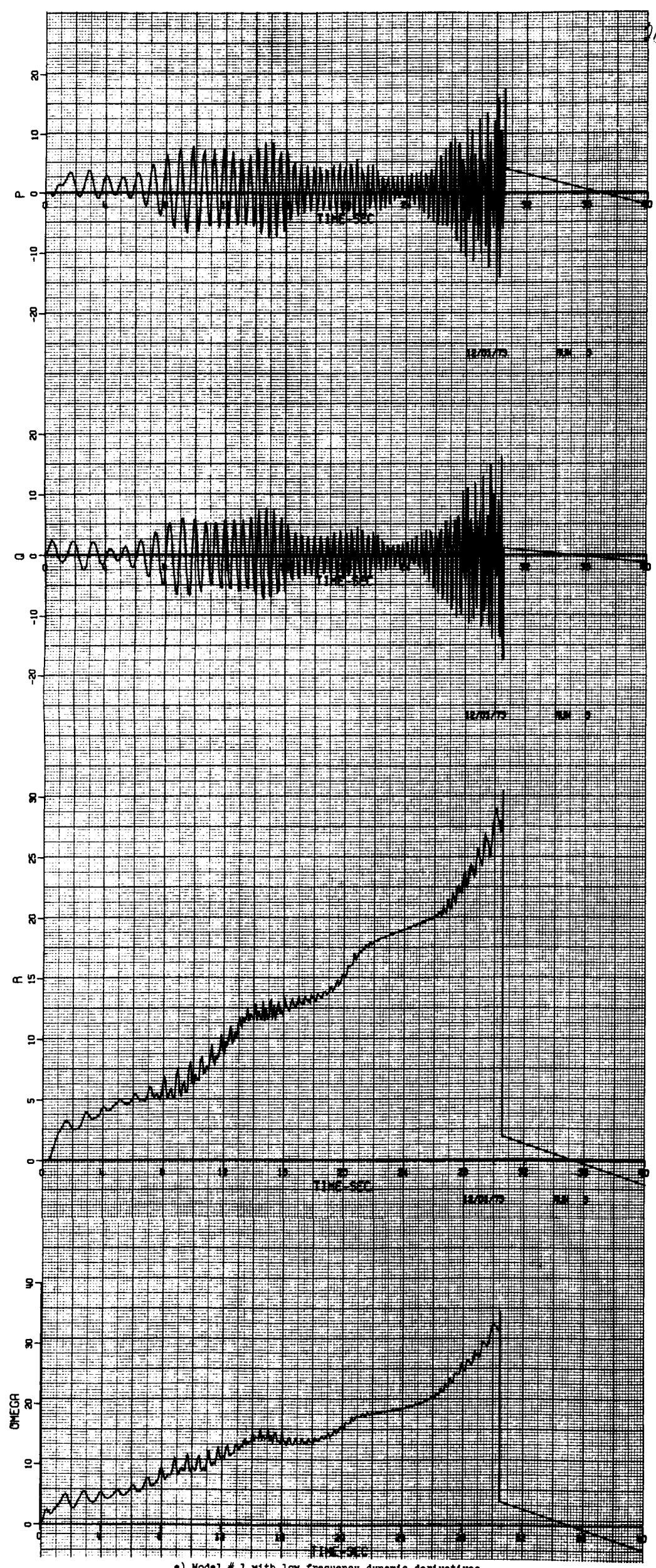
d) Model # 1 with high frequency dynamic derivatives.

Figure 7.- Continued.



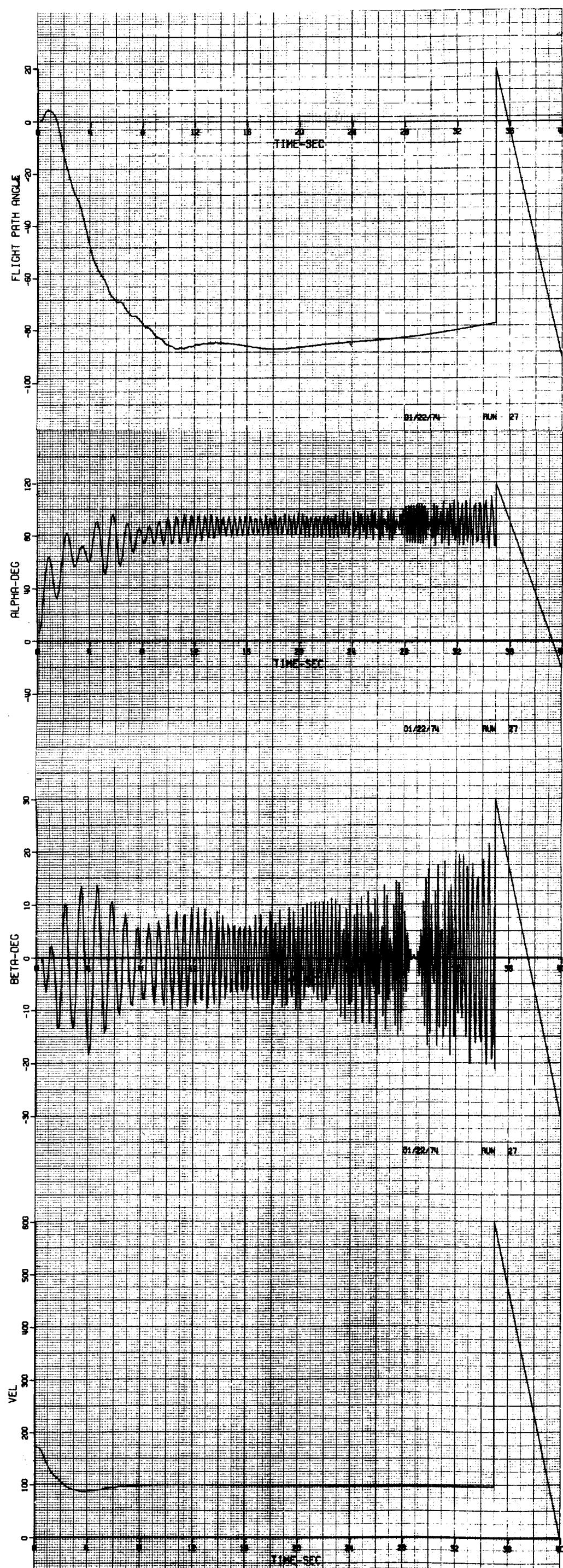
a) Model # 1 with low frequency dynamic derivatives.

Figure 7.- Continued.



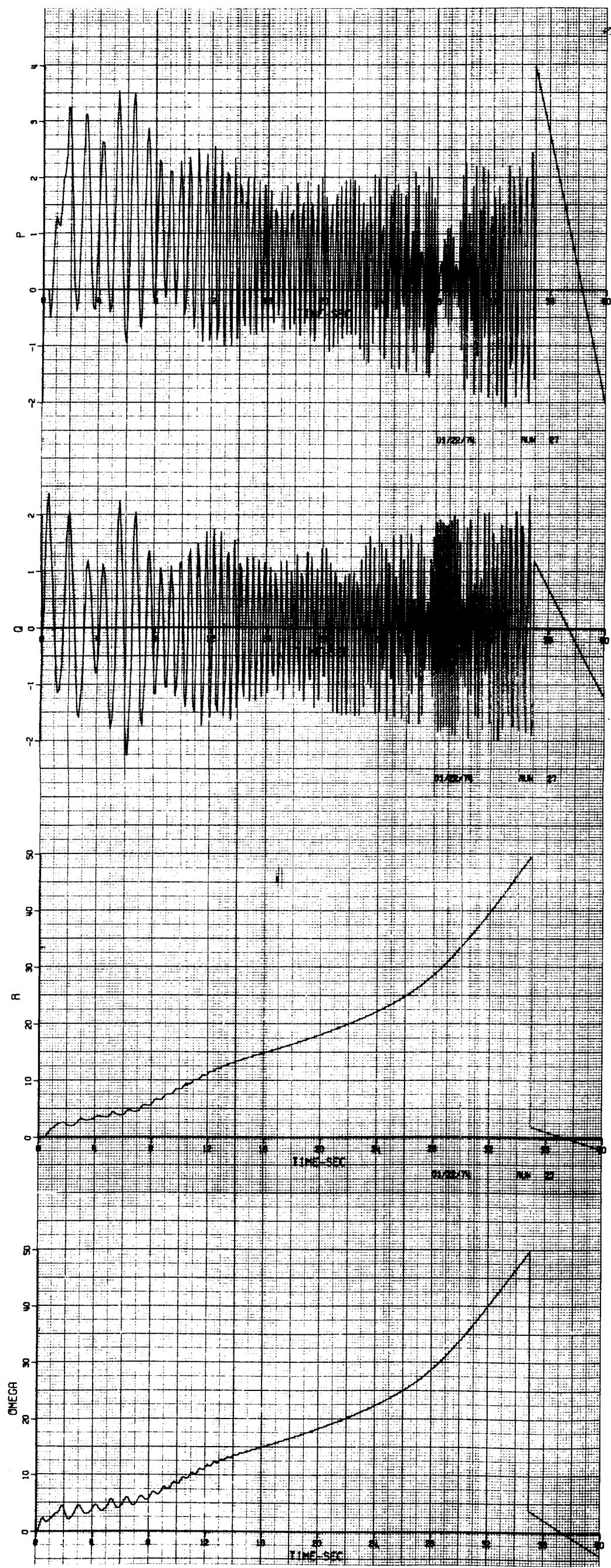
e) Model # 1 with low frequency dynamic derivatives.

Figure 7.- Continued.



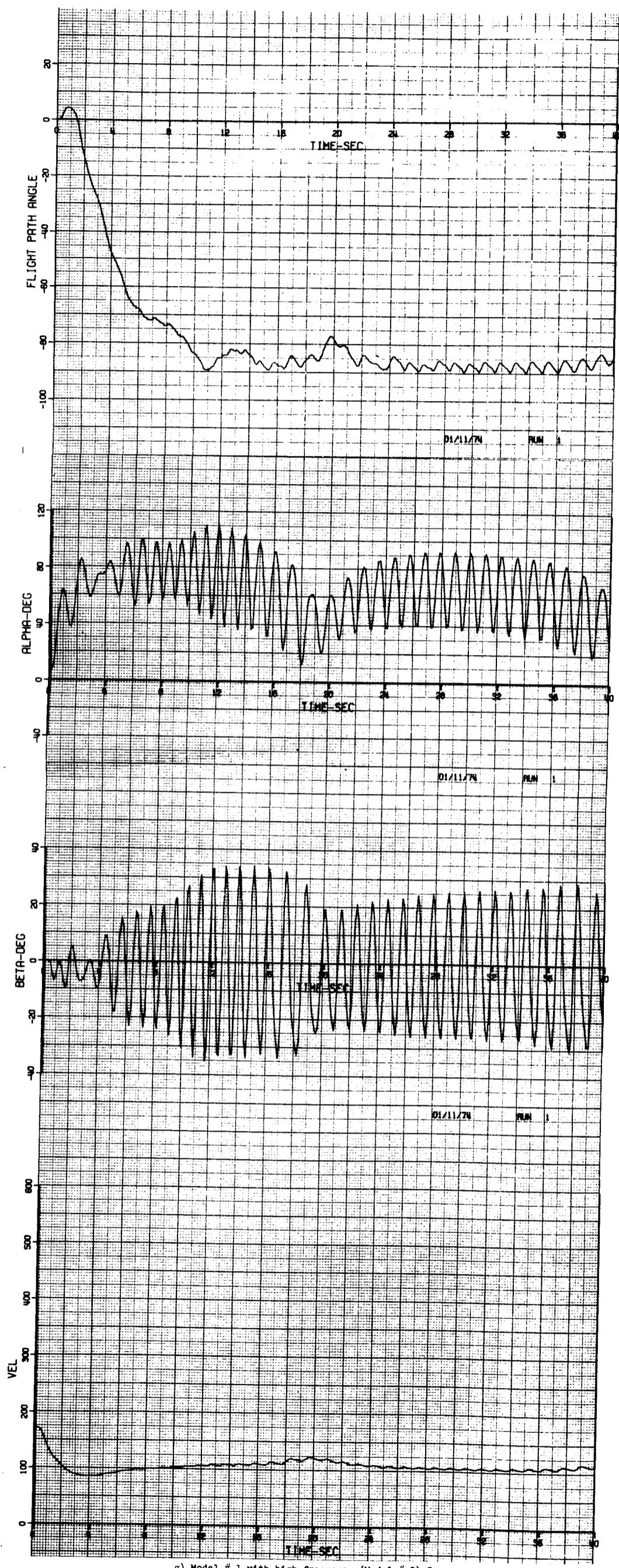
f) Model # 1 with high frequency (Model # 2) C_{n_r} .

Figure 7. - Continued.



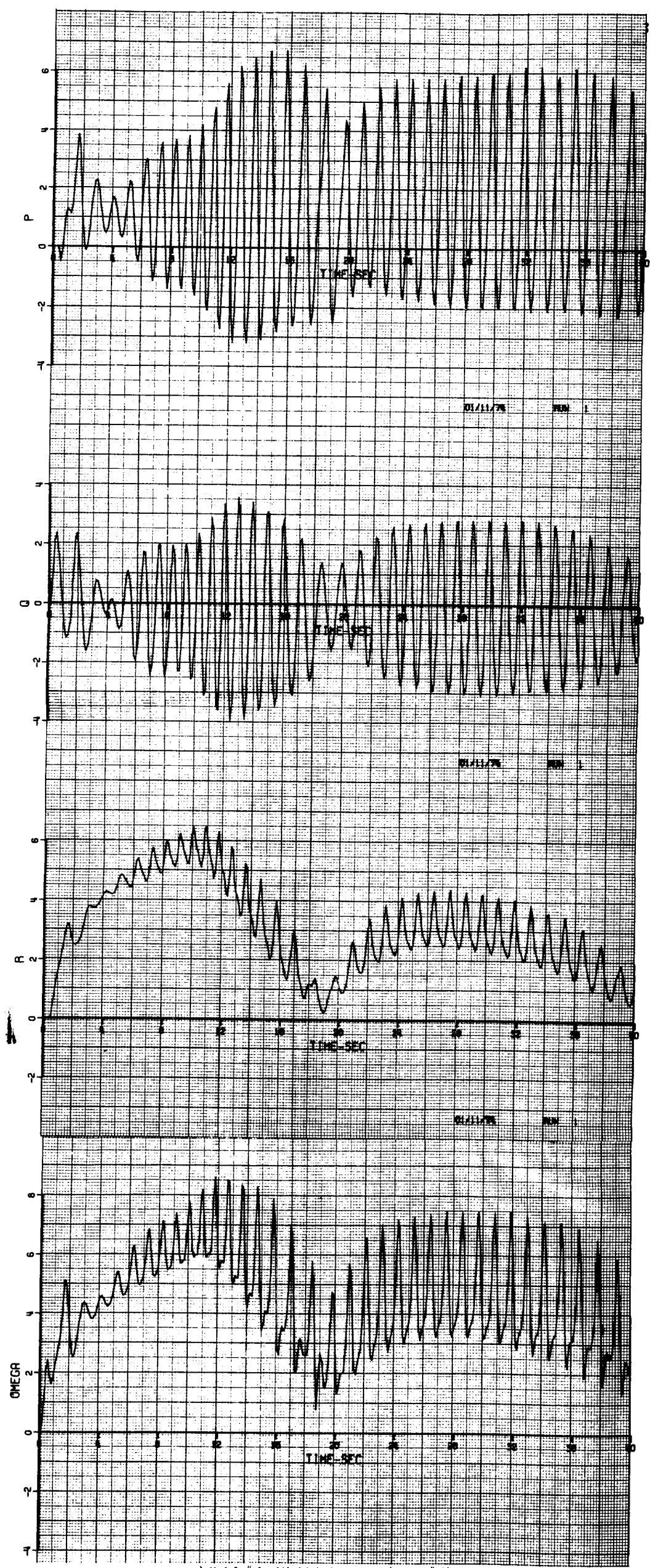
f) Model # 1 with high frequency (Model # 2) C_{n_r} .

Figure 7-- Continued.



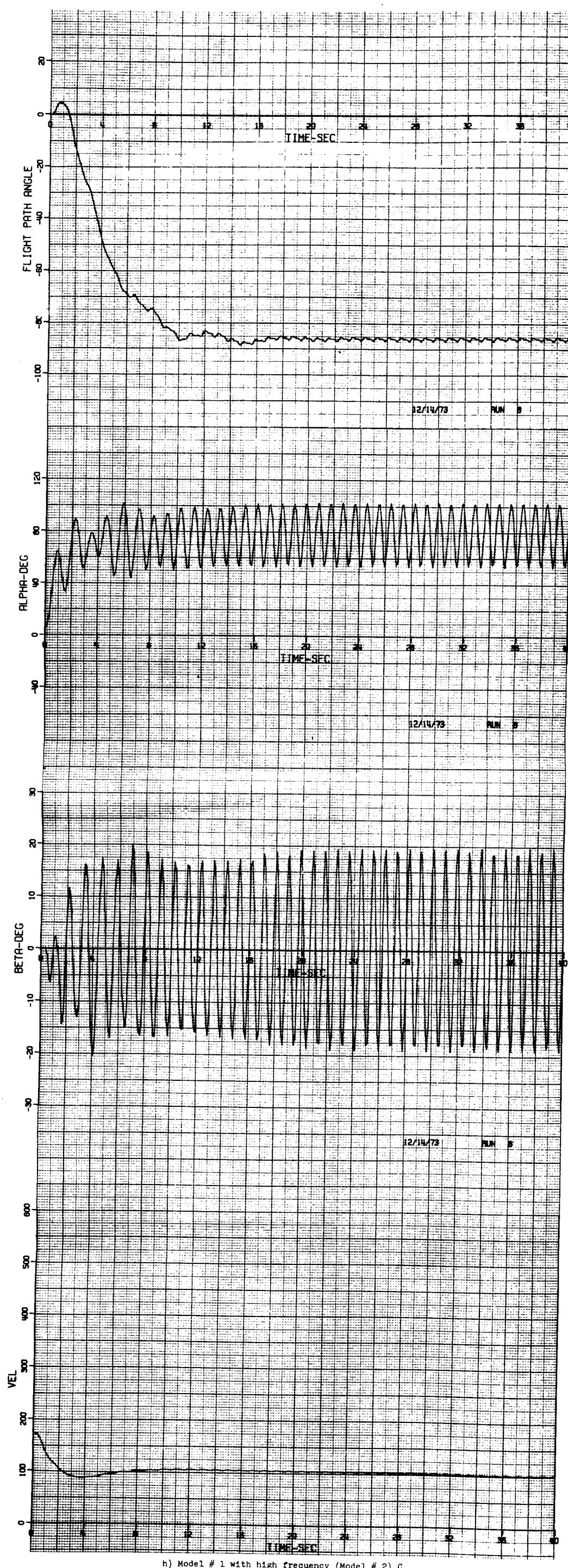
g) Model # 1 with high frequency (Model # 2) C_{I_r} .

Figure 7.- Continued.



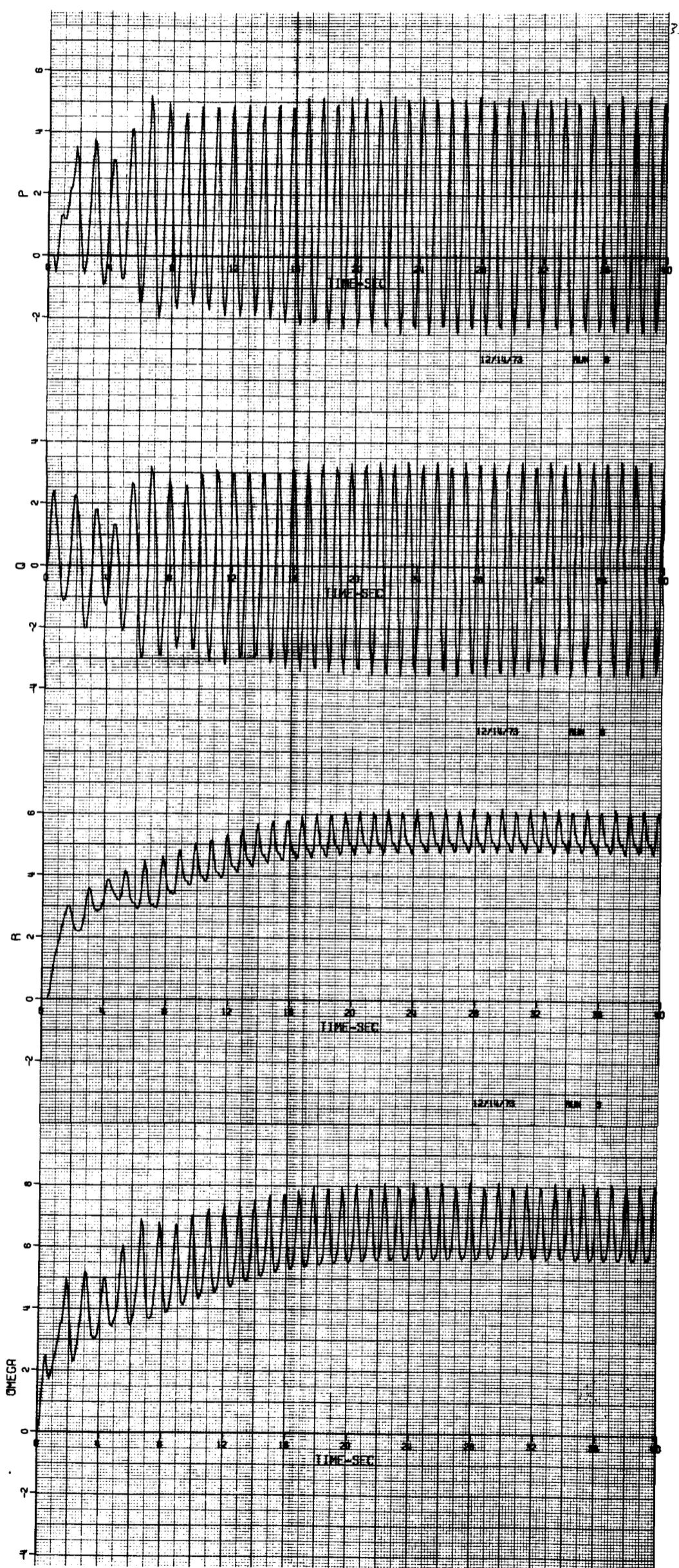
g) Model # 1 with high frequency (Model # 2) C_{A_2} .

Figure 7.- Continued.



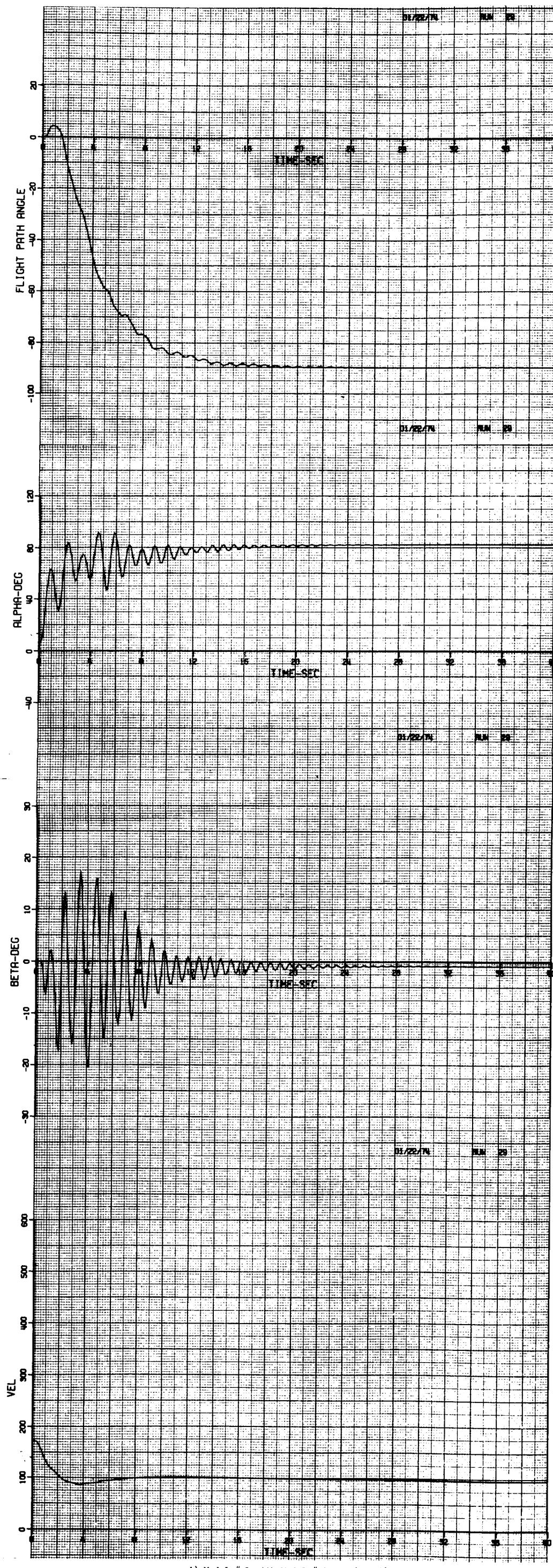
h) Model # 1 with high frequency (Model # 2) C_{m_q} .

Figure 7.- Continued.



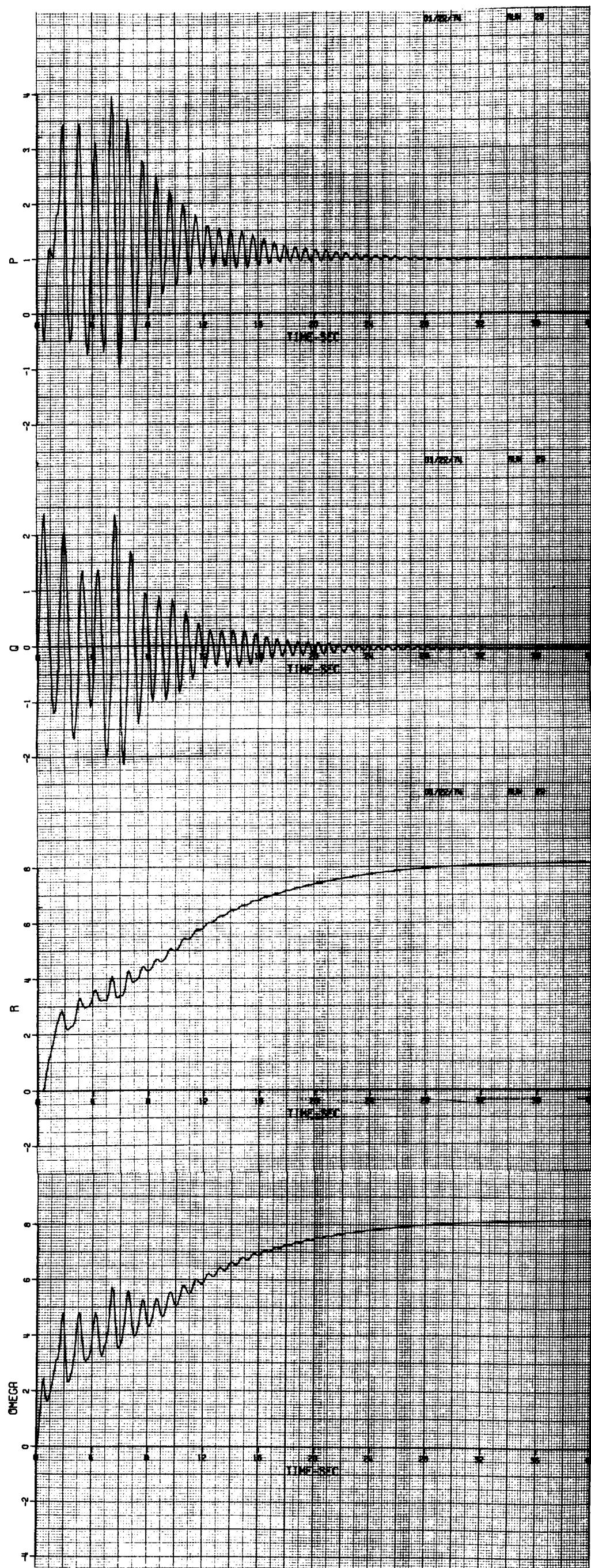
h) Model # 1 with high frequency (Model # 2) $C_{\alpha\beta}$.

Figure 7-- Continued.



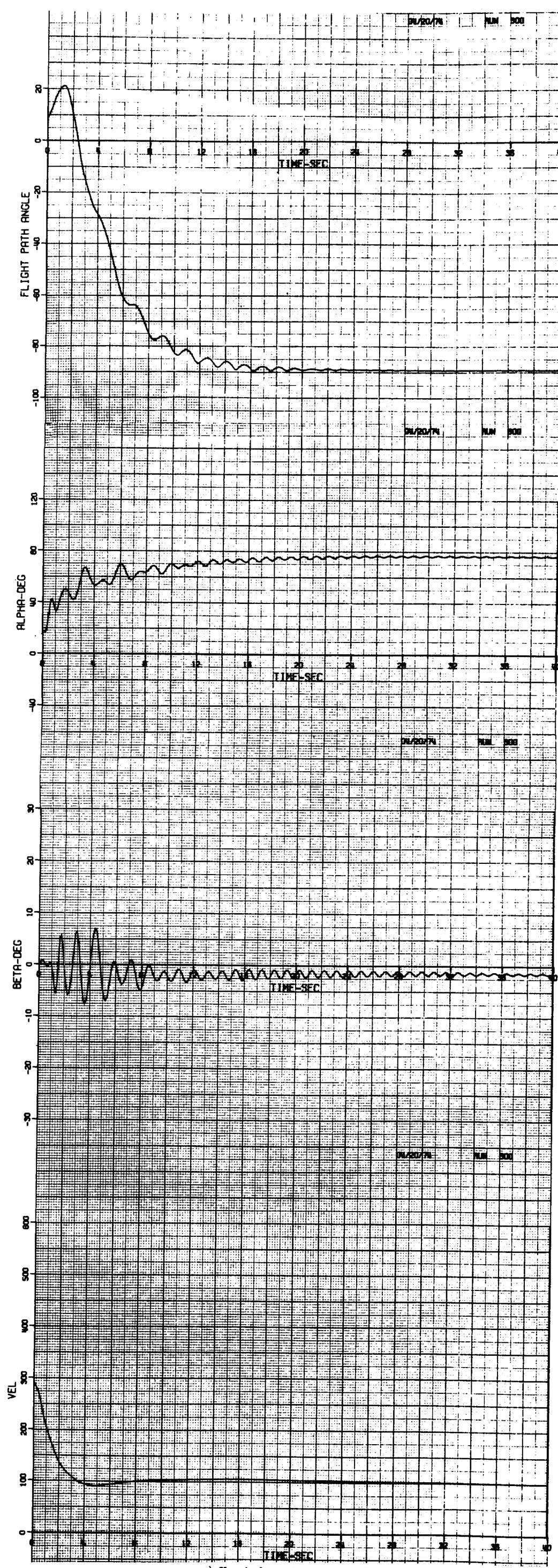
1) Model # 1 with Model # 2 C_n (α, β).

Figure 7.- Continued.



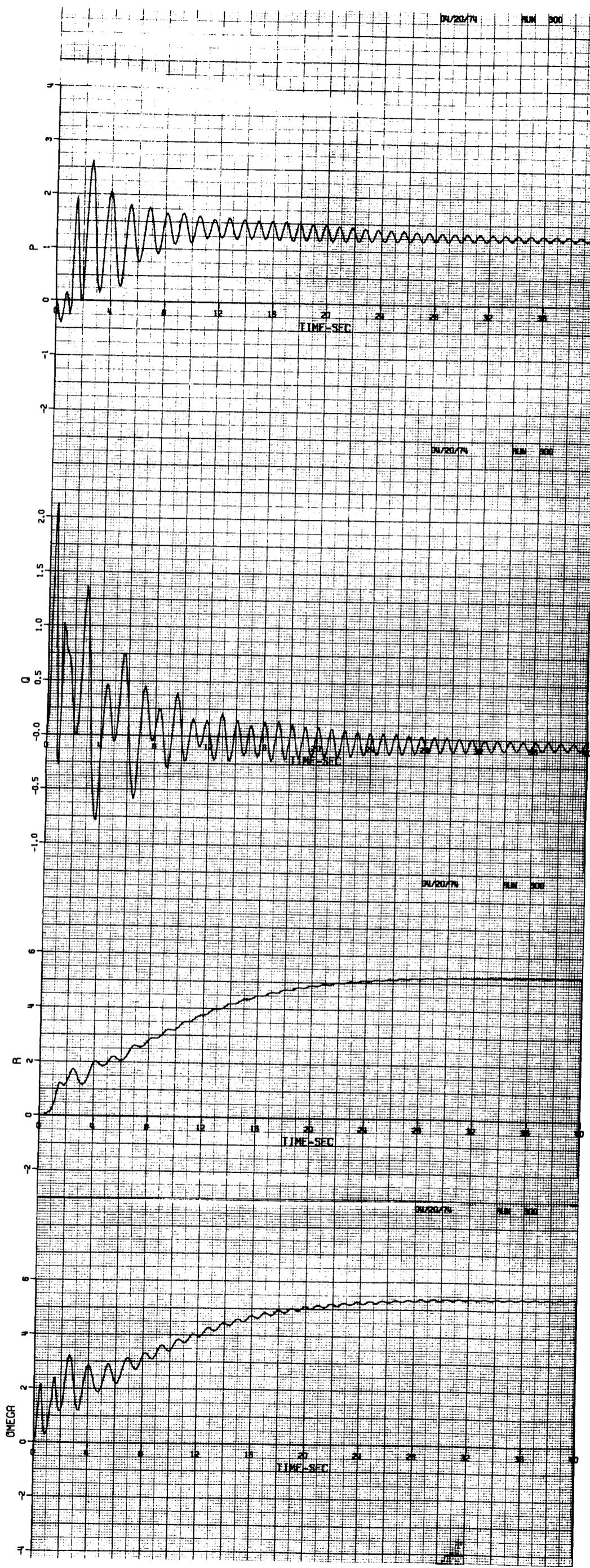
1) Model # 1 with Model # 2 C_n (α, β).

Figure 7.- Concluded.



a) Classical aerodynamic Model # 1.

Figure 8.- Influence of rotation-balance data on computed spinning motion.



a) Classical aerodynamic Model # 1

Figure 8.- Continued.

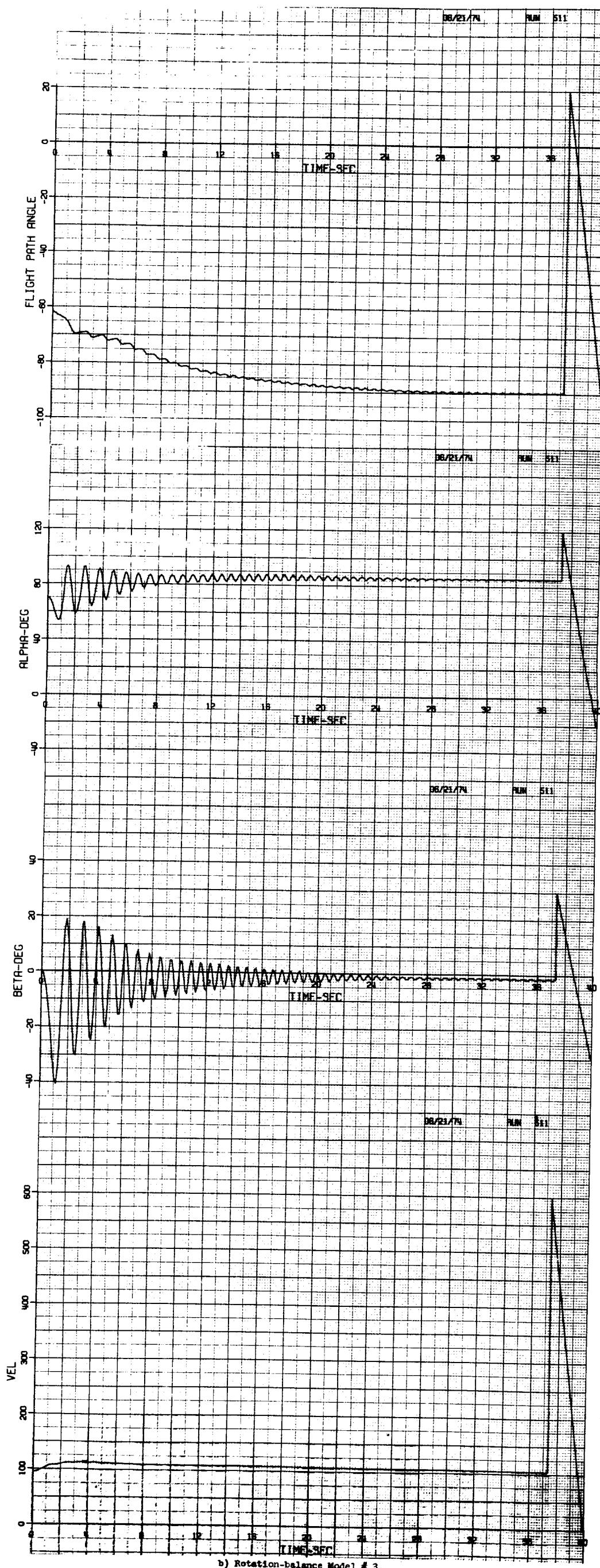
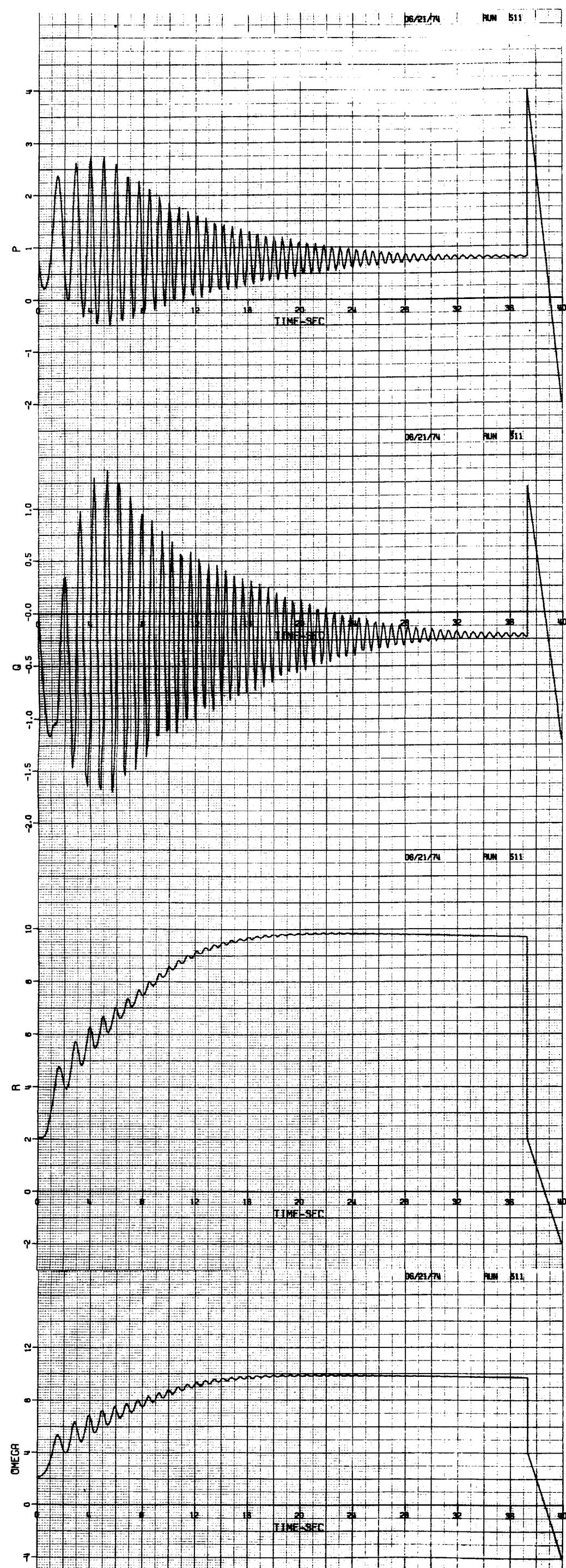
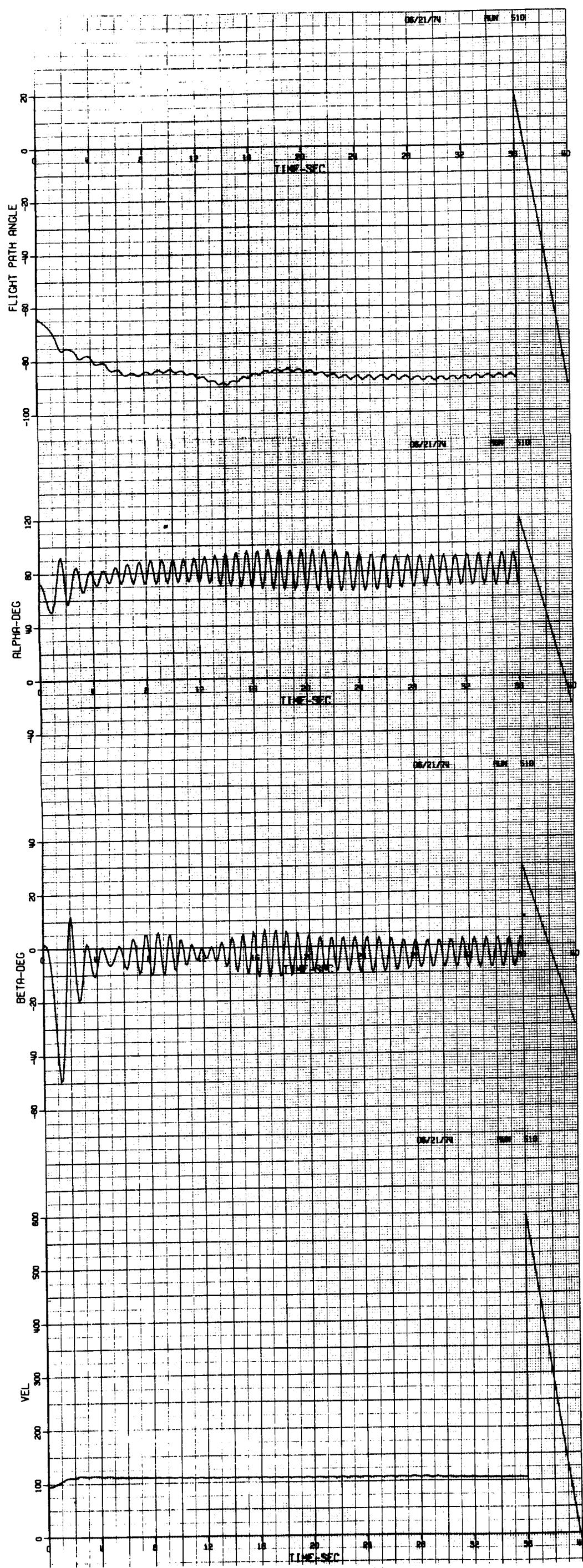


Figure 8.- Continued.

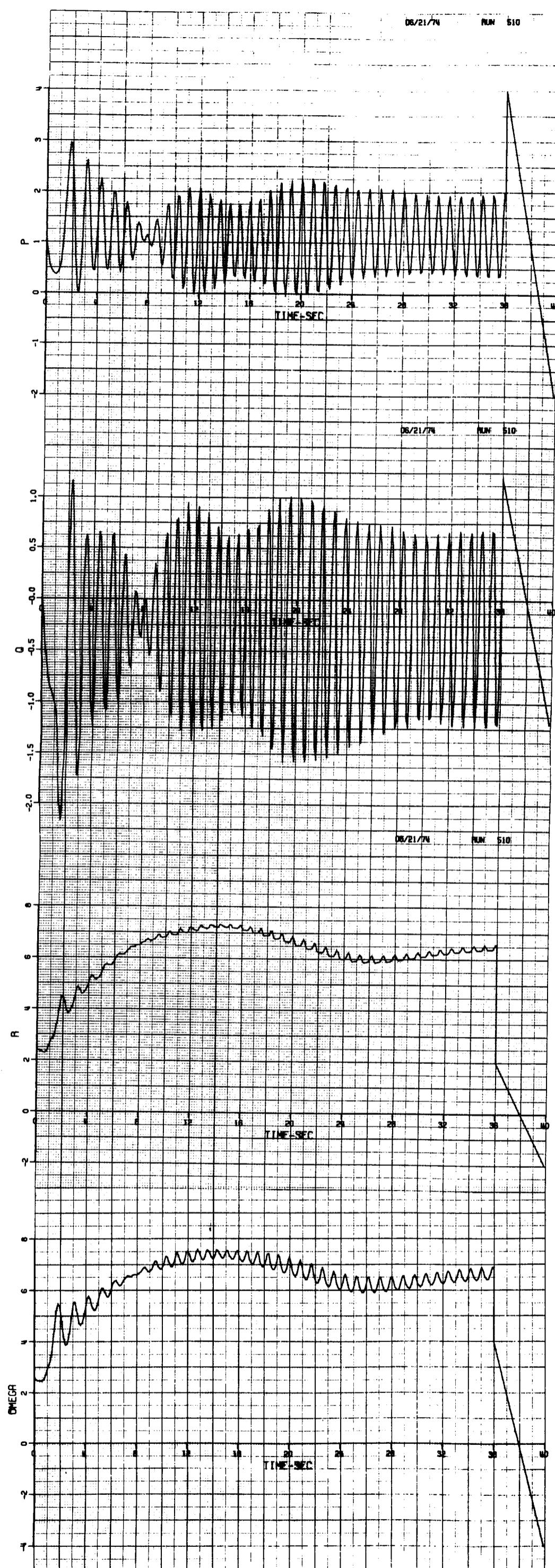


b) Rotation-balance Model # 3
Figure 8.- Continued.



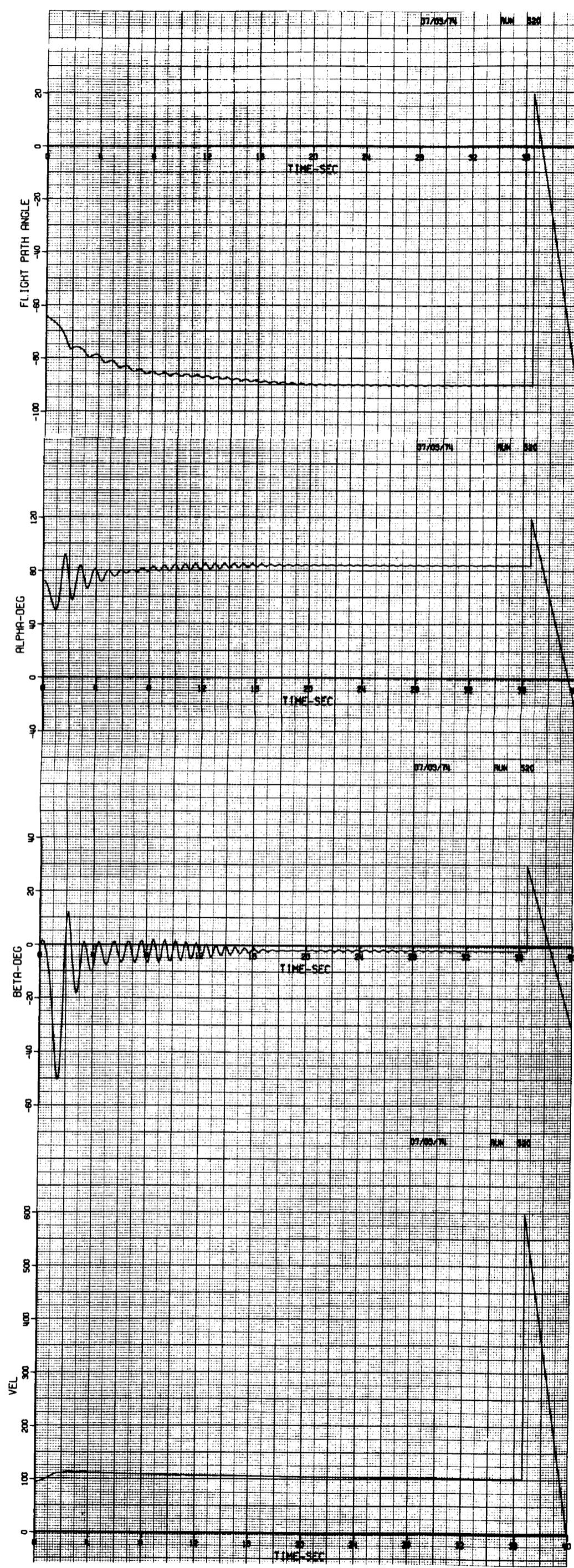
c) Rotation-balance Model # 4.

Figure 8.- Continued.



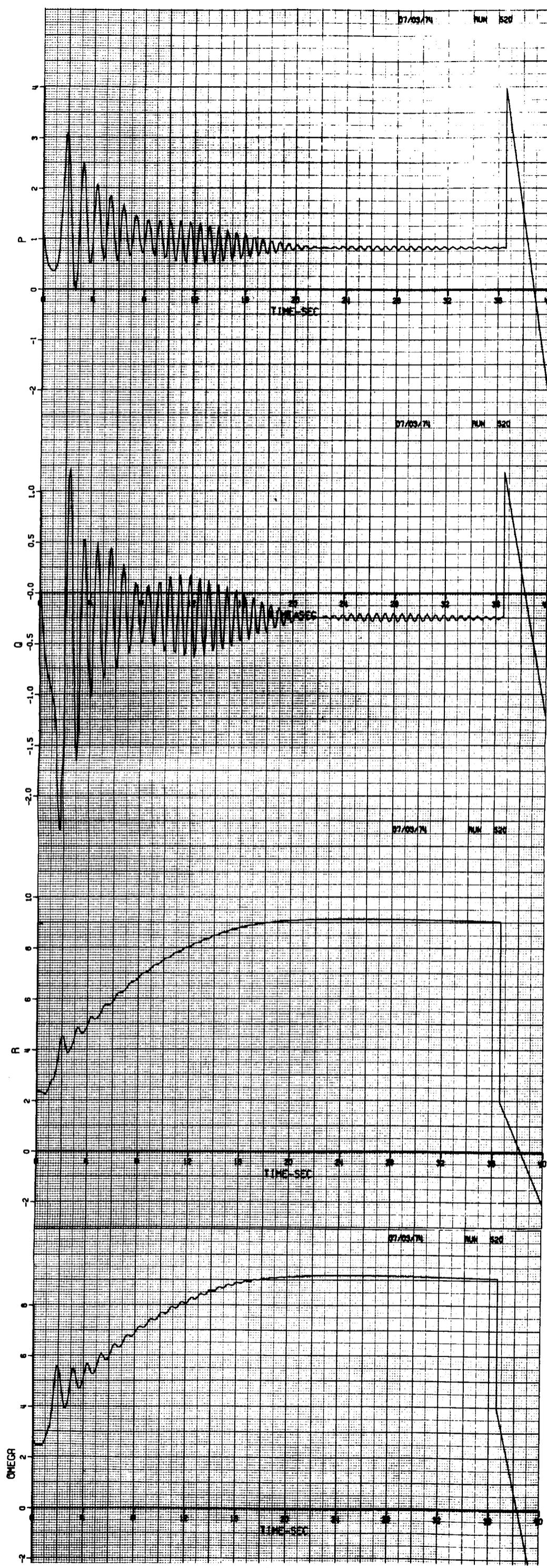
c) Rotation-balance Model # 4.

Figure 8.- Continued.



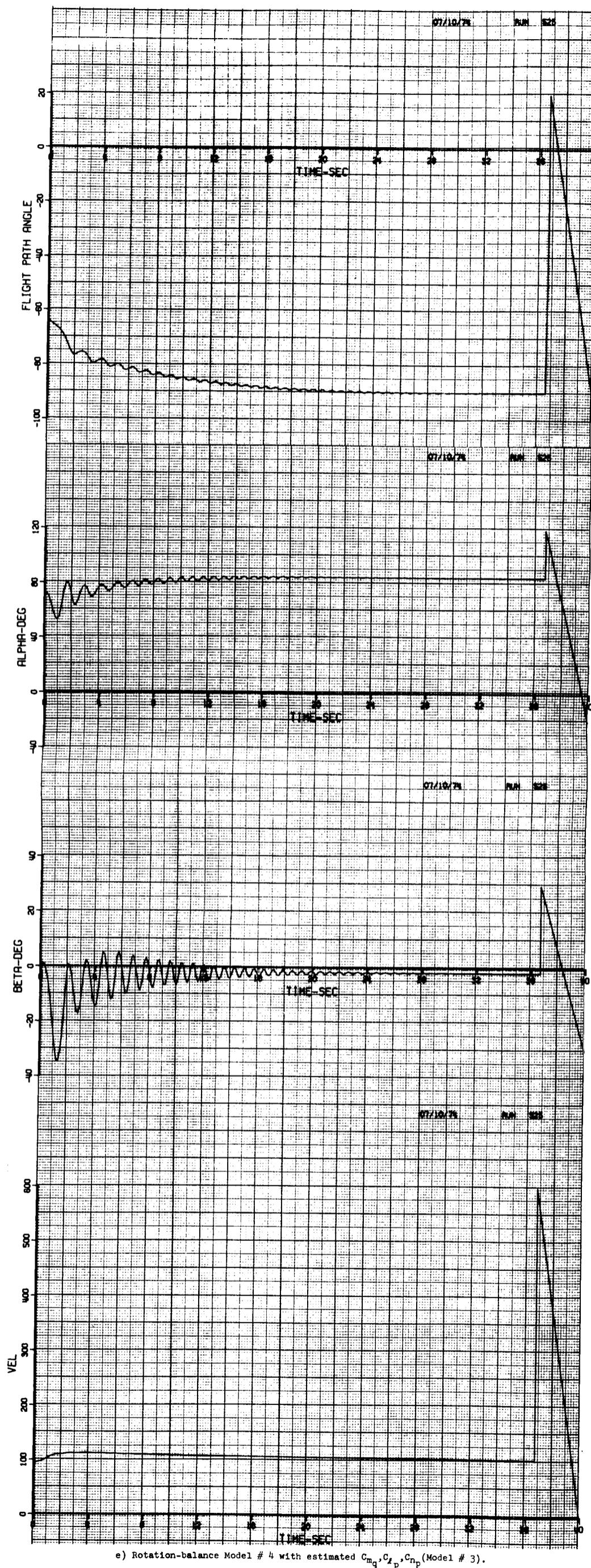
d) Rotation-balance Model # 4 with estimated C_{m_q} (Model # 3).

Figure 8.- Continued.



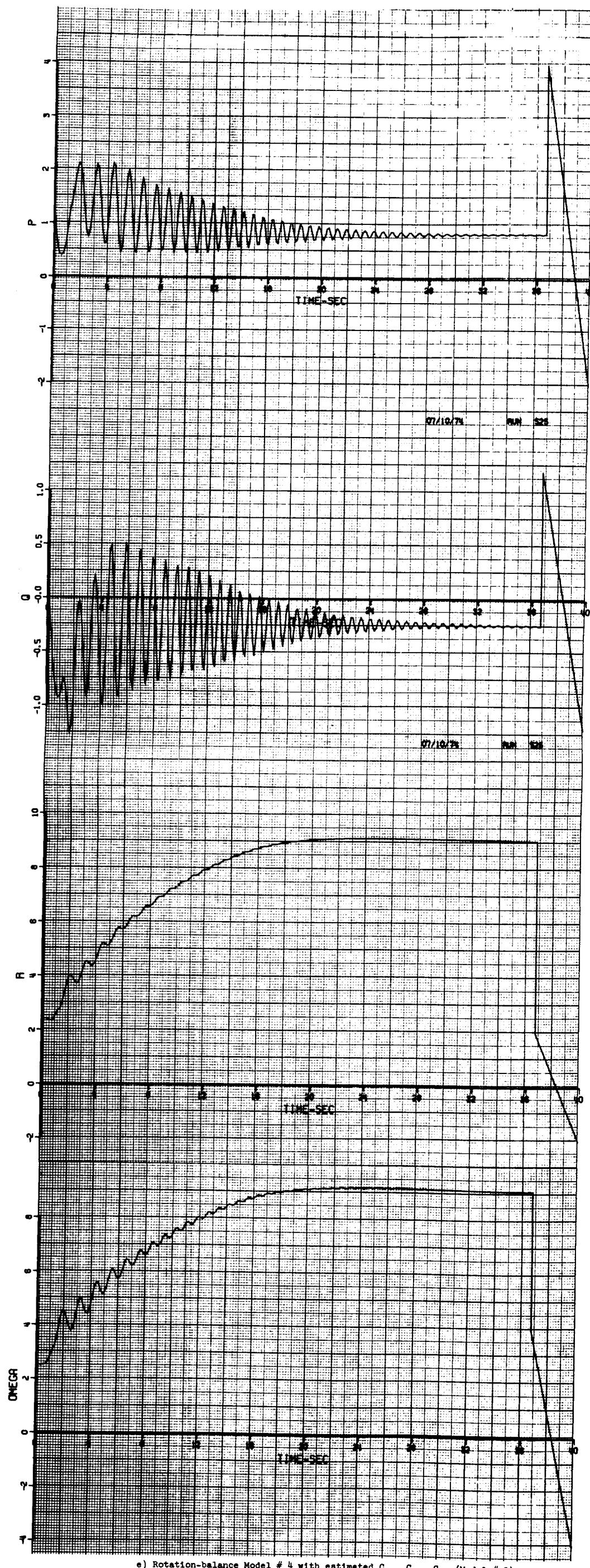
d) Rotation-balance Model # 4 with estimated C_{mq} (Model # 3).

Figure 8.- Continued



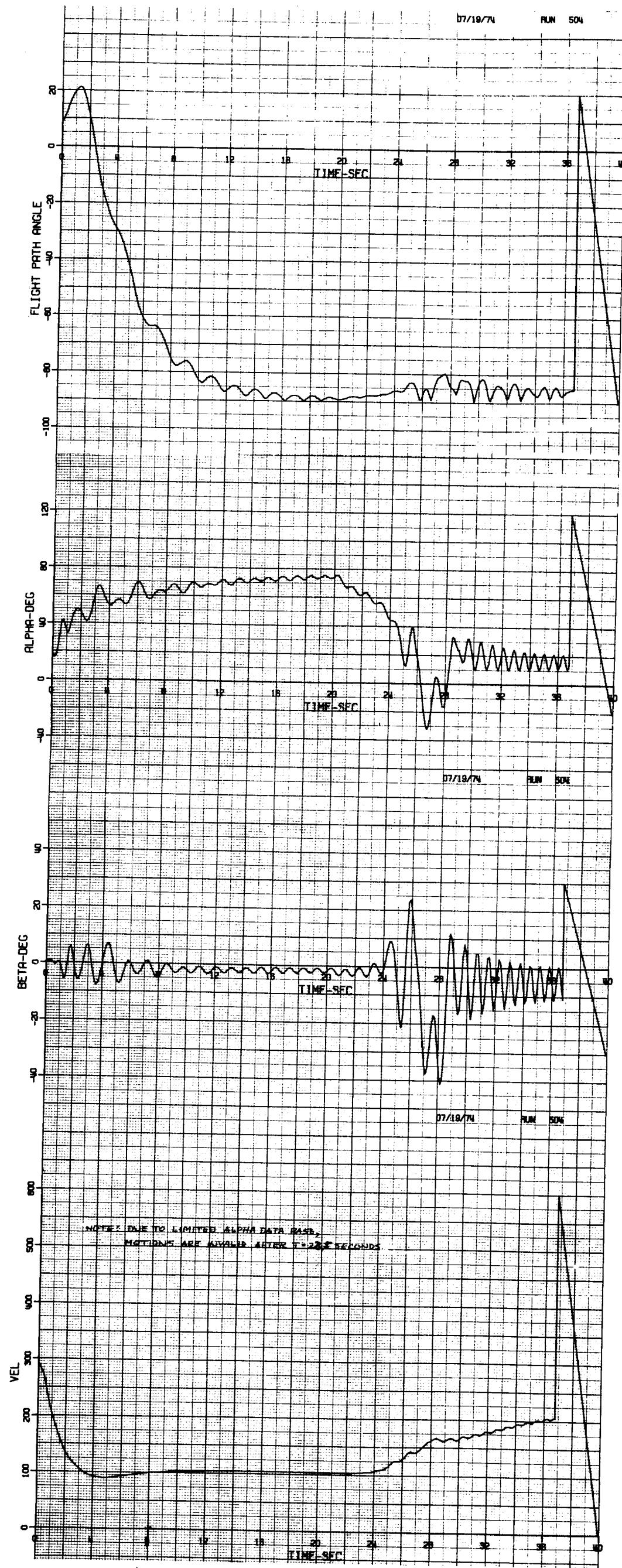
e) Rotation-balance Model # 4 with estimated C_{m_q} , C_{l_p} , C_{n_p} (Model # 3).

Figure 8.- Continued.



e) Rotation-balance Model # 4 with estimated C_{m_q} , C_{α_p} , C_{n_p} (Model # 3).

Figure 8.- Concluded.



a) Full opposite spin controls at $t = 20$ sec., classical Model # 1
 Figure 9.- Influence of rotation-balance data on computed recovery characteristics.

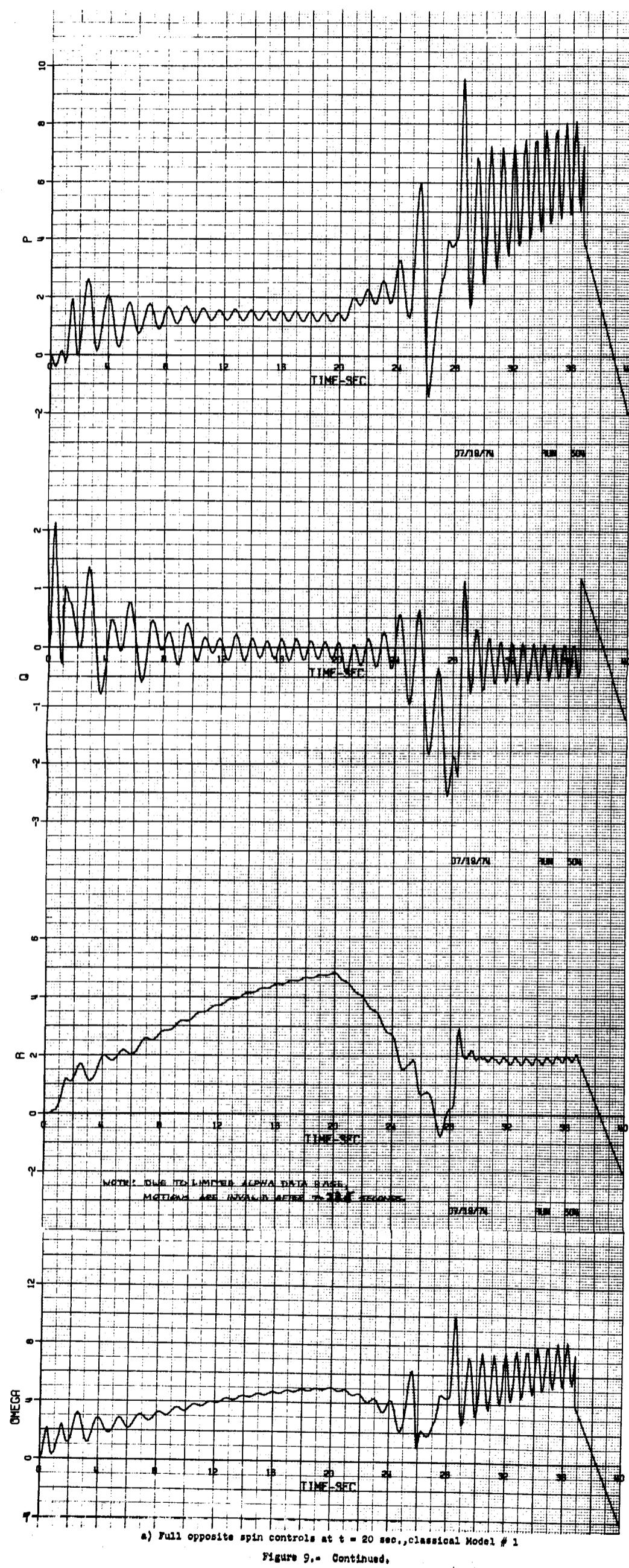
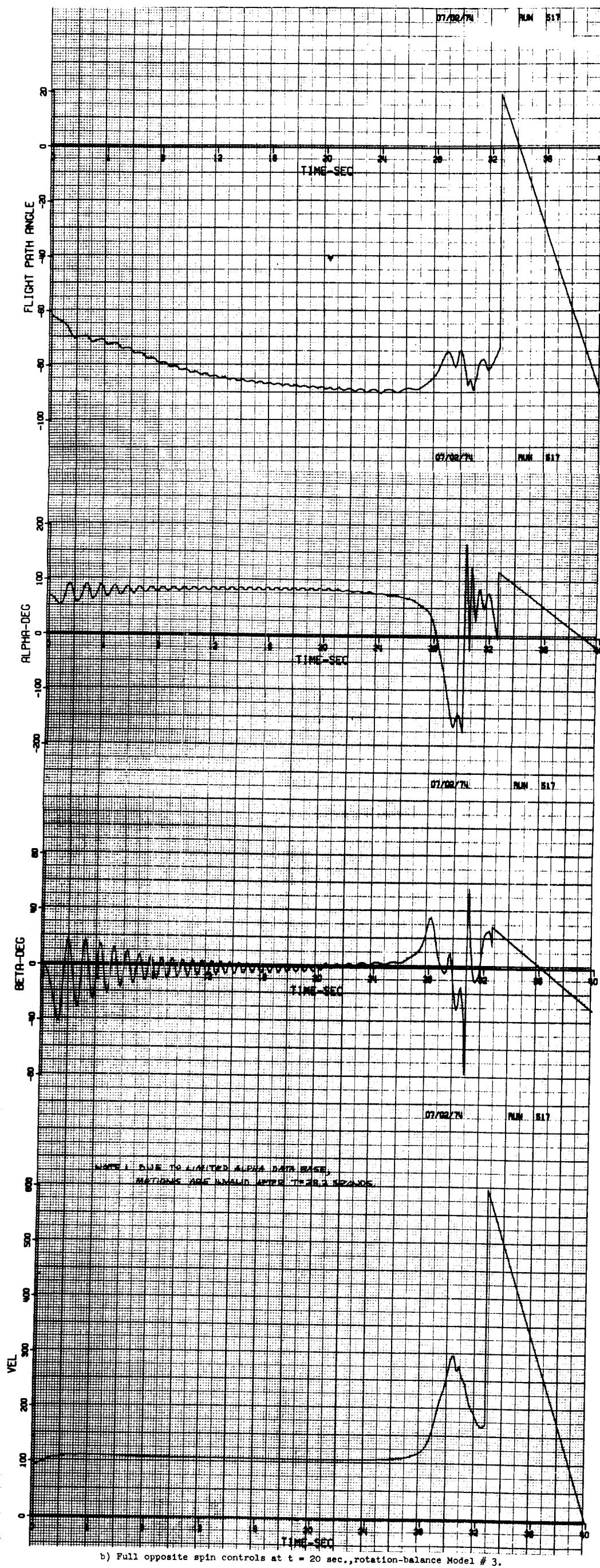
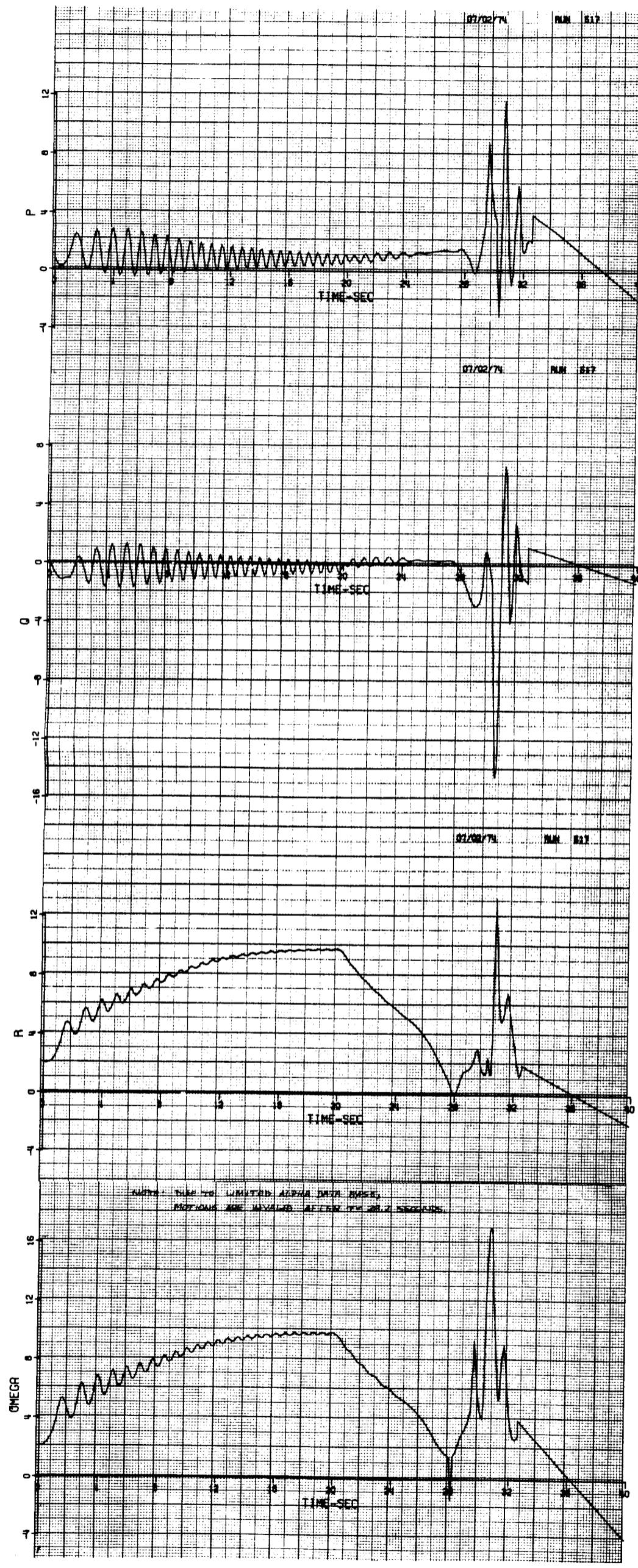


Figure 9.- Continued.



b) Full opposite spin controls at $t = 20$ sec., rotation-balance Model # 3.

Figure 9.- Continued.



b) Full opposite spin controls at $t = 20$ sec., rotation-balance Model # 3.
Figure 9.- Concluded.

Figure 9.- Concluded.

APPENDIX A

EQUATIONS OF MOTION AND ASSOCIATED FORMULAS

The dynamical equations required to specify the translational and rotational motions of a rigid body moving through space are described in this appendix. The familiar six degree of freedom differential equations representing linear and angular accelerations of a moving body axis system having its origin at the aircraft center of mass are presented below.

$$\dot{u} = -g \sin \theta_e + vr - wq + \frac{\sum F_x aero}{m}$$

$$\dot{v} = g \cos \theta_e \sin \phi_e + wp - ur + \frac{\sum F_y aero}{m}$$

$$\dot{w} = g \cos \theta_e \cos \phi_e + uq - vp + \frac{\sum F_z aero}{m}$$

$$\dot{p} = \frac{I_y - I_z}{I_x} qr + \frac{I_{xz}}{I_x} (\dot{r} + pq) + \frac{\sum L aero}{I_x}$$

$$\dot{q} = \frac{I_z - I_x}{I_y} pr - \frac{I_{xz}}{I_y} (p^2 - r^2) + \frac{\sum M aero}{I_y}$$

$$\dot{r} = \frac{I_x - I_y}{I_z} pq + \frac{I_{xz}}{I_z} (p - qr) + \frac{\sum N aero}{I_z}$$

In addition, the following formulas were used:

$$\alpha = \tan^{-1} \left(\frac{w}{u} \right)$$

$$\beta = \sin^{-1} \left(\frac{v}{v_R} \right)$$

$$v_R = \sqrt{u^2 + v^2 + w^2}$$

$$\Omega = \sqrt{p^2 + q^2 + r^2}$$

$$\text{Turns in spin} = \frac{\int \dot{\psi}_e dt}{2\pi}$$

$$\dot{\psi}_e = \frac{\dot{\theta}_e - p}{\sin \theta_e}$$

$$\theta_e = \sin^{-1} \left(\frac{\sin \phi}{\cos \theta_e} \right)$$

$$\dot{\theta}_e = q \cos \theta_e - r \sin \theta_e$$

$$\dot{\phi}_e = p + r \tan \theta_e \cos \theta_e + q \tan \theta_e \sin \theta_e$$

$$p = p_r + p_o$$

$$q = q_r + q_o$$

$$r = r_r + r_o$$

These total angular velocities (p, q, r) consist of steady rotation (p_r , q_r , r_r) components upon which oscillatory (p_o , q_o , and r_o) components are superimposed. These components are defined as follows:

$$p_r = -\dot{\psi}_e \sin \theta_e \quad p_o = \dot{\phi}_e$$

$$q_r = \dot{\psi}_e \cos \theta_e \sin \theta_e \quad q_o = \dot{\theta}_e \cos \theta_e$$

$$r_r = \dot{\psi}_e \cos \theta_e \cos \theta_e \quad r_o = -\dot{\theta}_e \sin \theta_e$$

For the conventional model, the following total derivatives were used

$$C_N' = C_N + C_{N_{is}} + C_{N_q} \frac{q_c}{2v}$$

$$C_c' = C_c + C_{c_{is}}$$

$$C_y' = C_y + C_{y_{\delta a}} \delta a + C_{y_{\delta r}} \delta r + C_{y_r} \frac{rb}{2v} + C_{y_p} \frac{pb}{2v}$$

$$C_l' = C_l + C_{l_{\delta a}} \delta a + C_{l_{\delta r}} \delta r + C_{l_r} \frac{rb}{2v} + C_{l_p} \frac{pb}{2v}$$

$$C_m' = C_m + C_{m_{is}} + C_{m_q} \frac{q_c}{2v}$$

$$C_n' = C_n + C_{n_{\delta a}} \delta a + C_{n_{\delta r}} \delta r + C_{n_r} \frac{rb}{2v} + C_{n_p} \frac{pb}{2v}$$

For the rotation balance model, the following total derivatives were employed, where C_x , C_y , C_z , etc. are rotation balance data

$$C_N' = -C_z + C_{n_q} \frac{q_c}{2v}$$

$$C_c' = -C_x$$

$$C_y' = C_y + C_{y_r} \frac{r_o b}{2v} + C_{y_p} \frac{p_o b}{2v}$$

$$C_l' = C_l + C_{l_r} \frac{r_o b}{2v} + C_{l_p} \frac{p_o b}{2v}$$

$$C_m' = C_m + C_{m_q} \frac{q_c}{2v}$$

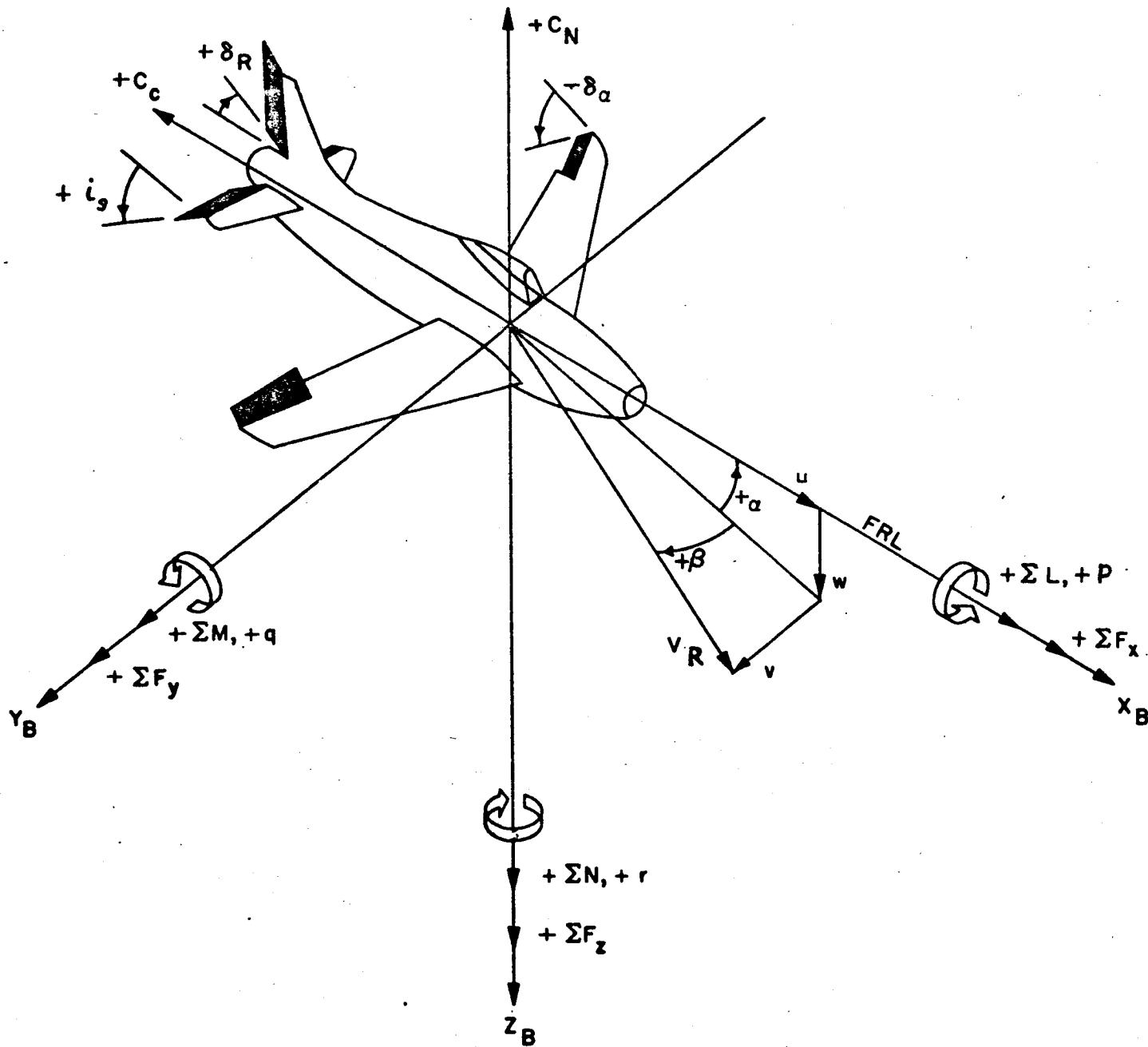
$$C_n' = C_n + C_{n_r} \frac{r_o b}{2v} + C_{n_p} \frac{p_o b}{2v}$$

APPENDIX B

SYMBOLS

Measurements and calculations were made in the U.S. Customary Units. Factors for converting these units to the International Systems of Units may be found in reference 6.

The Body Axes System is used with the origin of the axes system located at the aircraft center of gravity. The X axis is parallel to the aircraft Fuselage Reference Line (FRL) and is positive forward, the Y axis is positive towards the right wing tip and the Z axis is positive downward. The following illustration shows this axis system and the positive direction of the angles, forces and moments associated with it.

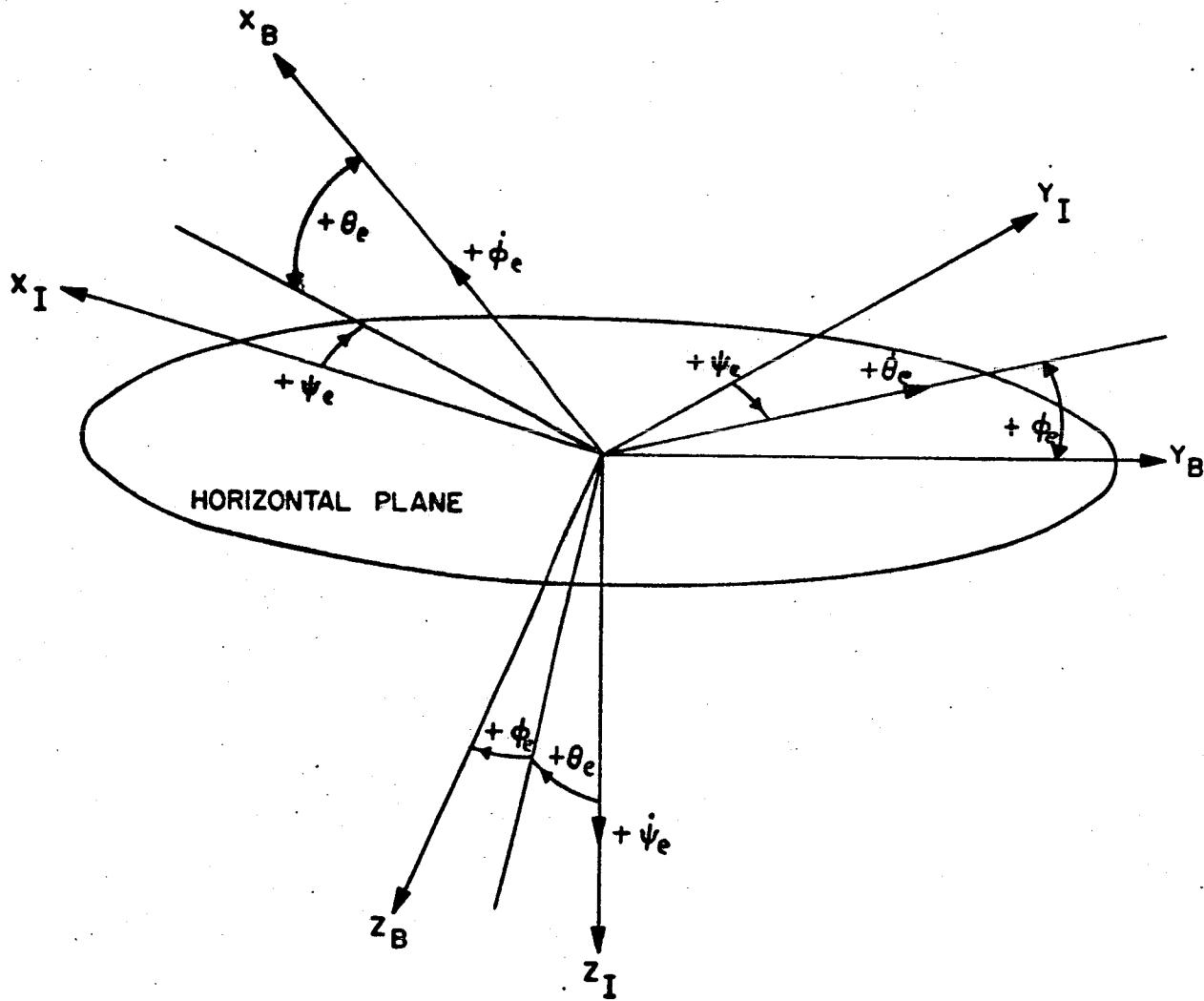


In the following definitions a dot (\cdot) over a quantity denotes one differentiation with respect to time and a zero subscript ($_0$) denotes the initial value of the quantity.

I_x, I_y, I_z	moments of inertia about the X, Y and Z body axes, respectively	slug-ft ²
I_{xz}	product of inertia, positive when the principle X axis is inclined below the X body axis at the aircraft nose	slug-ft ²
m	aircraft mass ($=W/g$)	slug's
W	aircraft weight ($=mg$)	lbs
S	wing area	ft ²
b	wing span	ft
\bar{c}	wing mean aerodynamic chord	ft
W/S	wing loading	lb/ft ²
$(I_y - I_z)/mb^2$	inertia rolling moment parameter	-
$(I_z - I_x)/mb^2$	inertia pitching moment parameter	-
$(I_x - I_y)/mb^2$	inertia yawing moment parameter	-
t	time	sec
ρ	atmospheric density	slug/ft ³
\bar{q}	dynamic pressure ($= \frac{\rho V^2}{2}$)	lb/ft ²
H	vertical height	ft
α	angle of attack, measured between the X body axis and the projection in the X-Z plane of the relative wind vector, positive when the X axis is above the projected relative wind vector	deg

x_I, y_I, z_I , inertial axes

x_B, y_B, z_B body axes



BODY AXIS SYSTEM LOCATED IN INERTIAL SPACE

POSITIVE DIRECTION OF EULER ANGLES AND RATES

β	angle of sideslip, measured between the relative wind vector and its projection in the X-Z plane, positive when the relative wind vector is to the right of the X-Z plane	deg
θ_e	inertial pitch attitude angle, measured in a vertical plane between the X body axis and the horizontal plane, positive when the X axis is above the horizontal plane	deg
ϕ_e	inertial roll attitude angle, measured in the Y-Z plane between the Y body axis and the horizontal plane, positive when the Y axis is moving clockwise as viewed from behind the aircraft	deg
ψ_e	inertial yaw attitude angle, measured between the initial flight direction and the projection in the horizontal plane of the X body axis, positive when the X axis is moving clockwise as viewed from above	deg
θ	angle between Y body axis and horizontal measured in vertical plane, positive for erect spins when right wing is downward and for inverted spins when left wing is downward	deg
γ	flight path angle, measured in a vertical plane between the horizontal plane and the resultant velocity vector, positive when the resultant velocity vector points above the horizontal plane	deg
δ_a	differential horizontal tail deflection (half angle), positive to produce left rolling moment	deg
i_s	control deflection-stabilizer, positive direction trailing edge down	deg
δ_R	control deflection-rudder, positive direction trailing edge left	deg

V_R	total linear velocity vector	ft/sec
V	free-stream velocity	ft/sec
u, v, w	components of the total linear velocity vector (V_R) along the X, Y and Z body axes, respectively	ft/sec
$\dot{u}, \dot{v}, \dot{w}$	components of the relative linear acceleration vector along the X, Y and Z body axes, respectively	ft/sec ²
p, q, r	components of the total angular velocity vector along the X, Y and Z body axes, respectively	radians/sec
ω	frequency of for ed-oscillation tests	radians/sec
η	total angular velocity vector	radians/sec
g	acceleration due to gravity	ft/sec ²
$F_{x,aero}, F_{y,aero},$	components of the aerodynamic forces along the X, Y and Z body axes, respectively,	lbs
$F_{z,aero}$	excluding the contributions due to the rate derivatives $C_{N\dot{\alpha}}$ and $C_{y\dot{\beta}}$	
$L_{aero}, M_{aero},$	components of the aerodynamic moments about the X, Y and Z body axes,	ft-lbs
N_{aero}	respectively	
T	total engine thrust force	lbs
$C'_c = \frac{-F_x}{\bar{q} S}$	total chordwise force coefficient, positive along the negative X body axis	

$$C'_y = \frac{F'_y \text{ aero}}{\bar{q} S}$$

total sideforce coefficient, excluding the contribution due to $C_{y\beta}$, positive along the positive Y body axis

$$C'_N = \frac{-F'_z \text{ aero}}{\bar{q} S}$$

total normal force coefficient, excluding the contribution due to $C_{N\alpha}$, positive along the negative Z body axis

$$C'_L = \frac{L \text{ aero}}{\bar{q} S_b}$$

total rolling moment coefficient, positive direction of moment drives the right wing tip down

$$C'_m = \frac{M \text{ aero}}{\bar{q} S_c}$$

total pitching moment coefficient about the aerodynamic center, positive direction of moment drives the nose up

$$C'_n = \frac{N \text{ aero}}{\bar{q} S_b}$$

total yawing moment coefficient, positive direction of moment drives the nose right

$$C_c(\alpha)$$

variation in chordwise force coefficient due to angle of attack

$$C_y(\beta, \alpha)$$

variation in side force coefficient due to sideslip angle and angle of attack

$$C_N(\alpha)$$

variation in normal force coefficient due to angle of attack

$$C_L(\beta, \alpha)$$

variation in rolling moment coefficient due to sideslip angle and angle of attack

$$C_m(\alpha)$$

variation in pitching moment coefficient due to angle of attack

$$C_n(\beta, \alpha)$$

variation in yawing moment coefficient due to sideslip angle and angle of attack

$$C_{y\beta} = \frac{\partial C_y}{\partial \beta} \quad \text{per deg}$$

$$C_{L\beta} = \frac{\partial C_L}{\partial \beta} \quad \text{per deg}$$

$$c_{n\beta} = \frac{\partial C_n}{\partial \beta} \quad \text{per deg}$$

$$c_{y_p} = \frac{\partial C_y}{\frac{\partial b}{2V_R}} \quad \text{per radian}$$

$$c_{\ell_p} = \frac{\partial C_\ell}{\frac{\partial b}{2V_R}} \quad \text{per radian}$$

$$c_{n_p} = \frac{\partial C_n}{\frac{\partial b}{2V_R}} \quad \text{per radian}$$

$$c_{N_q} = \frac{\partial C_N}{\partial \left(\frac{qc}{2V_R} \right)} \quad \text{per radian}$$

$$c_{m_q} = \frac{\partial C_m}{\partial \left(\frac{qc}{2V_R} \right)} \quad \text{per radian}$$

$$c_{y_r} = \frac{\partial C_y}{\partial \left(\frac{rb}{2V_R} \right)} \quad \text{per radian}$$

$$c_{\ell_r} = \frac{\partial C_\ell}{\partial \left(\frac{rb}{2V_R} \right)} \quad \text{per radian}$$

$$c_{n_r} = \frac{\partial C_n}{\partial \left(\frac{rb}{2V_R} \right)} \quad \text{per radian}$$

$$C_{y\delta_a} = \frac{\partial C_y}{\partial \delta_a} \quad \text{per deg}$$

$$C_{L\delta_a} = \frac{\partial C_L}{\partial \delta_a} \quad \text{per deg}$$

$$C_{n\delta_a} = \frac{\partial C_n}{\partial \delta_a} \quad \text{per deg}$$

$$C_{y\delta_R} = \frac{\partial C_y}{\partial \delta_R} \quad \text{per deg}$$

$$C_{L\delta_R} = \frac{\partial C_L}{\partial \delta_R} \quad \text{per deg}$$

$$C_{n\delta_R} = \frac{\partial C_n}{\partial \delta_R} \quad \text{per deg}$$

$$C_{c_i_s} = \frac{\partial C_c}{\partial i_s} \quad \text{per deg}$$

$$C_{N_i_s} = \frac{\partial C_N}{\partial i_s} \quad \text{per deg}$$

$$C_{m_i_s} = \frac{\partial C_m}{\partial i_s} \quad \text{per deg}$$

$$C_Z = -C_N \quad \text{per deg}$$

$$C_X = C_r \quad \text{per deg}$$

APPENDIX C

AERODYNAMIC DATA EMPLOYED IN ANALYTICAL INVESTIGATION

LIST OF FIGURES

Figure No.	Title	Page
MODEL # 1: STATIC AND DYNAMIC DATA USED IN PREVIOUS INVESTIGATION		
C-1	Effect of angle of attack on longitudinal-control effectiveness. Lamda = 22°.	109
C-2	Effect of angle of attack on directional-control effectiveness. Lamda = 22°.	110
C-3	Effect of angle of attack on side force coefficient due to directional control. Lamda = 22°.	111
C-4	Effect of angle of attack on lateral-control effectiveness. Lamda = 22°.	112
C-5	Effect of angle of attack and sideslip angle on force characteristics. Lamda = 22°.	
a)	C_N	113
b)	C_c	114
c)	C_y	115
C-6	Effect of angle of attack and longitudinal-control deflection on pitching-moment coefficient. Lamda = 22°.	116
C-7	Effect of angle of attack and sideslip angle on rolling-moment coefficient. Lamda = 22°.	117
C-8	Effect of angle of attack and longitudinal-control deflection on yawing-moment coefficient. Lamda = 22°.	
a)	$\beta = 5^\circ$	118
b)	$\beta = 10^\circ$	119
c)	$\beta = 15^\circ$	120
d)	$\beta = 20^\circ$	121
e)	$\beta = 30^\circ$	122
C-9	Effect of angle of attack on damping derivatives. Lamda = 22°.	
a)	C_{m_q}	123
b)	C_{ℓ_p}	124
c)	C_{n_r}	125

LIST OF FIGURES (cont'd.)

Figure No.	Title	Page
C-10	Effect of angle of attack on cross derivatives. Lamda = 22°.	
a)	C_{n_p}	126
b)	C_{λ_r}	127
C-11	Aerodynamic derivatives assigned zero values.	128
MODEL # 2: STATIC AND DYNAMIC DATA MEASURED IN 30' x 60' FACILITY		
C-12	Effect of angle of attack on longitudinal-control characteristics. Lamda = 22°.	
a)	$C_{m_{is}}$	129
b)	$C_{c_{is}}$	130
c)	$C_{N_{is}}$	131
C-13	Effect of angle of attack and sideslip angle on lateral-control characteristics. Lamda 22°.	
a)	$C_{n_{\delta_R}}$	132
b)	$C_{\lambda_{\delta_R}}$	133
c)	$C_{y_{\delta_R}}$	134
C-14	Effect of angle of attack and sideslip angle on lateral-control characteristics. Lamda = 22°.	
a)	$C_{\lambda_{\delta_a}}$	135
b)	$C_{n_{\delta_a}}$	136
c)	$C_{y_{\delta_a}}$	137
C-15	Effect of angle of attack and sideslip angle on force characteristics. Lamda = 22°.	
a)	C_N	138
b)	C_c	139
c)	C_y	140

Figure No.	Title	Page
C-16	Effect of angle of attack on pitching-moment coefficient; $\alpha_s = 0^\circ$. $\lambda = 22^\circ$.	141
C-17	Effect of angle of attack and sideslip angle on rolling-moment coefficient. $\lambda = 22^\circ$.	142
C-18	Effect of angle of attack and longitudinal-control deflection on yawing-moment coefficient. $\lambda = 22^\circ$.	
	a) $\beta = 5^\circ$	143
	b) $\beta = 10^\circ$	144
	c) $\beta = 20^\circ$	145
	d) $\beta = 30^\circ$	146
C-19	Effect of angle of attack and forced-oscillation frequency on normal-force coefficient due to pitch rate. $\lambda = 22^\circ$.	147
C-20	Effect of angle of attack and forced-oscillation frequency on side-force coefficient due to roll and yaw rate. $\lambda = 22^\circ$.	148
C-21	Effect of angle of attack and forced-oscillation frequency on damping derivatives. $\lambda = 22^\circ$.	
	a) C_{m_q}	149
	b) C_{l_p}	150
	c) C_{n_r}	151
C-22	Effect of angle of attack and forced-oscillation frequency on cross derivatives. $\lambda = 22^\circ$.	
	a) C_{n_p}	152
	b) C_{l_r}	153

Figure No.	Title	Page
ROTATION-BALANCE DATA MEASURED IN 30' x 60' FACILITY		
C-23	Effect of rotation rate and pitch and roll attitude angles on the longitudinal coefficients for all neutral controls. Lamda = 22°.	
	a) $\phi = 0^\circ, \theta = 55, 60, 65^\circ$	154
	b) $\phi = 0^\circ, \theta = 70, 75, 80^\circ$	155
	c) $\phi = 0^\circ, \theta = 85, 90^\circ$	156
	d) $\phi = 5^\circ, \theta = 55, 60, 65^\circ$	157
	e) $\phi = 5^\circ, \theta = 70, 75, 80^\circ$	158
	f) $\phi = 5^\circ, \theta = 85, 90^\circ$	159
C-24	Effect of rotation rate and pitch and roll attitude angles on the longitudinal coefficients for $i_s = -30^\circ$. Lamda = 22°.	
	a) $\phi = 0^\circ, \theta = 55, 60, 65^\circ$	160
	b) $\phi = 0^\circ, \theta = 70, 75, 80^\circ$	161
	c) $\phi = 0^\circ, \theta = 85, 90^\circ$	162
	d) $\phi = 5^\circ, \theta = 55, 60, 65^\circ$	163
	e) $\phi = 5^\circ, \theta = 70, 75, 80^\circ$	164
	f) $\phi = 5^\circ, \theta = 85, 90^\circ$	165
C-25	Effect of rotation rate and pitch and roll attitude angles on the longitudinal coefficients for right pro-spin controls. Lamda = 22°.	
	a) $\phi = 0^\circ, \theta = 55, 60, 65^\circ$	166
	b) $\phi = 0^\circ, \theta = 70, 75, 80^\circ$	167
	c) $\phi = 0^\circ, \theta = 85, 90^\circ$	168
	d) $\phi = 5^\circ, \theta = 55, 60, 65^\circ$	169
	e) $\phi = 5^\circ, \theta = 70, 75, 80^\circ$	170
	f) $\phi = 5^\circ, \theta = 85, 90^\circ$	171

Figure No.	Title	Page
C-26	Effect of rotation rate and pitch and roll attitude angles on the longitudinal coefficients for left pro-spin controls. Lamda = 22°.	
	a) $\phi = 0^\circ, \theta = 55, 60, 65^\circ$	172
	b) $\phi = 0^\circ, \theta = 70, 75, 80^\circ$	173
	c) $\phi = 0^\circ, \theta = 85, 90^\circ$	174
	d) $\phi = 5^\circ, \theta = 55, 60, 65^\circ$	175
	e) $\phi = 5^\circ, \theta = 70, 75, 80^\circ$	176
	f) $\phi = 5^\circ, \theta = 85, 90^\circ$	177
C-27	Effect of rotation rate and pitch and roll attitude angles on the lateral-directional coefficients for all neutral controls. Lamda = 22°.	
	a) $\phi = 0^\circ, \theta = 55, 60, 65^\circ$	178
	b) $\phi = 0^\circ, \theta = 70, 75, 80^\circ$	179
	c) $\phi = 0^\circ, \theta = 85, 90^\circ$	180
	d) $\phi = 5^\circ, \theta = 55, 60, 65^\circ$	181
	e) $\phi = 5^\circ, \theta = 70, 75, 80^\circ$	182
	f) $\phi = 5^\circ, \theta = 85, 90^\circ$	183
C-28	Effect of rotation rate and pitch and roll attitude angles on the lateral-direction coefficients for $i_s = -30^\circ$, Kanda = 22°.	
	a) $\phi = 0^\circ, \theta = 55, 60, 65^\circ$	184
	b) $\phi = 0^\circ, \theta = 70, 75, 80^\circ$	185
	c) $\phi = 0^\circ, \theta = 85, 90^\circ$	186
	d) $\phi = 5^\circ, \theta = 55, 60, 65^\circ$	187
	e) $\phi = 5^\circ, \theta = 70, 75, 80^\circ$	188
	f) $\phi = 5^\circ, \theta = 85, 90^\circ$	189

Figure No.	Title	Page
C-29	Effect of rotation rate and pitch and roll attitude angles on the lateral-directional coefficients for right pro-spin controls. $\Lambda_{ma} = 22^\circ$.	
a)	$\phi = 0^\circ, \theta = 55, 60, 65^\circ$	190
b)	$\phi = 0^\circ, \theta = 70, 75, 80^\circ$	191
c)	$\phi = 0^\circ, \theta = 85, 90^\circ$	192
d)	$\phi = 5^\circ, \theta = 55, 60, 65^\circ$	193
e)	$\phi = 5^\circ, \theta = 70, 75, 80^\circ$	194
f)	$\phi = 5^\circ, \theta = 85, 90^\circ$	195
C-30	Effect of rotation rate and pitch and roll attitude angles on the lateral-directional coefficients for left pro-spin controls. $\Lambda_{ma} = 22^\circ$.	
a)	$\phi = 0^\circ, \theta = 55, 60, 65^\circ$	196
b)	$\phi = 0^\circ, \theta = 70, 75, 80^\circ$	197
c)	$\phi = 0^\circ, \theta = 85, 90^\circ$	198
d)	$\phi = 5^\circ, \theta = 55, 60, 65^\circ$	199
e)	$\phi = 5^\circ, \theta = 70, 75, 80^\circ$	200
f)	$\phi = 5^\circ, \theta = 85, 90^\circ$	201

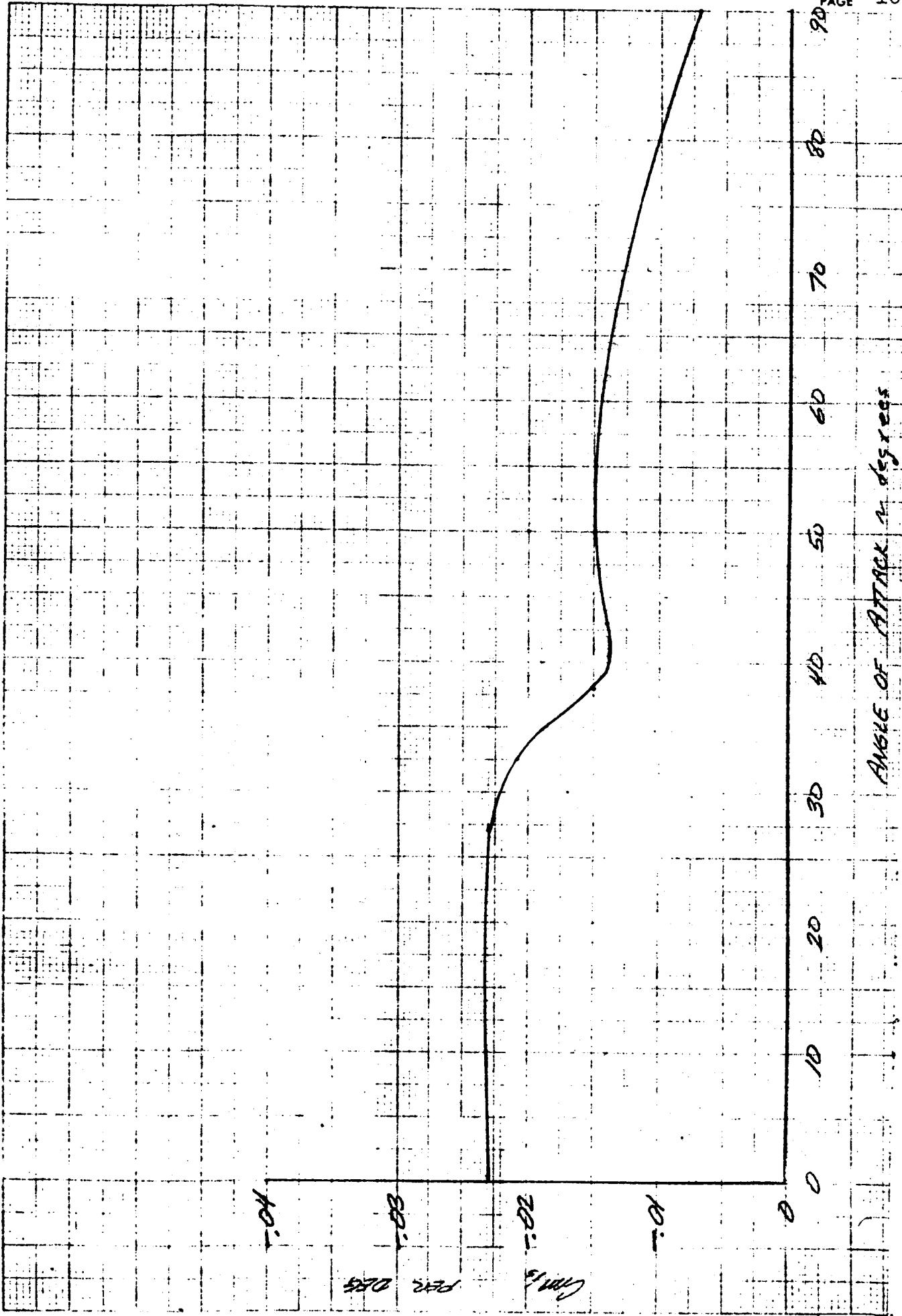


Figure C-1. - Effect of angle of attack on longitudinal-control effectiveness.
 $\text{Lambda} = 22^\circ$.

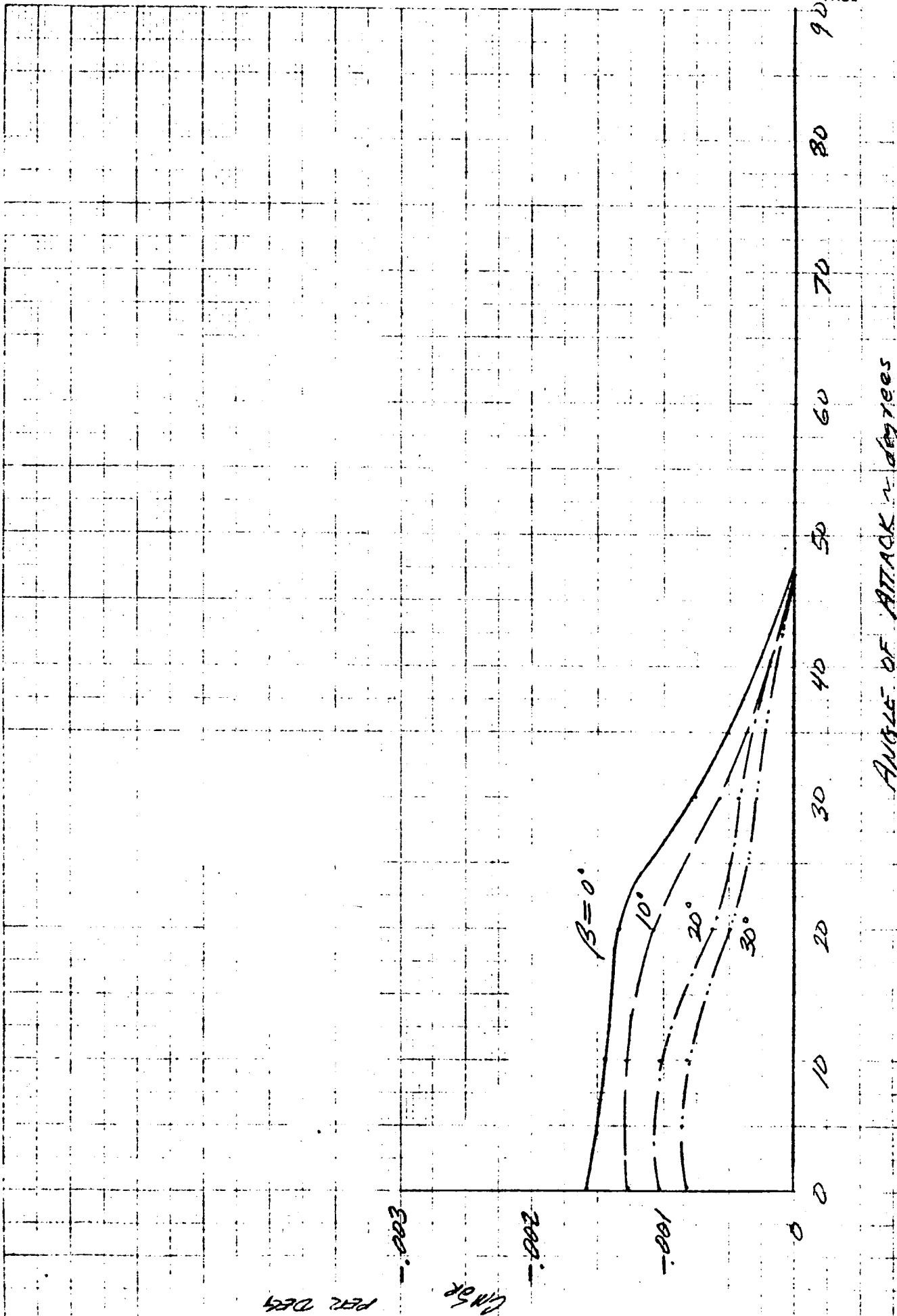


Figure C-2. - Effect of angle of attack on directional-control effectiveness. $\text{Lamda} = 22^\circ$.

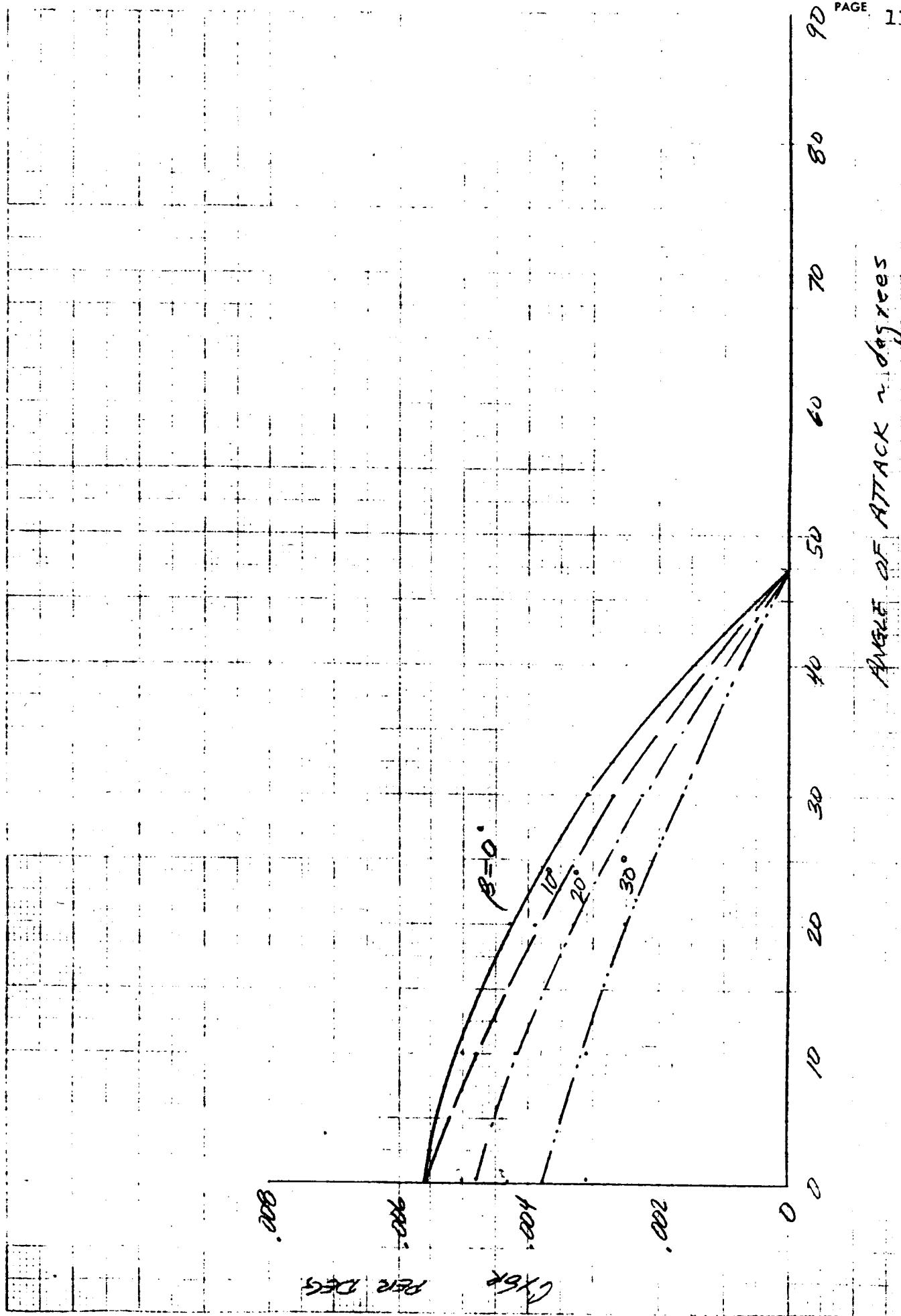


Figure C-3. - Effect of angle of attack on side force coefficient due to directional-control. $\Lambda_{mda}=22$

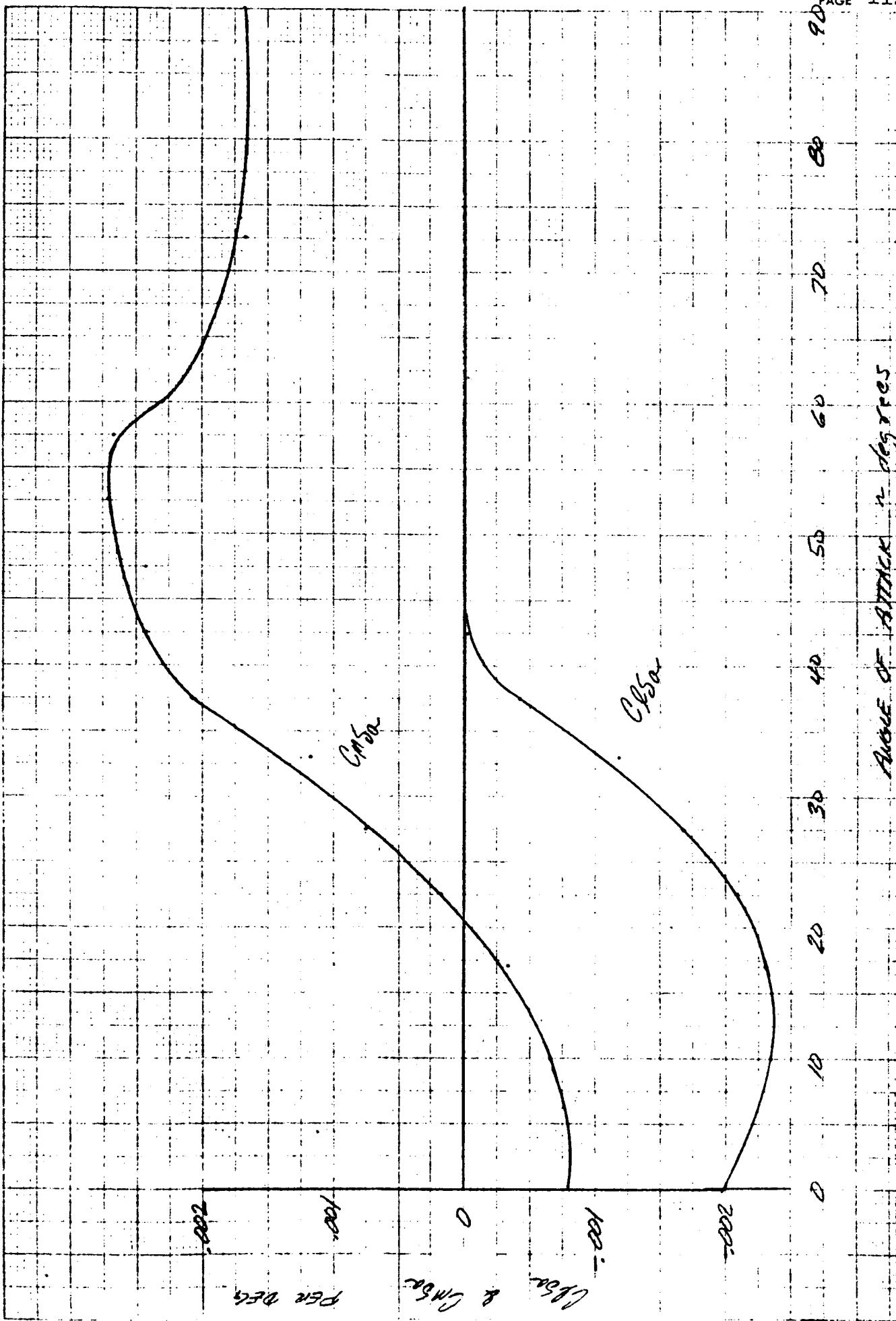
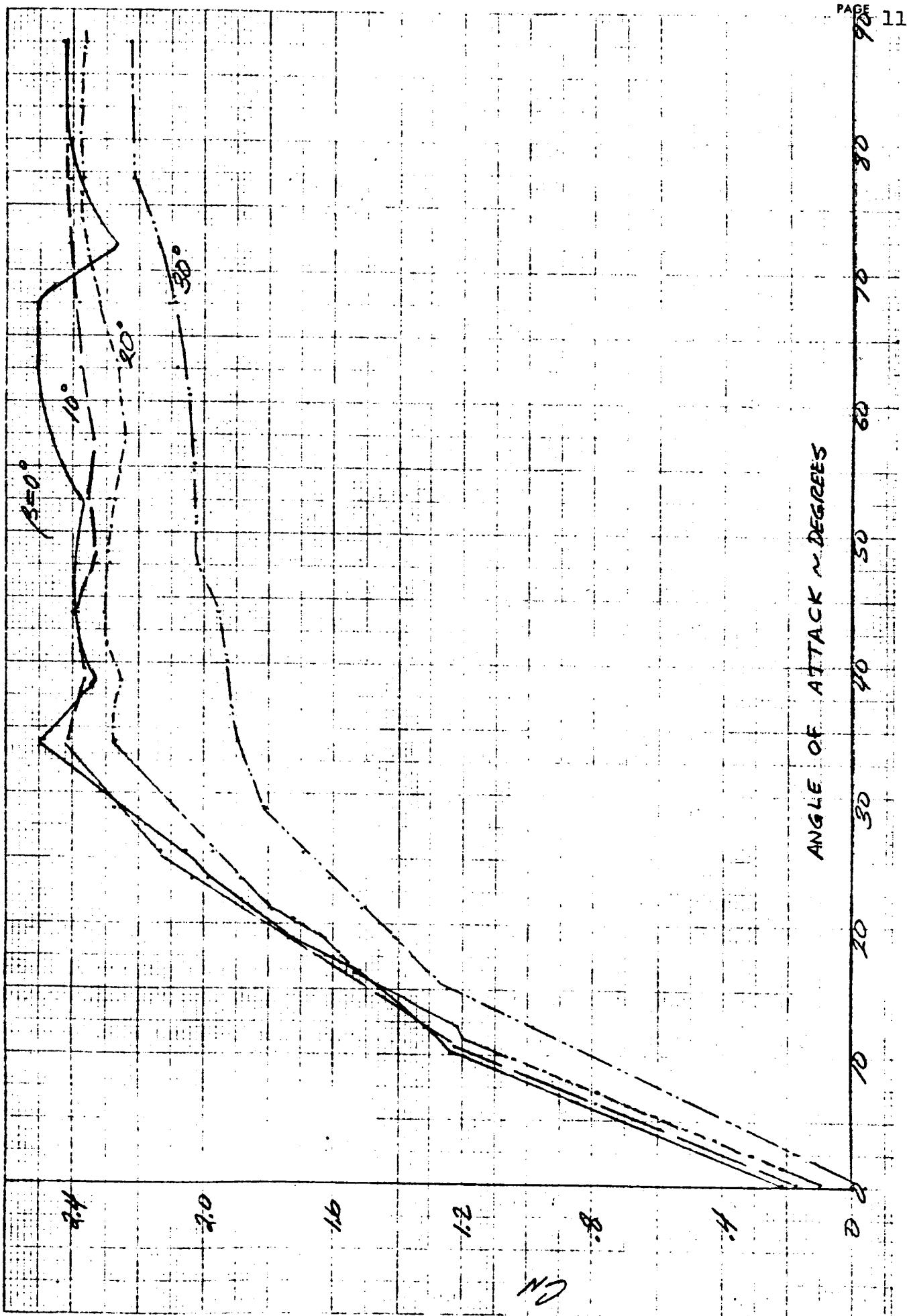


Figure C-4. - Effect of angle of attack on lateral-control effectiveness.
 $\lambda = 22$



Lamda = 22°

Figure C-5. - Effect of angle of attack and sideslip angle on force characteristics. Lamda = 22°.

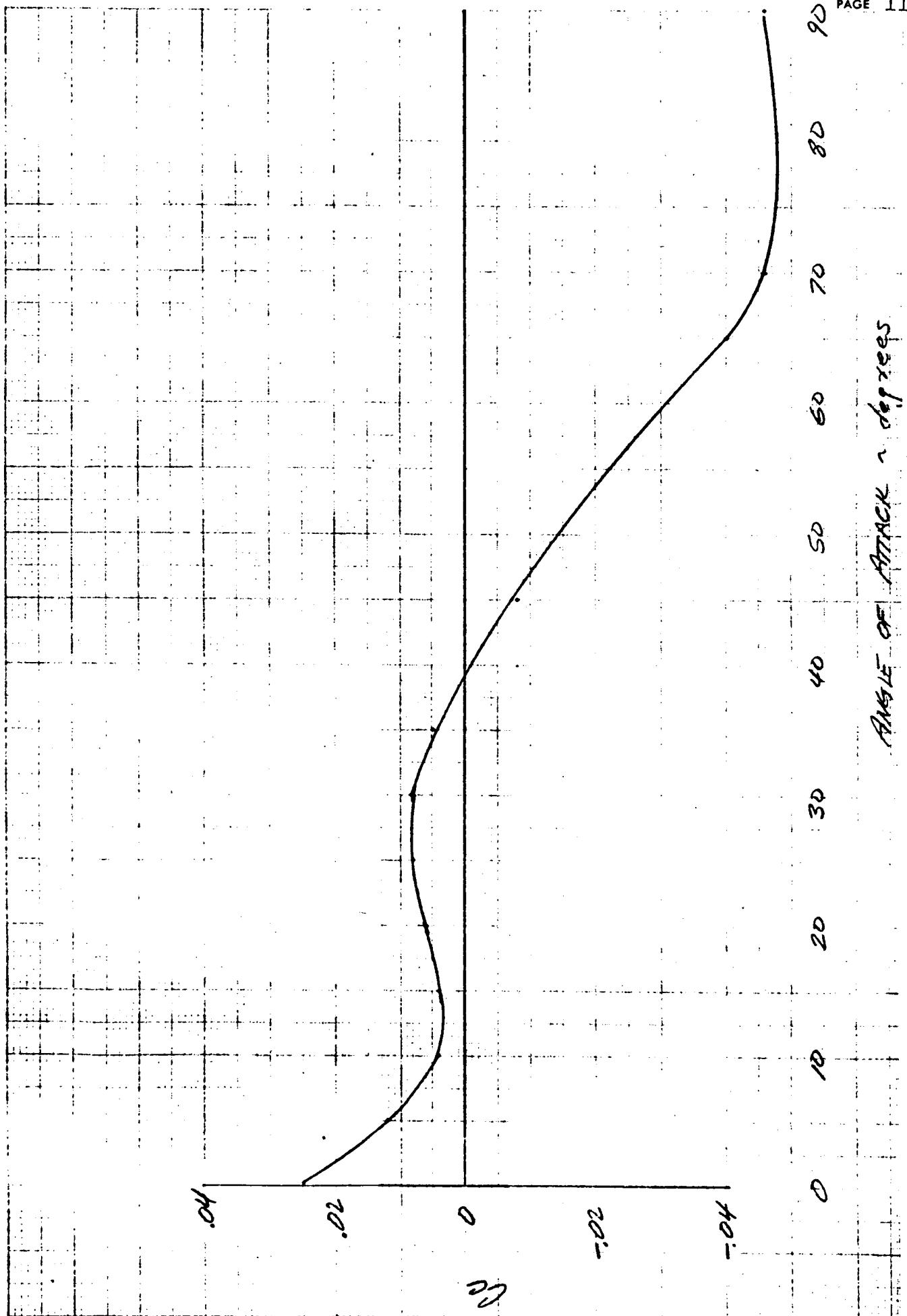


Figure C-5. - Continued.

c) C_y vs. α in degrees

90

70

60

50

40

30

20

10

0

TJ

6

4

2

REPORT
DATE

GRUMMAN AIRCRAFT DIVISION

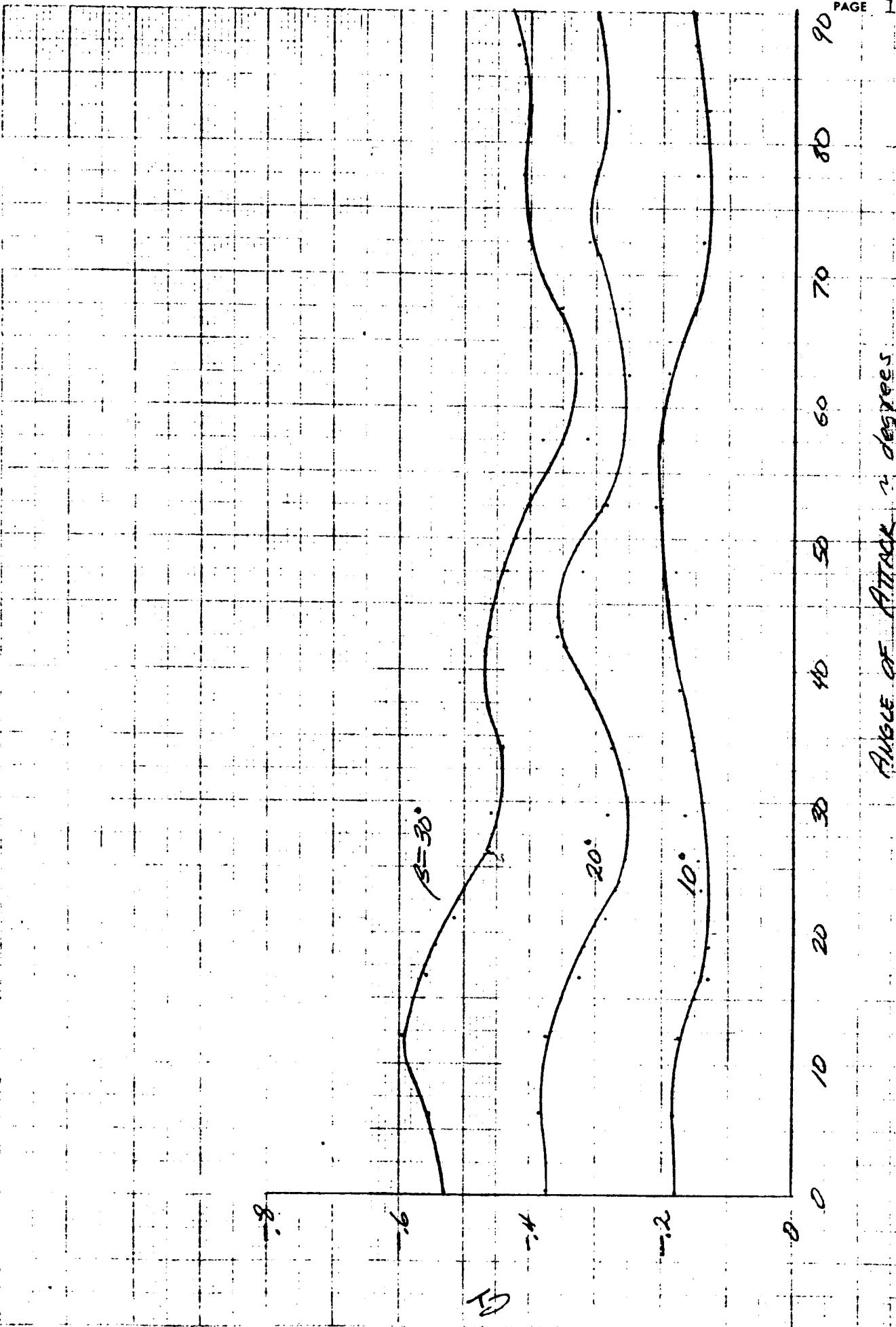


Figure C-5. - Concluded.

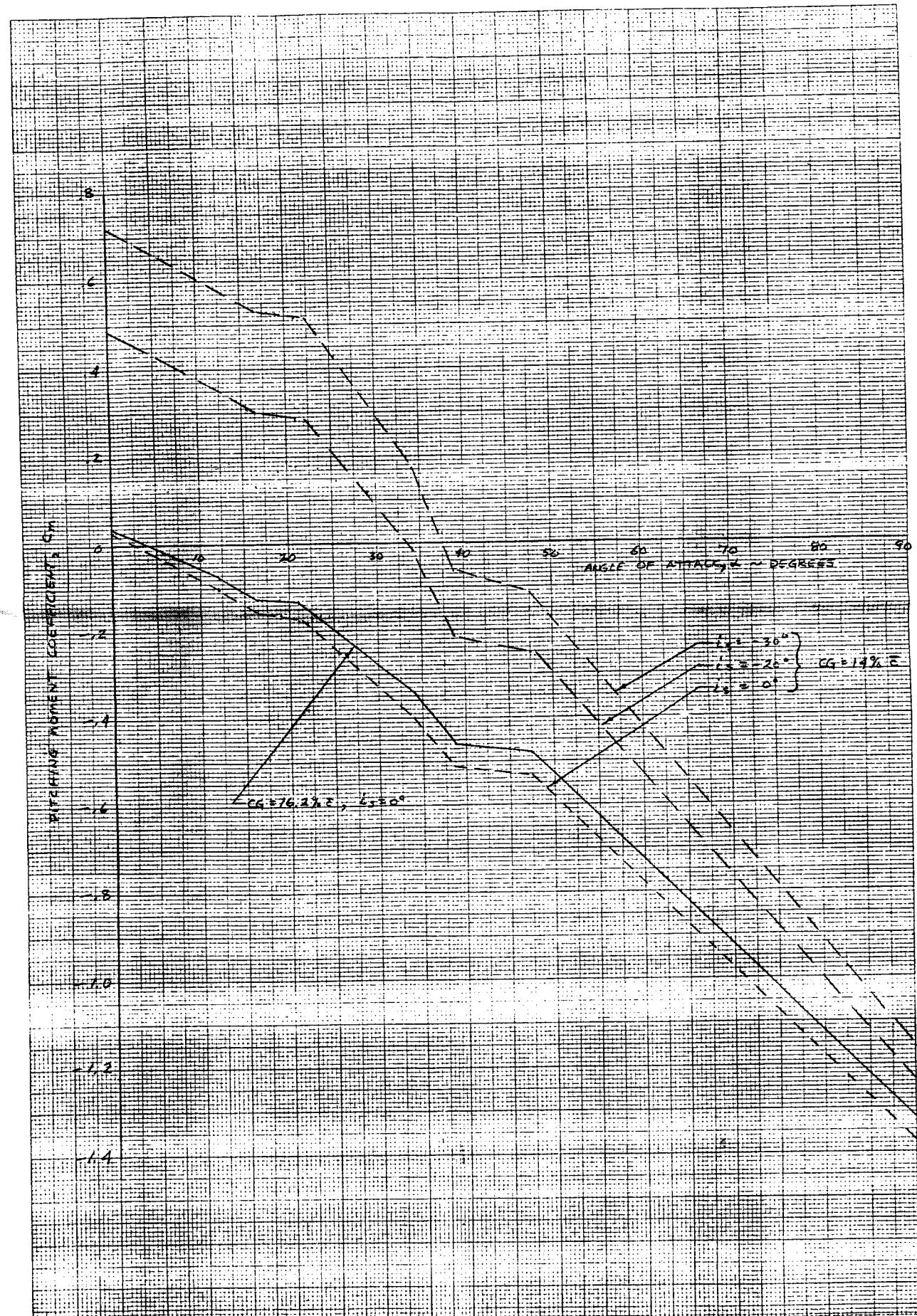
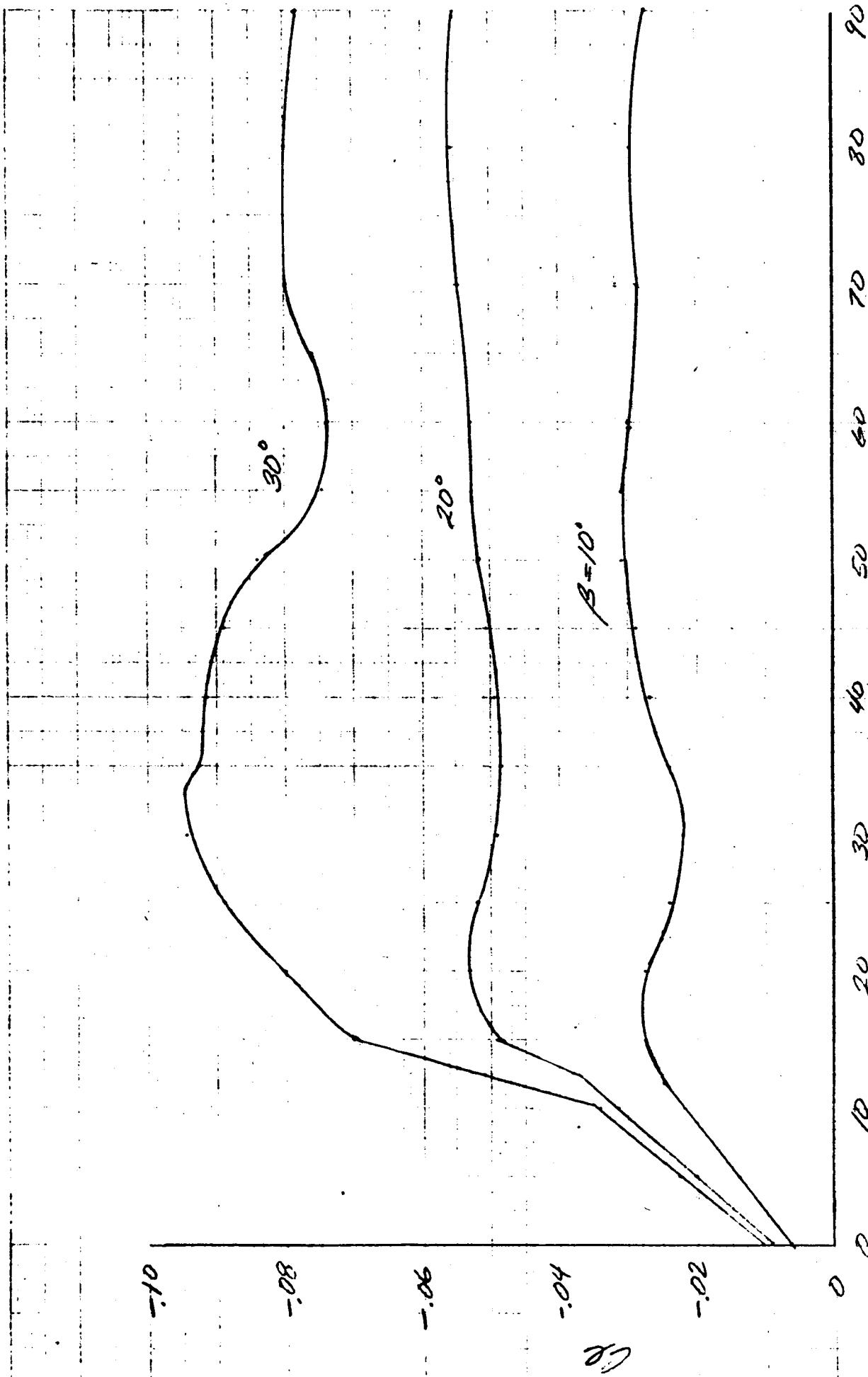


Figure C-6. - Effect of angle of attack and longitudinal-control deflection on pitching-moment coefficient. $\Lambda = 22^\circ$.



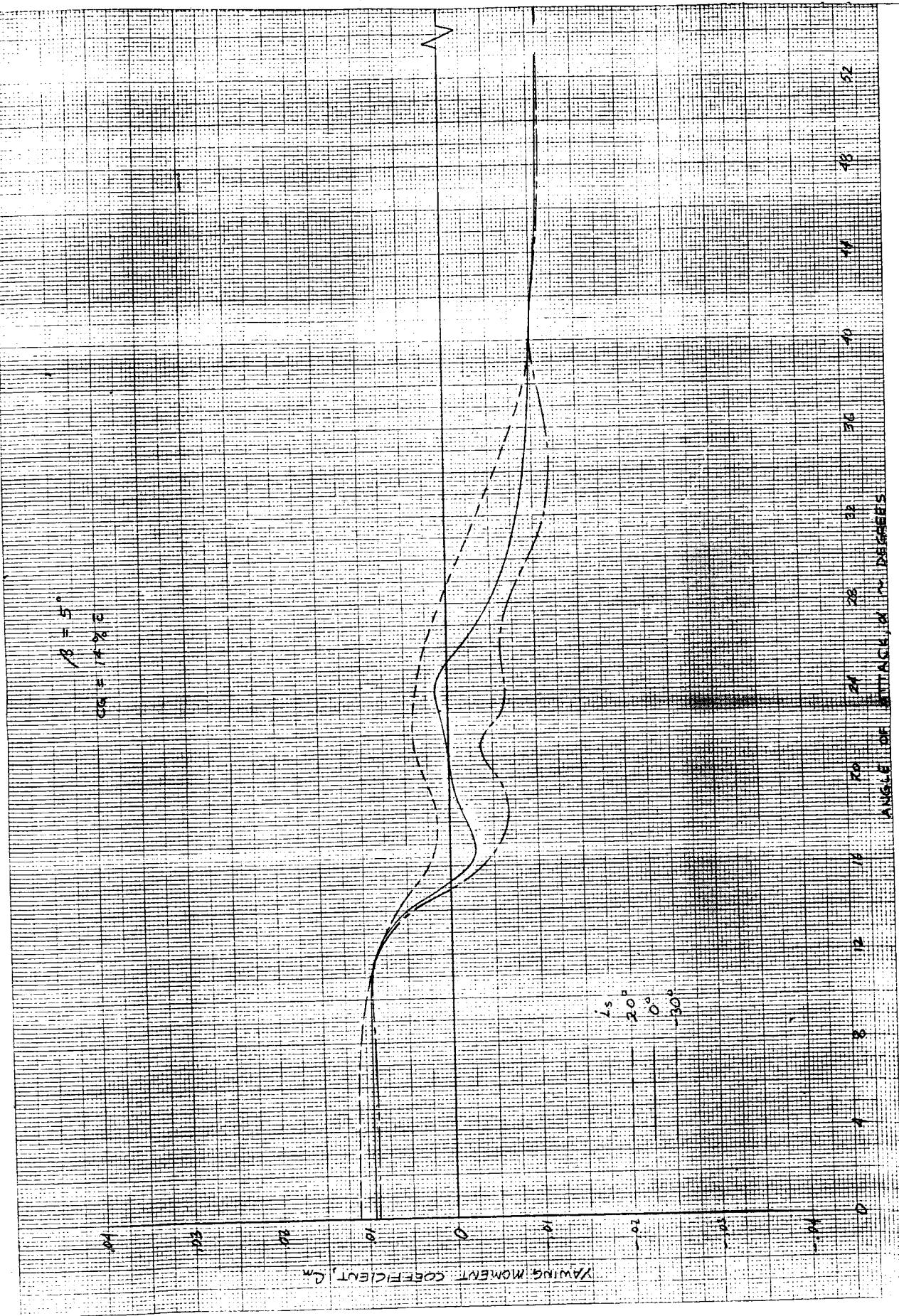
PAGE 117

ANGLE OF ATTACK in degrees

Figure C-7. - Effect of angle of attack and sideslip angle on rolling-moment coefficient. $\lambda = 22^{\circ}$

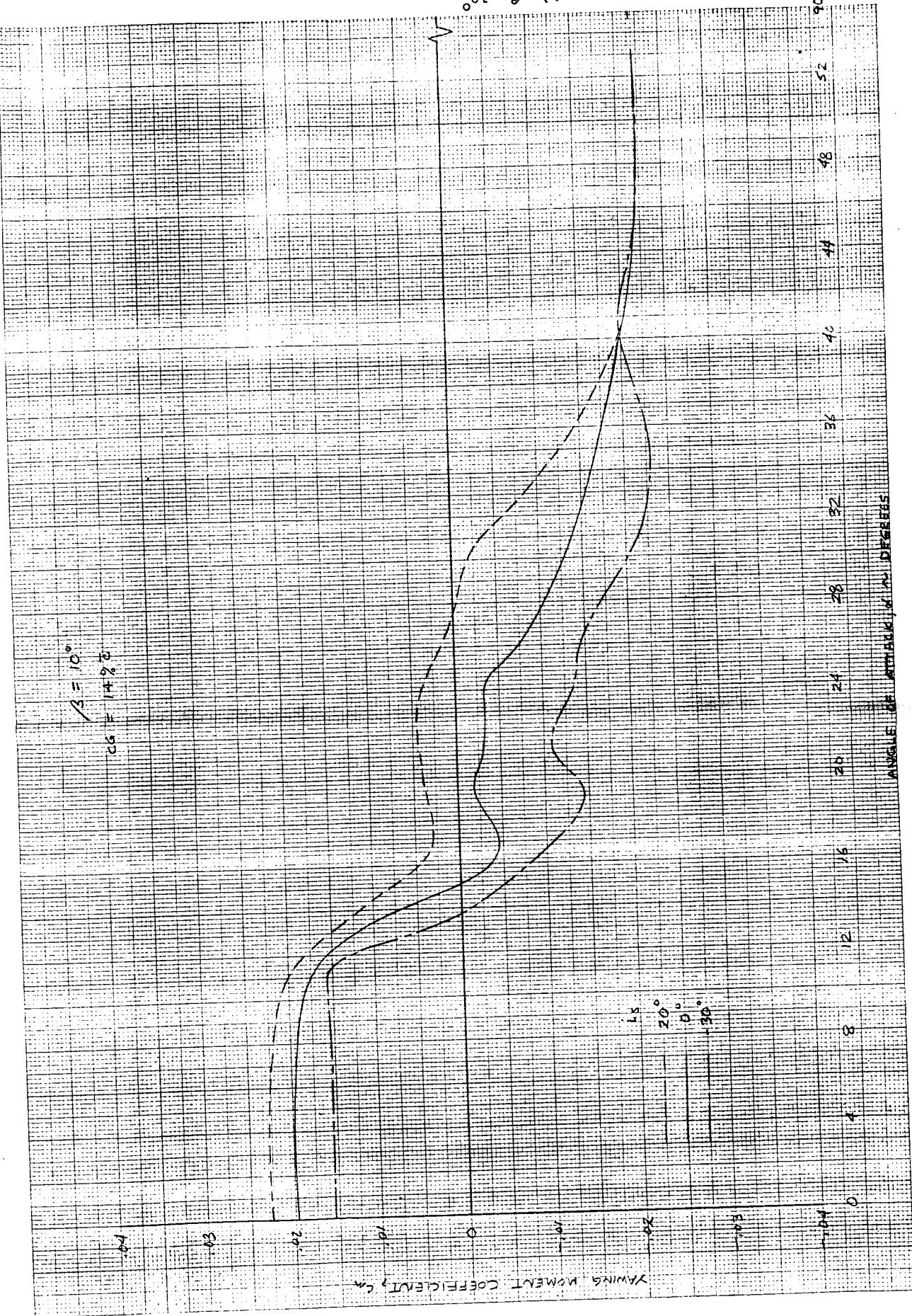
a) $\alpha = 5^\circ$

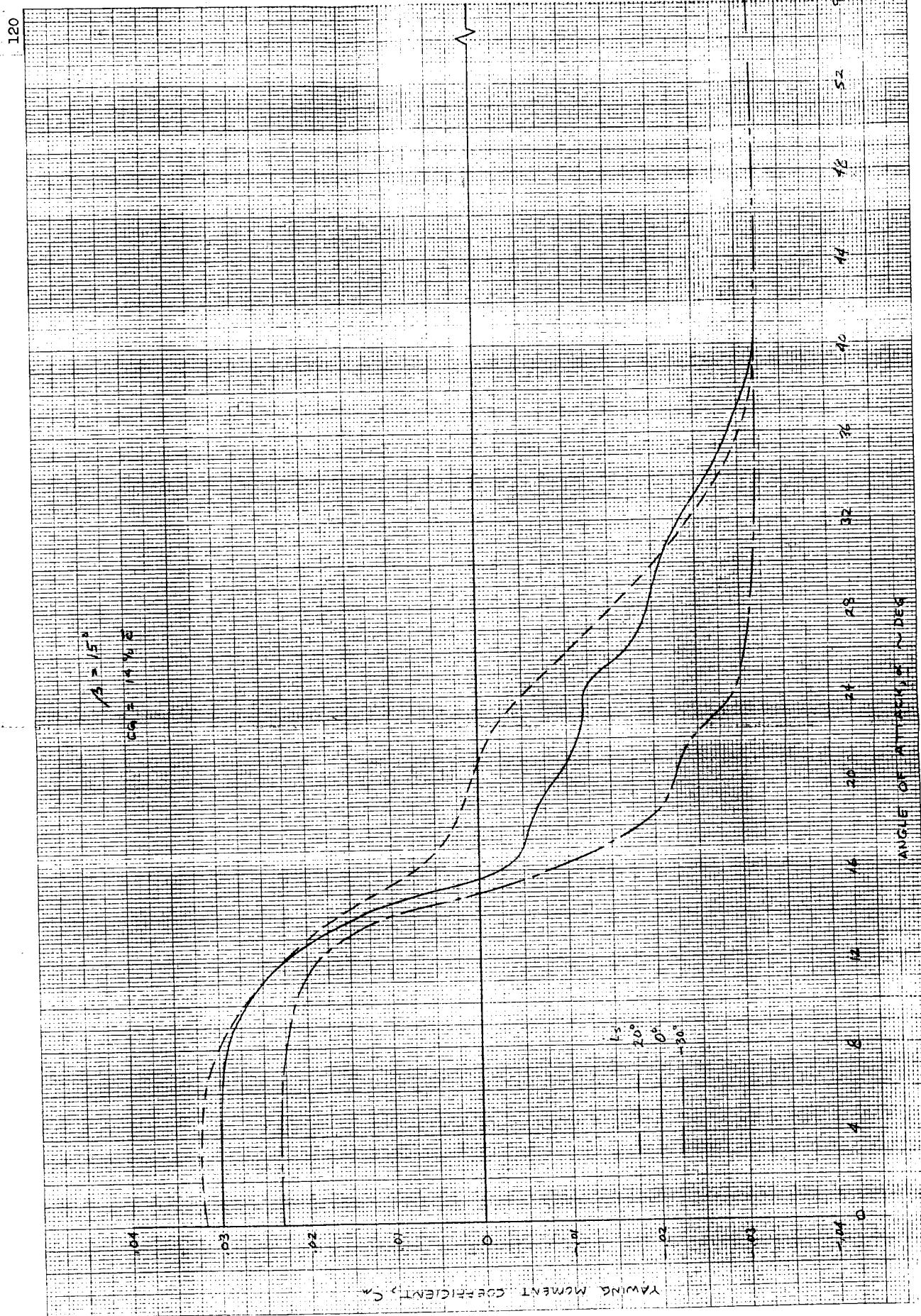
118



b) $\beta = 10^\circ$

119



c) $\beta = 15^\circ$ 

$$d) \beta = 20^\circ$$

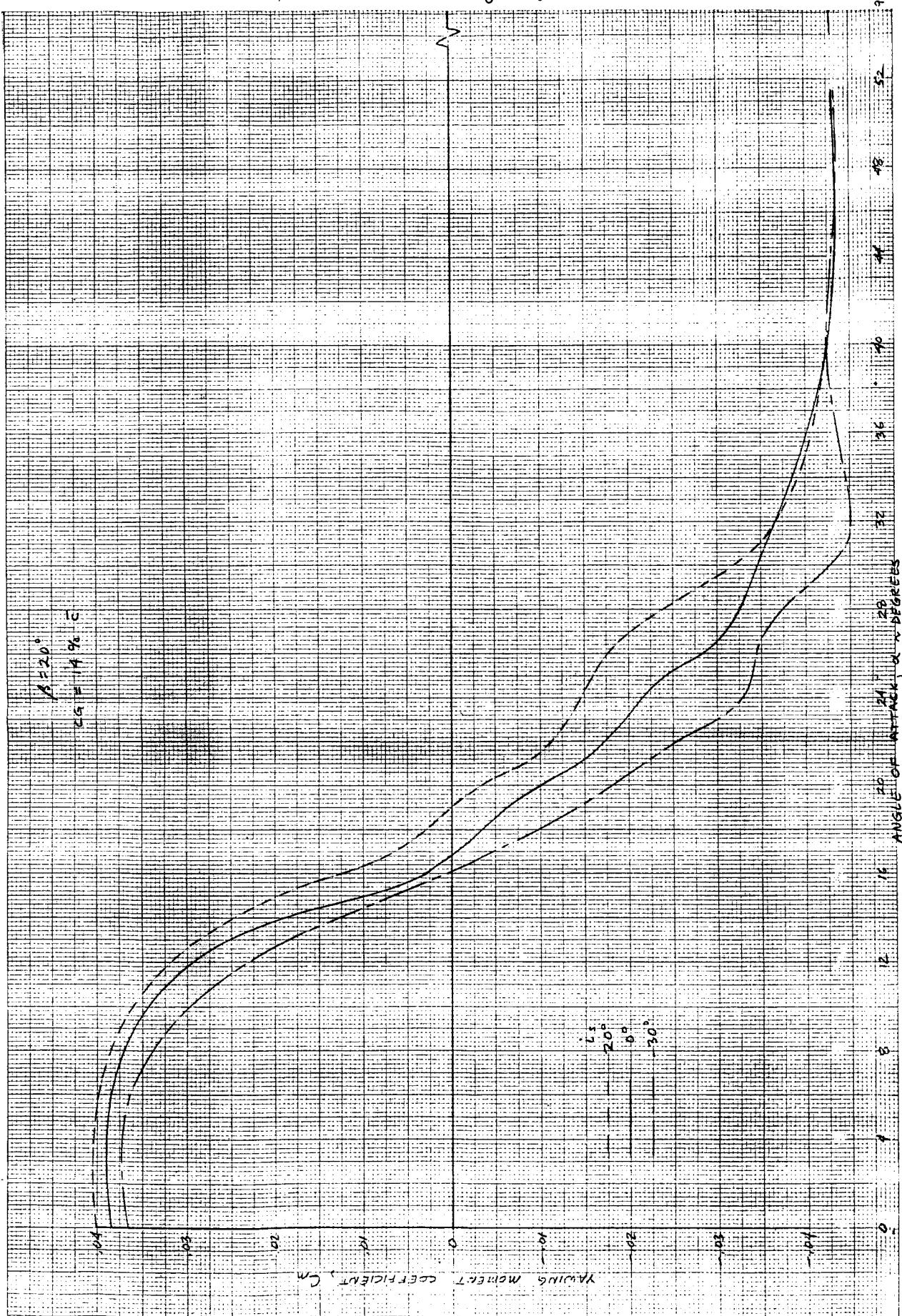
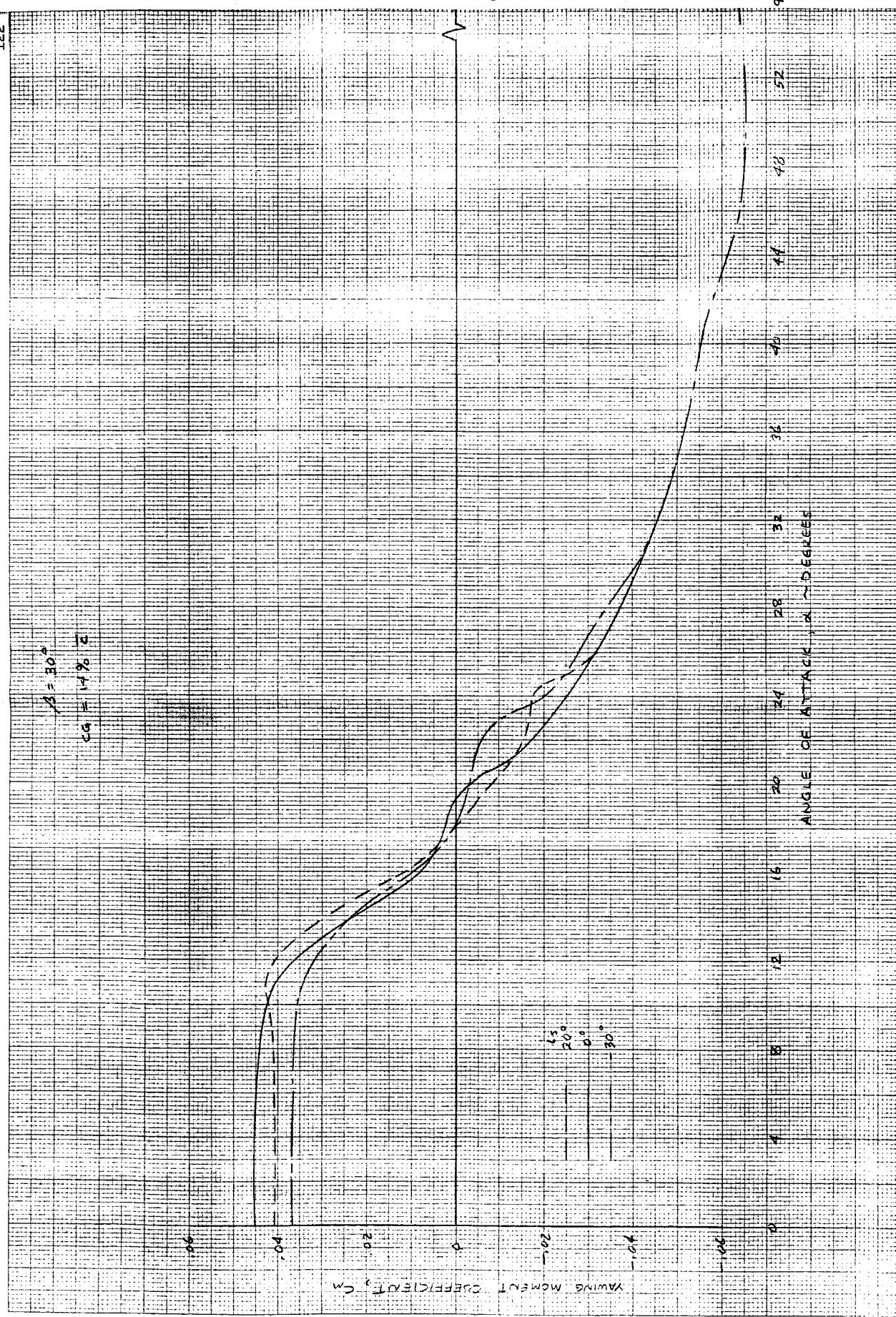


Figure C-8. - Concluded.

$$0^{\circ} = \beta (a)$$



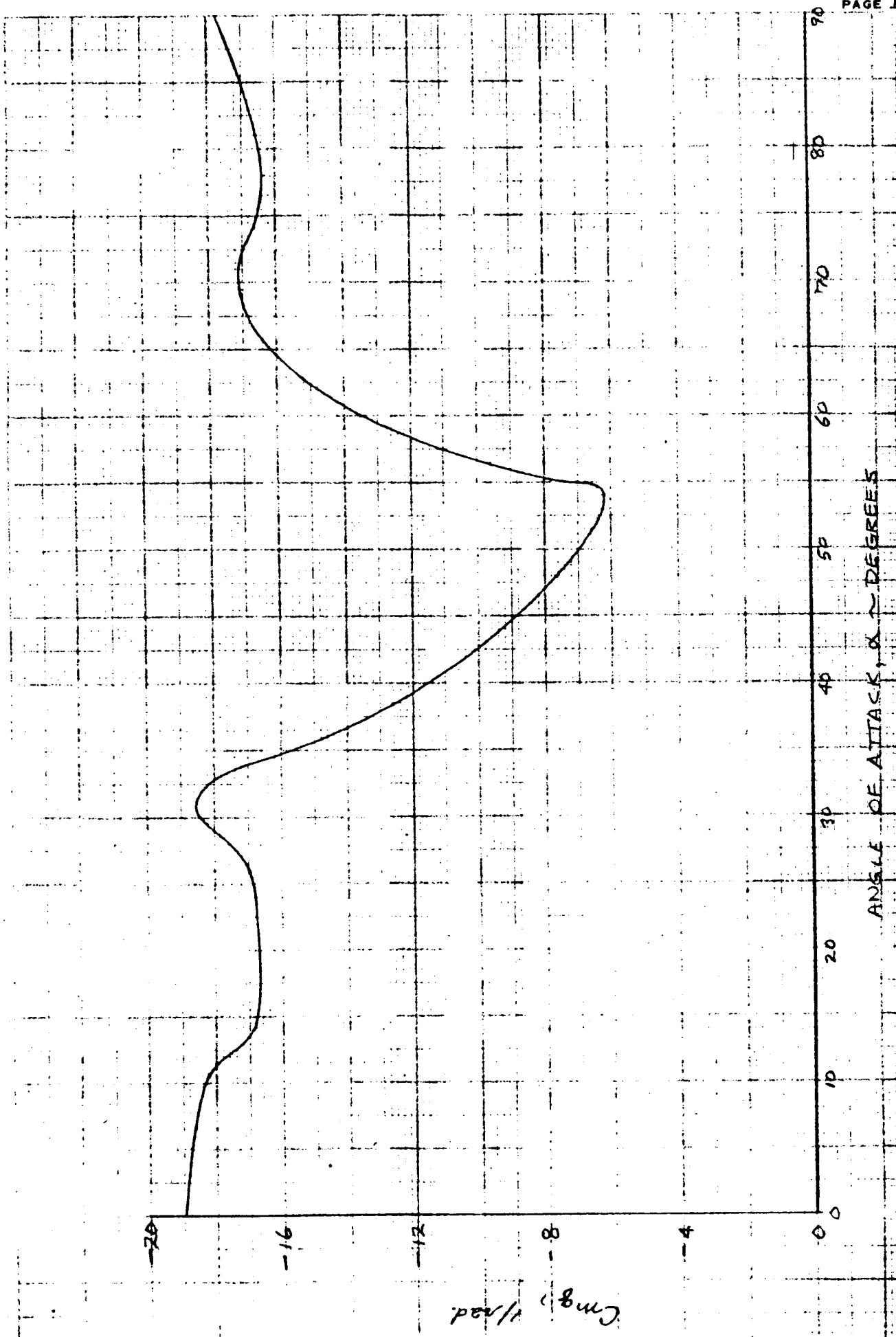
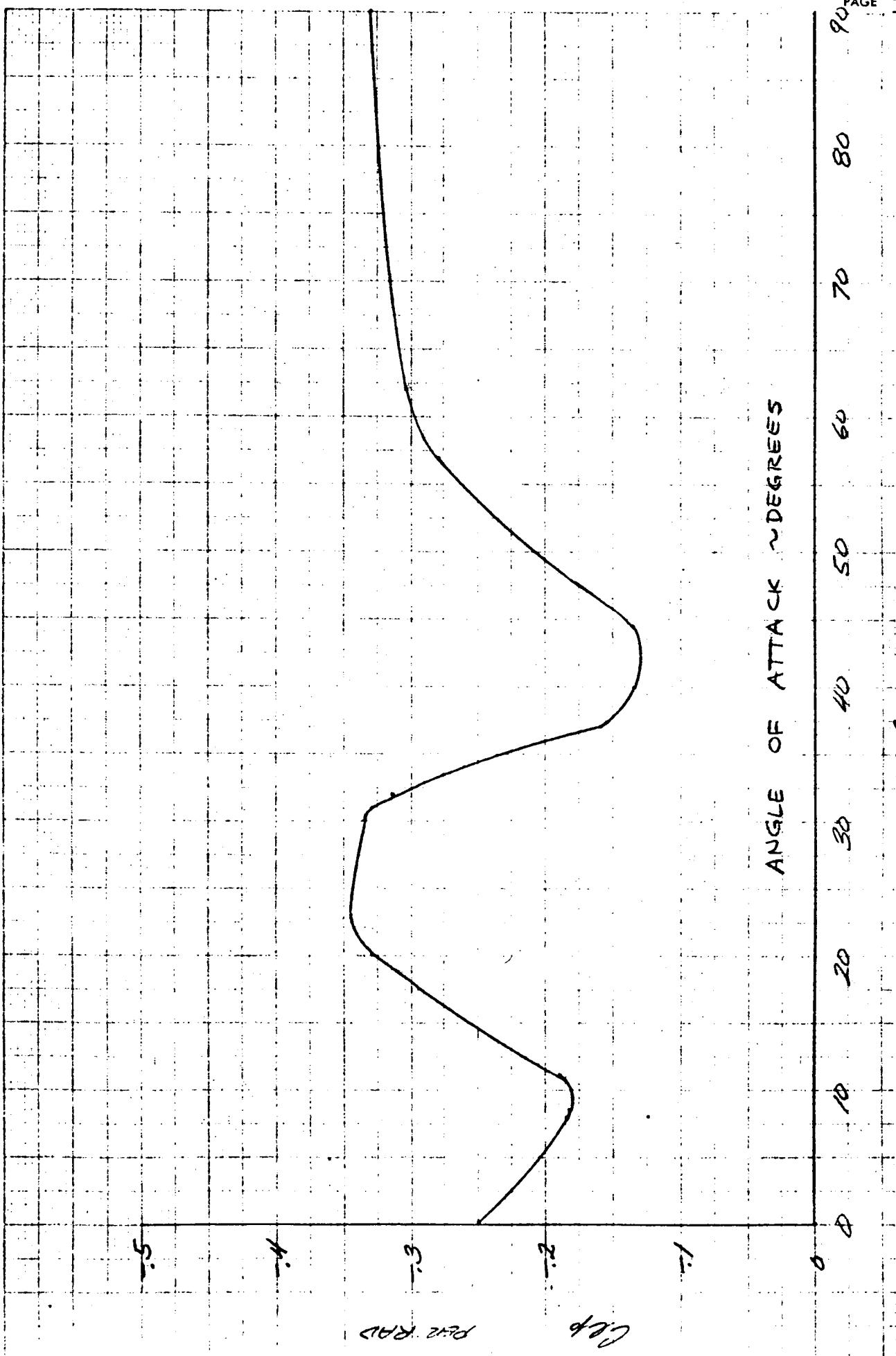
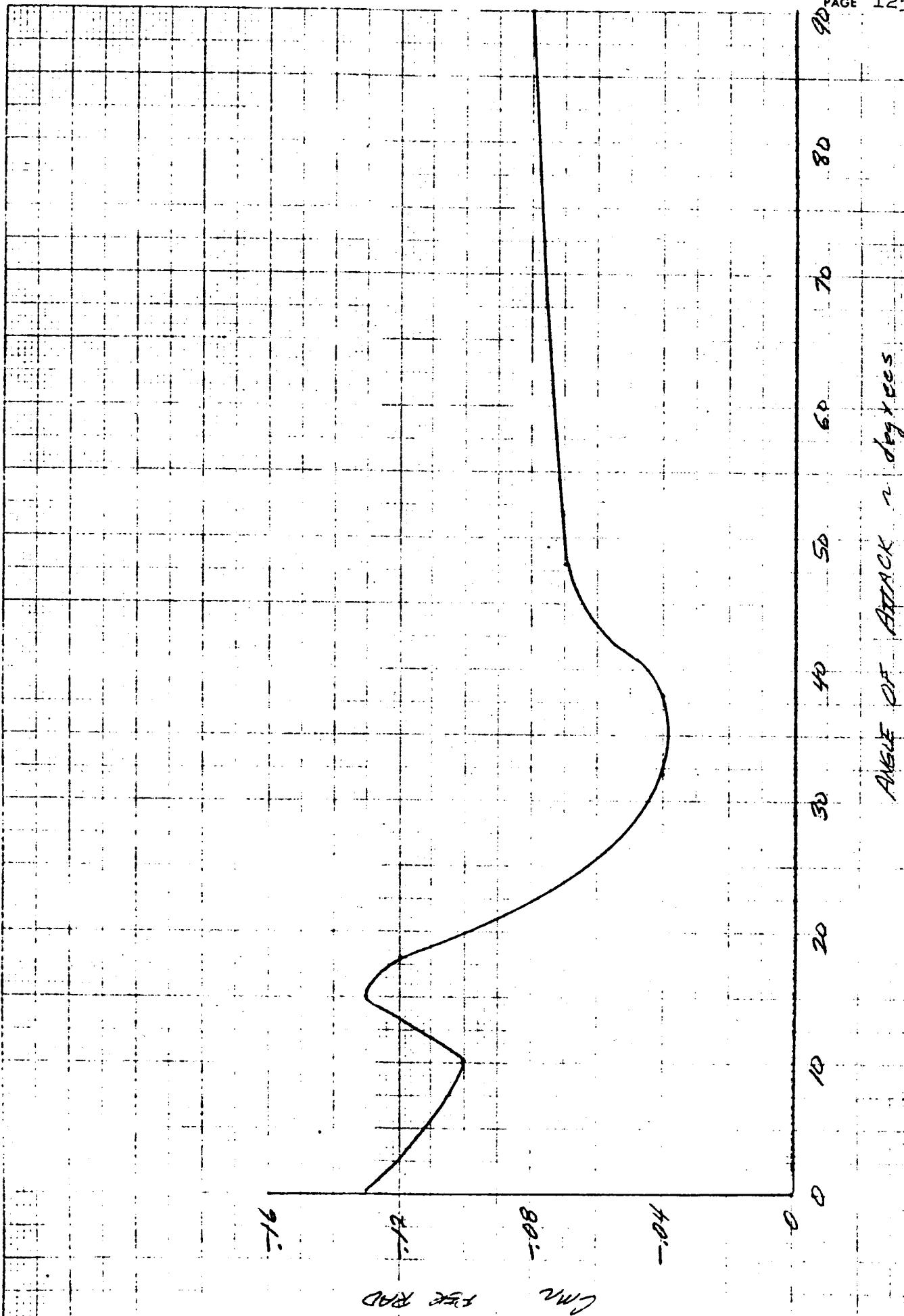


Figure C-9. - Effect of angle of attack on damping derivatives. $\Lambda = 22^\circ$. $\Lambda = 20^\circ$.



b) C_L
Figure C-9. - Continued.



22
a) C_{np}
ANGLE OF ATTACK in degrees

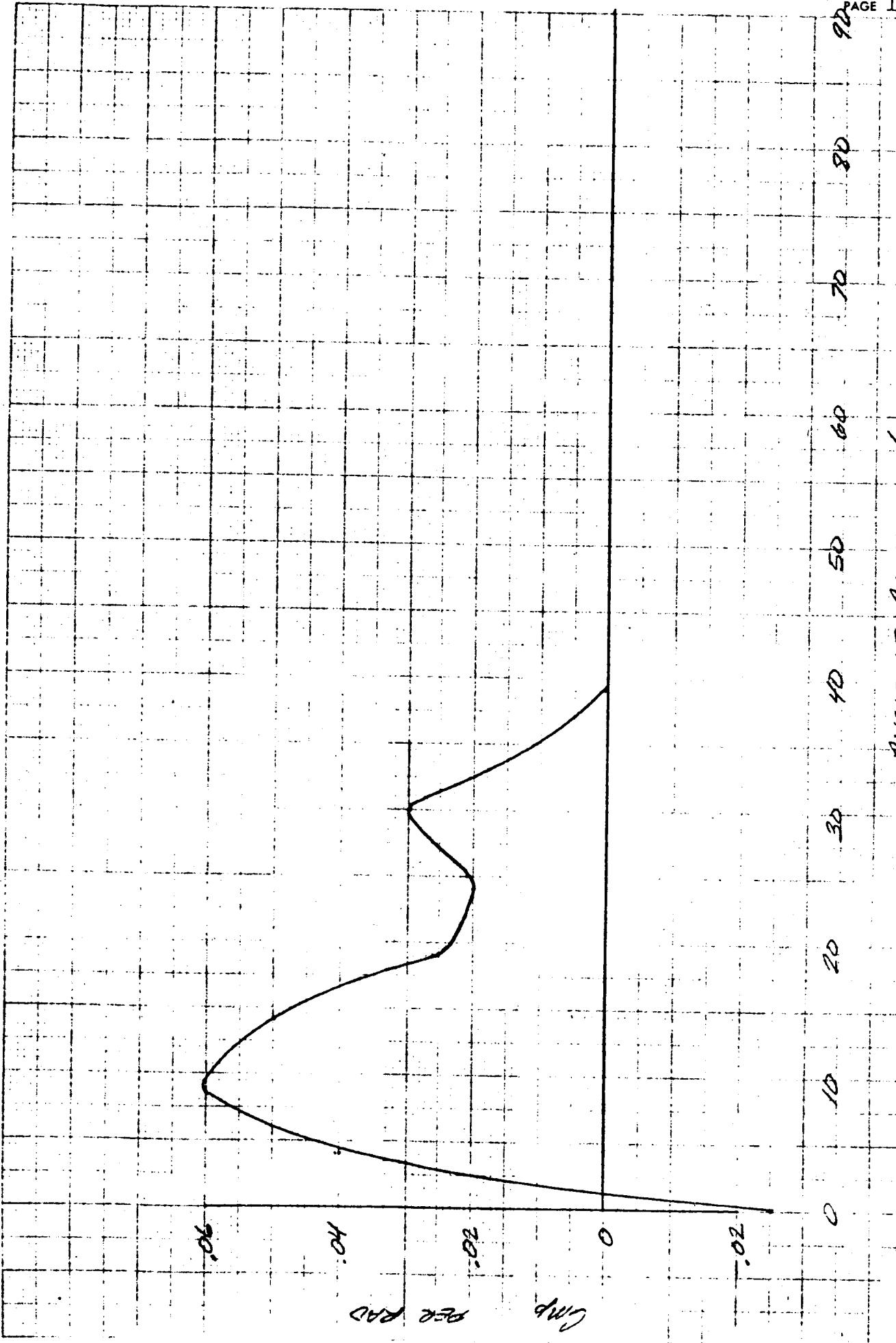


Figure C-10.- Effect of angle of attack on cross derivatives.
Lambda = 22°.

b) C_{L_r}

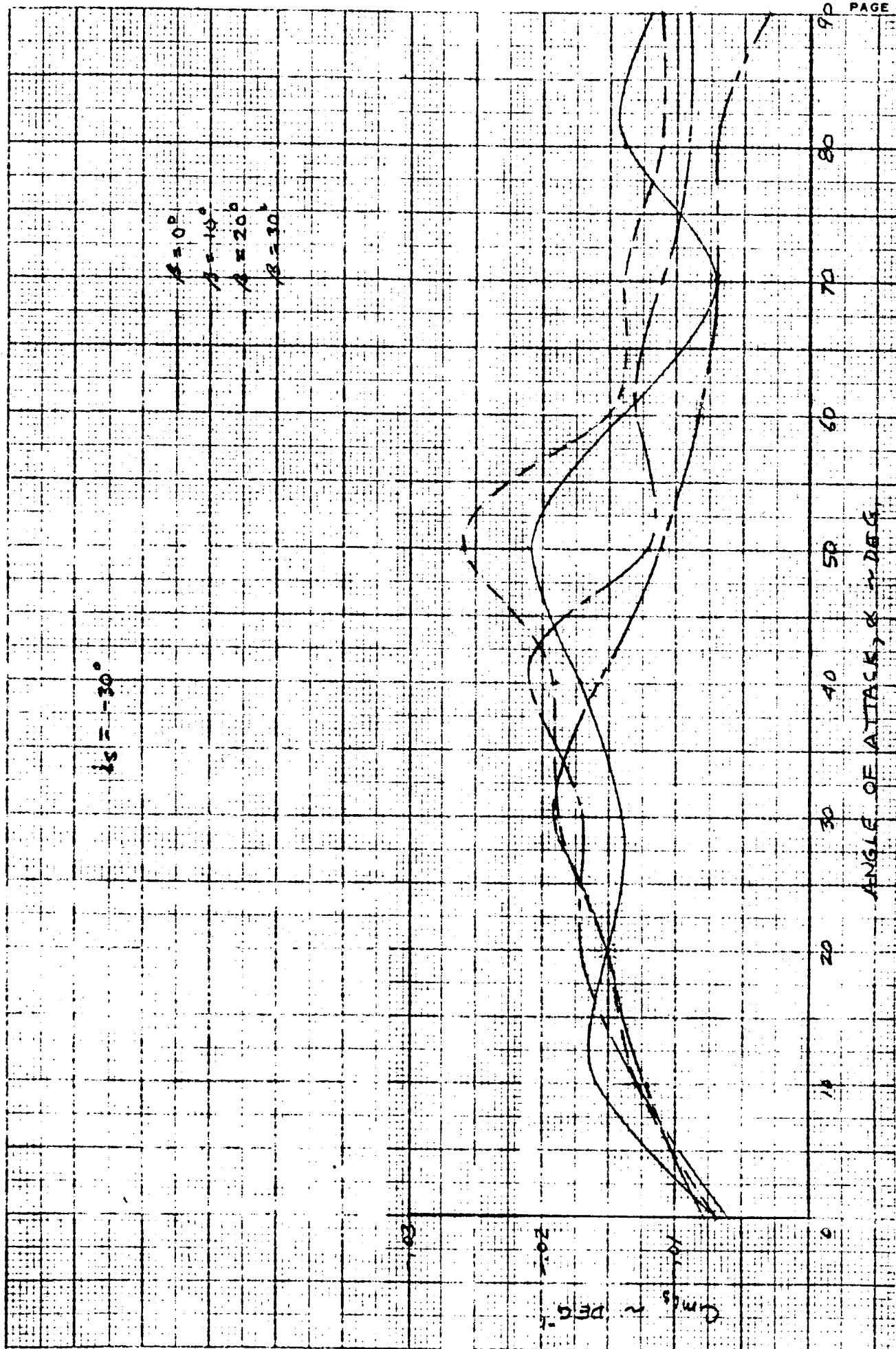
ANGLE OF ATTACK α ~ DEG.

Angle of Attack (α)	C_{L_r}
0	0.0
10	0.8
15	1.4
20	1.0
25	0.5
30	0.0
35	-0.2
40	-0.4
45	-0.4
50	-0.2
55	0.0
60	0.0

Figure C-10. - Concluded.

C_{N_1s}	$= 0$
C_{L_R}	$= 0$
C_{m_e}	$= 0$
C_{y_b}	$= 0$
C_{y_p}	$= 0$
C_{N_d}	$= 0$
C_{c_1s}	$= 0$
$C_{y_{ba}}$	$= 0$
C_{m_b}	$= 0$
$C_{N_{Rb}}$	$= 0$
C_{y_r}	$= 0$

Figure C-11. - Aerodynamic derivatives assigned zero values.



a) C_{m1s}

Figure C-12. - Effect of angle of attack on longitudinal-control characteristics. Λ = 22°

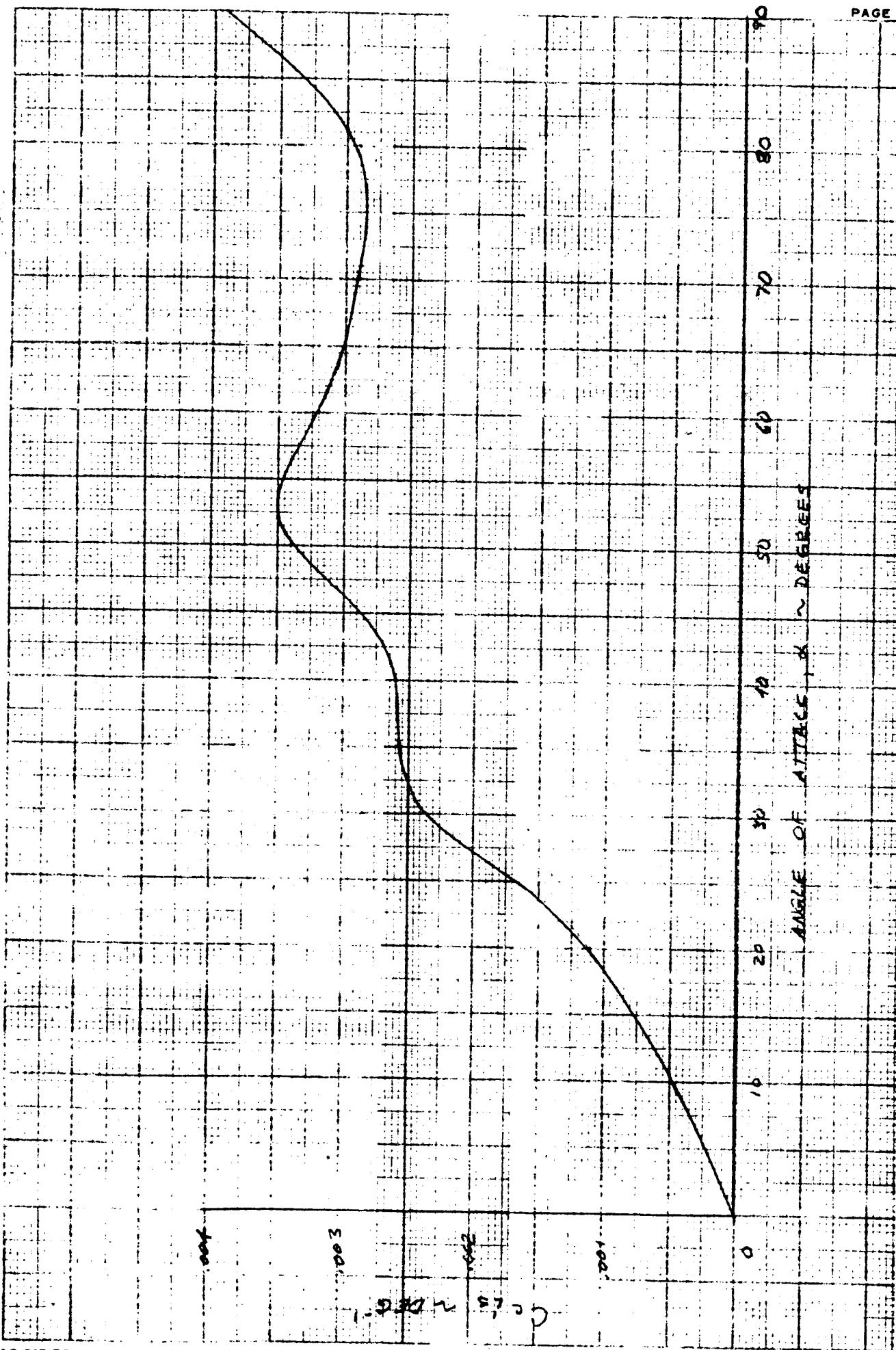


Figure C-12. - Continued.

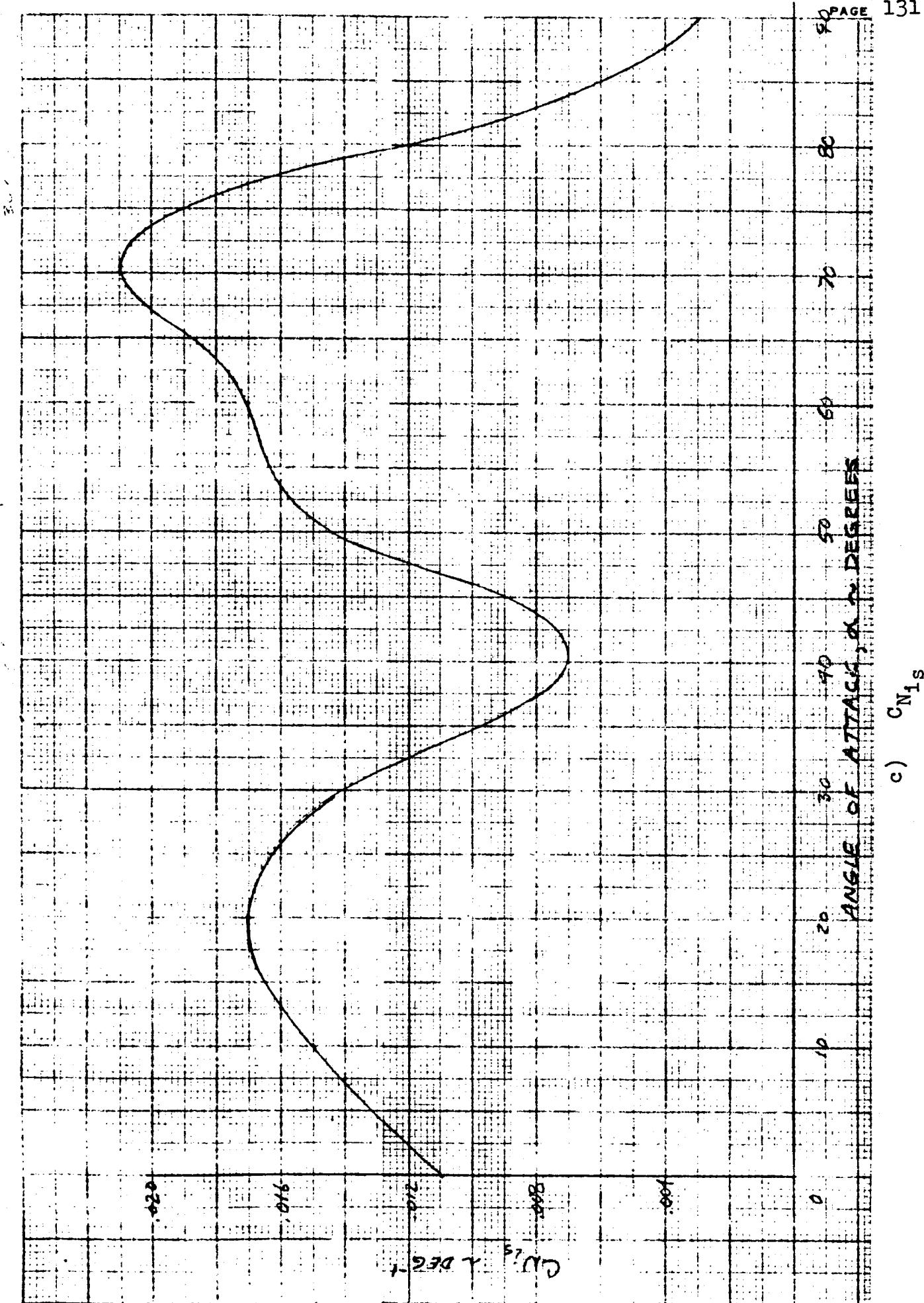
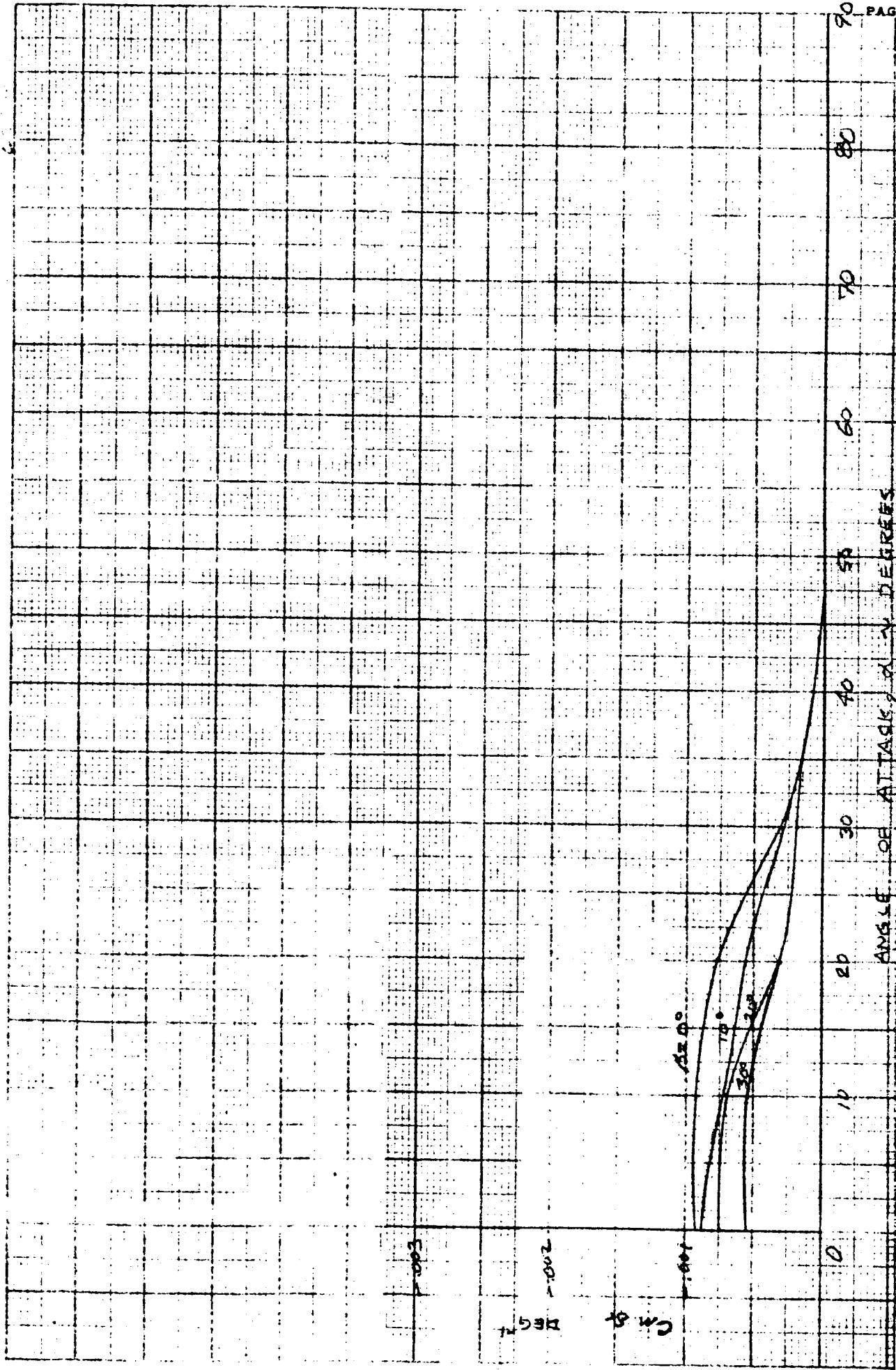
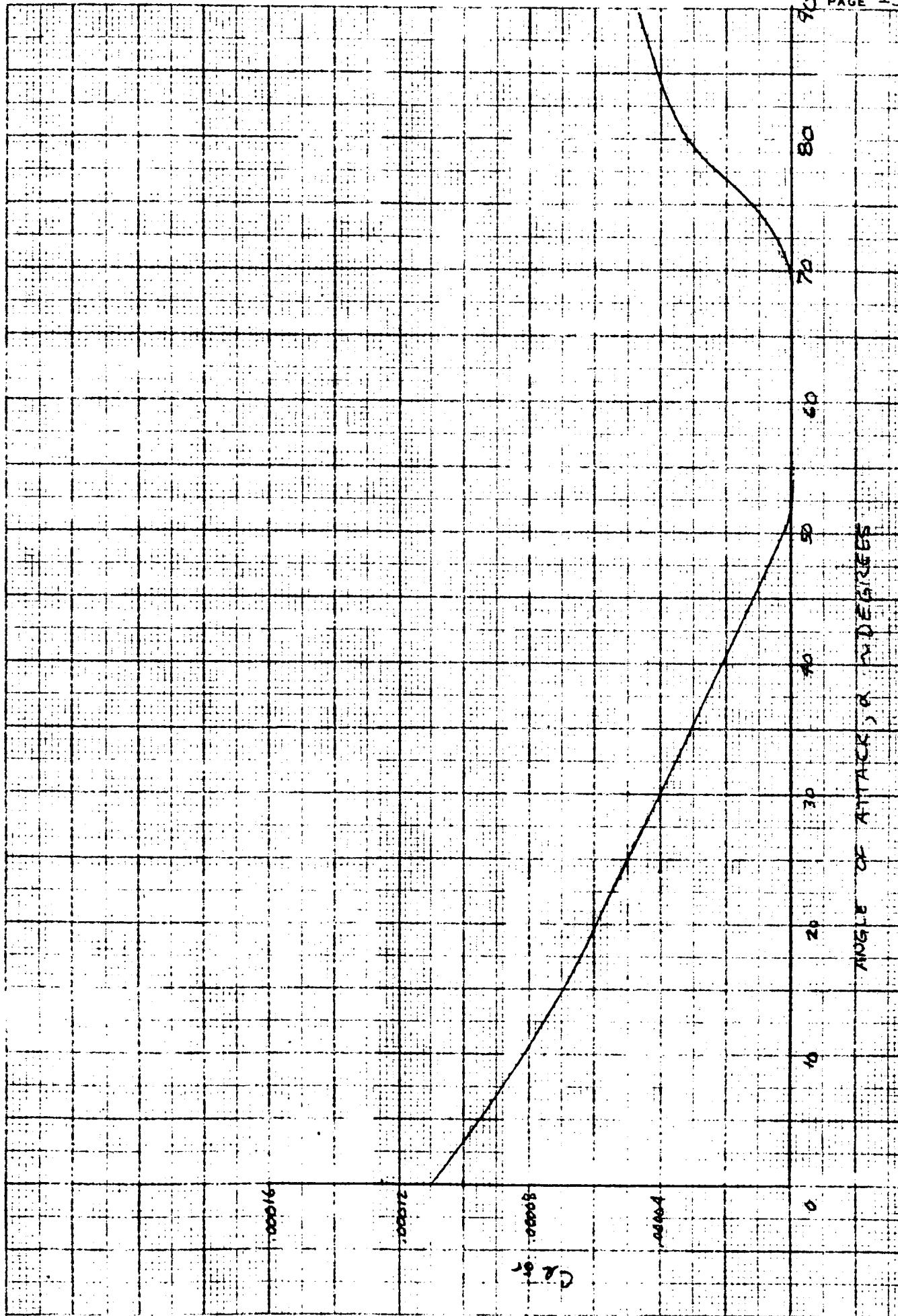


Figure C-12. - Concluded.

Figure C-13 - Effect of angle attack and sideslip angle on directional-control characteristics. Λ = 22°.

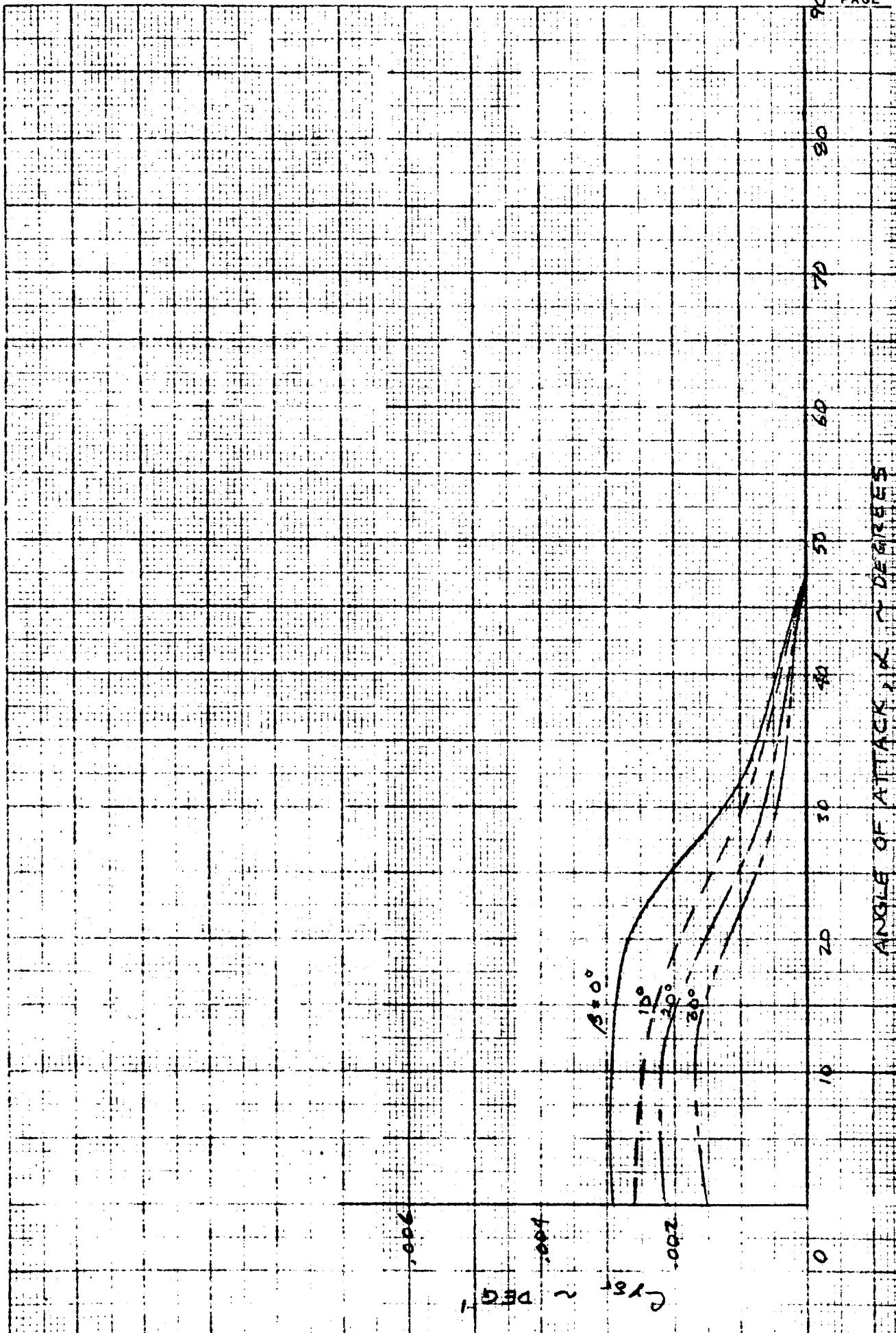
a) $C_n \delta_R$





c) $C_{y\delta R}$

ANGLE OF ATTACK AT DIVE



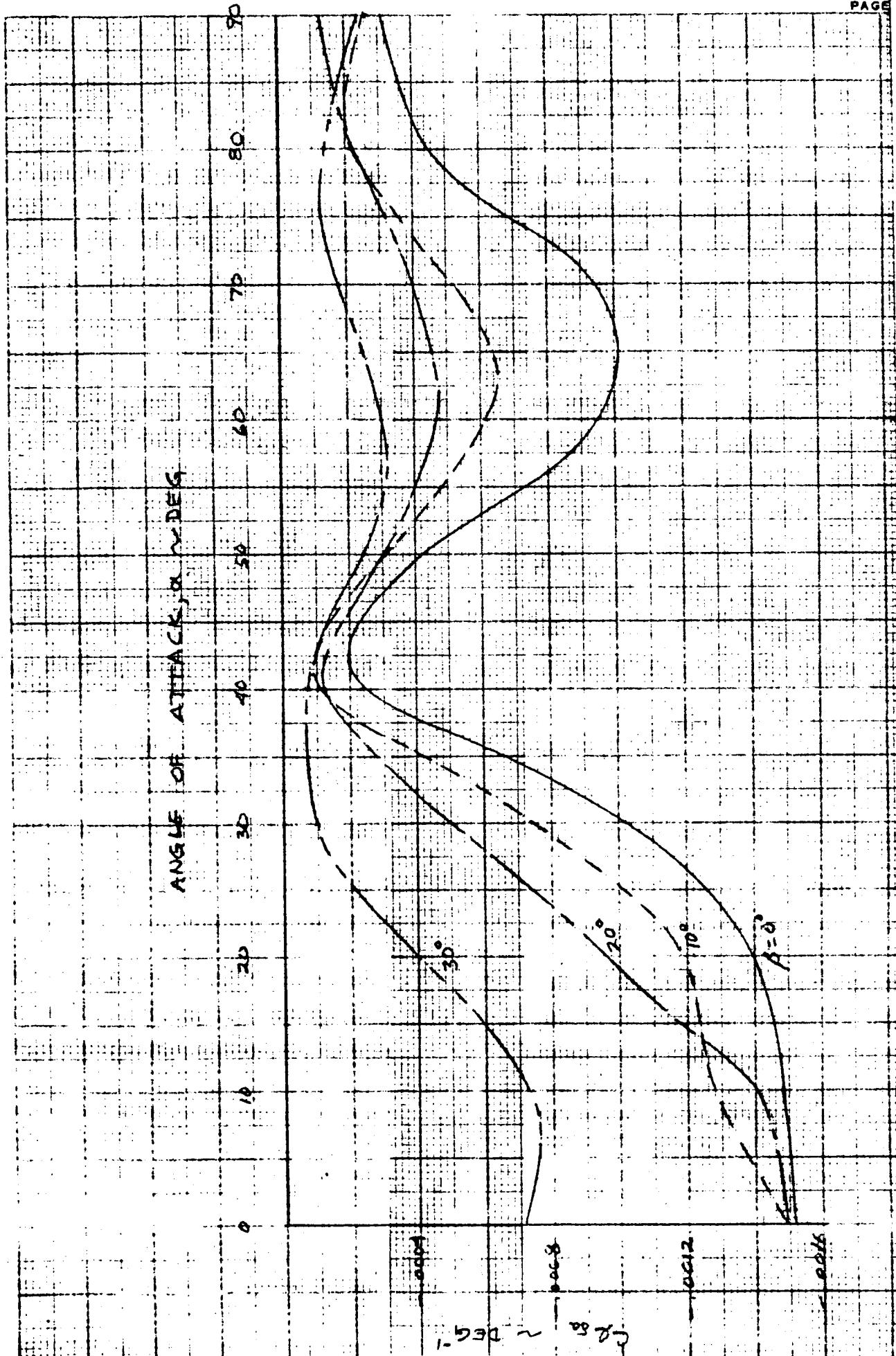


Figure C-14. - Effect of angle of attack and sideslip angle on lateral-control characteristics. Lamda 22°.

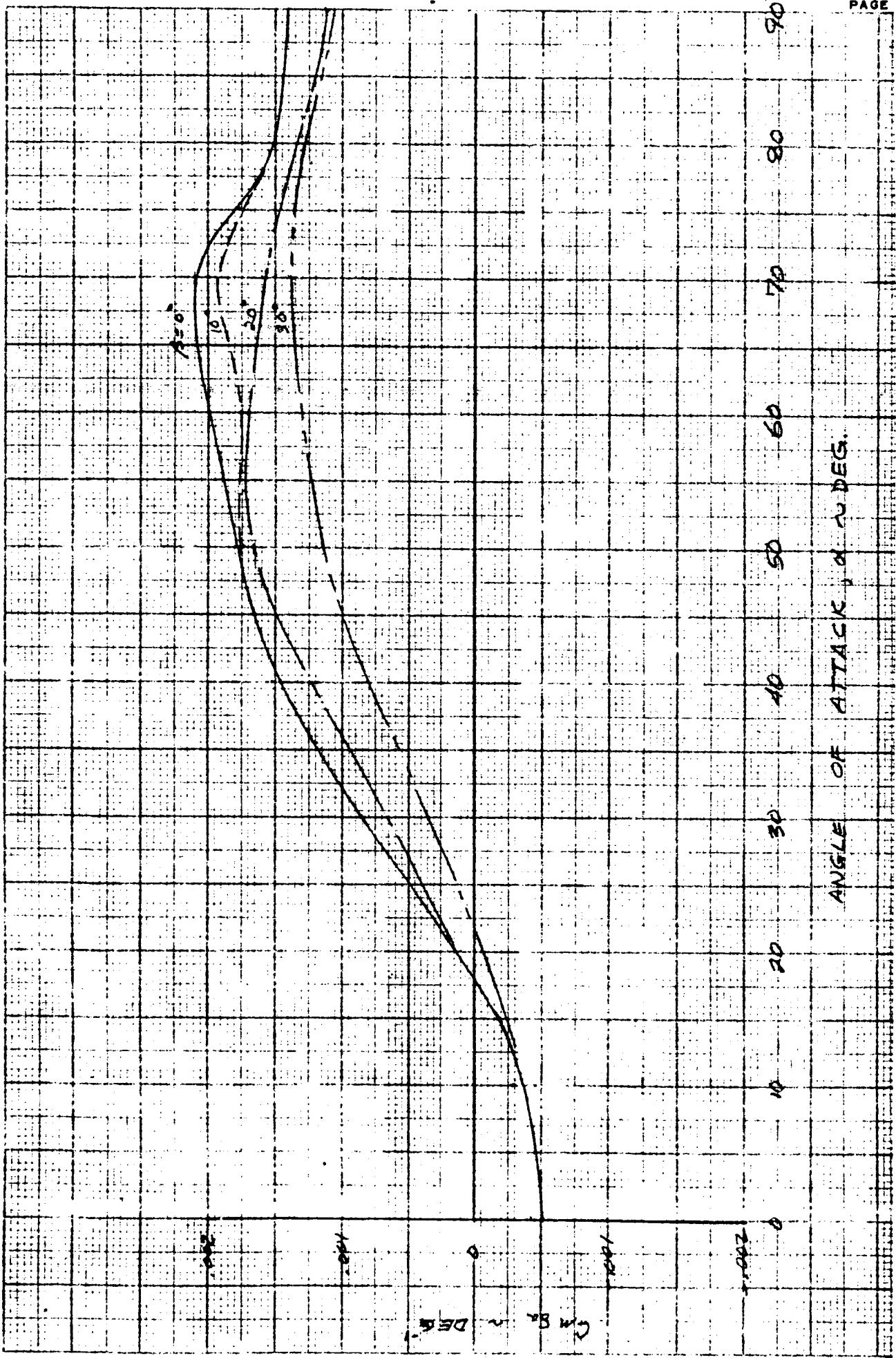


Figure C-14. - Continued.

c) C_{y6a} ANGLE OF ATTACK, α DEGREES100
80
60
40
20
010
20
30
40
50
60
70
80
900
-0.06
-0.04
-0.02-0.02
0
0.02
0.04

-150 ~ 150

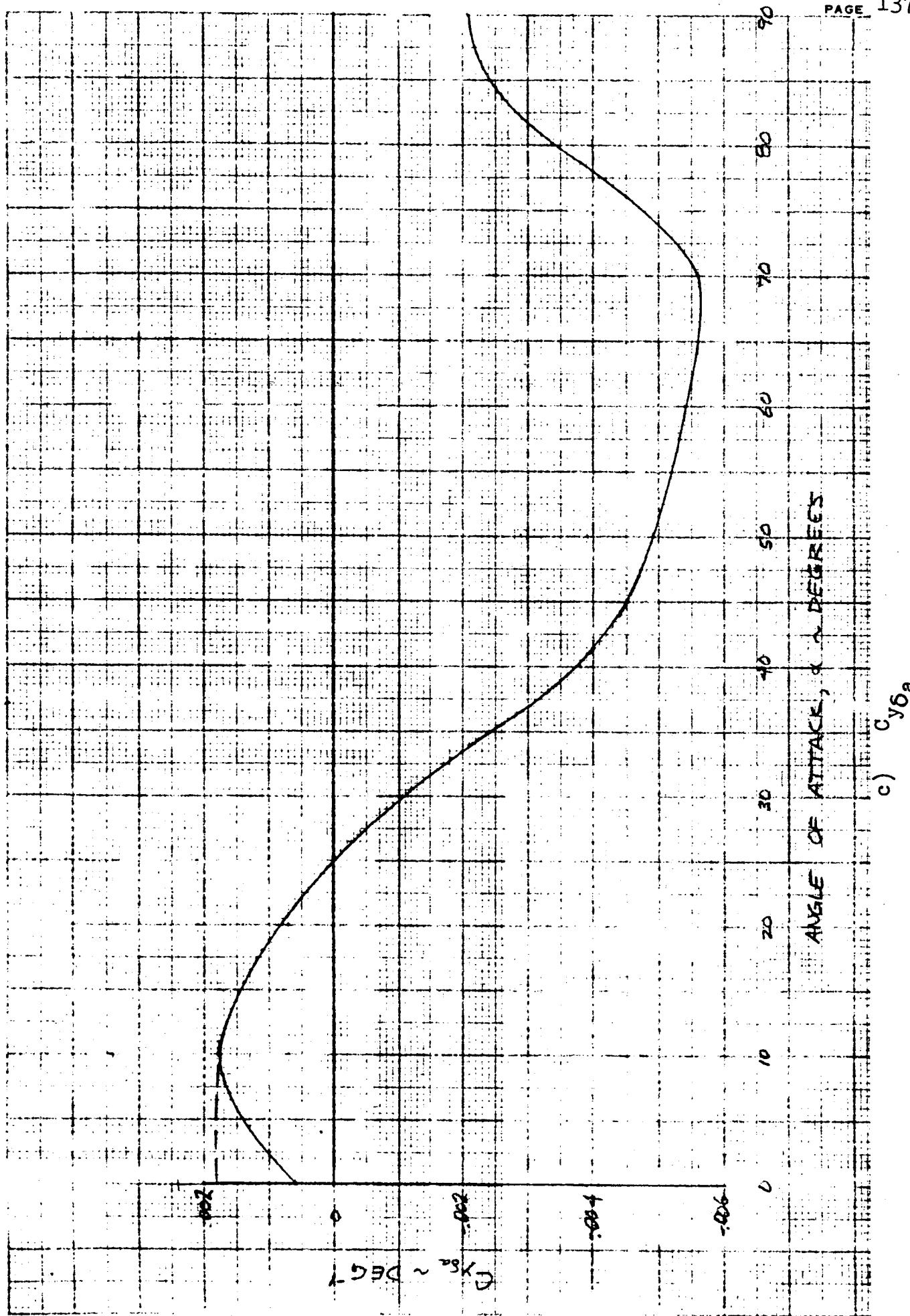


Figure C-14. - Concluded.

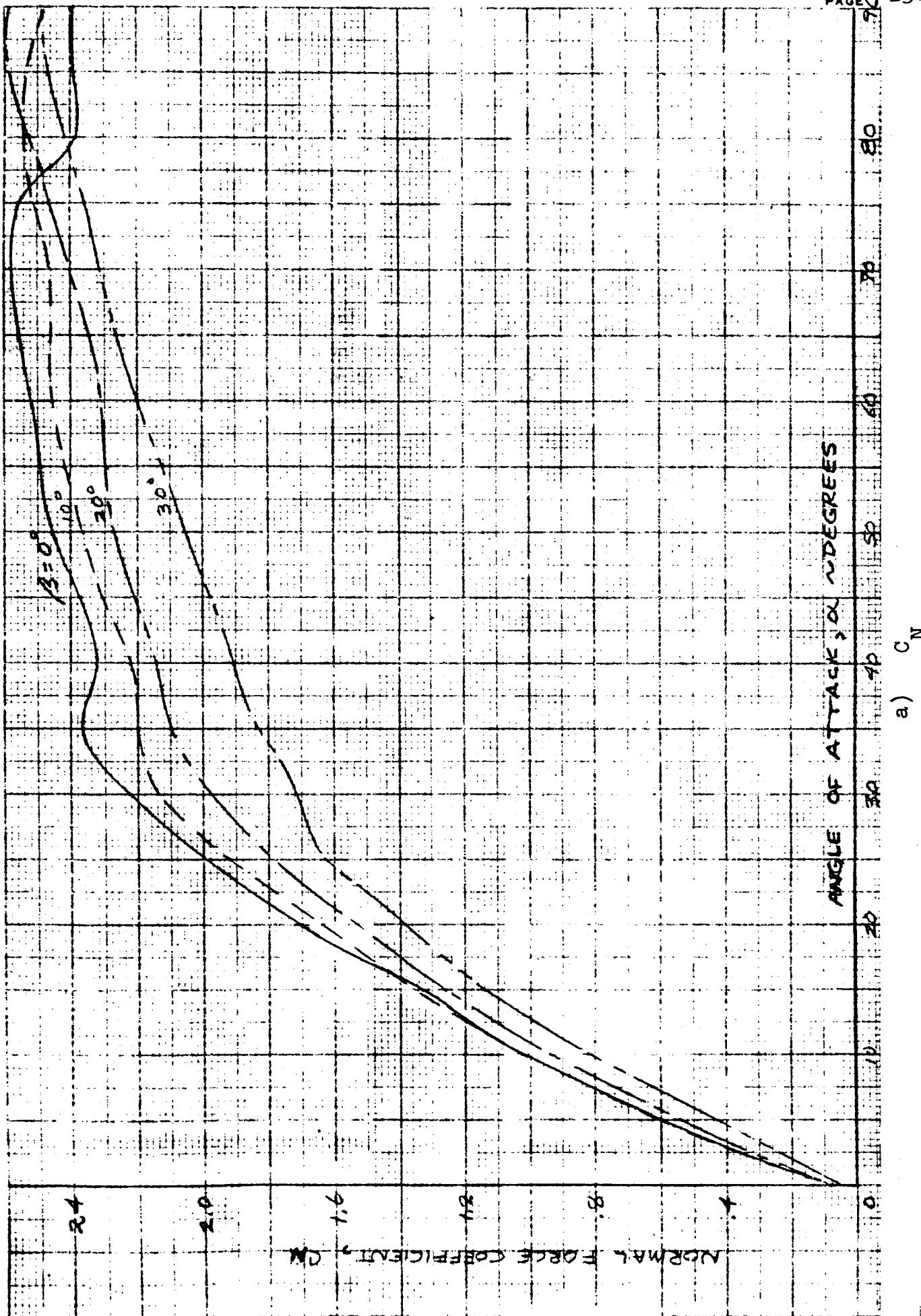


Figure C-15. - Effect of angle of attack and sideslip angle on force characteristics. $\Lambda = 22^\circ$.

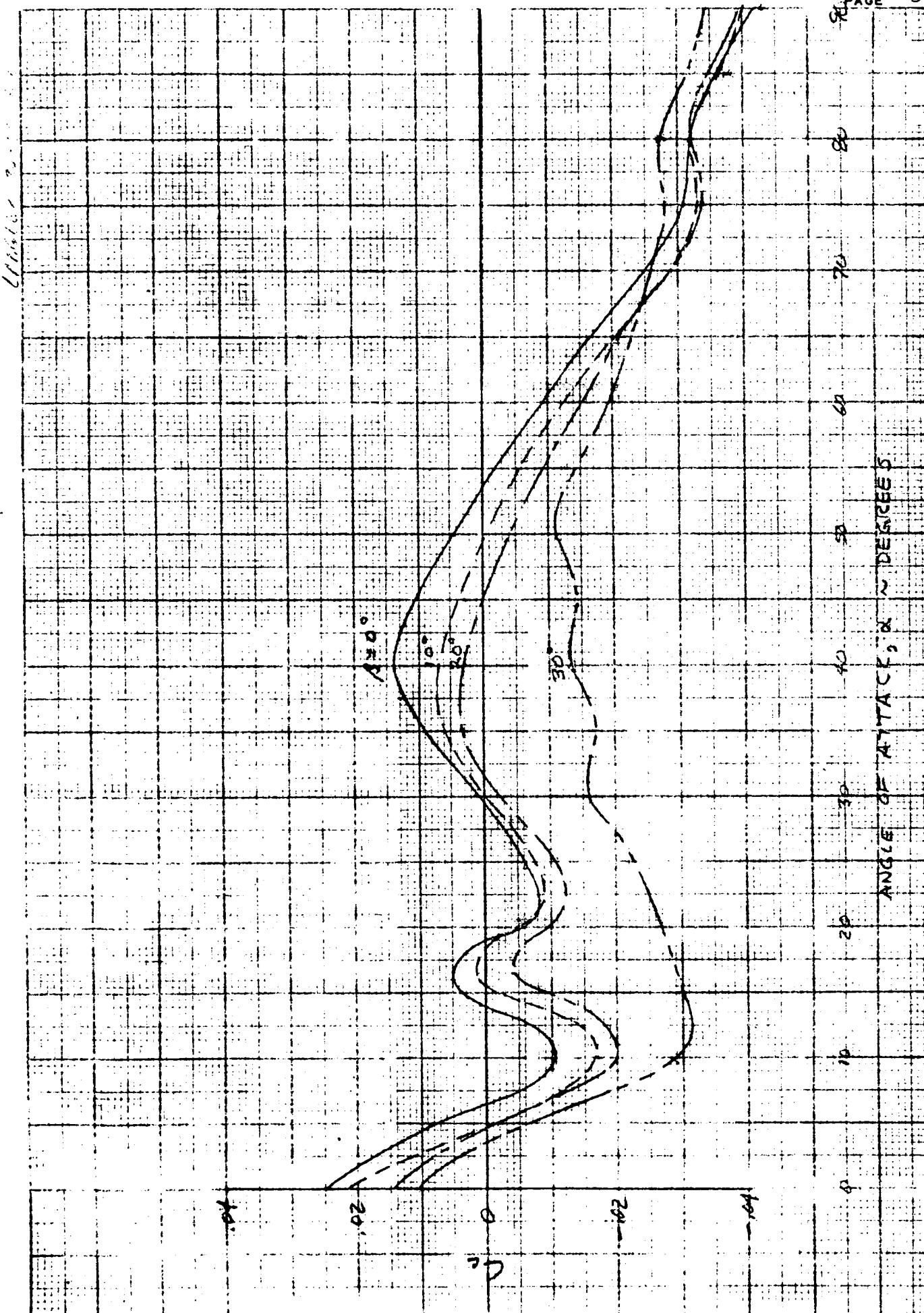
ANGLE OF ATTACK, α - DEGREESb) C_c 

Figure C-15. - Continued.

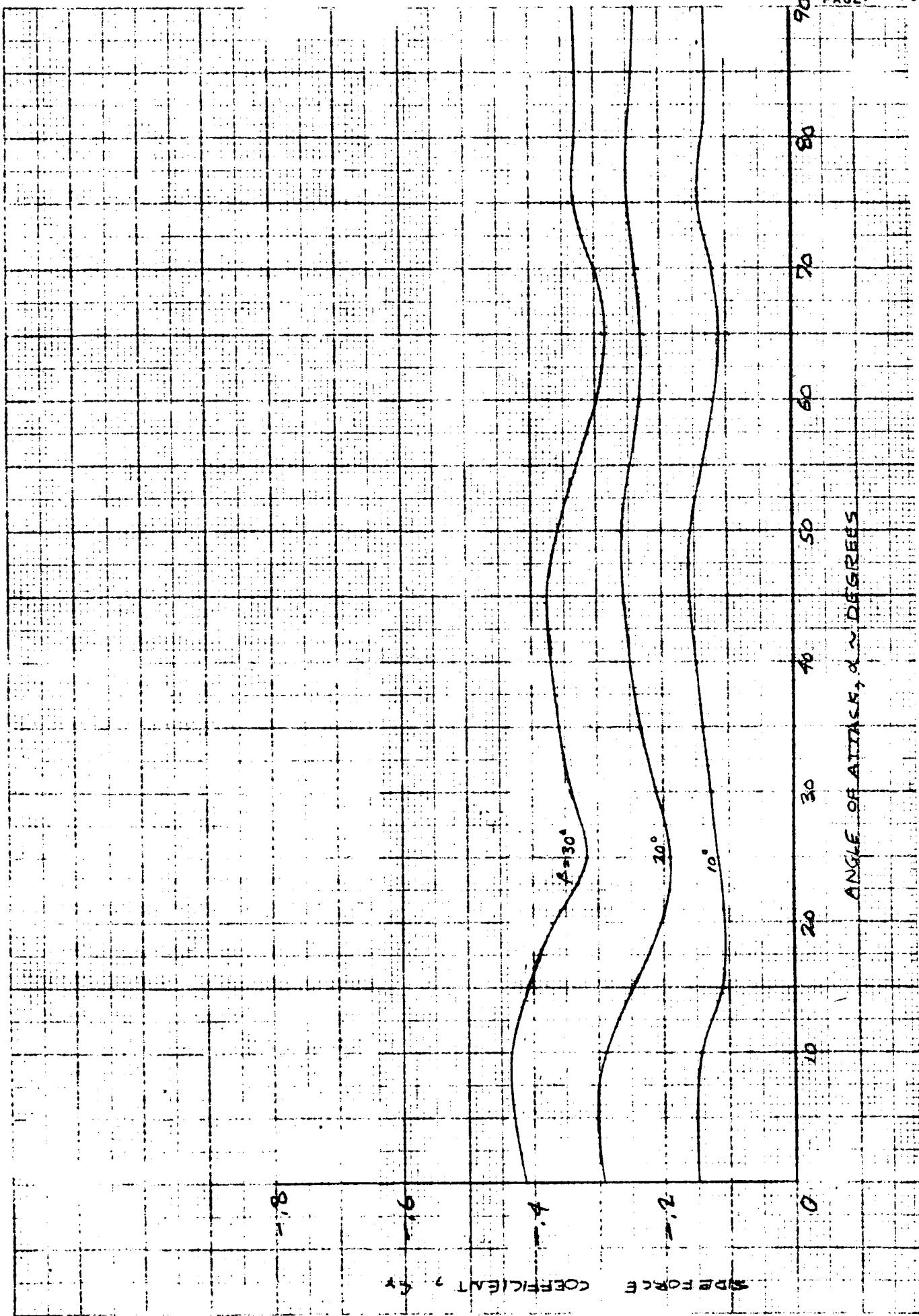


Figure C-15. - Concluded. -

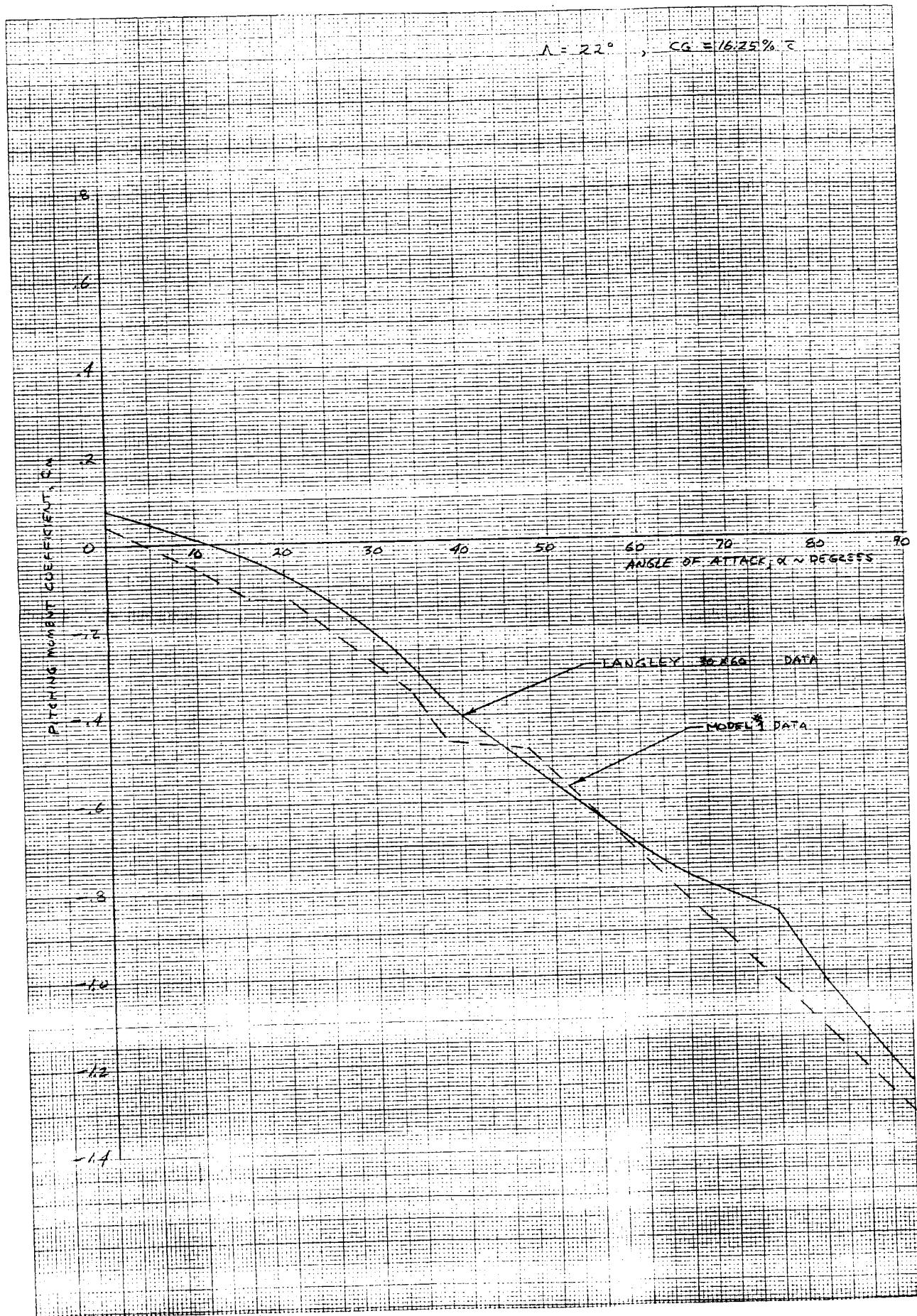


Figure C-16. - Effect of angle of attack on pitching-moment coefficient; $i_s = 0^\circ$. $\lambda = 22^\circ$.

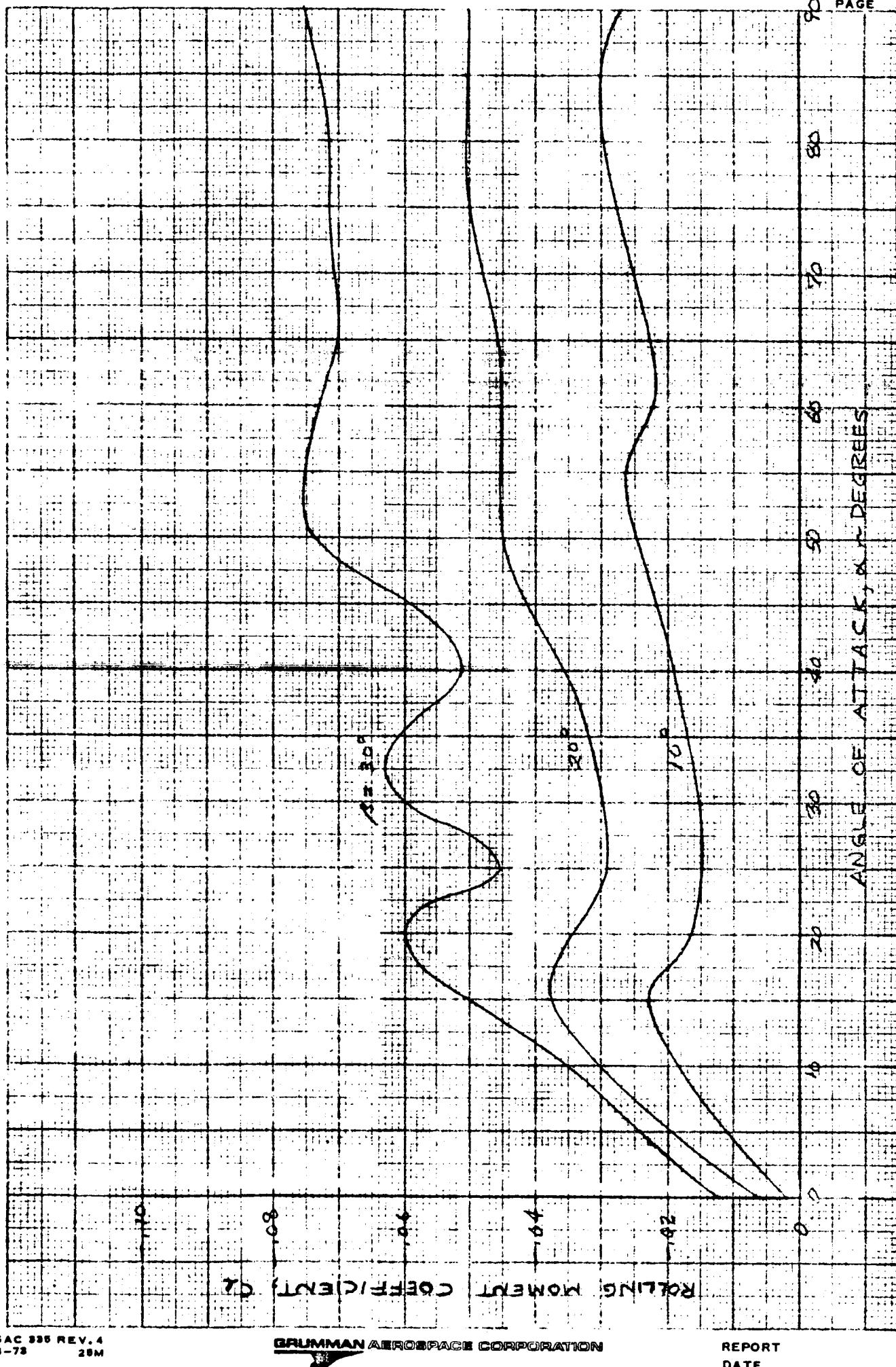


Figure C-17. - Effect of angle of attack and longitudinal-control deflection on rolling-moment coefficient. Λ = 220.

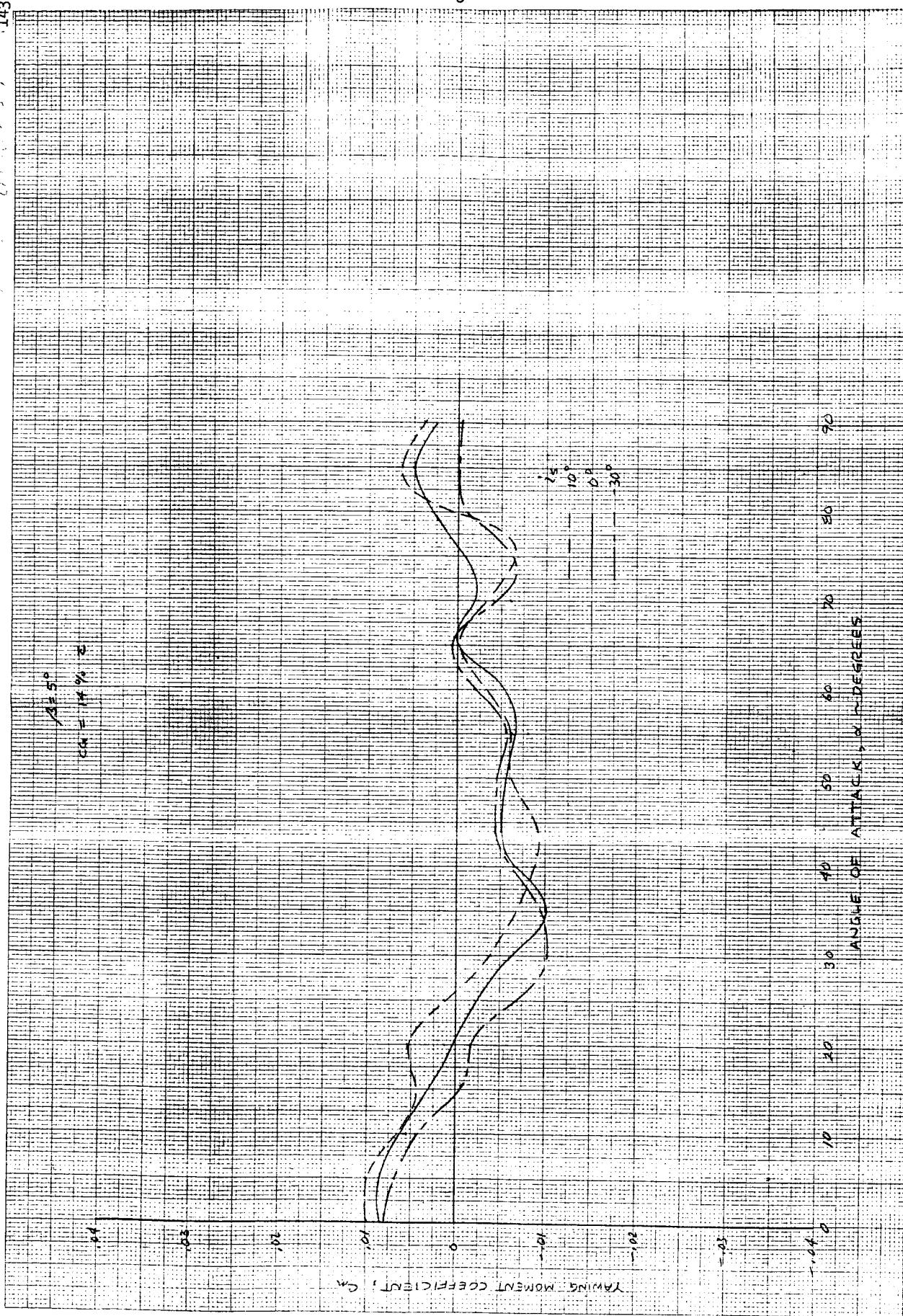
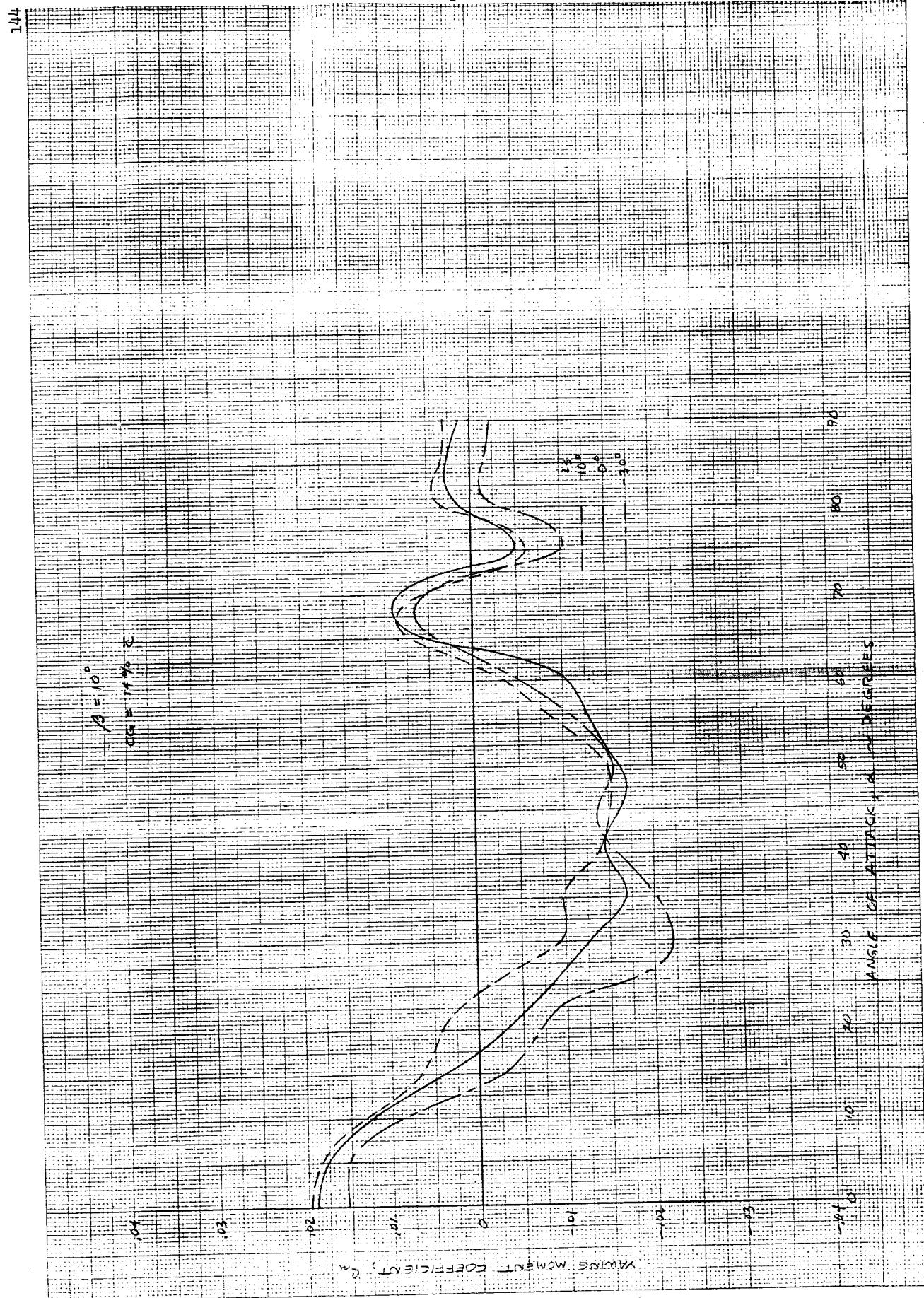
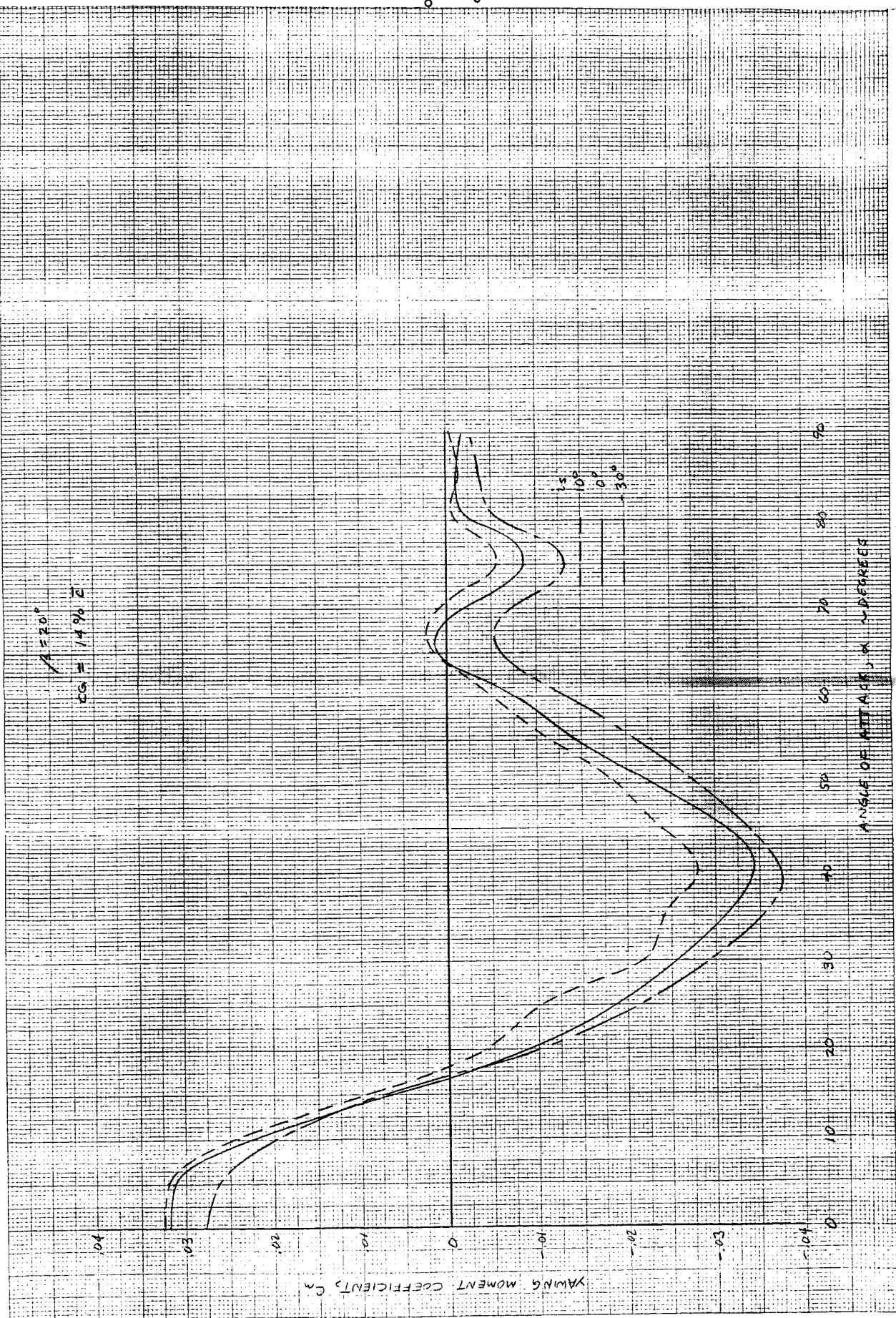


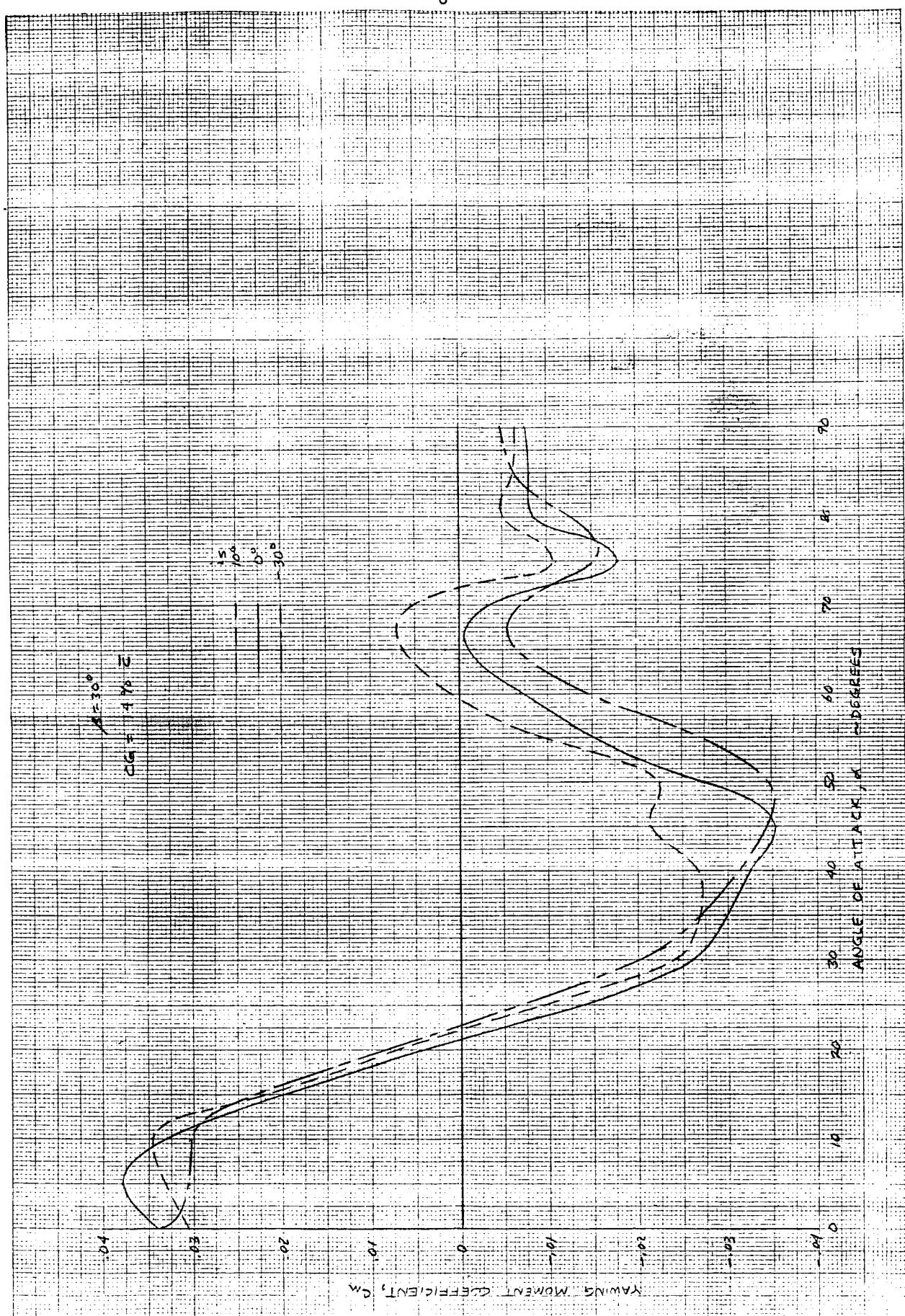
FIGURE C-18. - Continued.

b) $\beta = 10^\circ$



$$c) \quad \beta = 20^\circ$$



d) $\beta = 30^\circ$ 

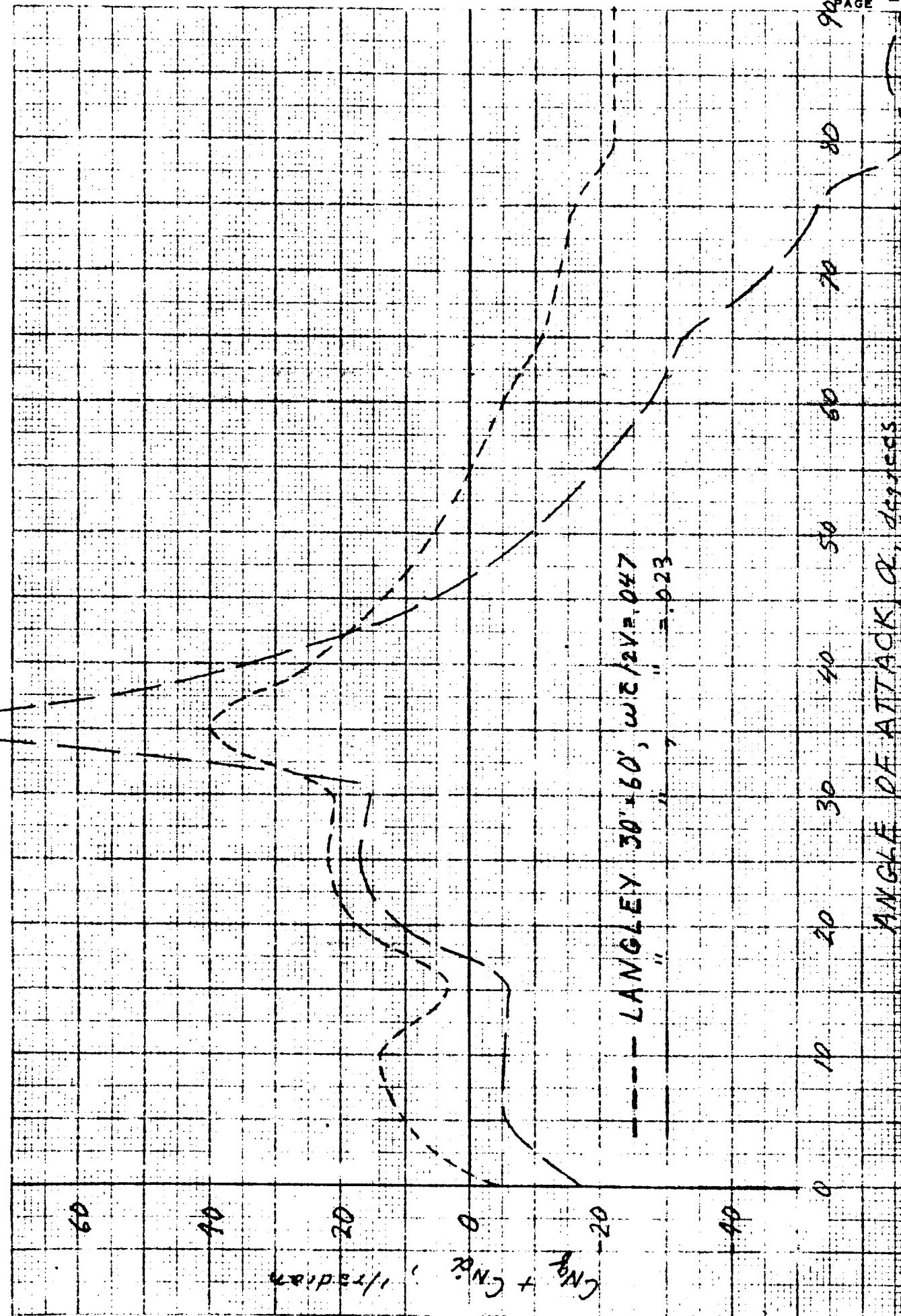


Figure C-19. - Effect of angle of attack and forced-oscillation frequency on normal-force coefficient due to pitch rate. $\lambda = 22$.

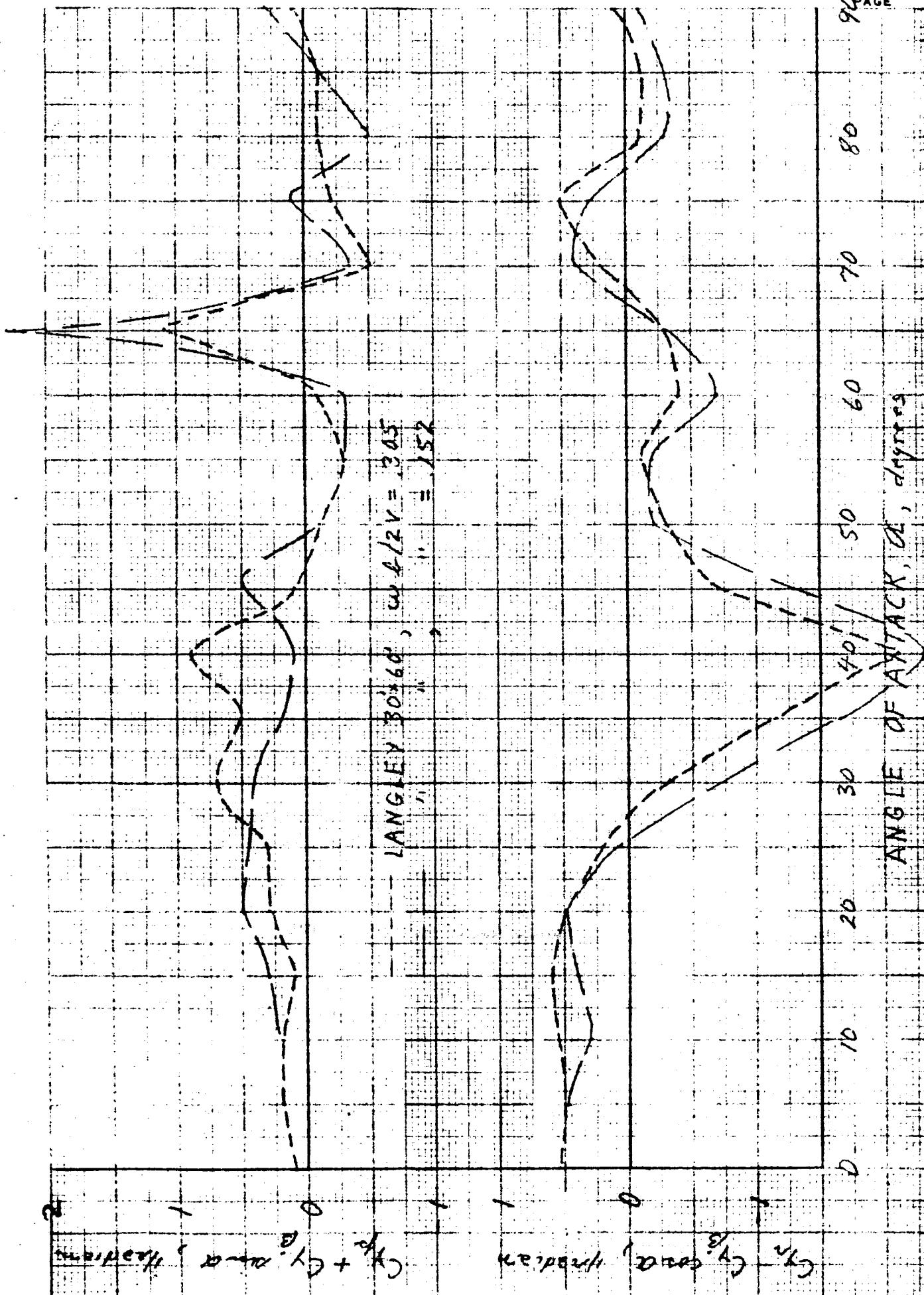


Figure C-20. - Effect of angle of attack and forced-oscillation frequency on side-force coefficient due to roll and yaw rate. $\Lambda = 22^\circ$.

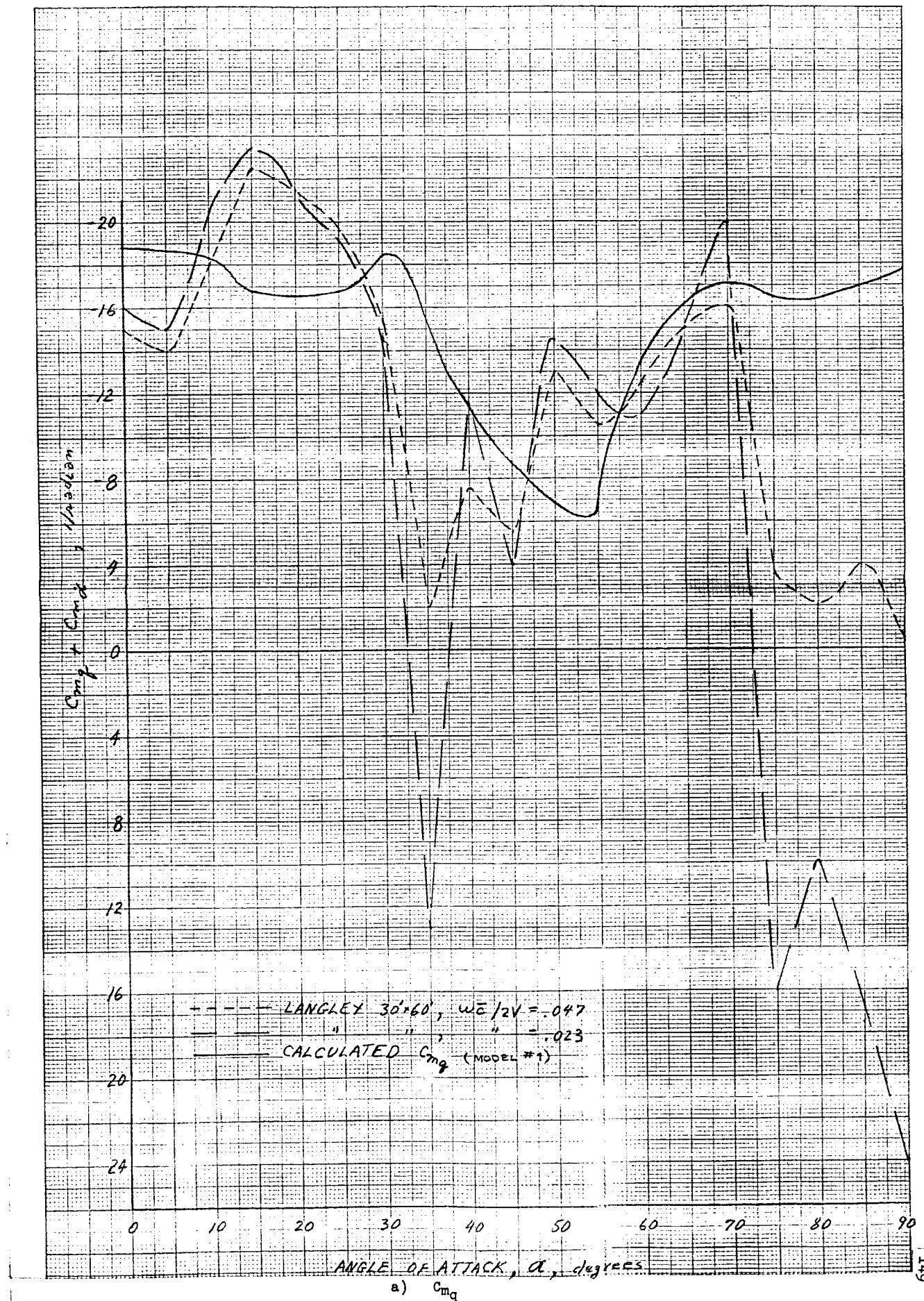
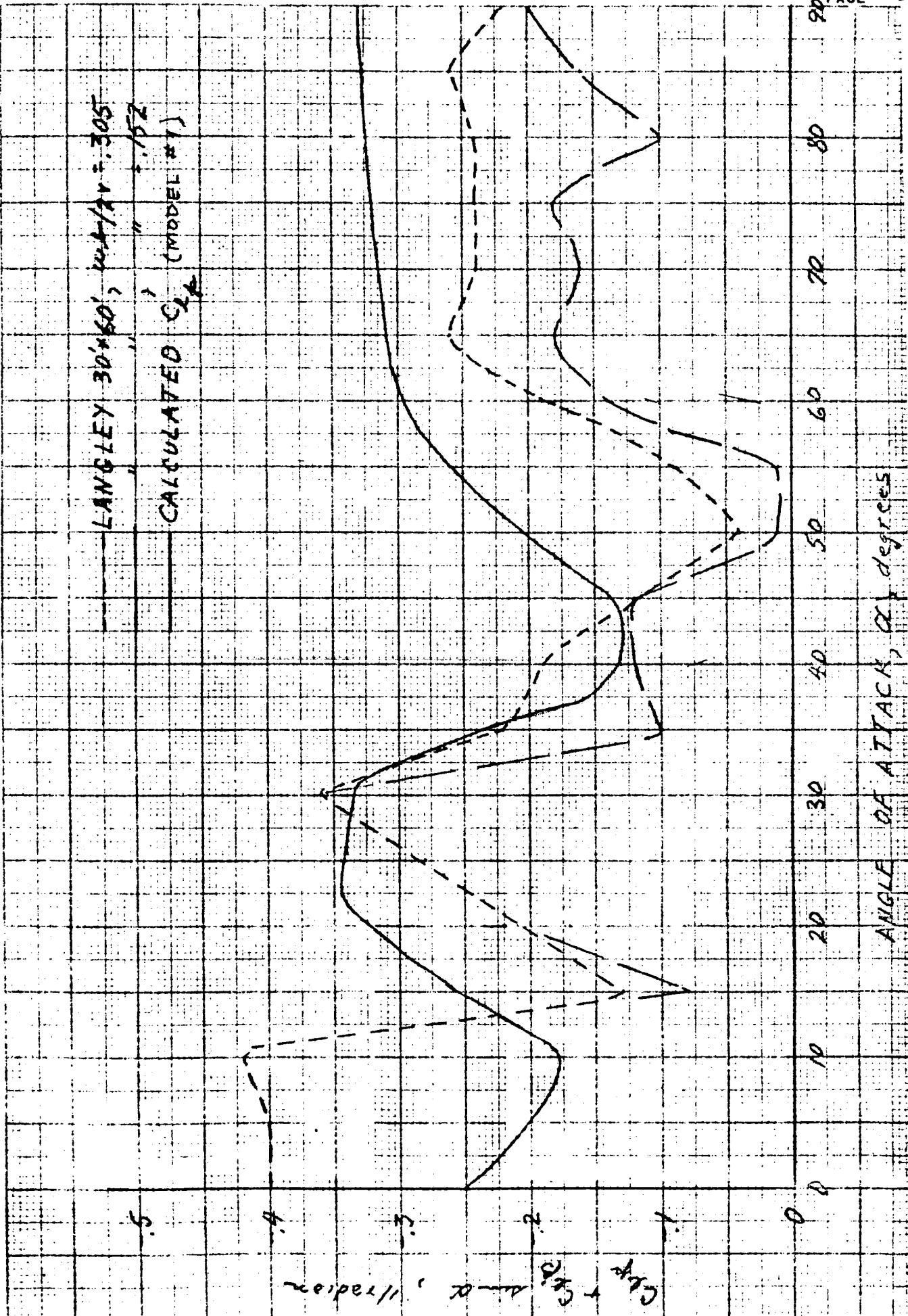


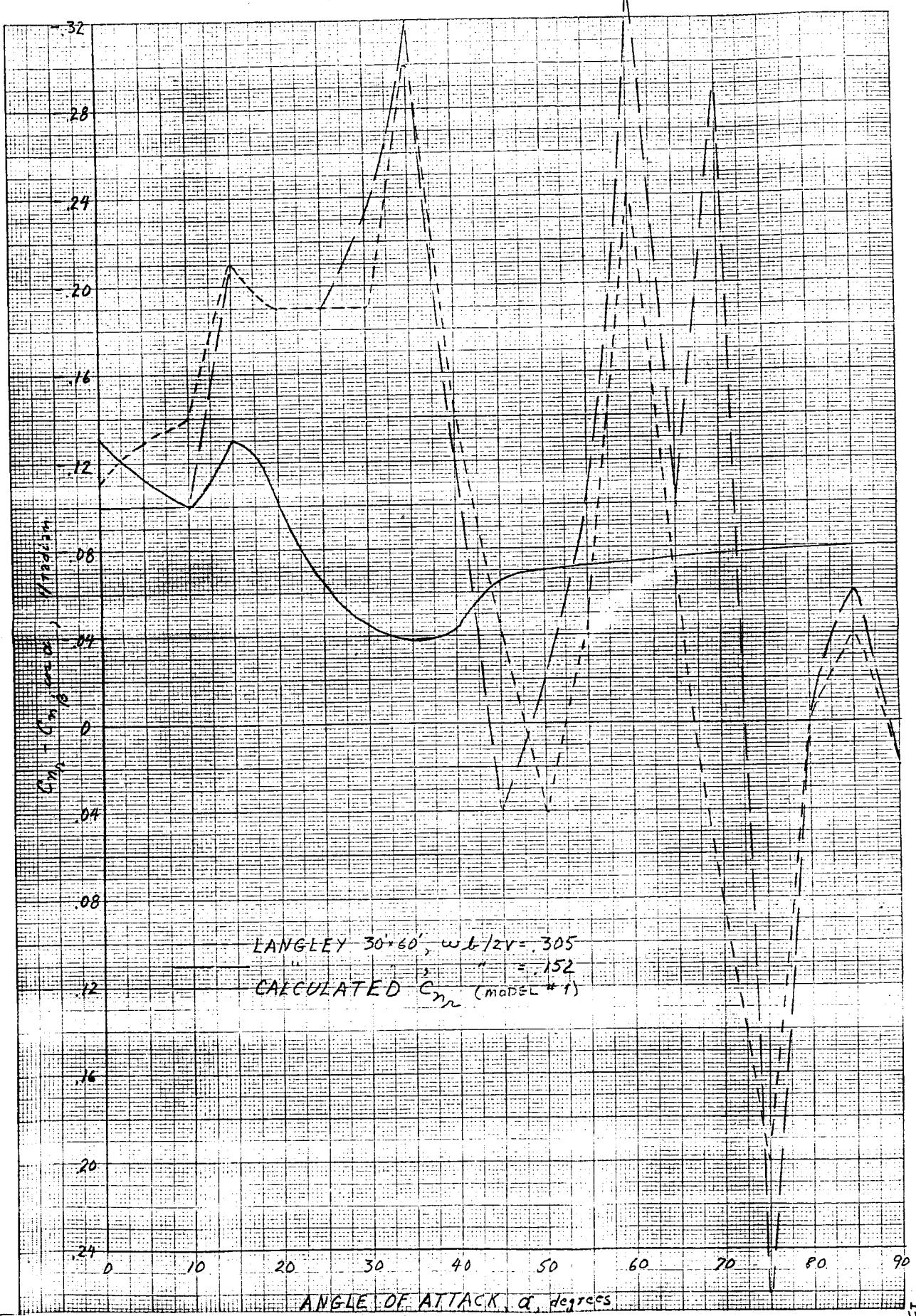
Figure C-21. - Effect of angle of attack and forced-oscillation frequency on damping derivatives. $\Lambda = 22^\circ$.

CALCULATED C₂ (MODEL #1)



b) C_2

Figure C-21: - Continued:



c) C_{n_r}
Figure C-21. - Concluded.

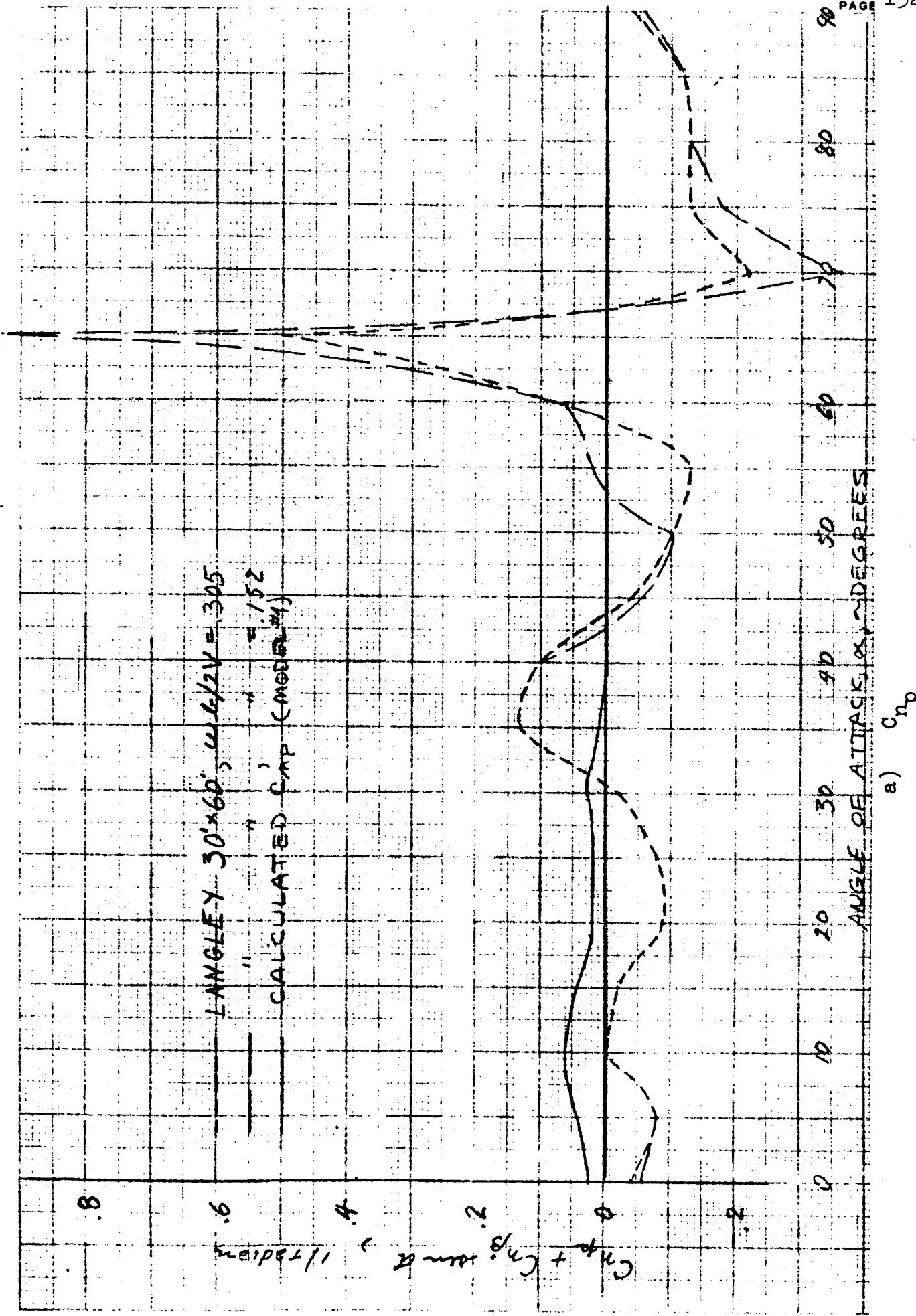
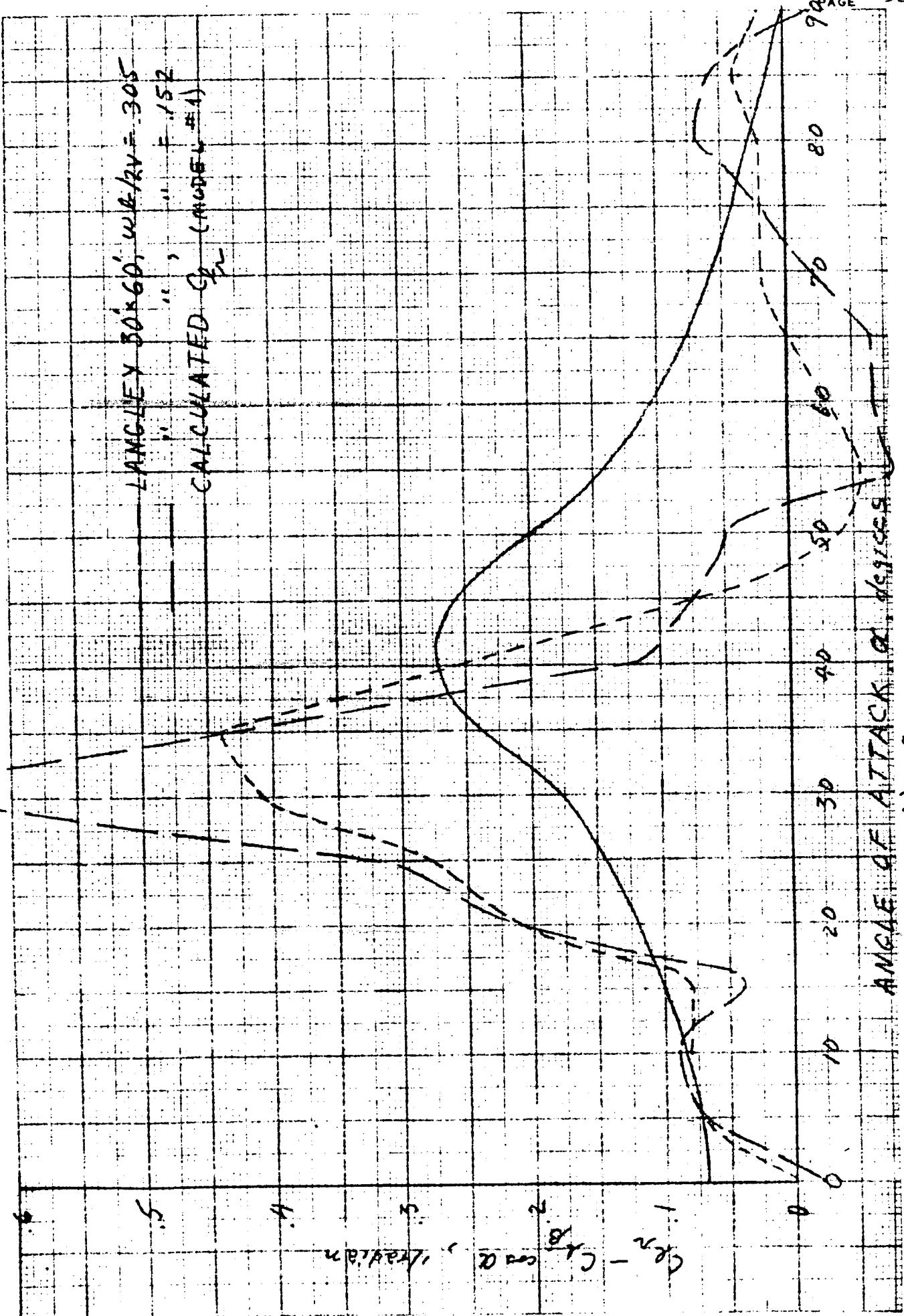
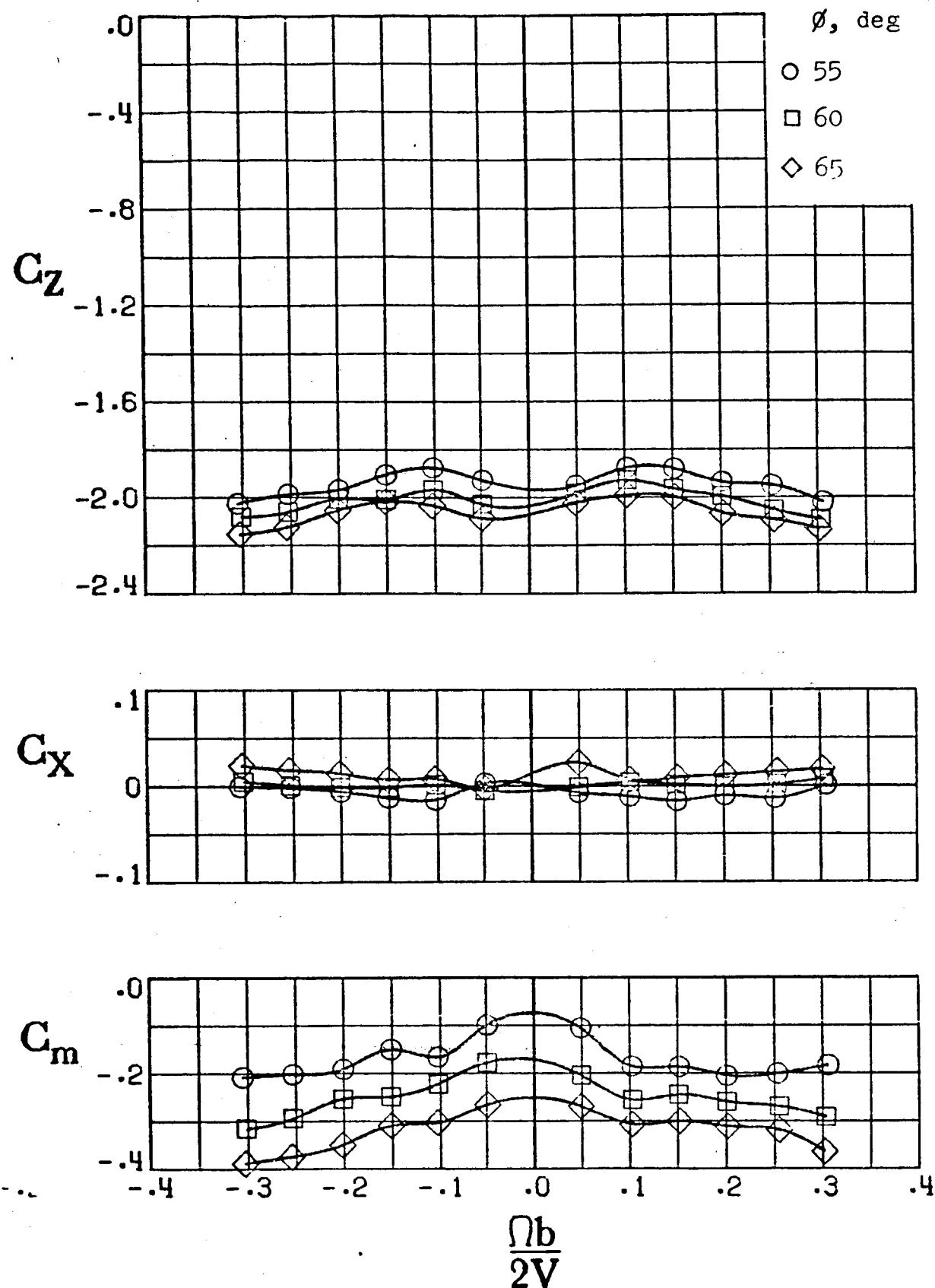


Figure C-22. - Effect of angle of attack and forced-oscillation frequency on cross derivatives.
 $\lambda = 220$

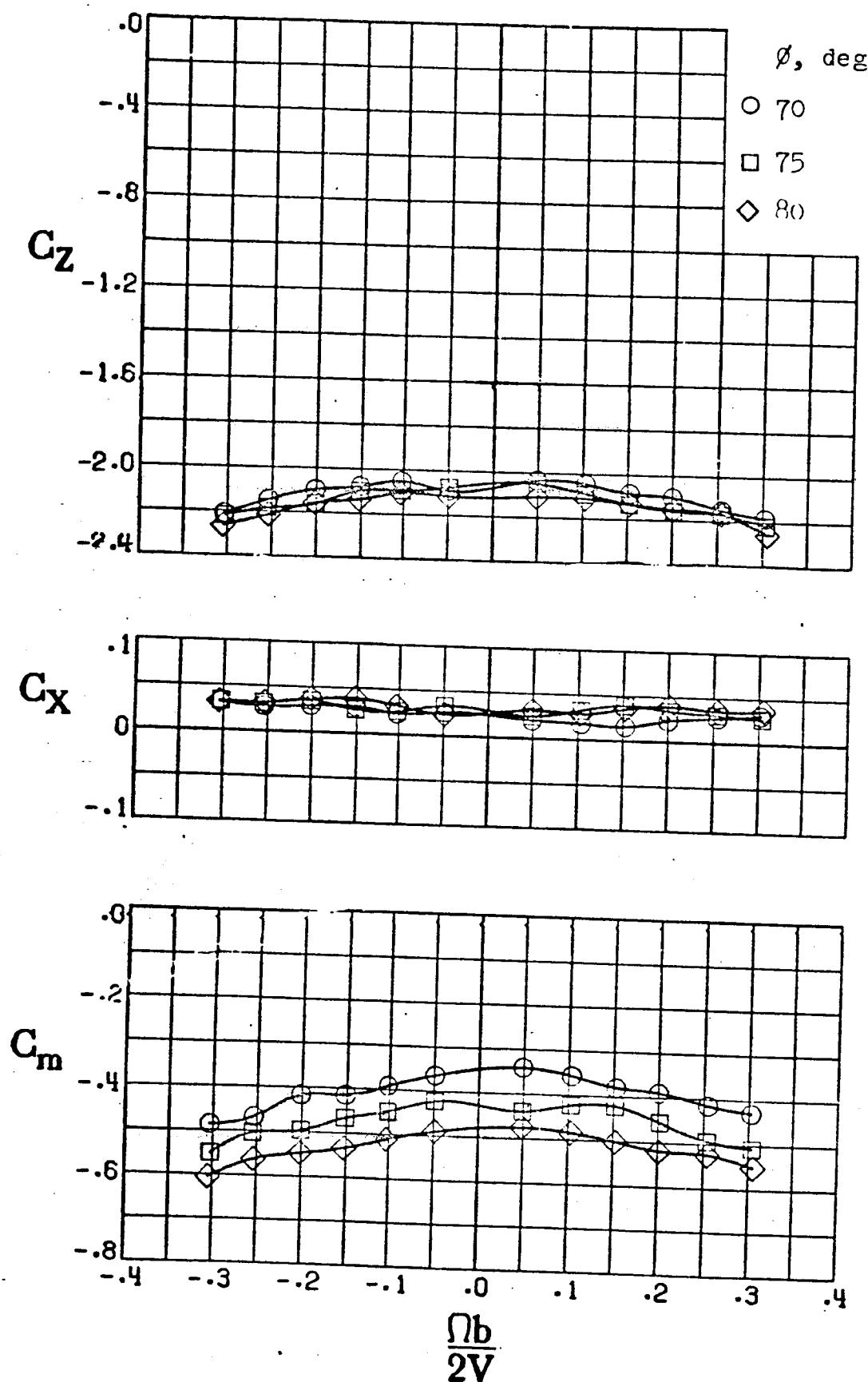
LANCEY 80' x 60', 102.424 = 305
CALCULATED Q_s (MUSEUM) 152





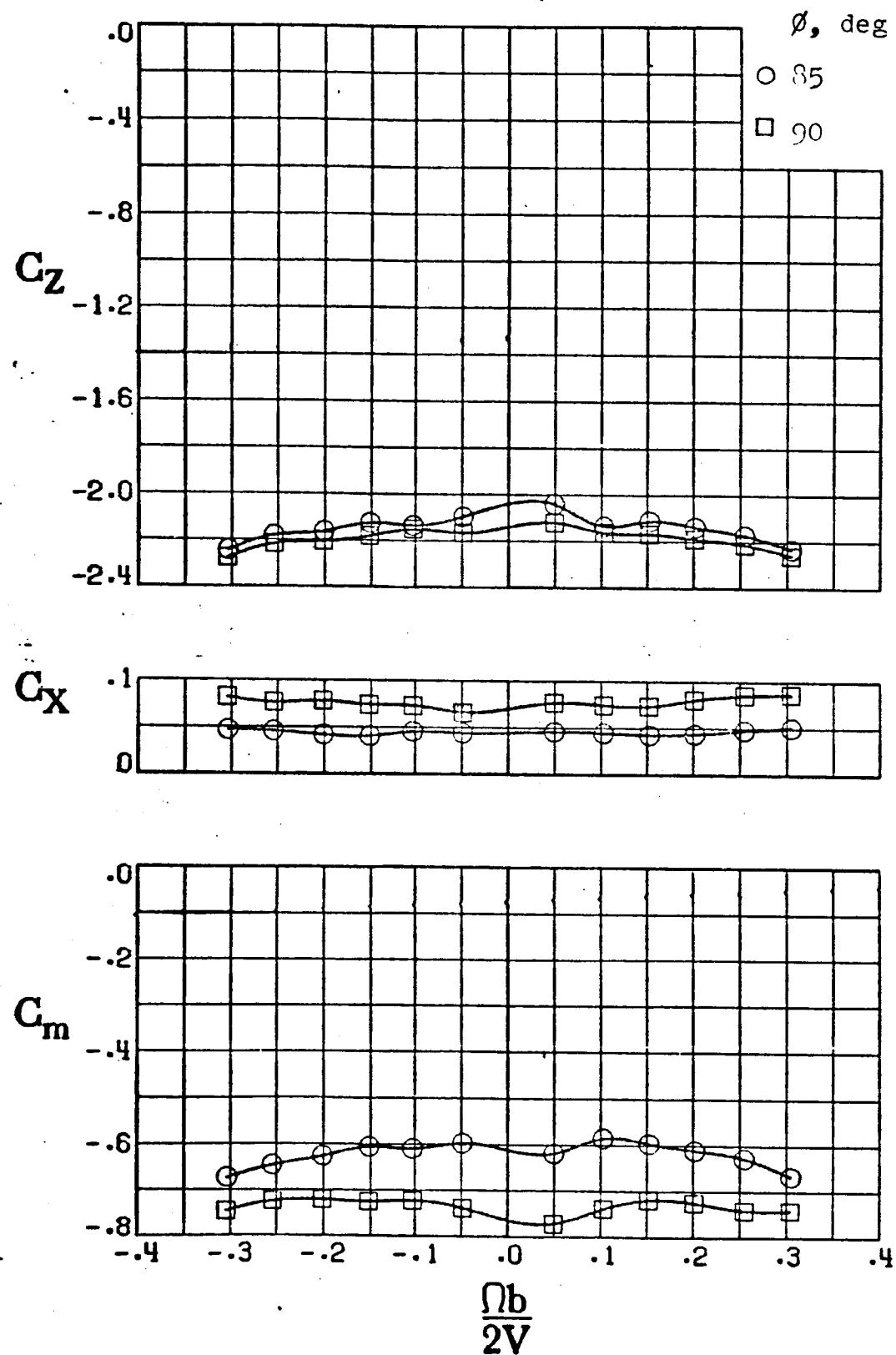
a) $\phi = 0^\circ$, $\theta = 55, 60, 65^\circ$

Figure C-23. - Effect of rotation rate and pitch and roll attitude angles on the longitudinal coefficients for all neutral controls. $\Lambda = 22^\circ$.



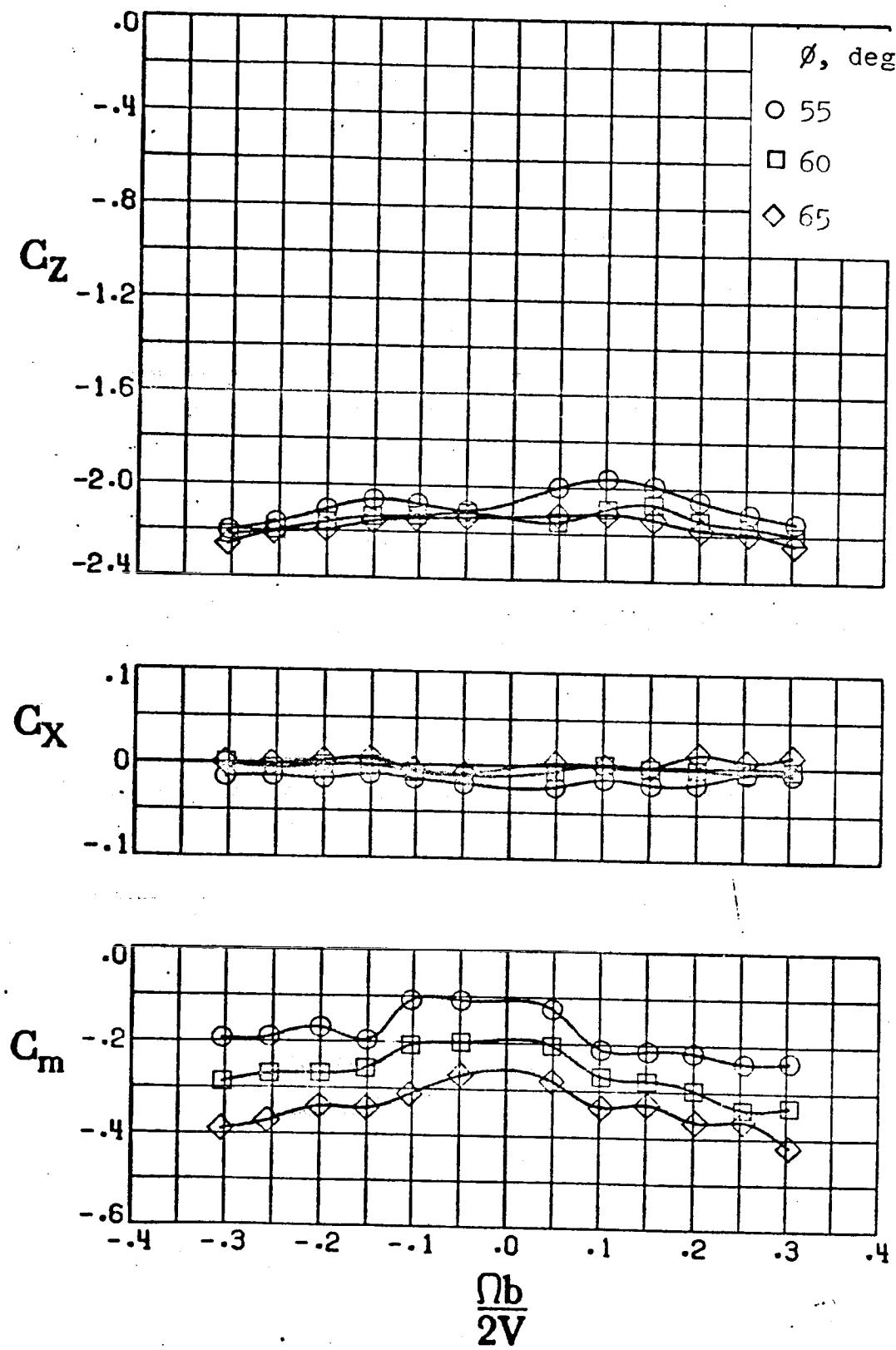
b) $\phi = 0^\circ$, $\theta = 70^\circ, 75^\circ, 80^\circ$

Figure C-23. - Continued.



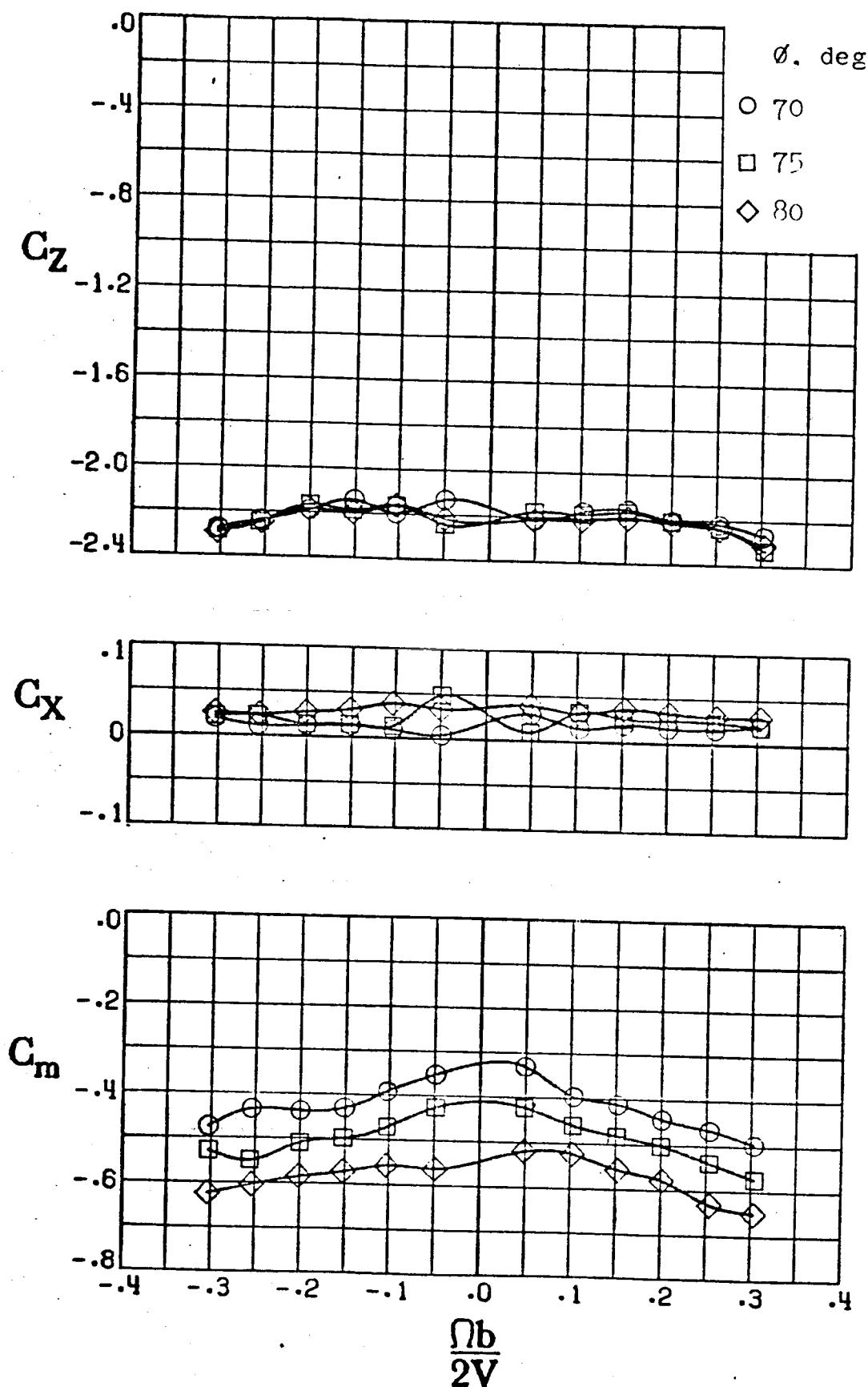
c) $\phi = 0^\circ$, $\theta = 85^\circ, 90^\circ$

Figure C-23. - Continued.



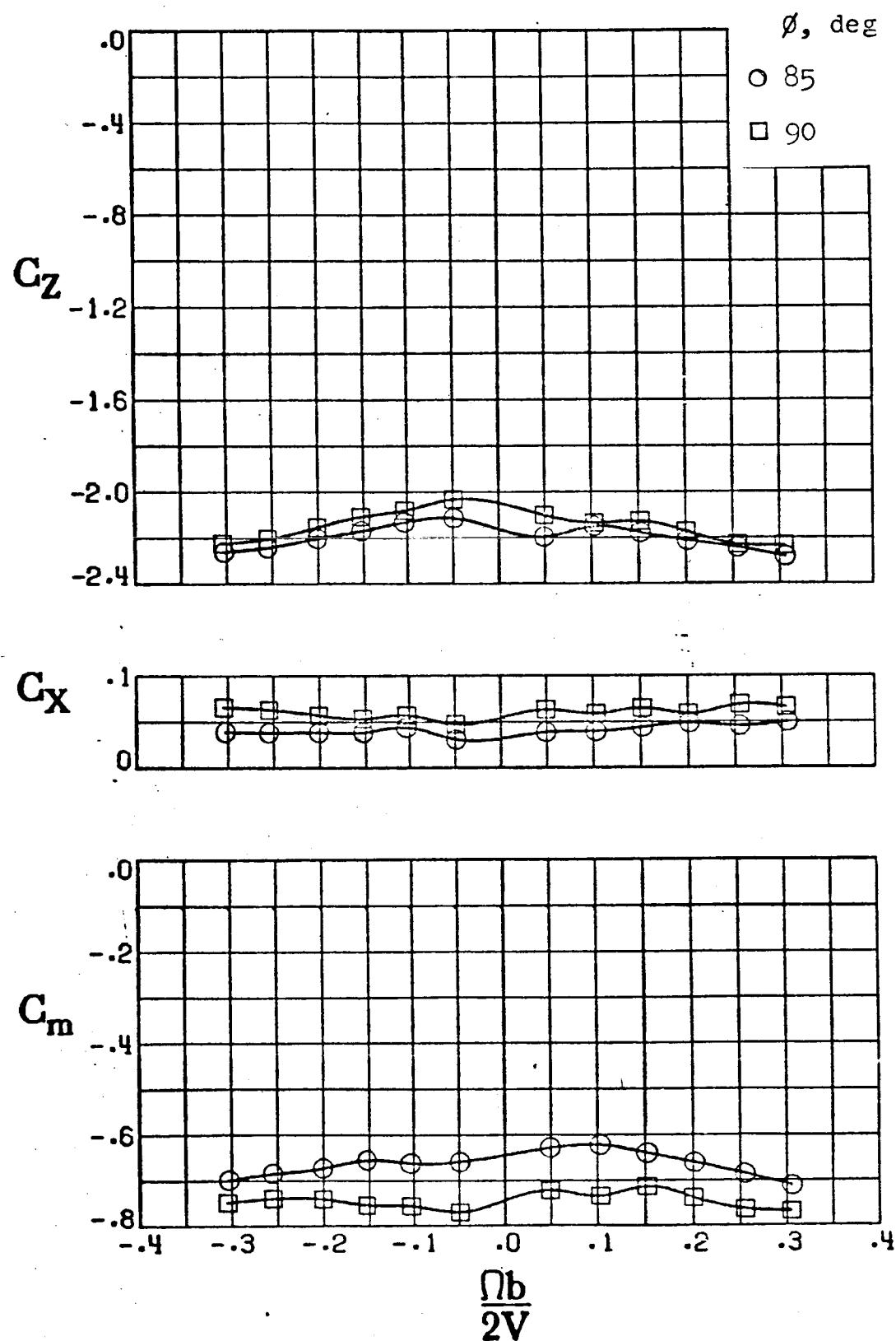
d) $\phi = 5^\circ$, $\theta = 55^\circ$, 60° , and 65°

Figure C-23. - Continued.



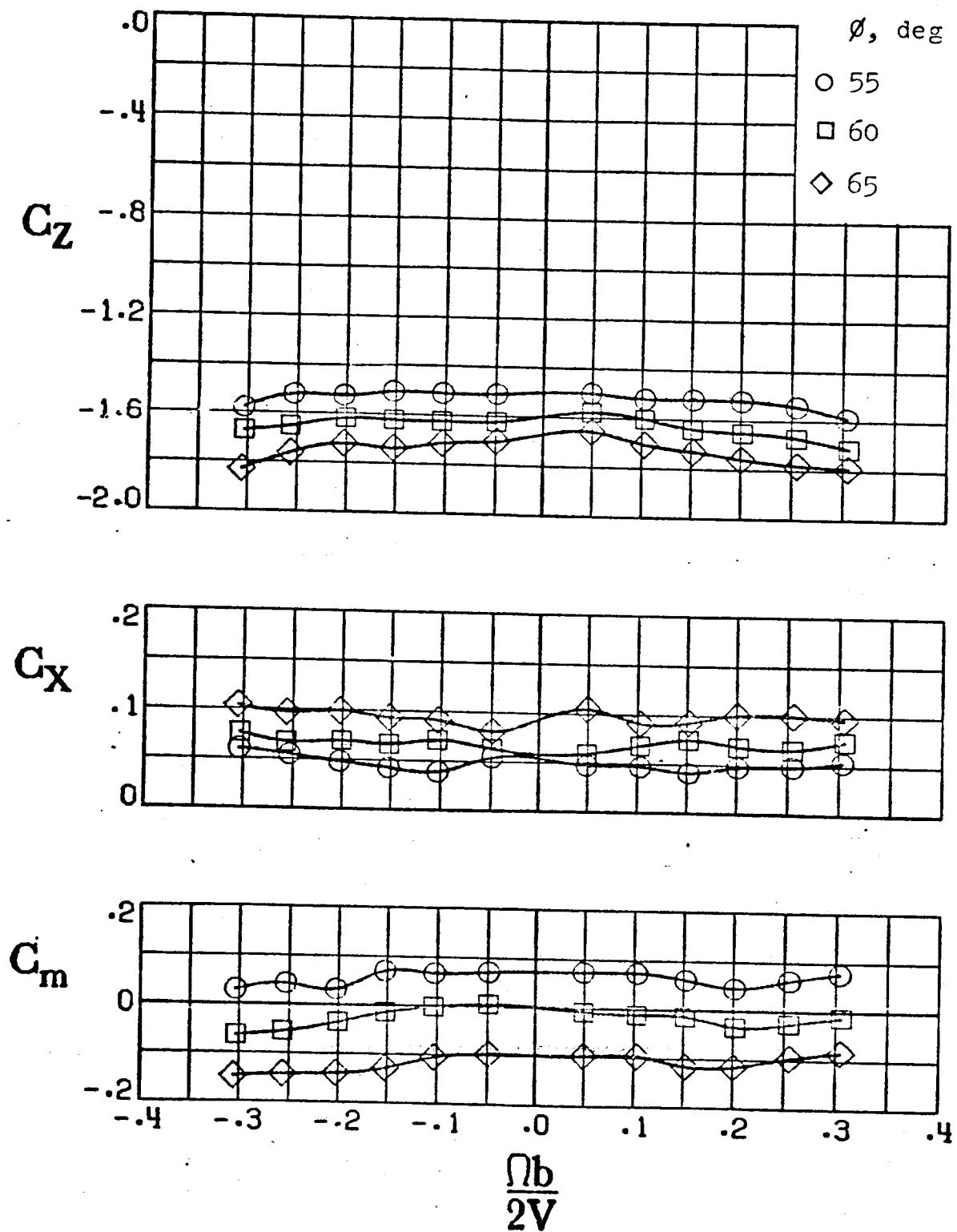
e) $\phi = 5^\circ$, $\theta = 70, 75$, and 80°

Figure C-23. - Continued.



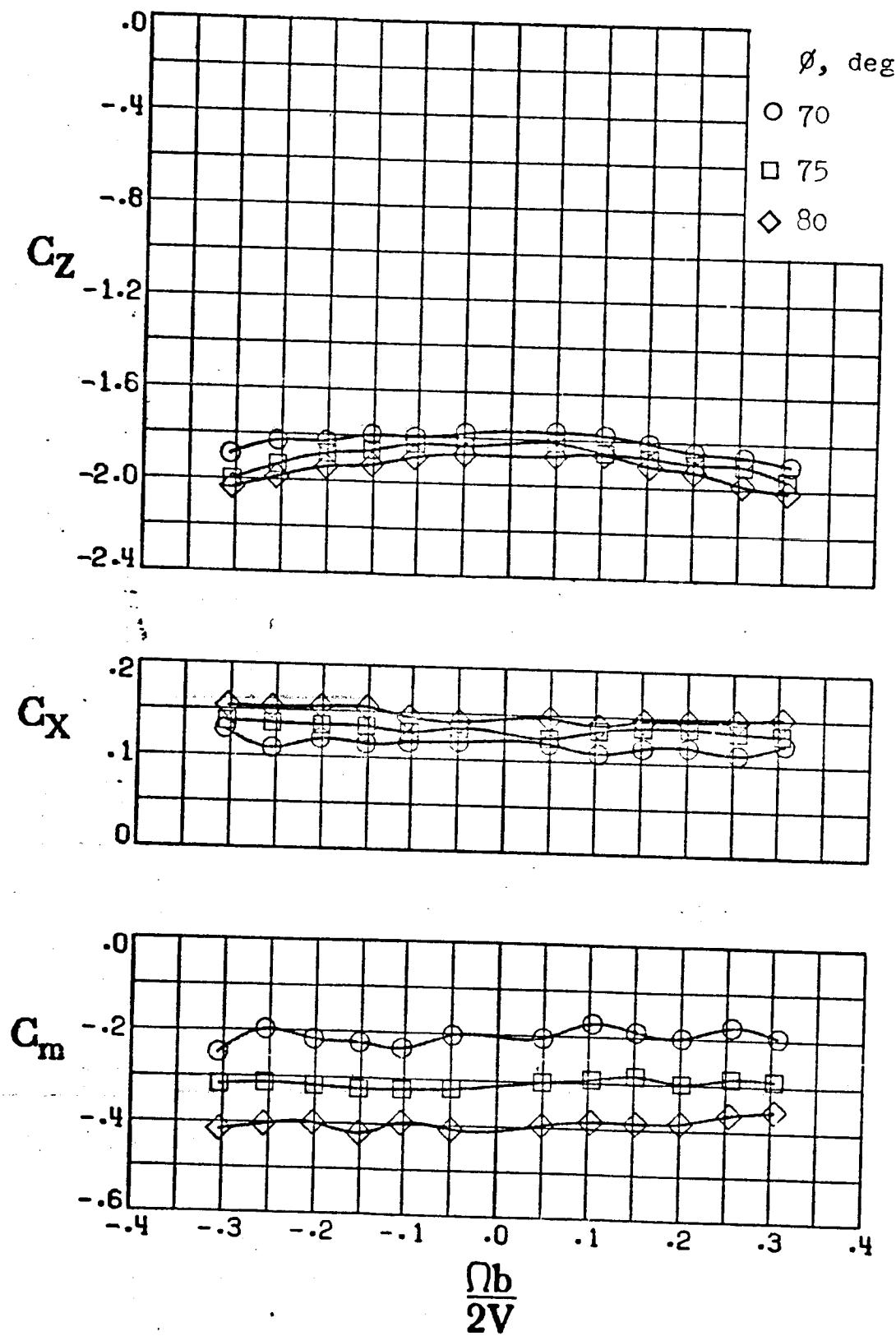
f) $\phi = 5^\circ, \theta = 85$ and 90°

Figure C-23. - Concluded.



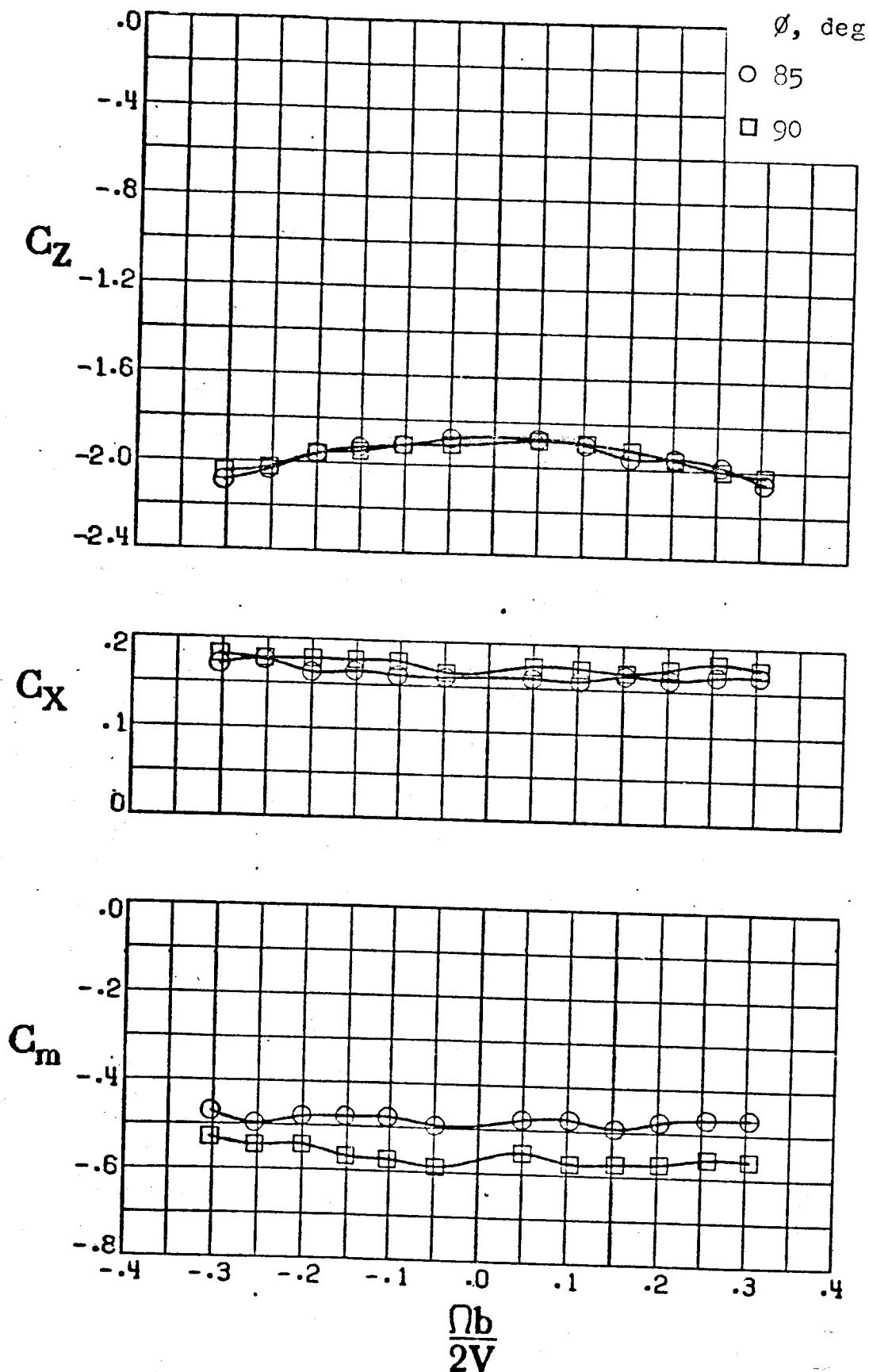
a) $\phi = 0^\circ, \theta = 55, 60, 65^\circ$

Figure C-24. - Effect of rotation rate and pitch and roll attitude angles on the longitudinal coefficients for $i_s = -30^\circ$. Lamda = 22



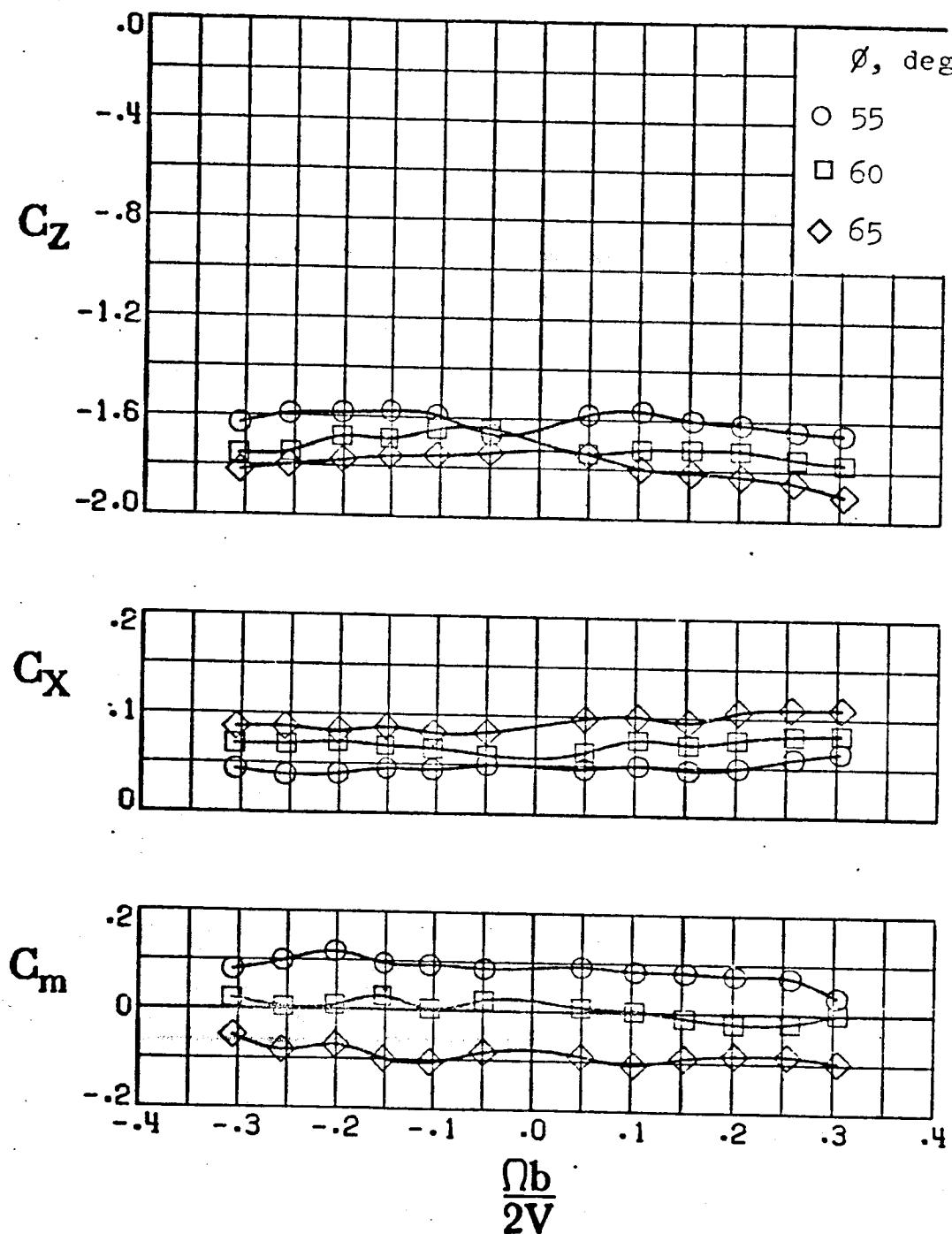
b) $\phi = 0^\circ$, $\theta = 70^\circ$, 75° and 80°

Figure C-24. - Continued.



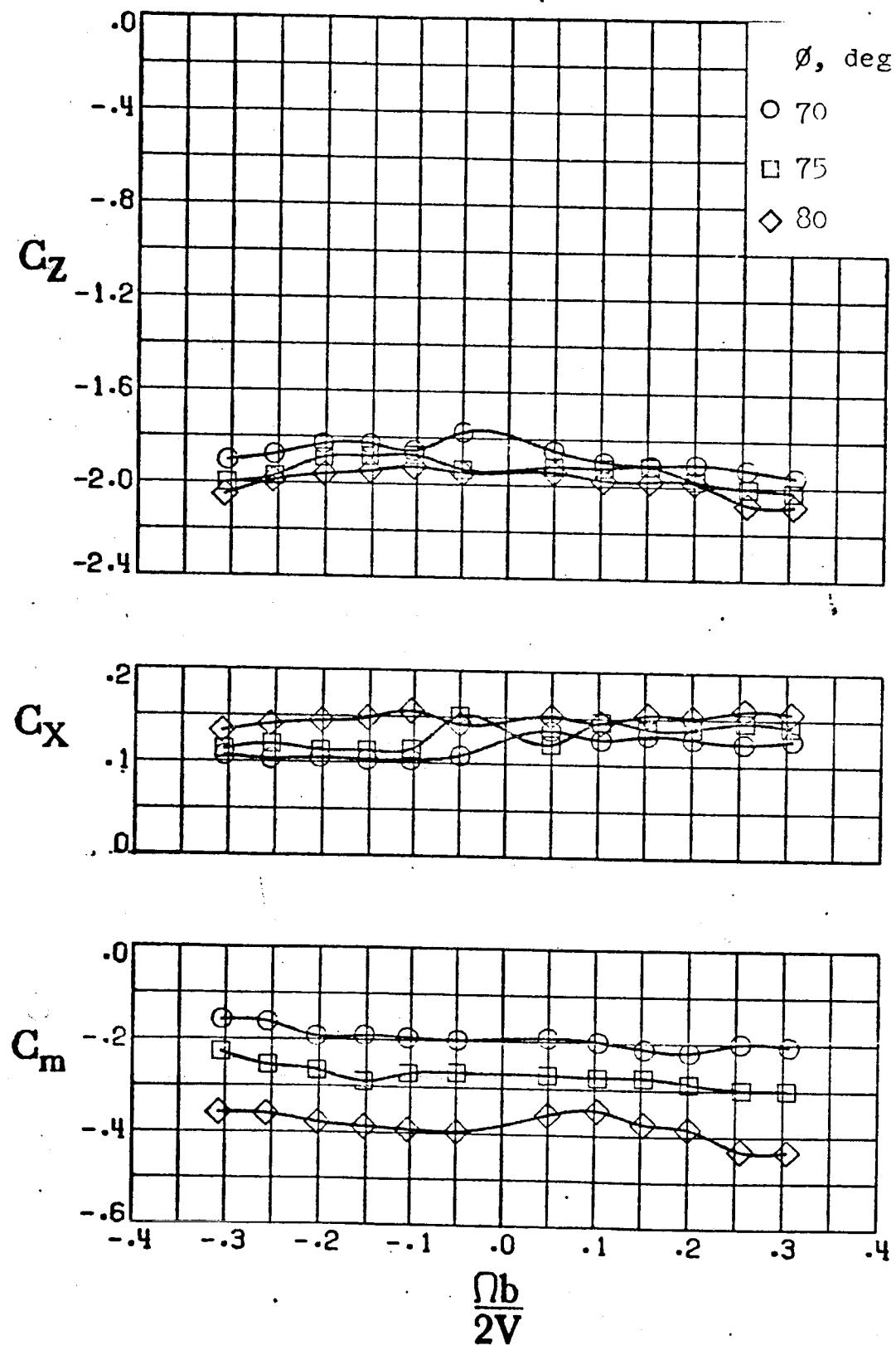
c) $\phi = 0^\circ, \theta = 85, 90^\circ$

Figure C-24. - Continued.



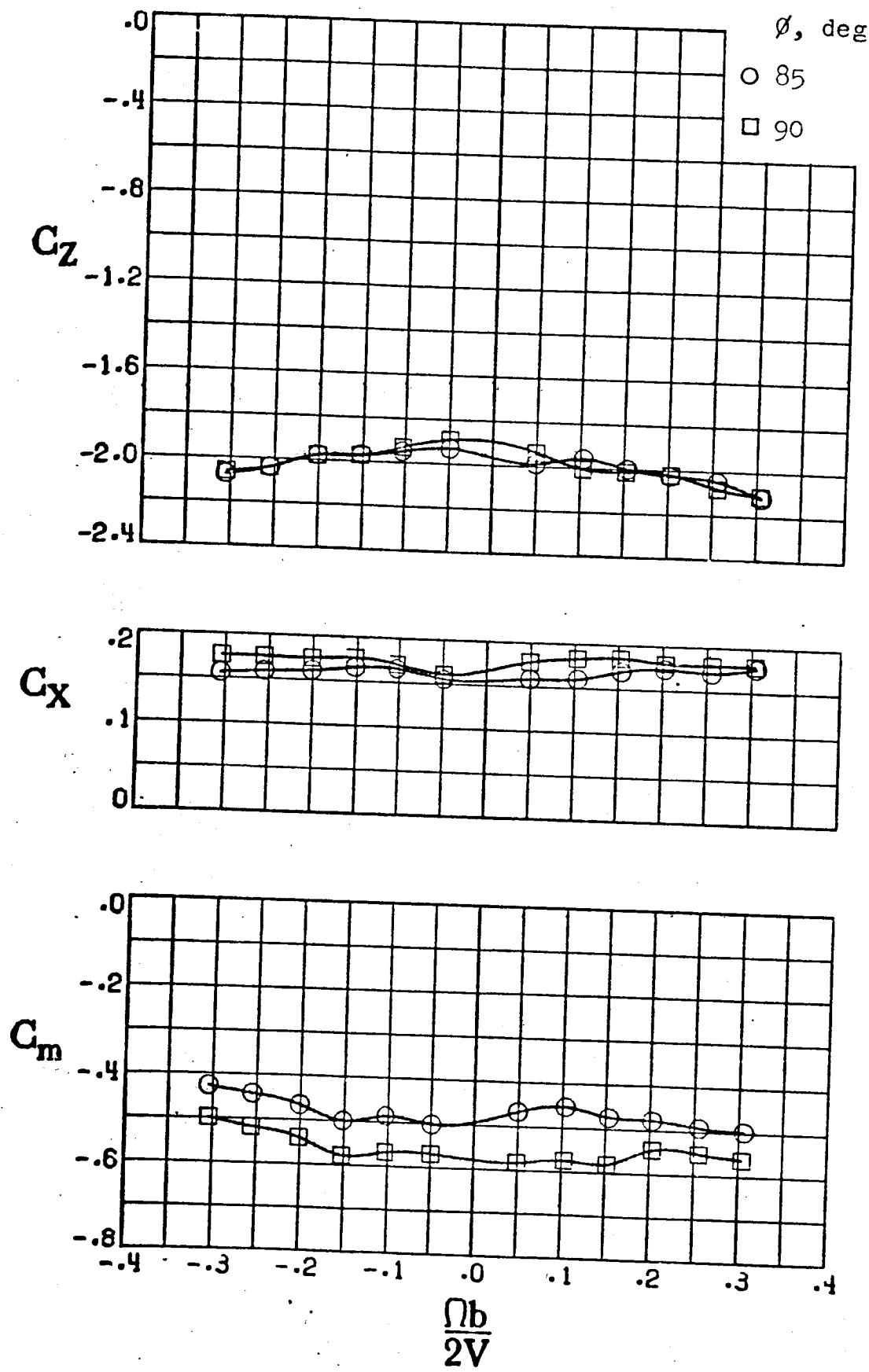
d) $\phi = 5^\circ, \theta = 55, 60, 65^\circ$

Figure C-24. - Continued.



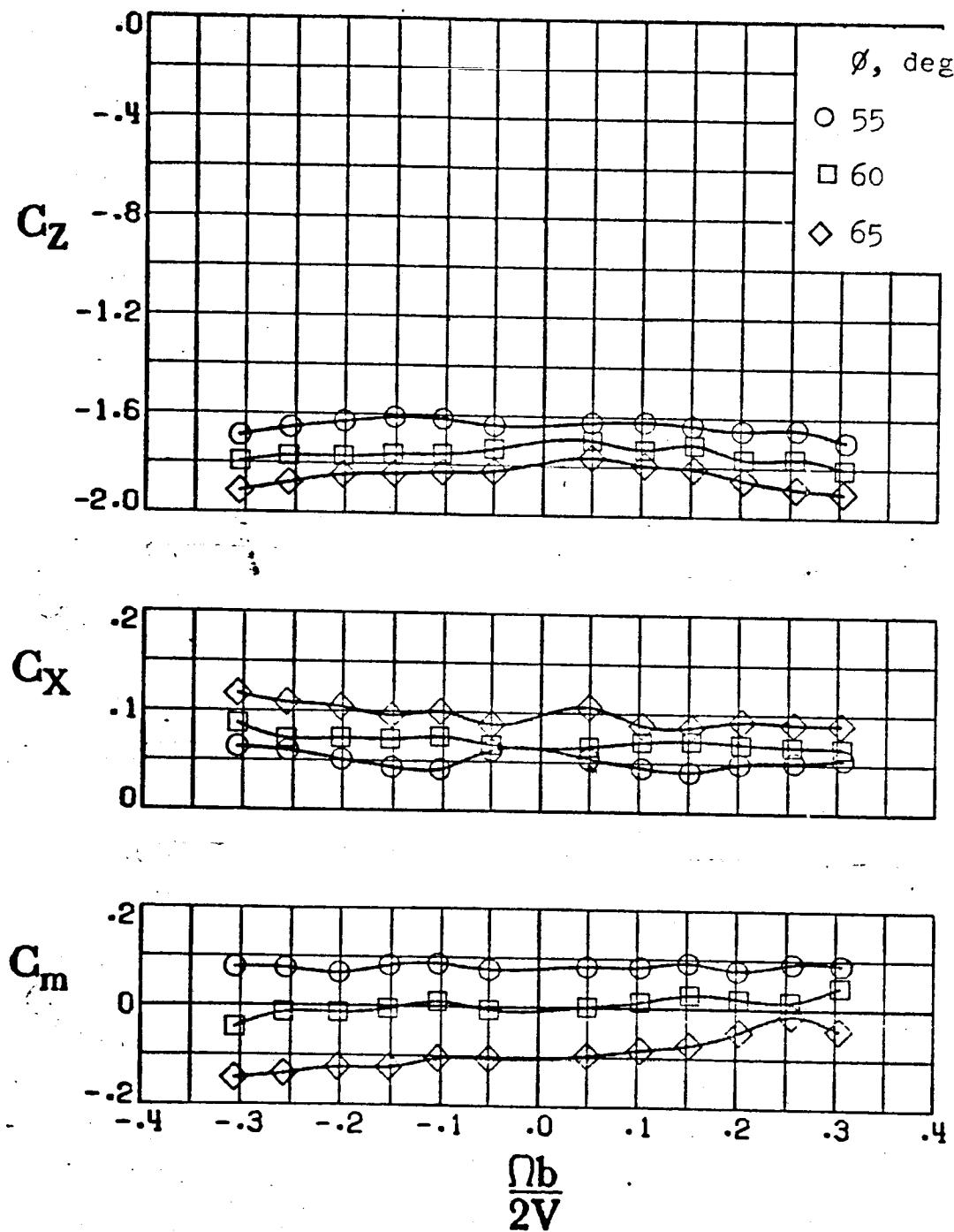
e) $\phi = 5^\circ$, $\theta = 70, 75, 80^\circ$

Figure C-24. - Continued.



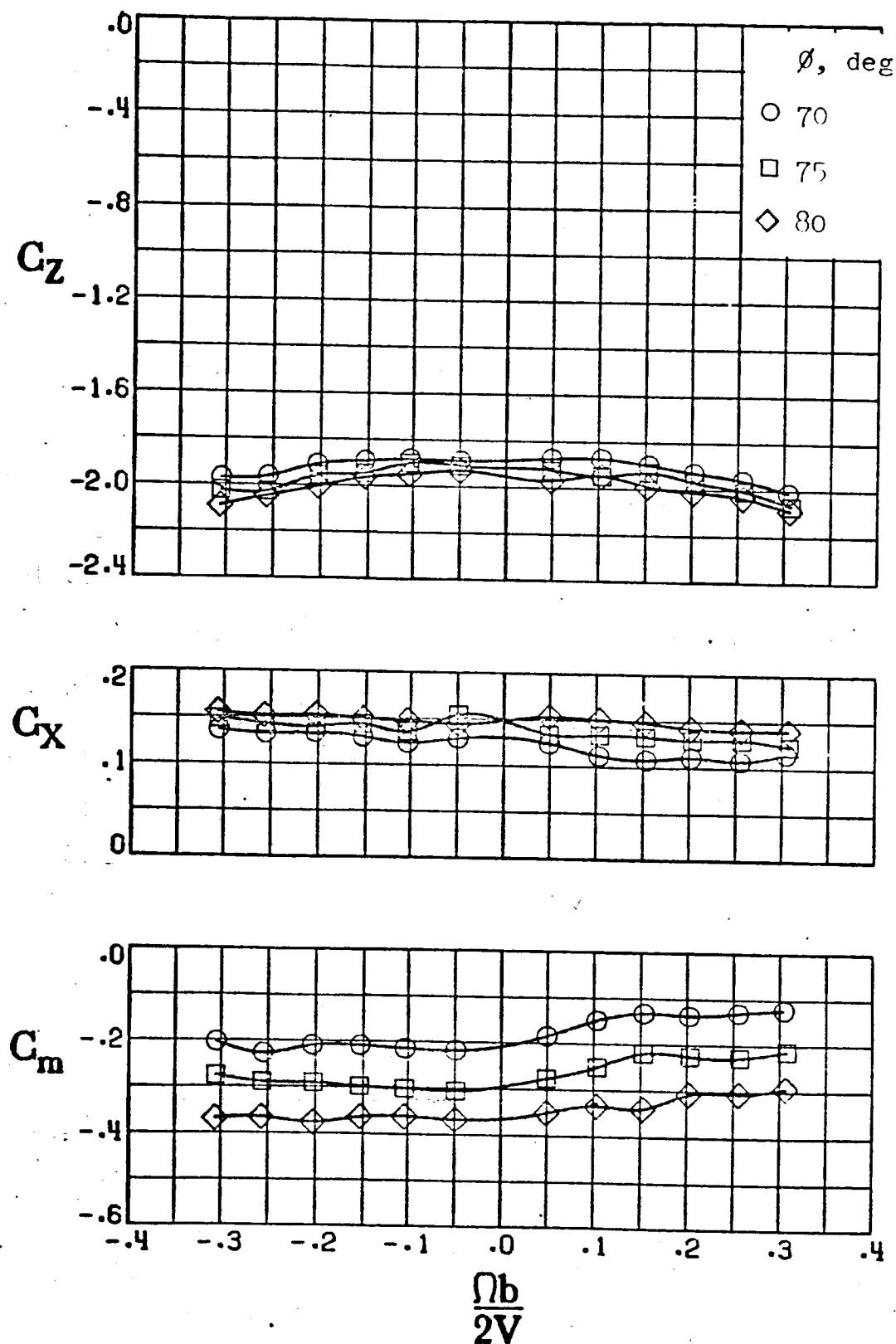
f) $\phi = 5^\circ, \theta = 85, 90^\circ$

Figure C-24. - Concluded.



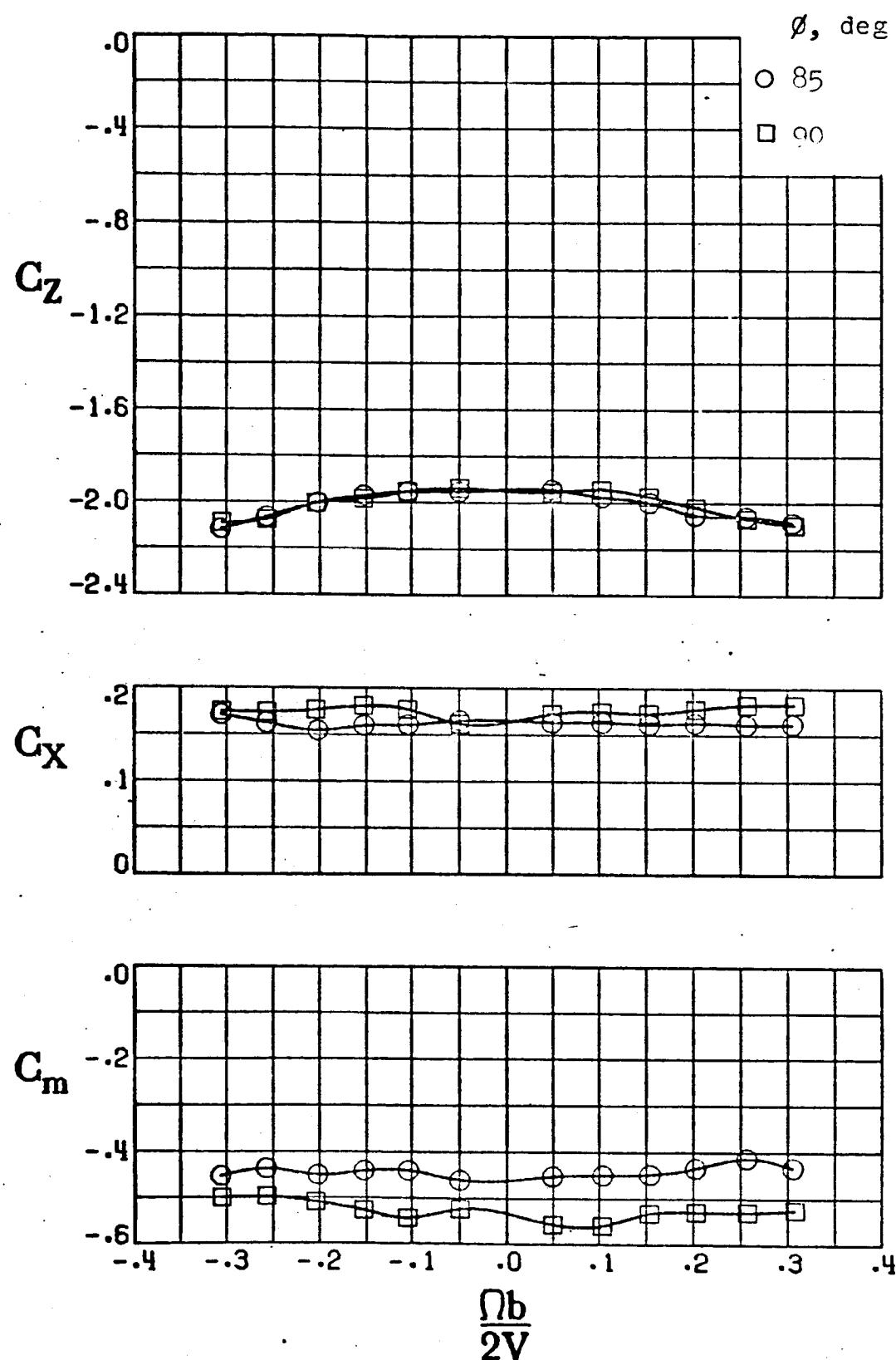
a) $\phi = 0^\circ, \theta = 55^\circ, 60^\circ, 65^\circ$

Figure C-25. - Effect of rotation rate and pitch and roll attitude angles on the longitudinal coefficients for right pro-spin controls. $\Lambda = 22^\circ$.



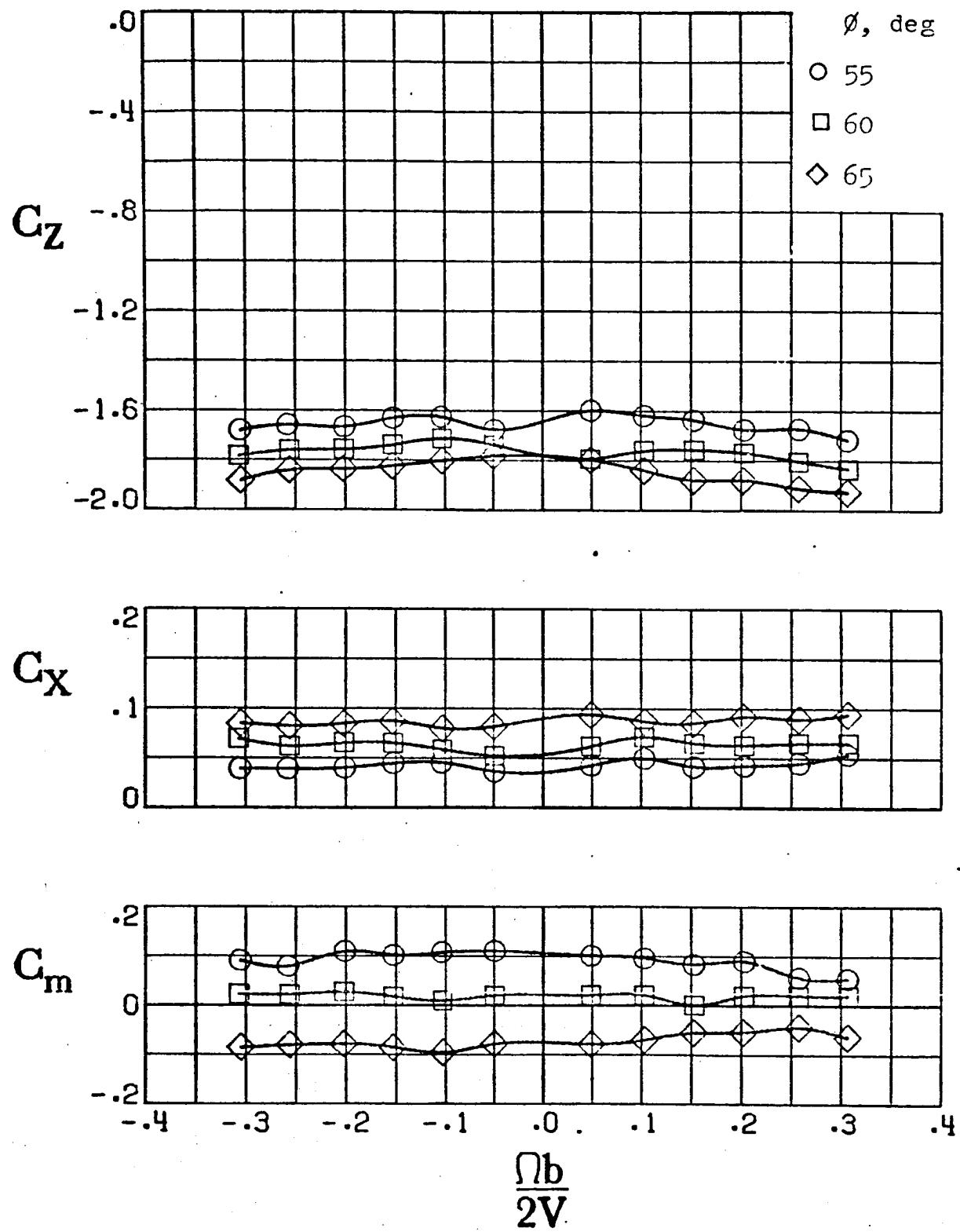
b) $\phi = 0^\circ$, $\theta = 70, 75, 80^\circ$

Figure C-25. - Continued.



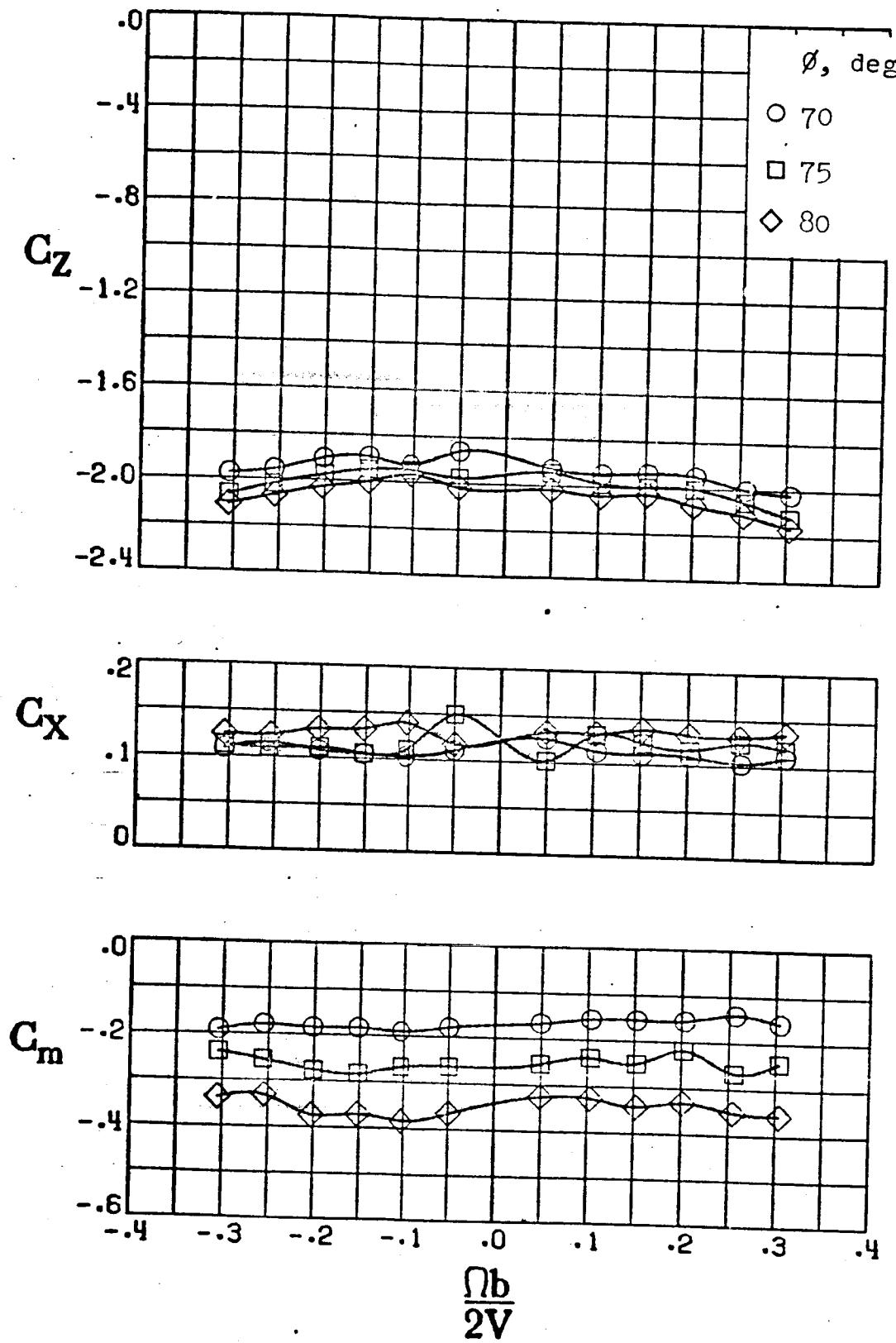
c) $\phi = 0^\circ, \theta = 85, 90^\circ$

Figure C-25. - Continued.



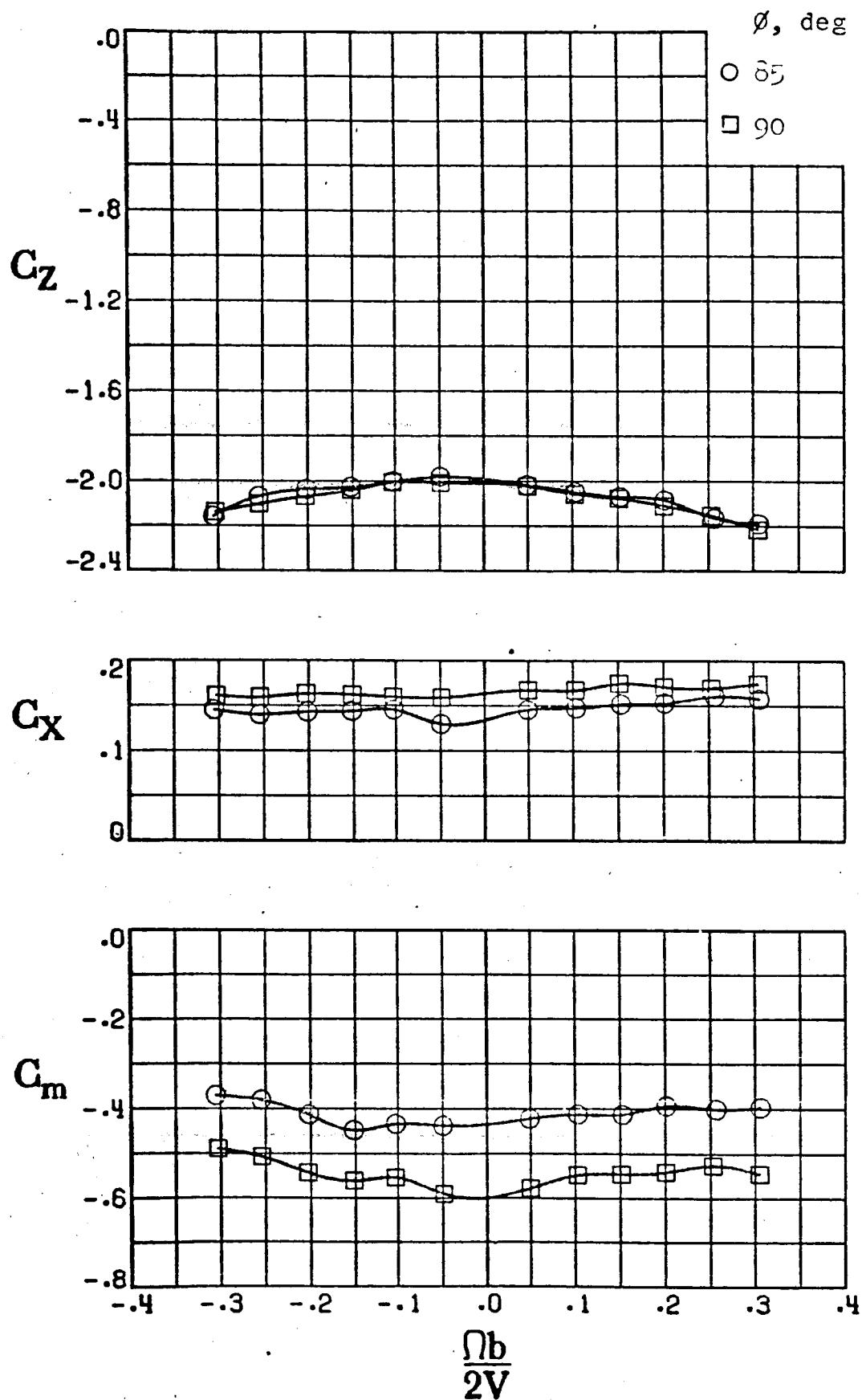
d) $\phi = 5^\circ, \theta = 55, 60, 65^\circ$

Figure C-25. - Continued.



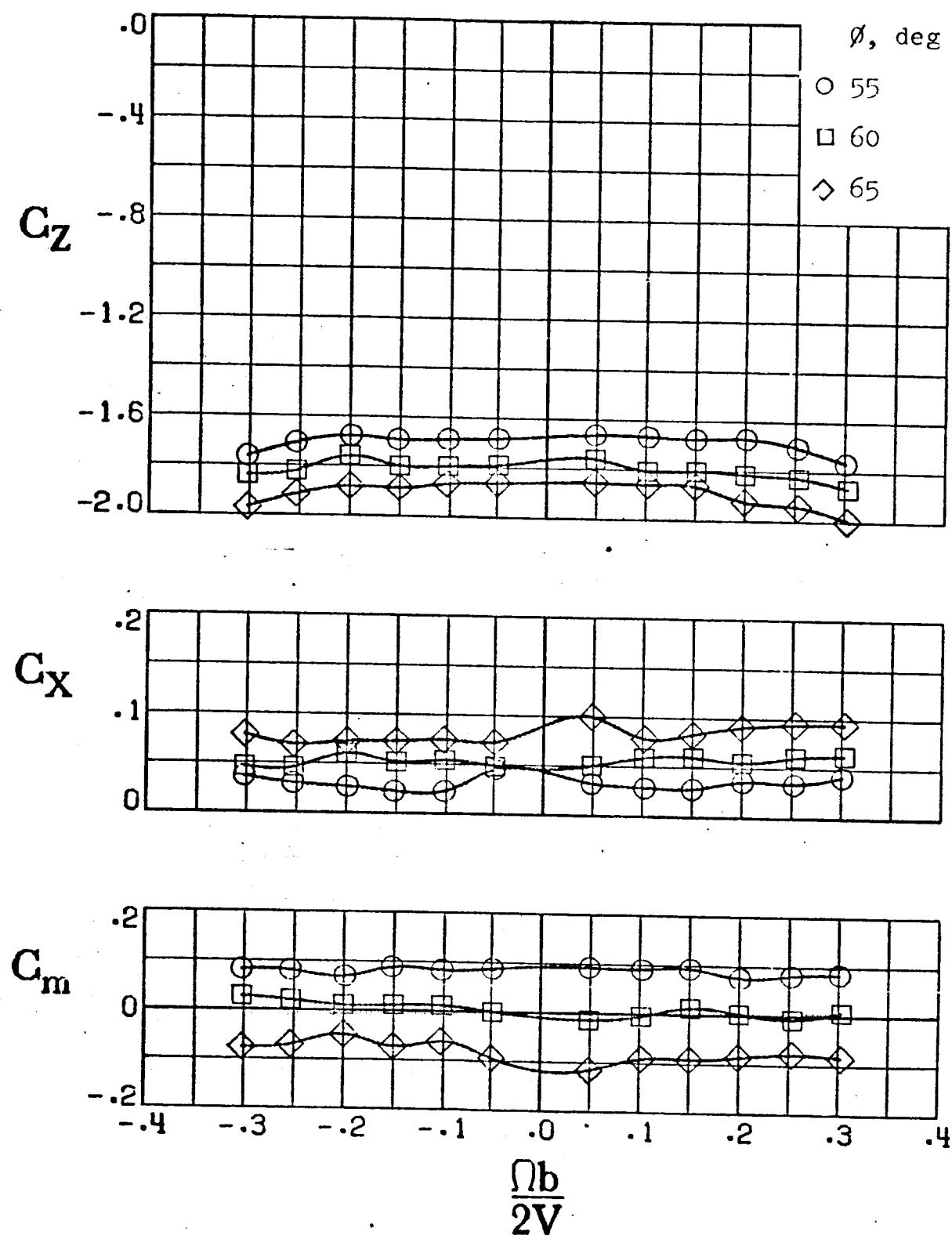
e) $\phi = 5^\circ, \theta = 70, 75, 80^\circ$

Figure C-25. - Continued.



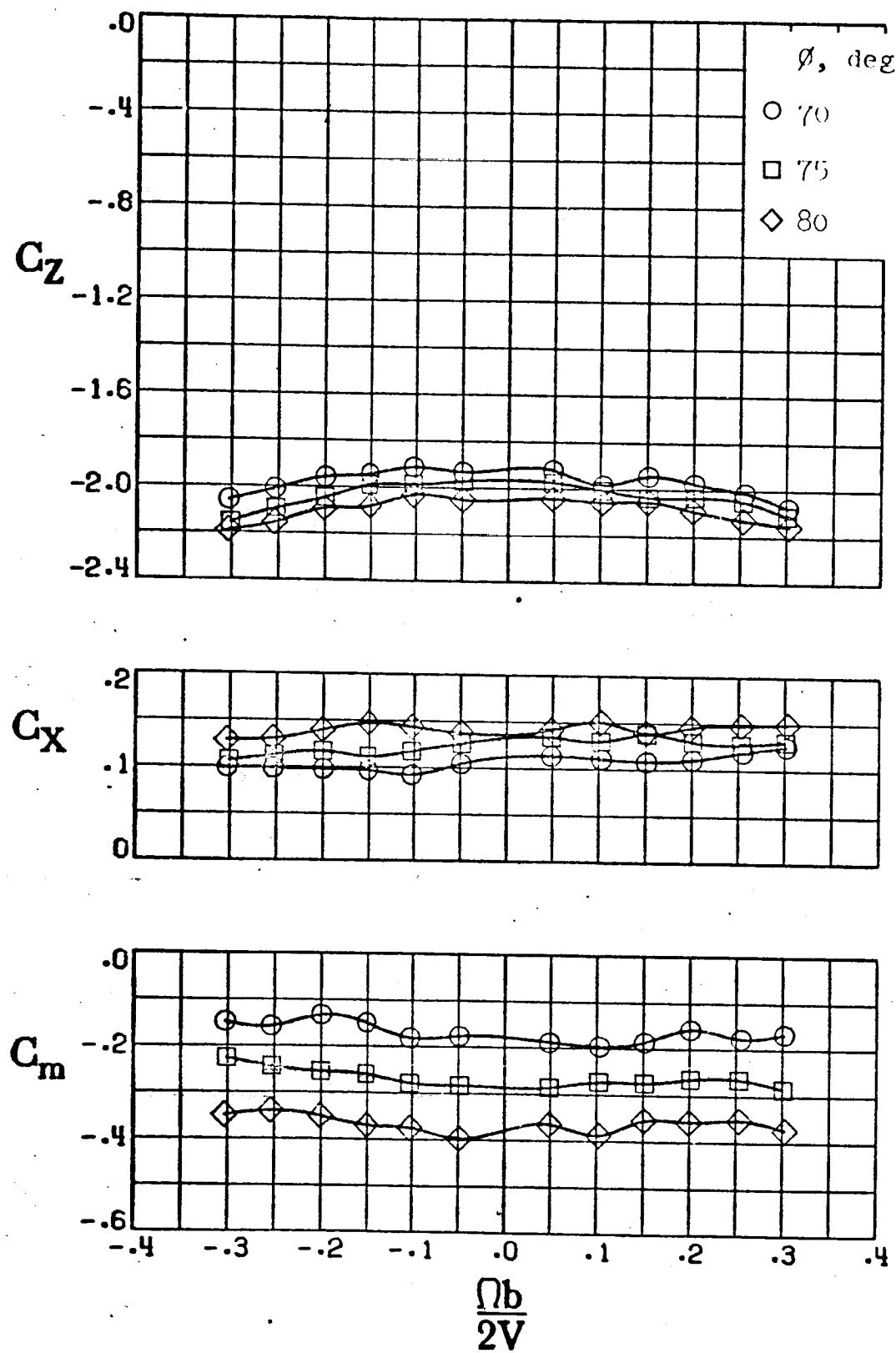
f) $\phi = 5^\circ$, $\theta = 85^\circ$, 90°

Figure C-25. - Concluded.



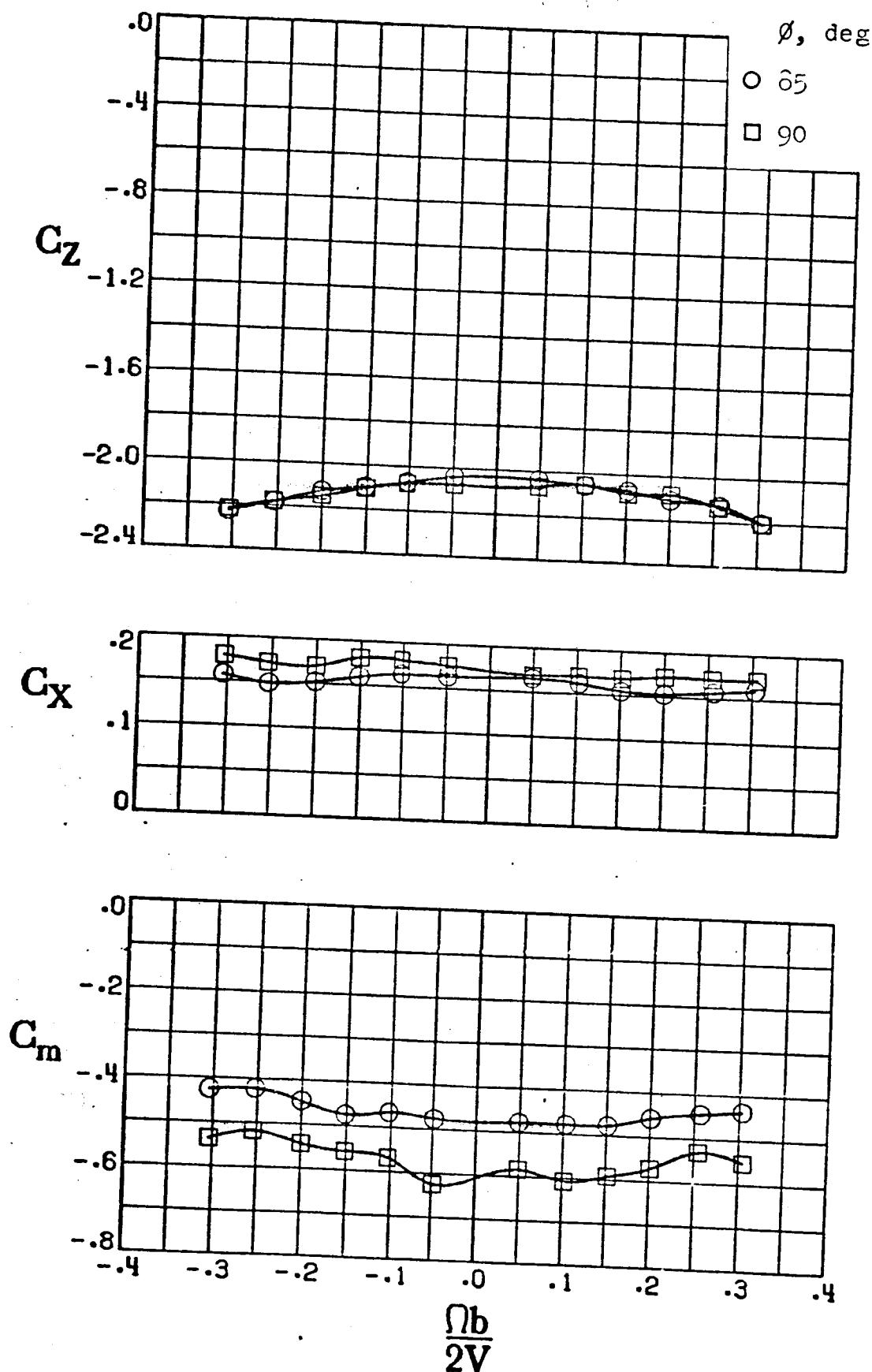
a) $\phi = \theta = 0^\circ, \theta = 55, 60, 65^\circ$

Figure C-26. - Effect of rotation rate and pitch and roll attitude angles on the longitudinal coefficients for left pro-spin controls. $\lambda = 22^\circ$.



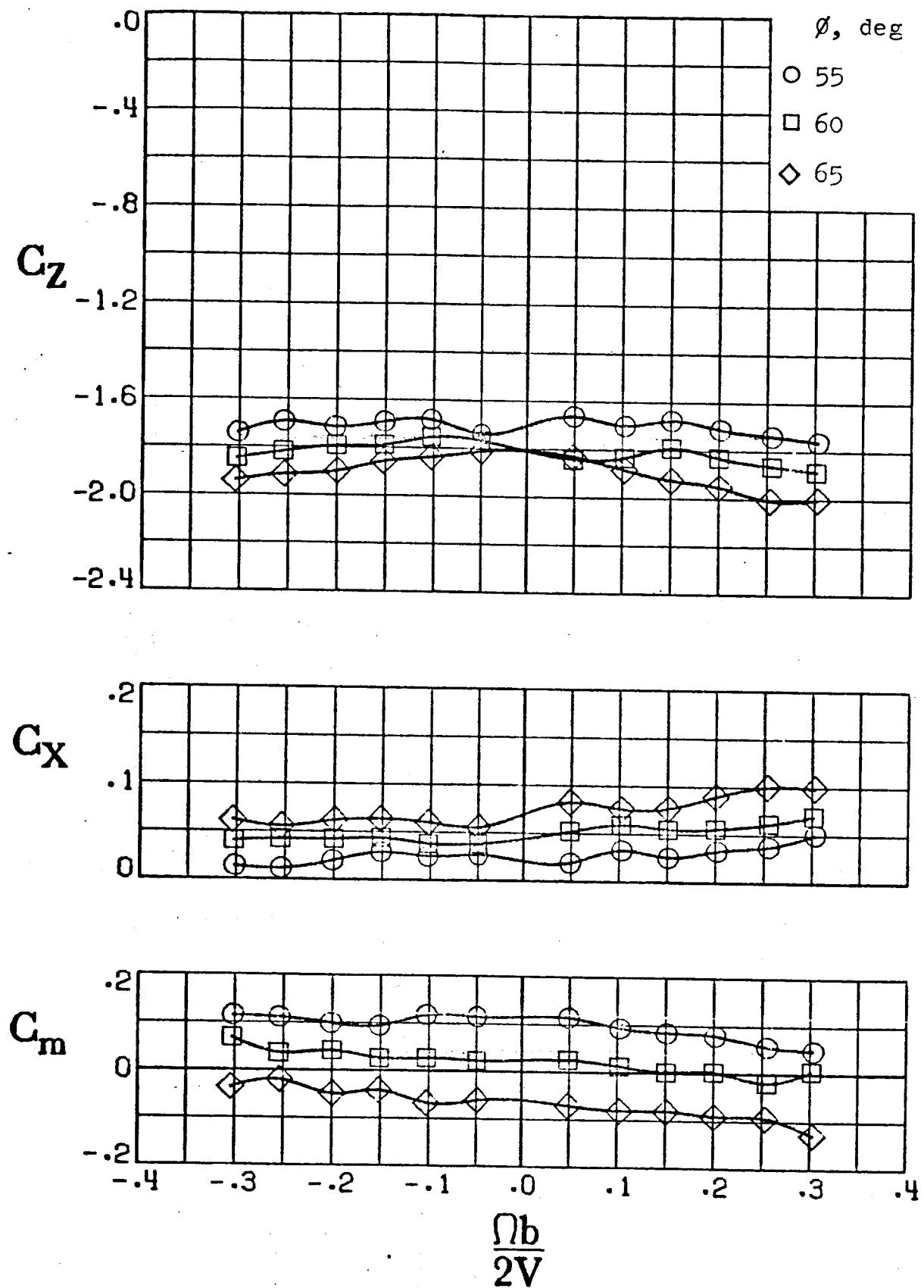
b) $\phi = 0^\circ$, $\theta = 70, 75, 80^\circ$

Figure C-26. - Continued.



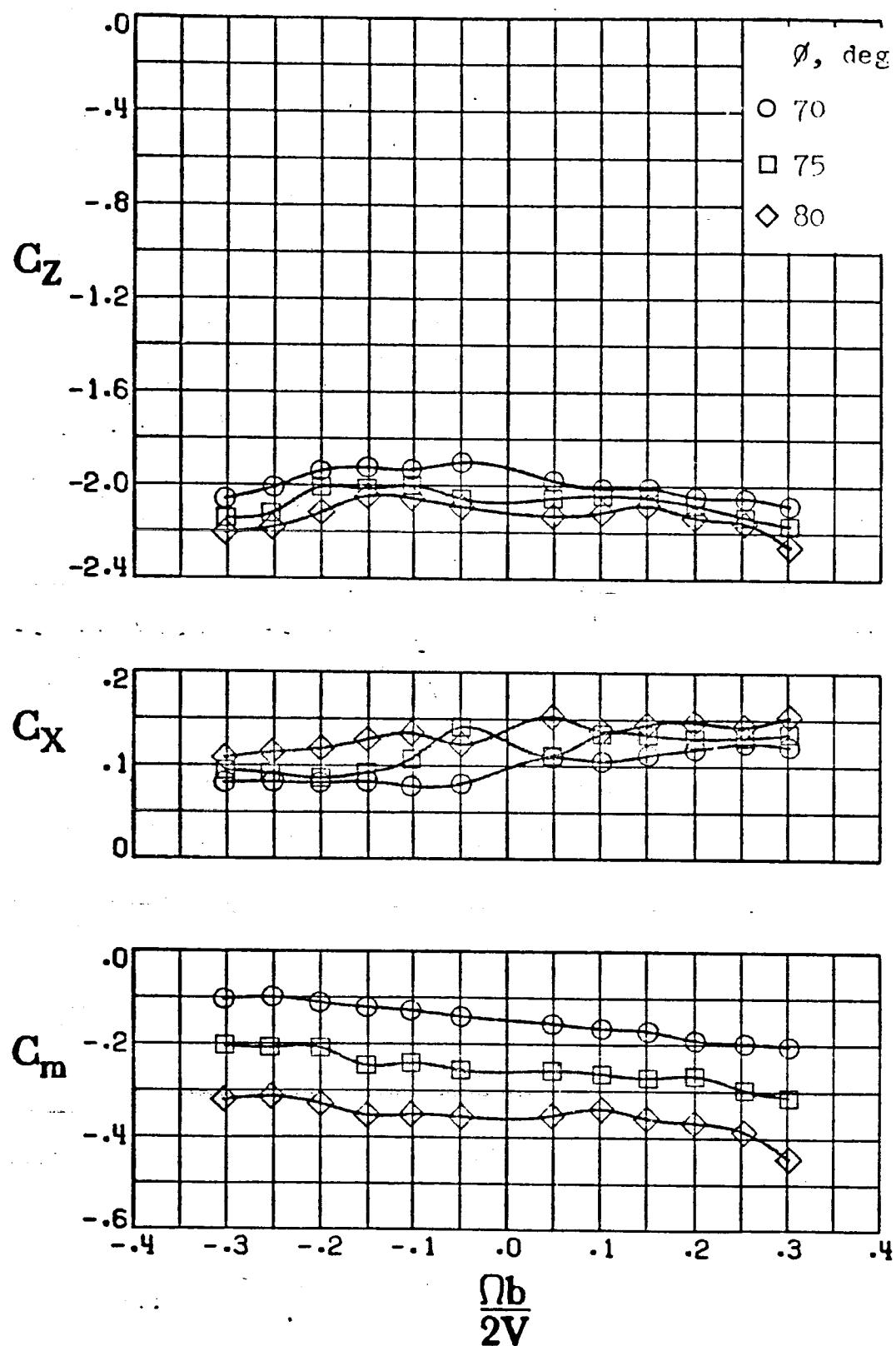
c) $\phi = 0^\circ$, $\theta = 85^\circ, 90^\circ$

Figure C-26. - Continued.



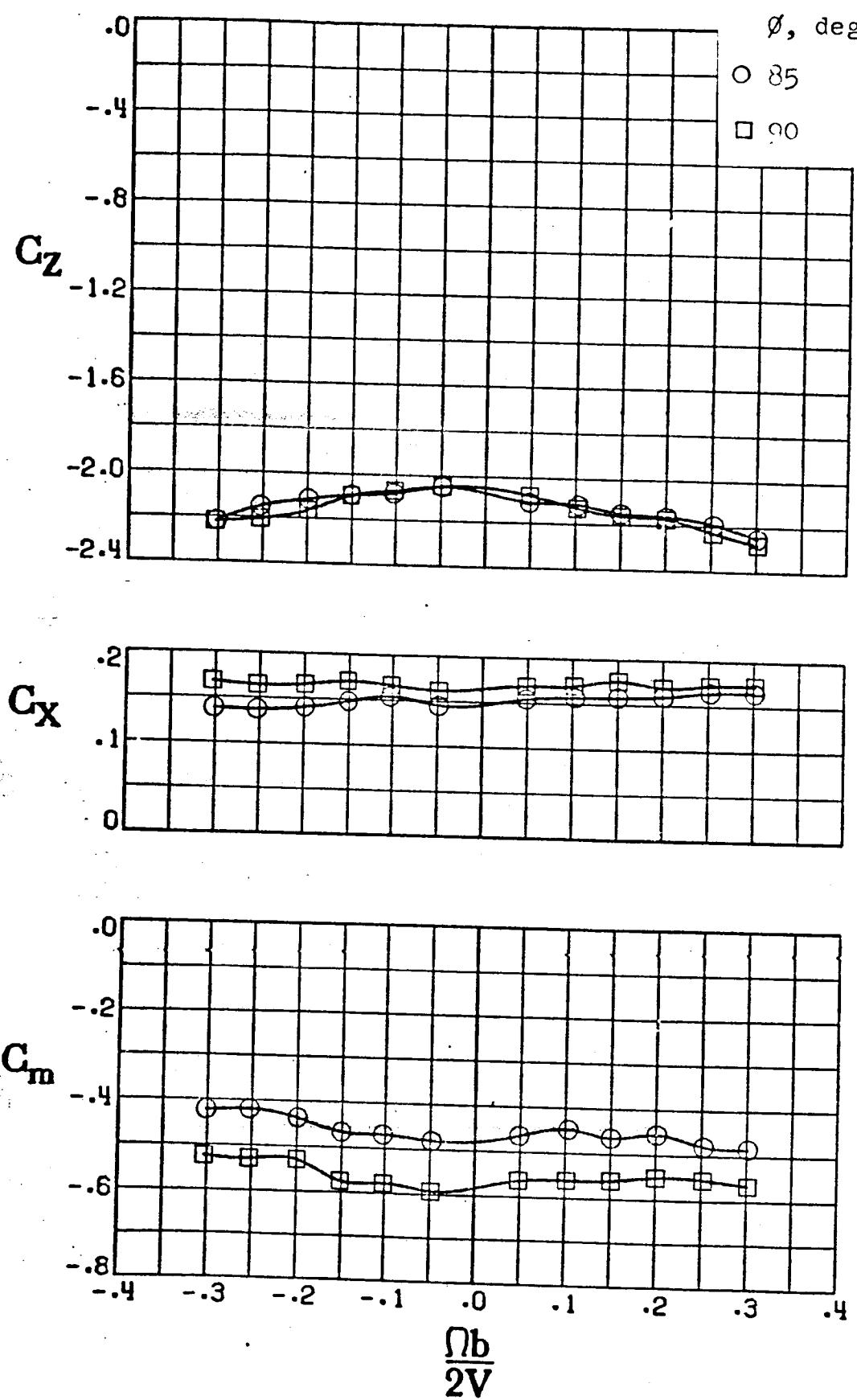
d) $\phi = 5^\circ, \theta = 55, 60, 65^\circ$

Figure C-26. - Continued.



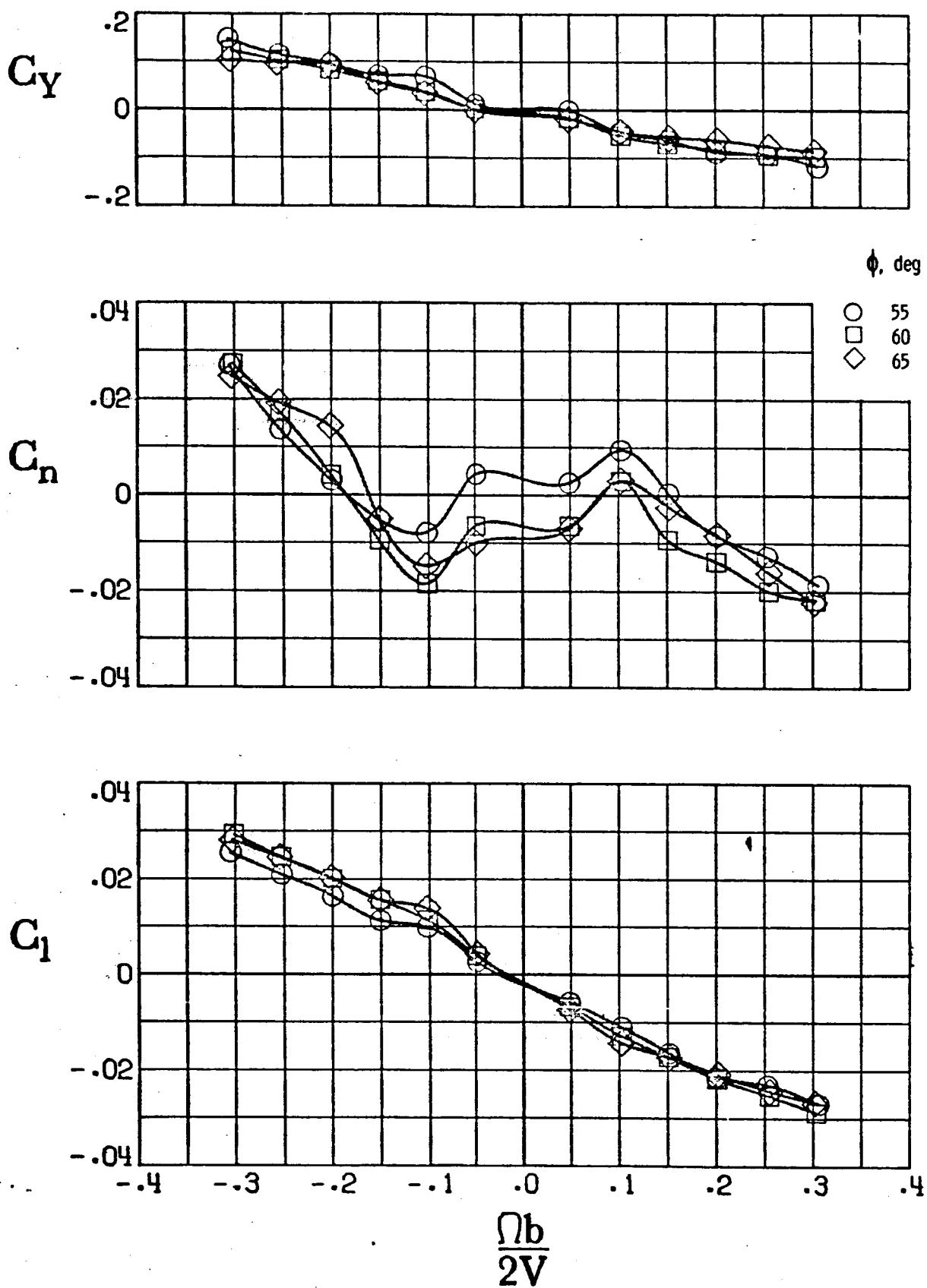
e) $\phi = 5^\circ$, $\theta = 70, 75, 80^\circ$

Figure C-26. - Continued.



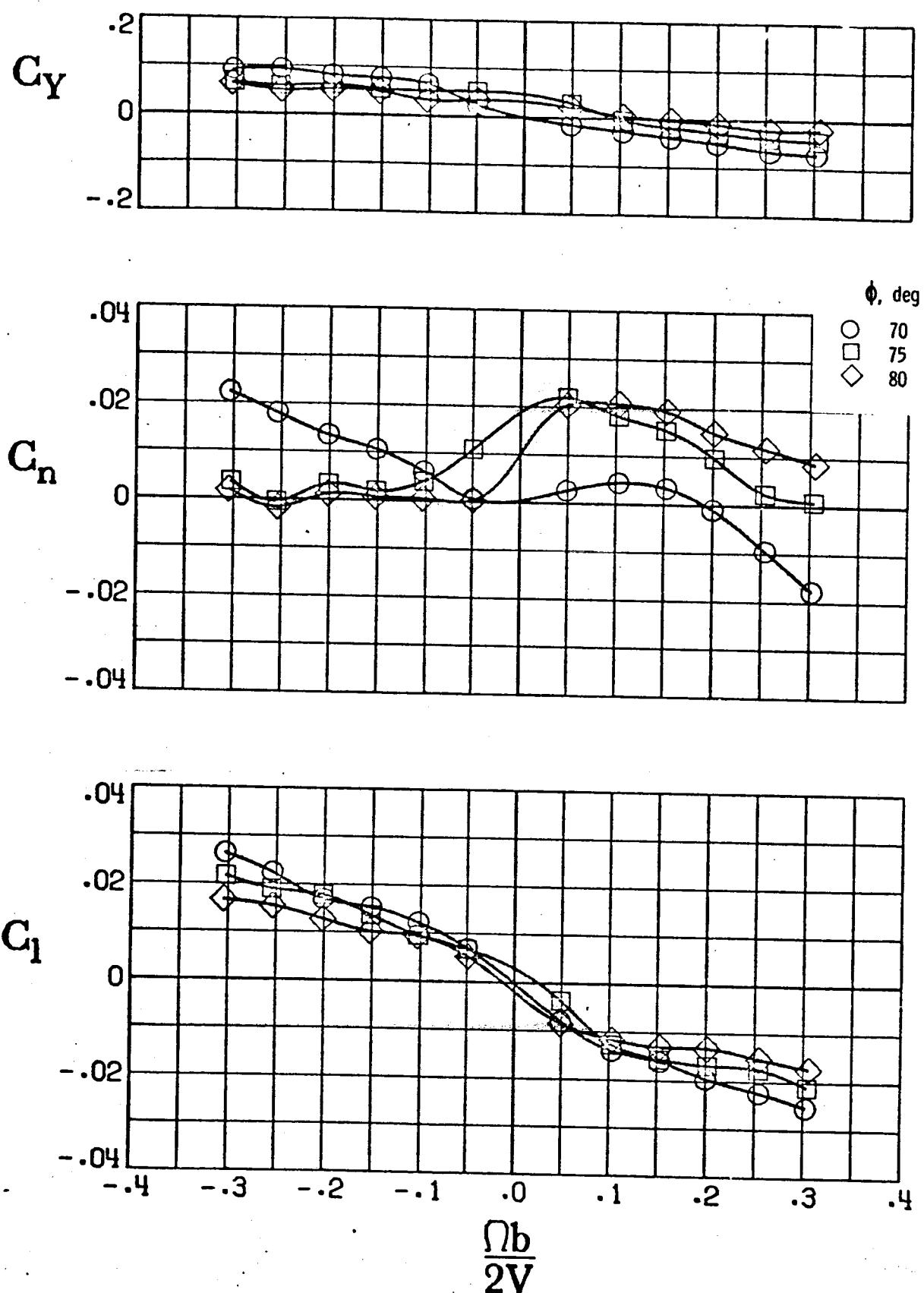
f) $\phi = 5^\circ, \theta = 85, 90^\circ$

Figure C-26. - Concluded.



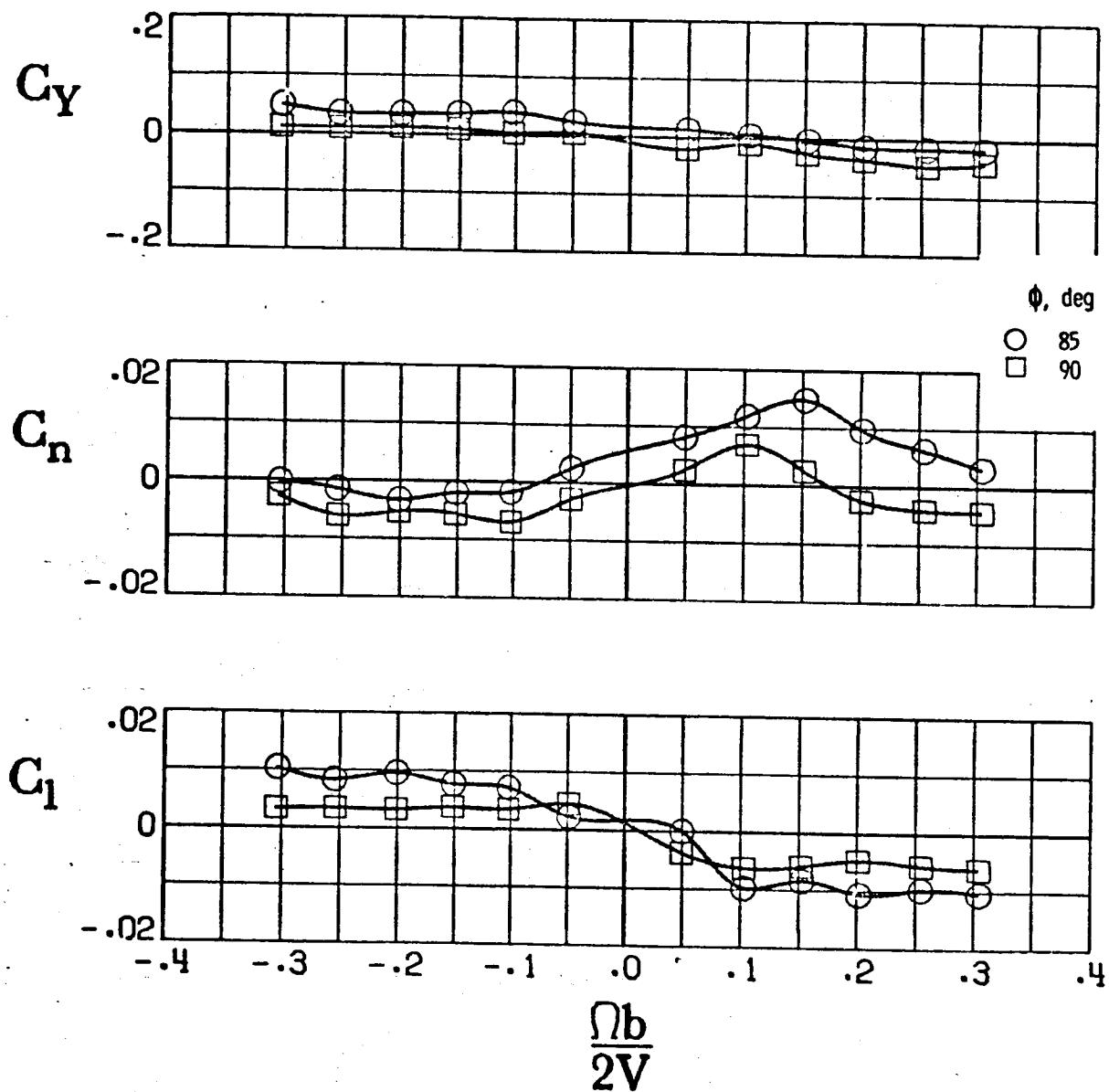
a) $\phi = 0^\circ, \theta = 55, 60, 65^\circ$

Figure C-27. - Effect of rotation rate and pitch and roll attitude angles on the lateral-directional coefficients for all neutral controls. $\Lambda = 22^\circ$.



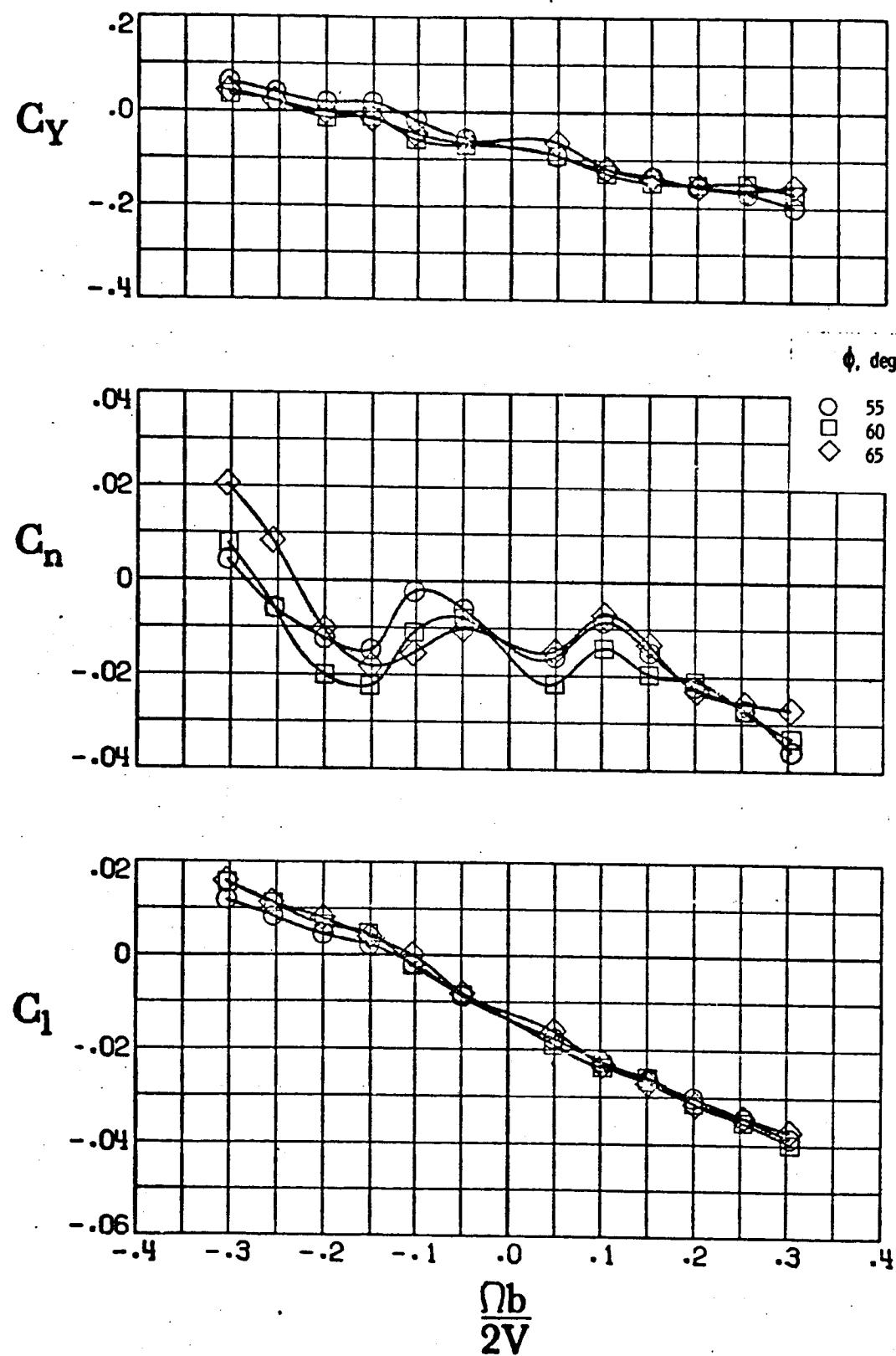
b) $\phi = 0^\circ$, $\theta = 70, 75$ and 80°

Figure C-27. - Continued.



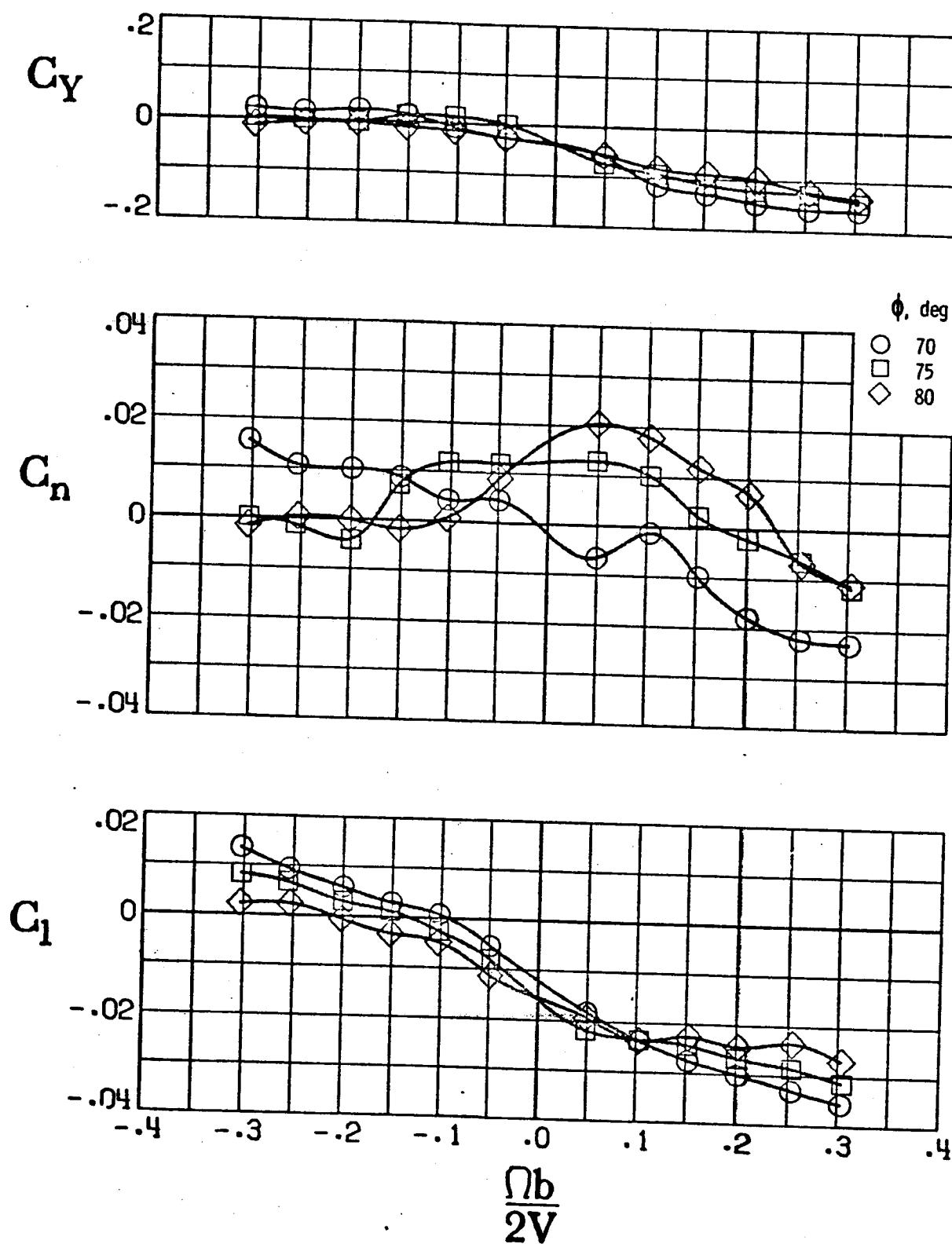
c) $\phi = 0^\circ$, $\theta = 85$ and 90°

Figure C-27. - Continued.



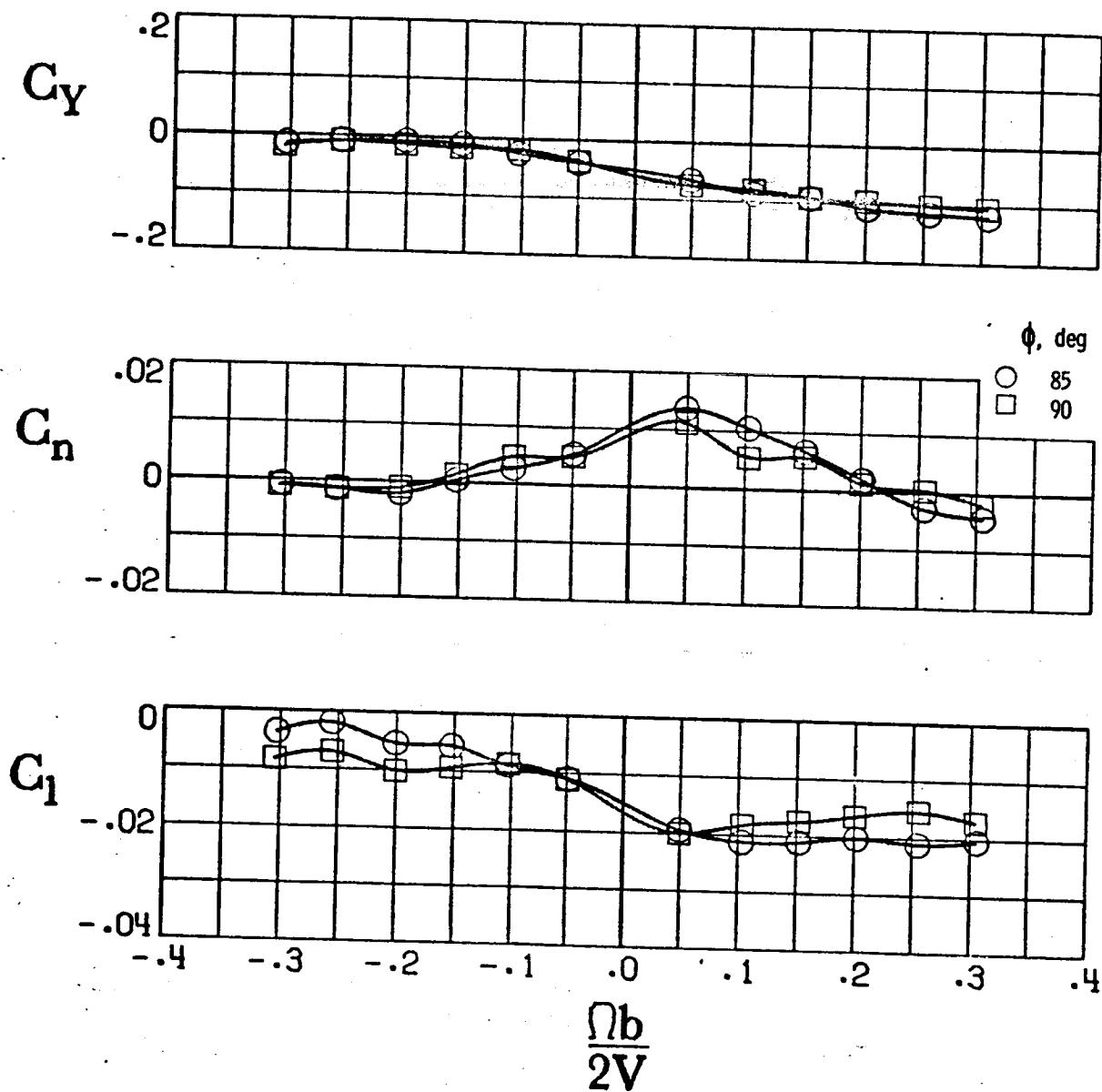
d) $\phi = 5^\circ$, $\theta = 55^\circ$, 60° and 65°

Figure C-27. - Continued.



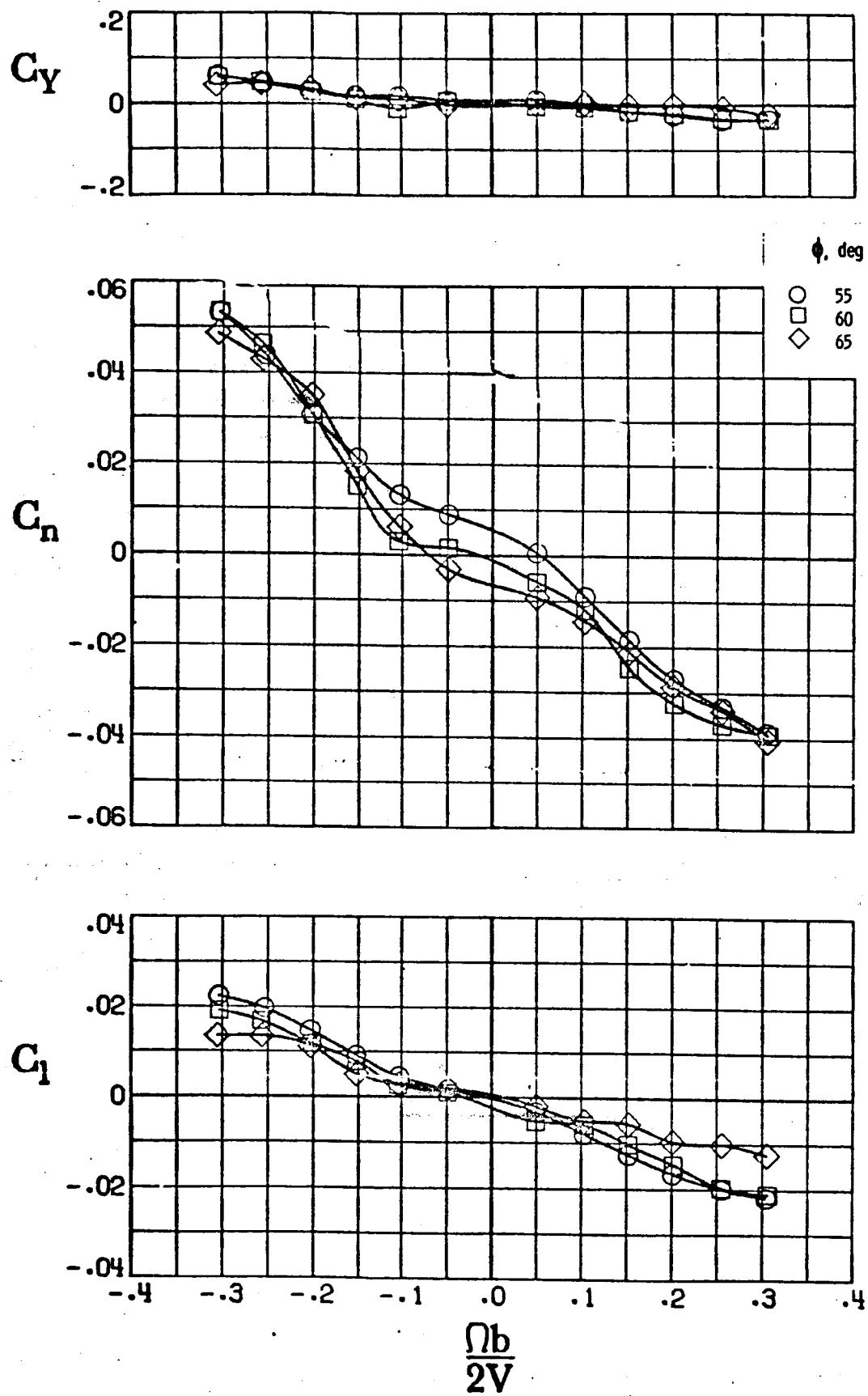
e) $\phi = 5^\circ$, $\theta = 70, 75$ and 80°

Figure C-27. - Continued.



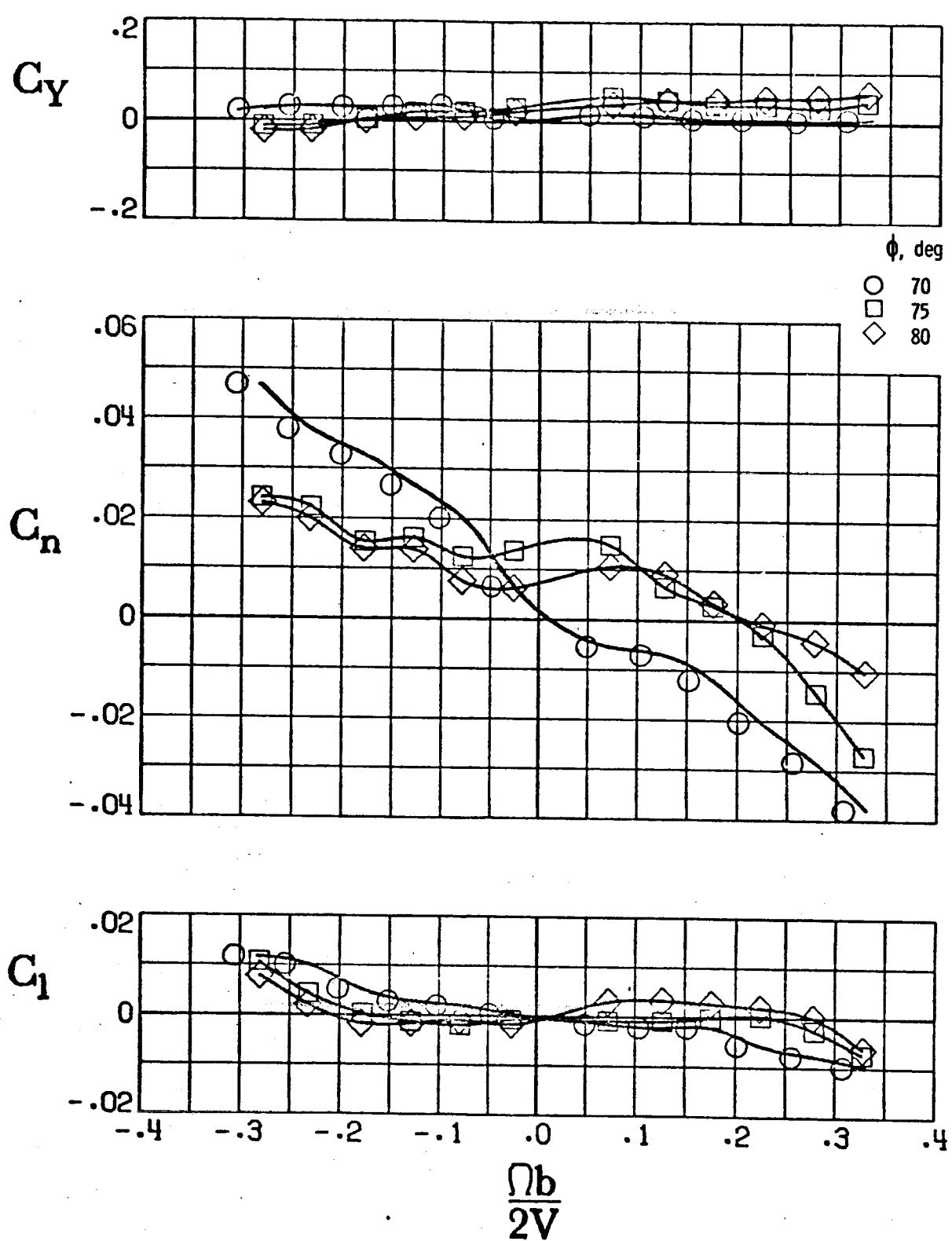
f) $\phi = 5^\circ$, $\theta = 85$ and 90°

Figure C-27. - Concluded.

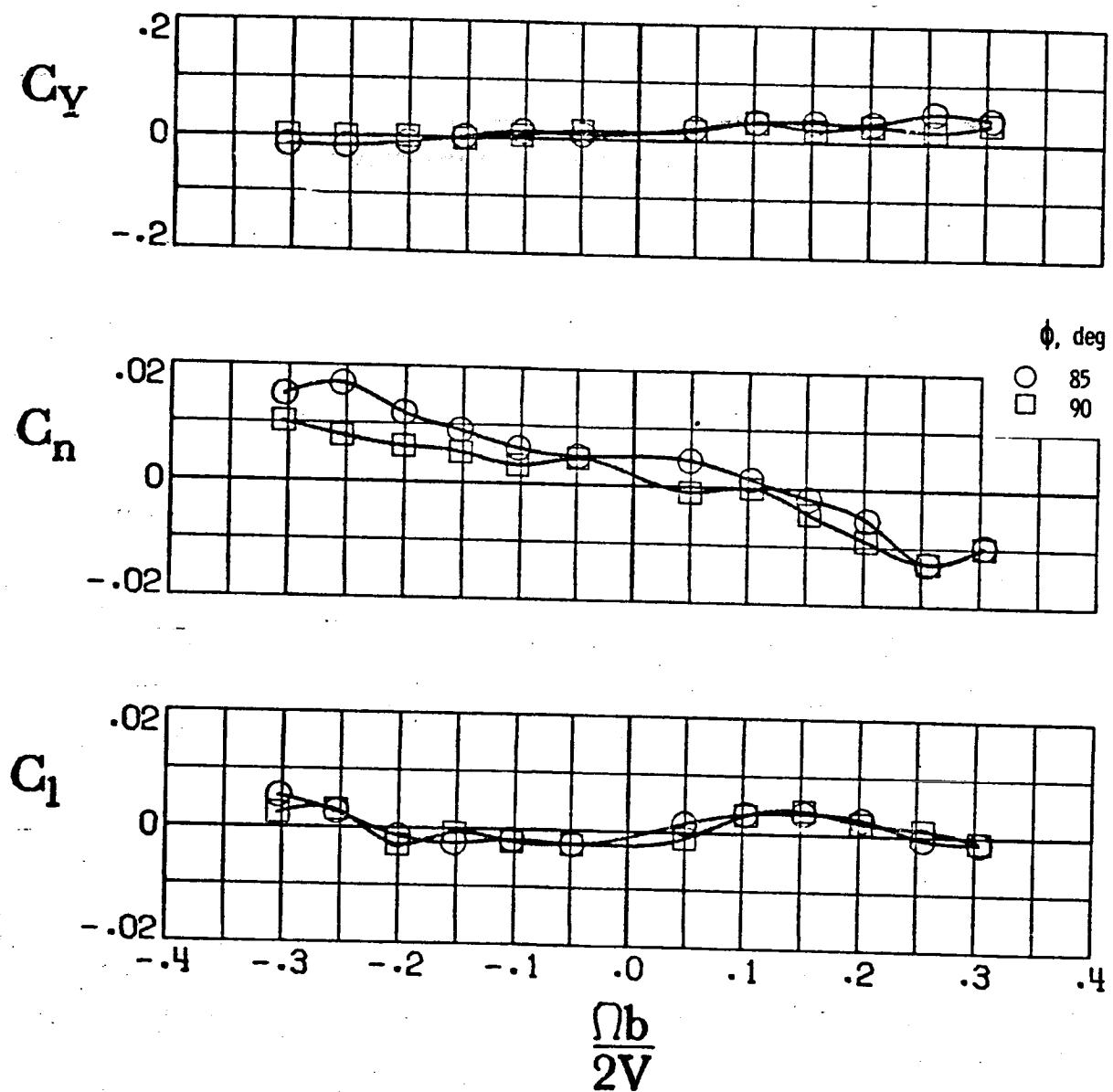


a) $\phi = 0^\circ, \theta = 55, 60, 65^\circ$

Figure C-28. - Effect of rotation rate and pitch and roll attitude angle on the lateral-directional coefficients for $i_s = -30^\circ$. Lamda = 220.

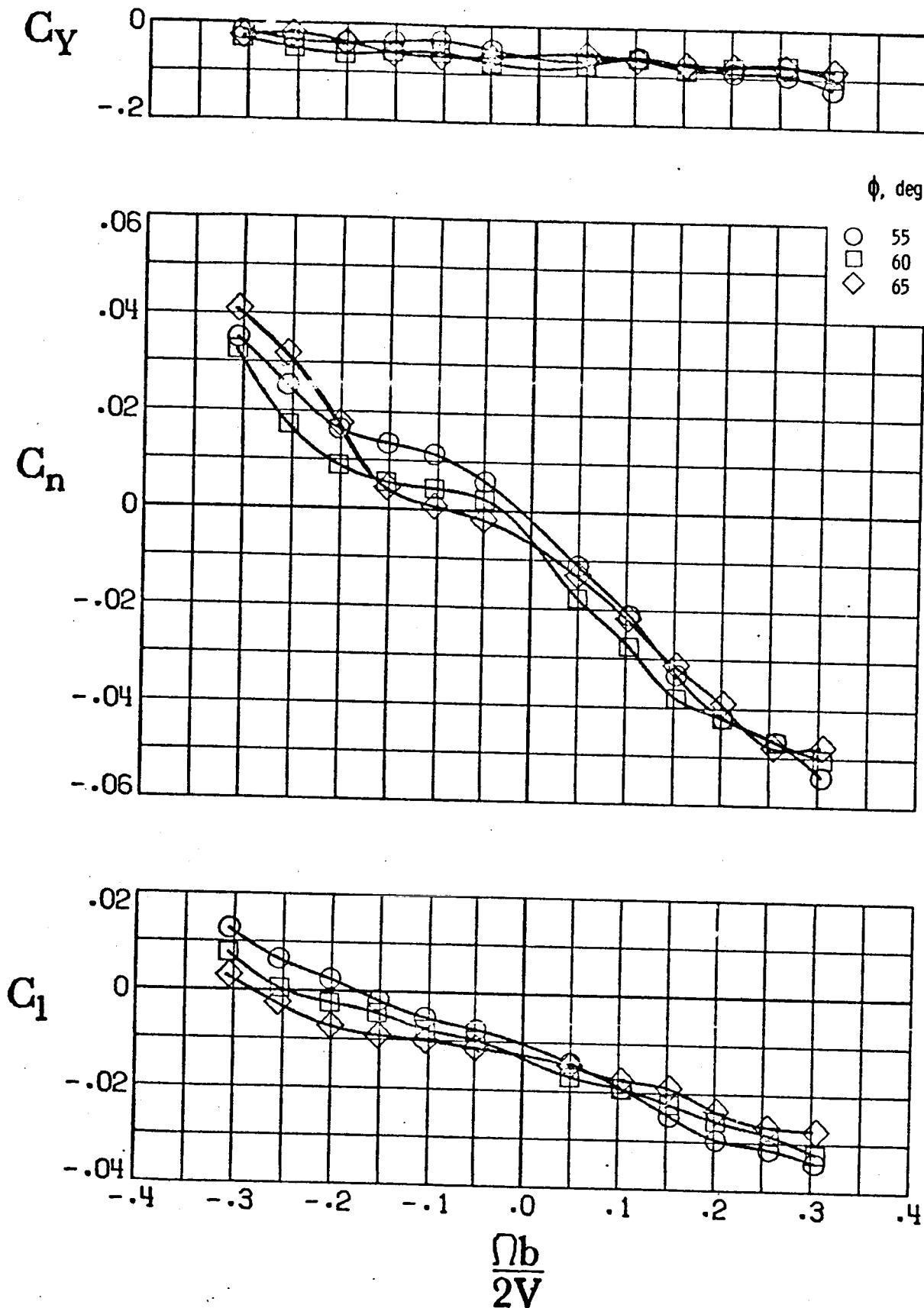


b) $\phi = 0^\circ$, $\theta = 70^\circ$, 75° and 80°
 Figure C-28. - Continued.



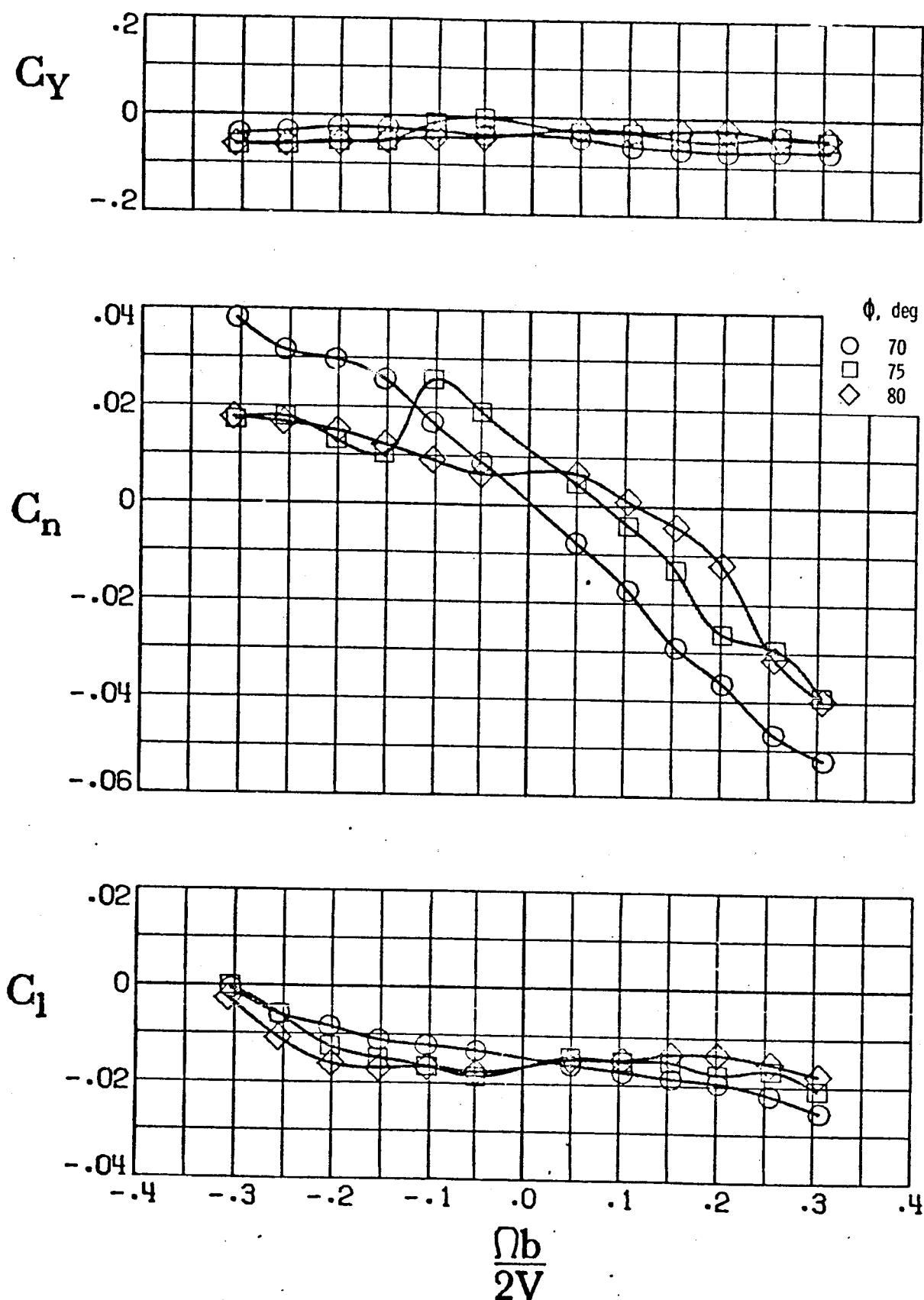
c) $\phi = 0^\circ, \theta = 85, 90^\circ$

Figure C-28. - Continued.



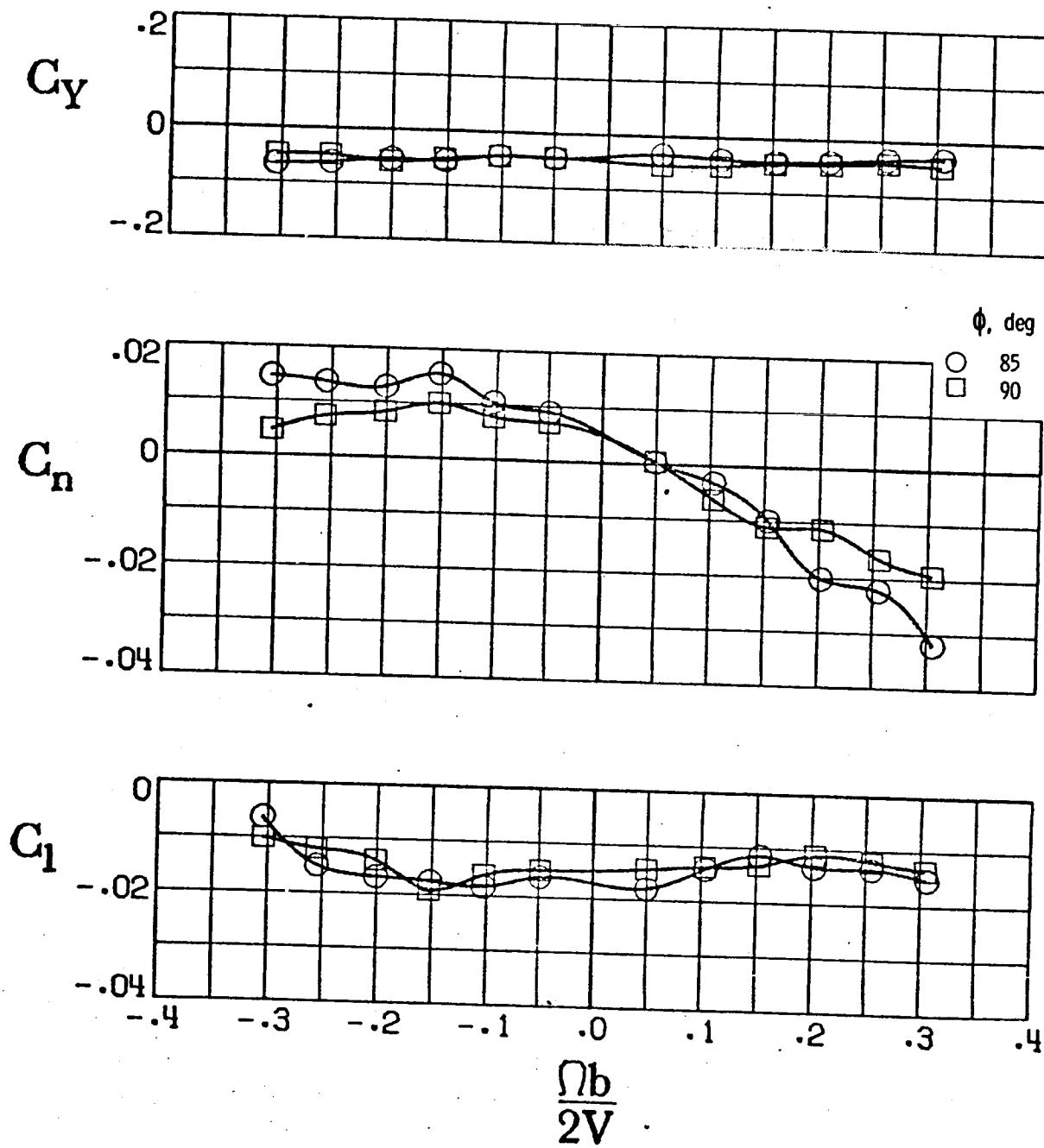
d) $\phi = 5^\circ, \theta = 55, 60, 65^\circ$

Figure C-28. - Continued.



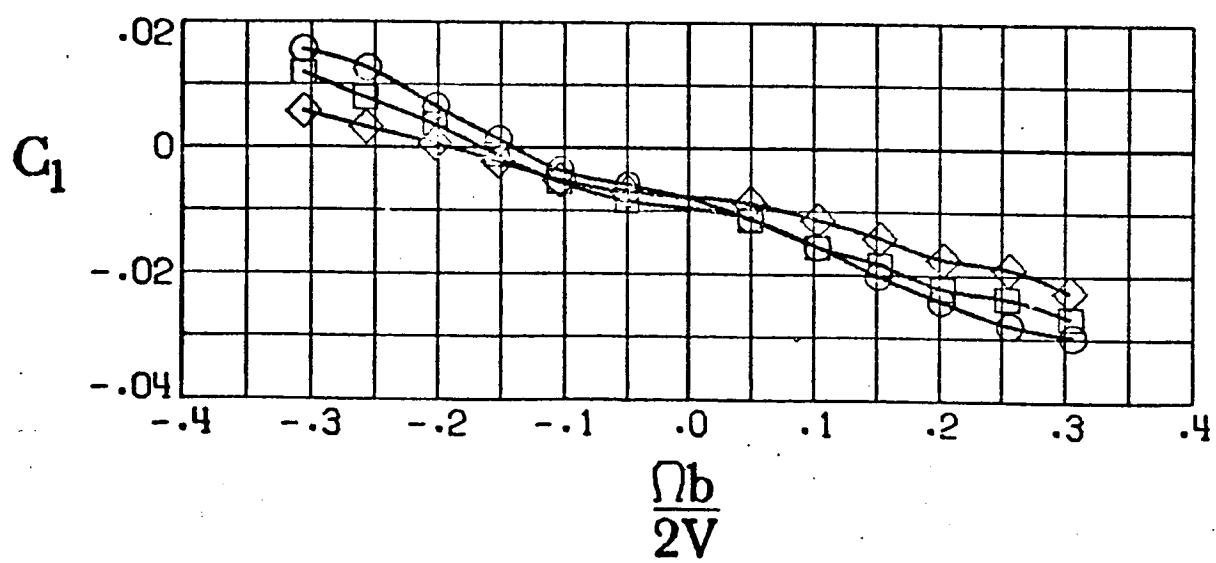
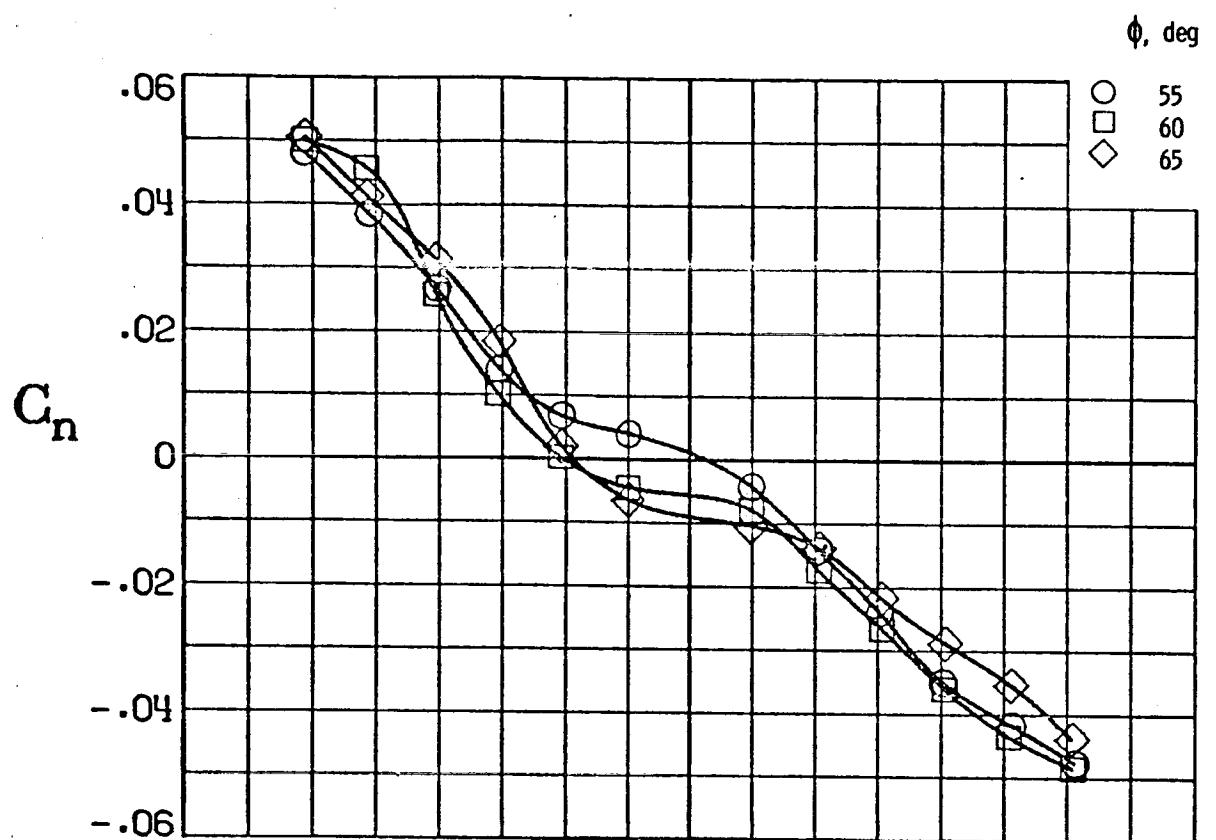
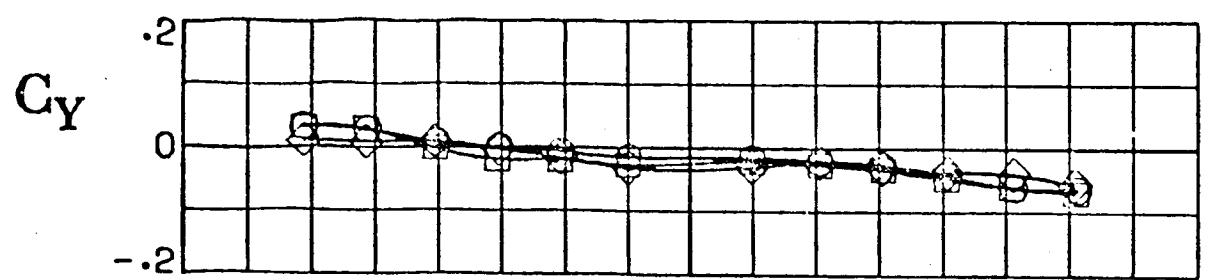
e) $\phi = 5^\circ$, $\theta = 70, 75, 80^\circ$

Figure C-28. - Continued.



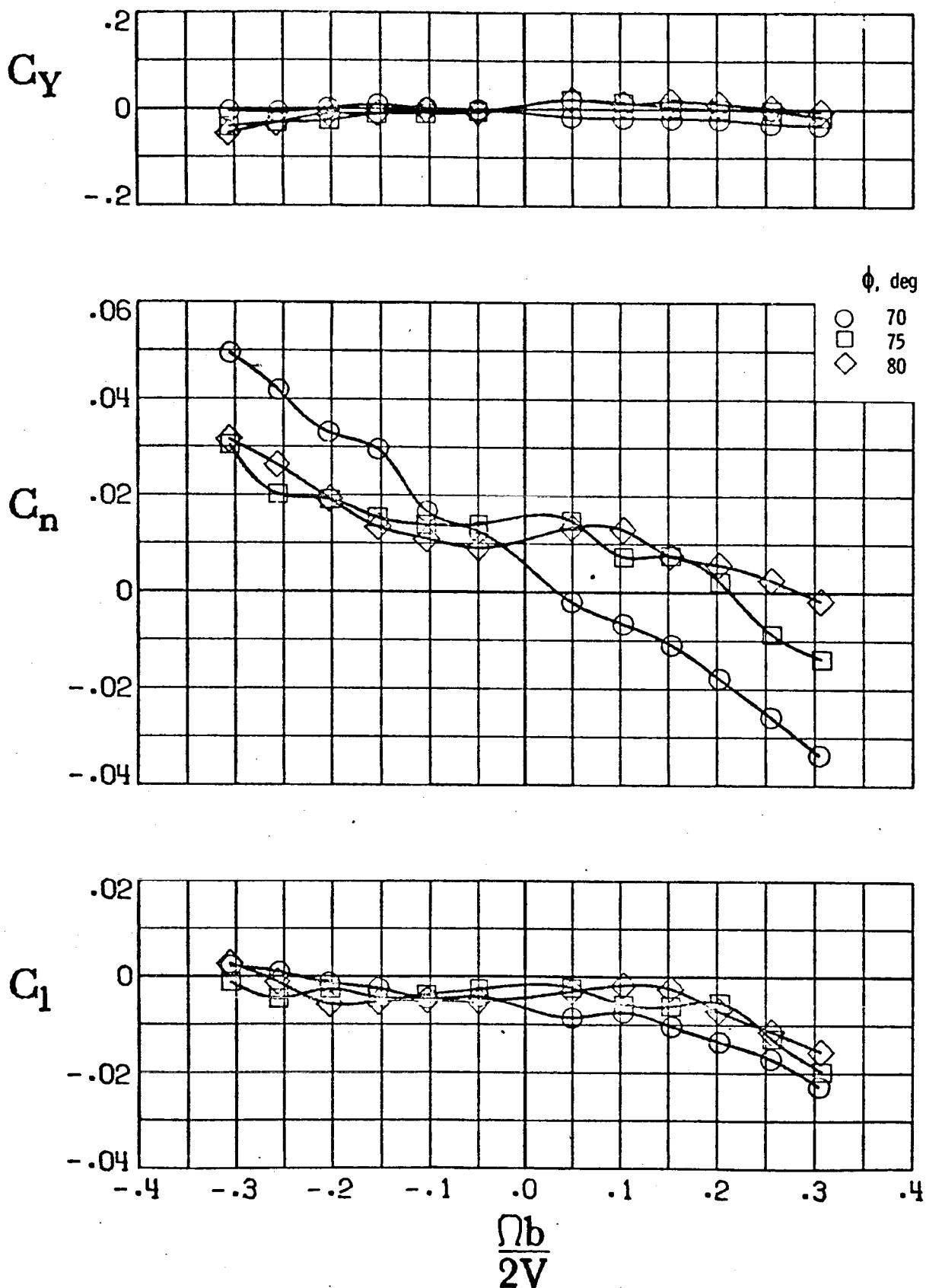
f) $\phi = 5^\circ, \theta = 85, 90^\circ$

Figure C-28. - Concluded.



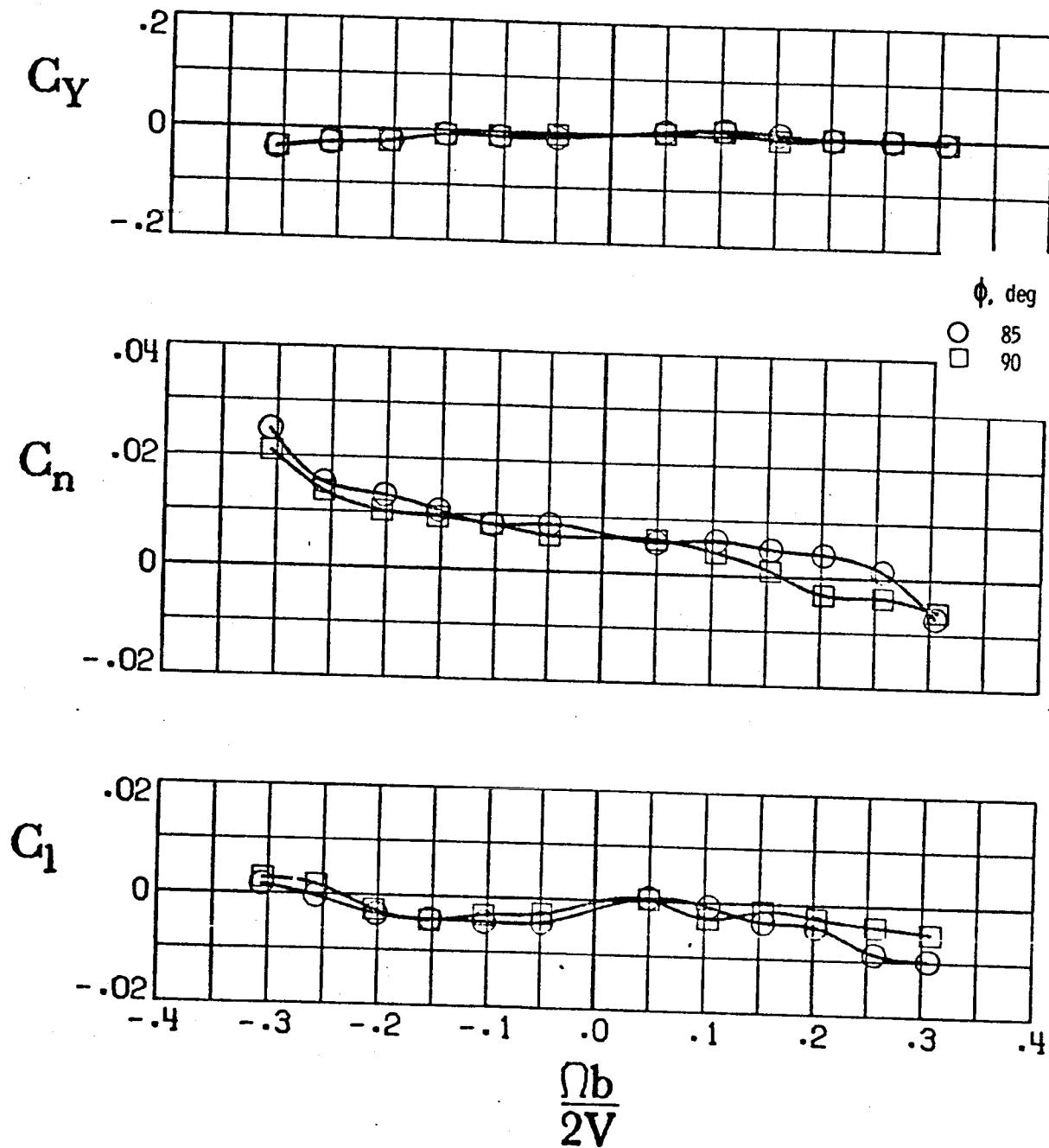
a) $\theta = 0^\circ, \theta = 55^\circ, 60^\circ, 65^\circ$

Figure C-29. - Effect of rotation rate and pitch and roll attitude angles on the lateral-directional coefficients for right pro-spin controls. Lamda = 22° .



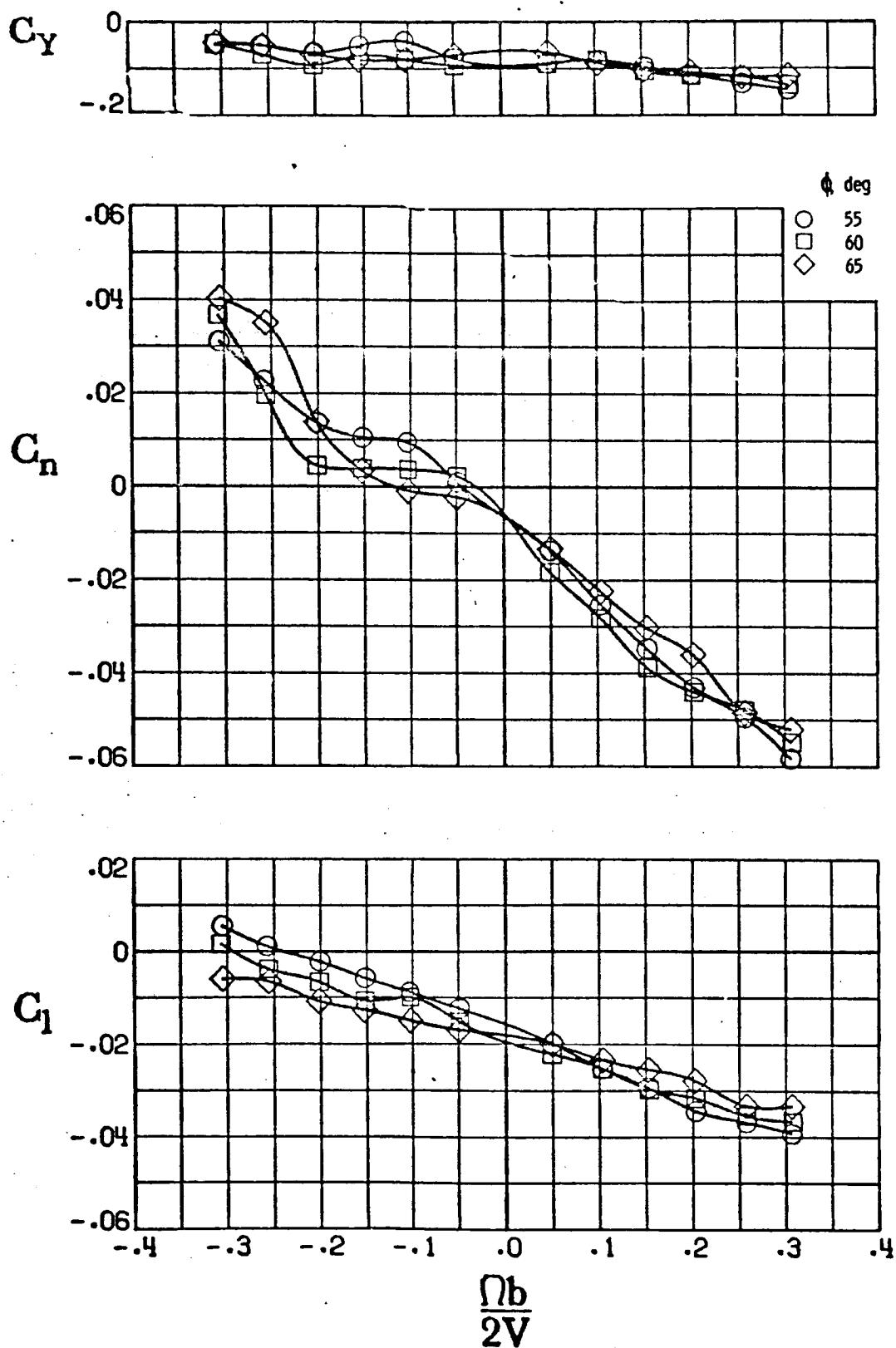
b) $\phi = 0^\circ$, $\theta = 70, 75, 80^\circ$

Figure C-29. - Continued.



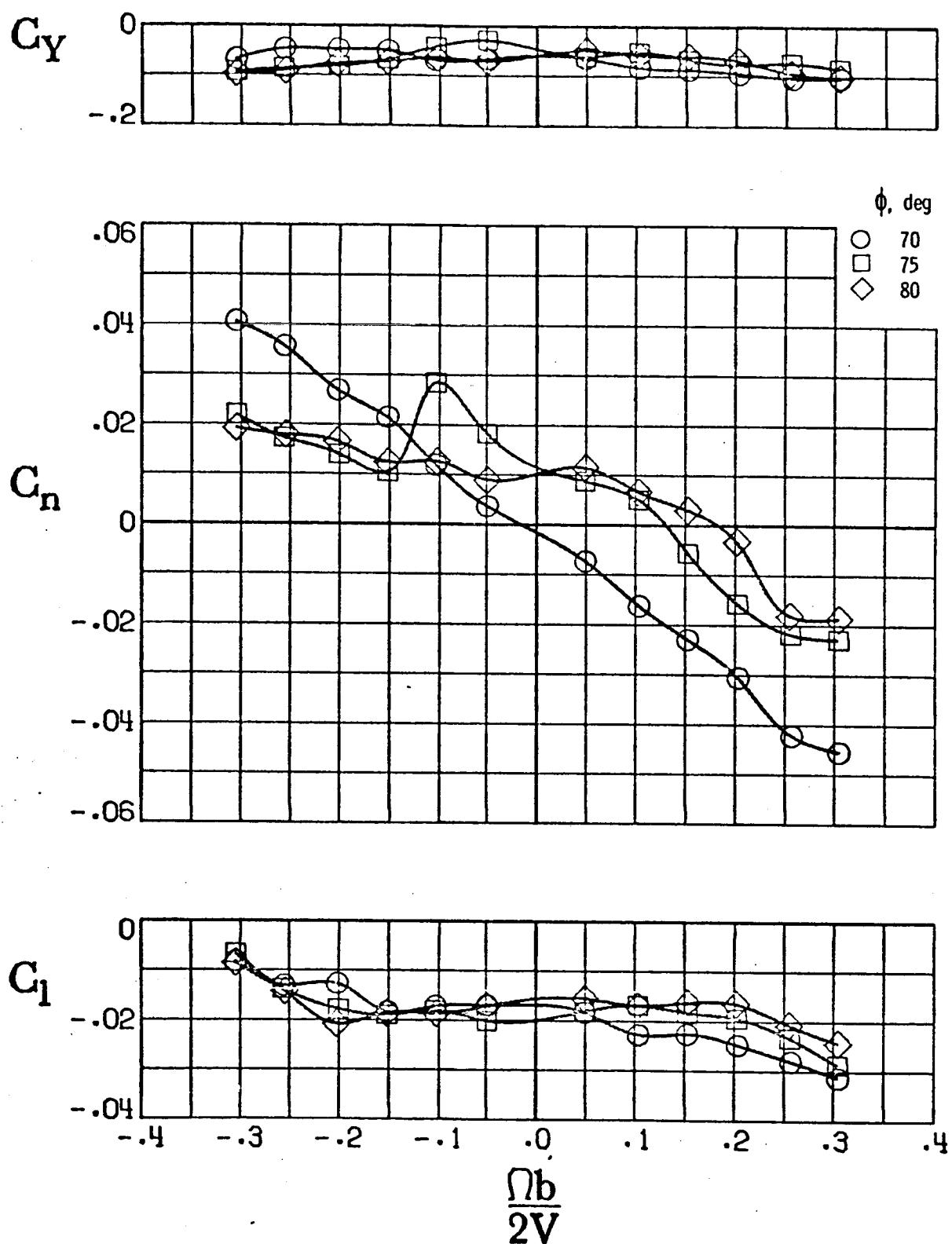
c) $\phi = 0^\circ, \theta = 85, 90^\circ$

Figure C-29. - Continued.



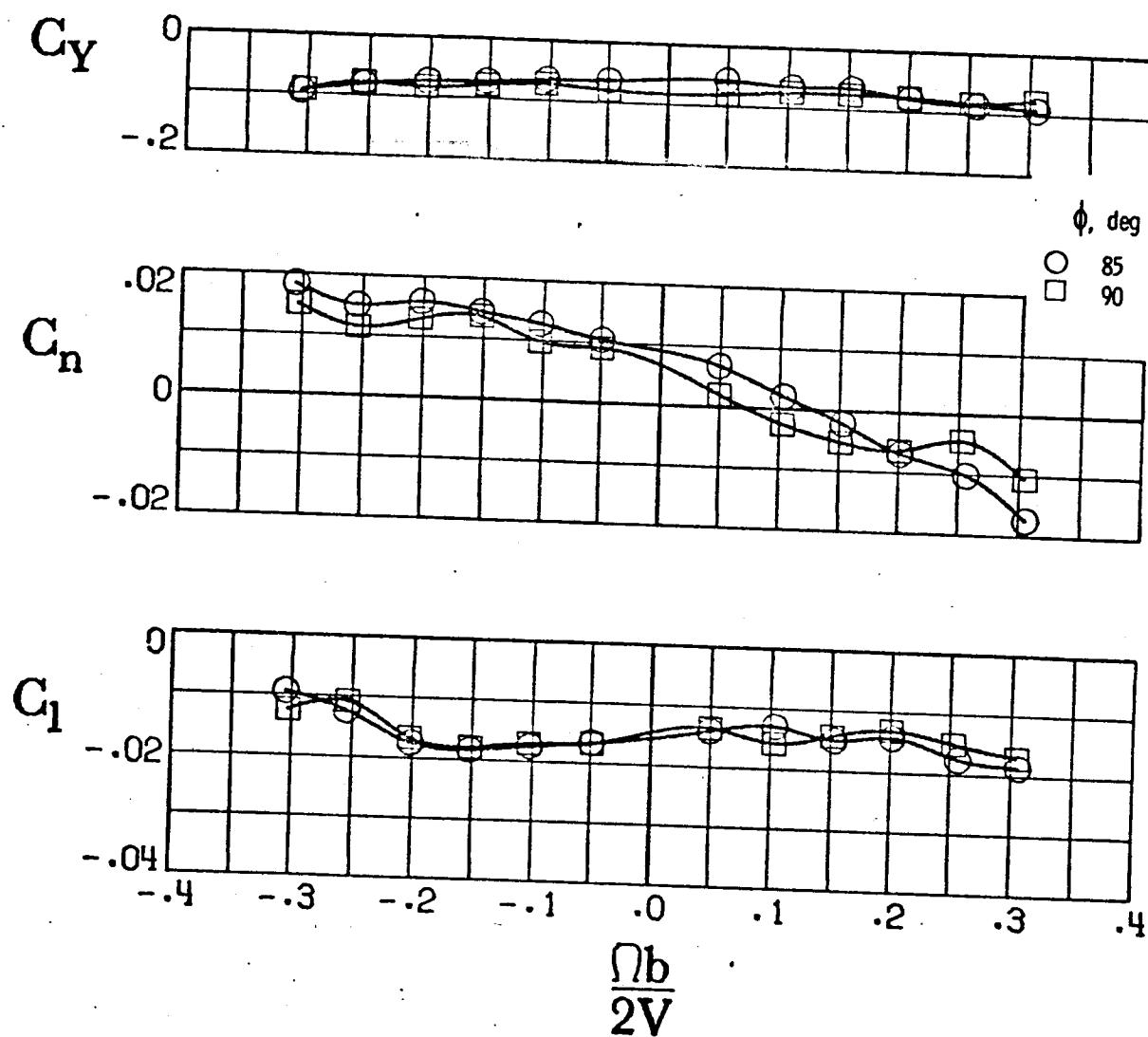
d) $\phi = 5^\circ, \theta = 55, 60, 65^\circ$

Figure C-29. - Continued.



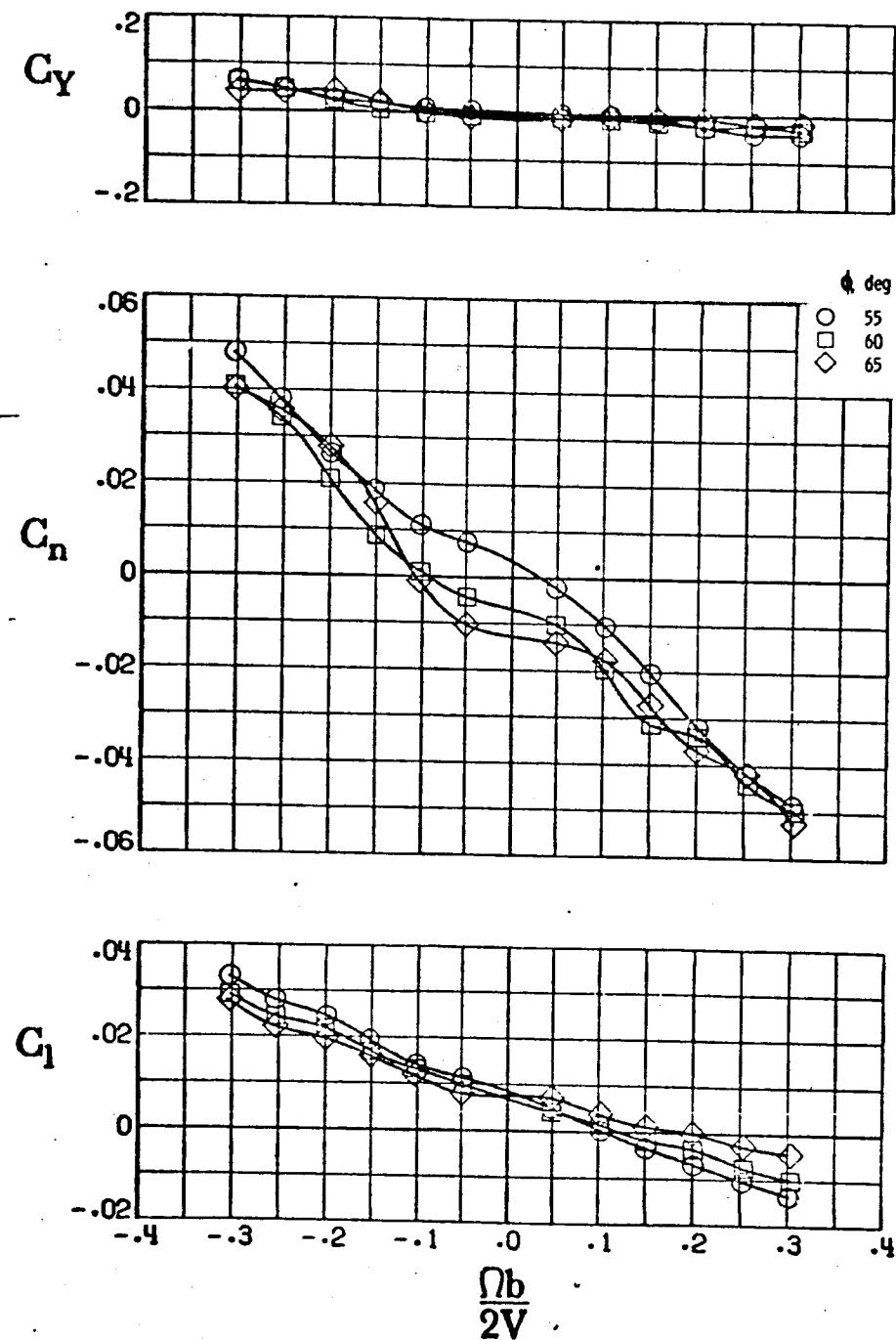
e) $\phi = 5^\circ$, $\theta = 70, 75, 80^\circ$

Figure C-29. - Continued.



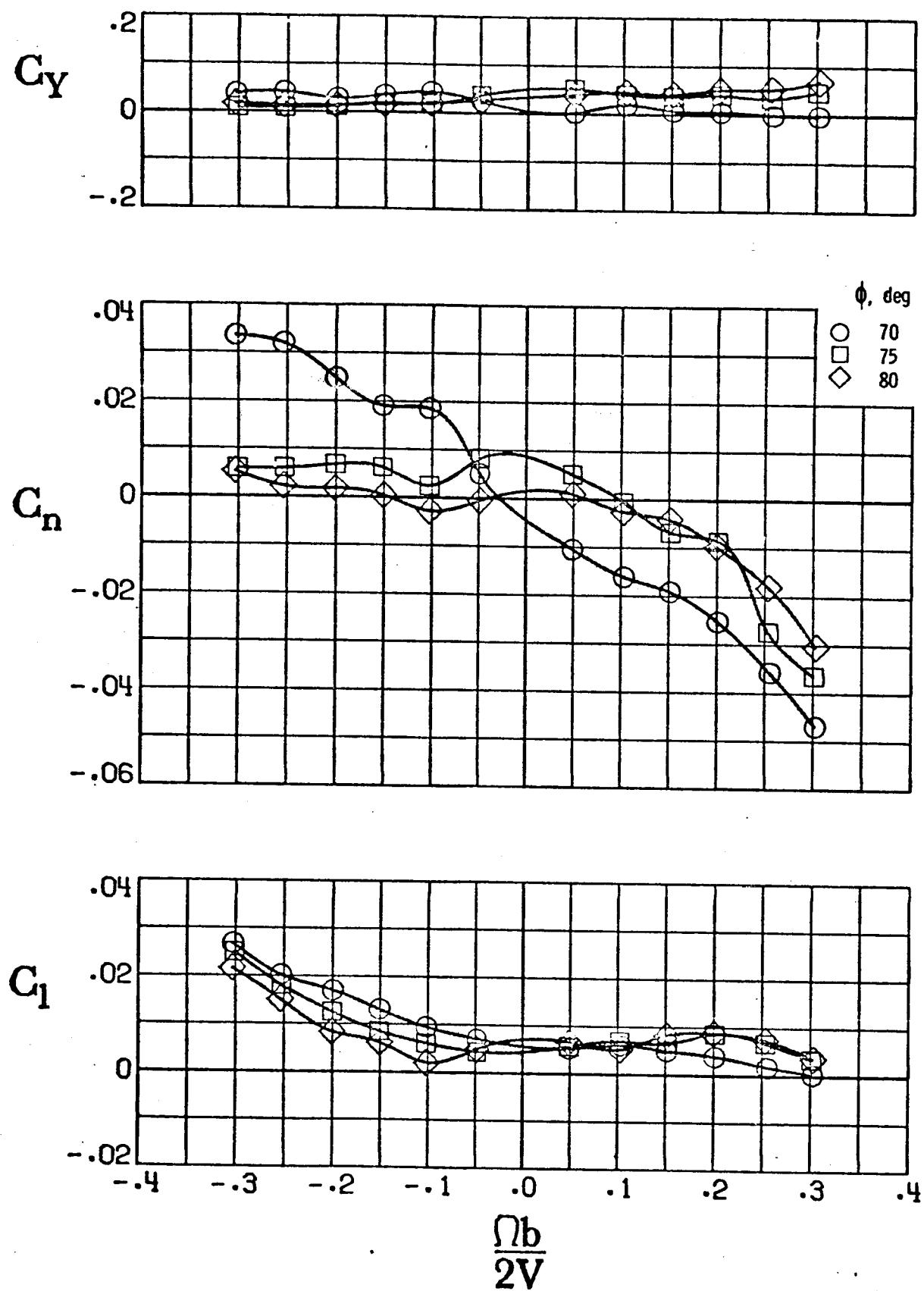
f) $\phi = 5^\circ$, $\theta = 85, 90^\circ$

Figure C-29. - Concluded.



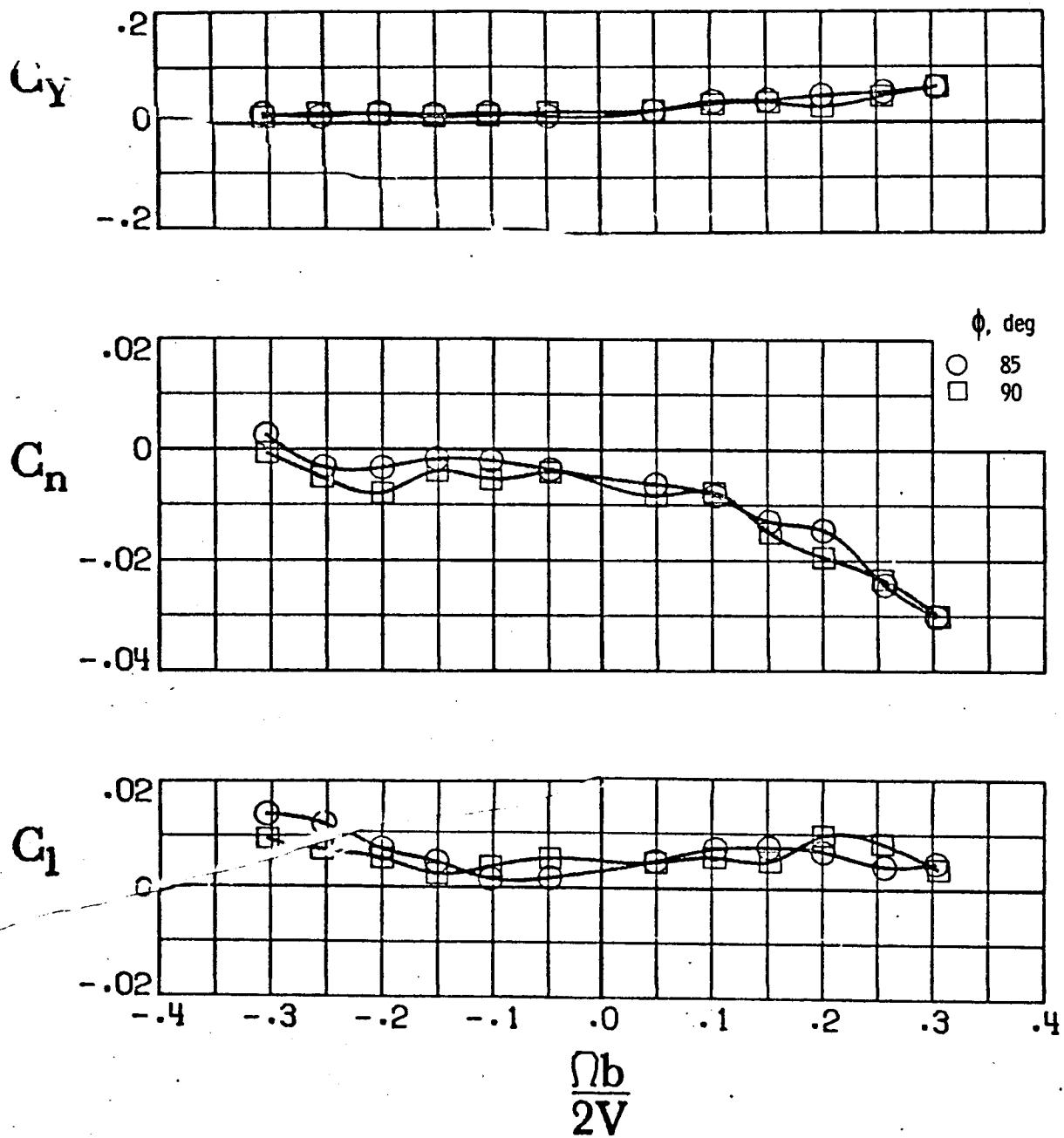
a) $\emptyset = 0^\circ$, $\theta = 55, 60, 65^\circ$

Figure C-30. - Effect of rotation rate and pitch and roll attitude angles on the lateral-directional coefficients for left pro-spin controls. Lamda = 22° .



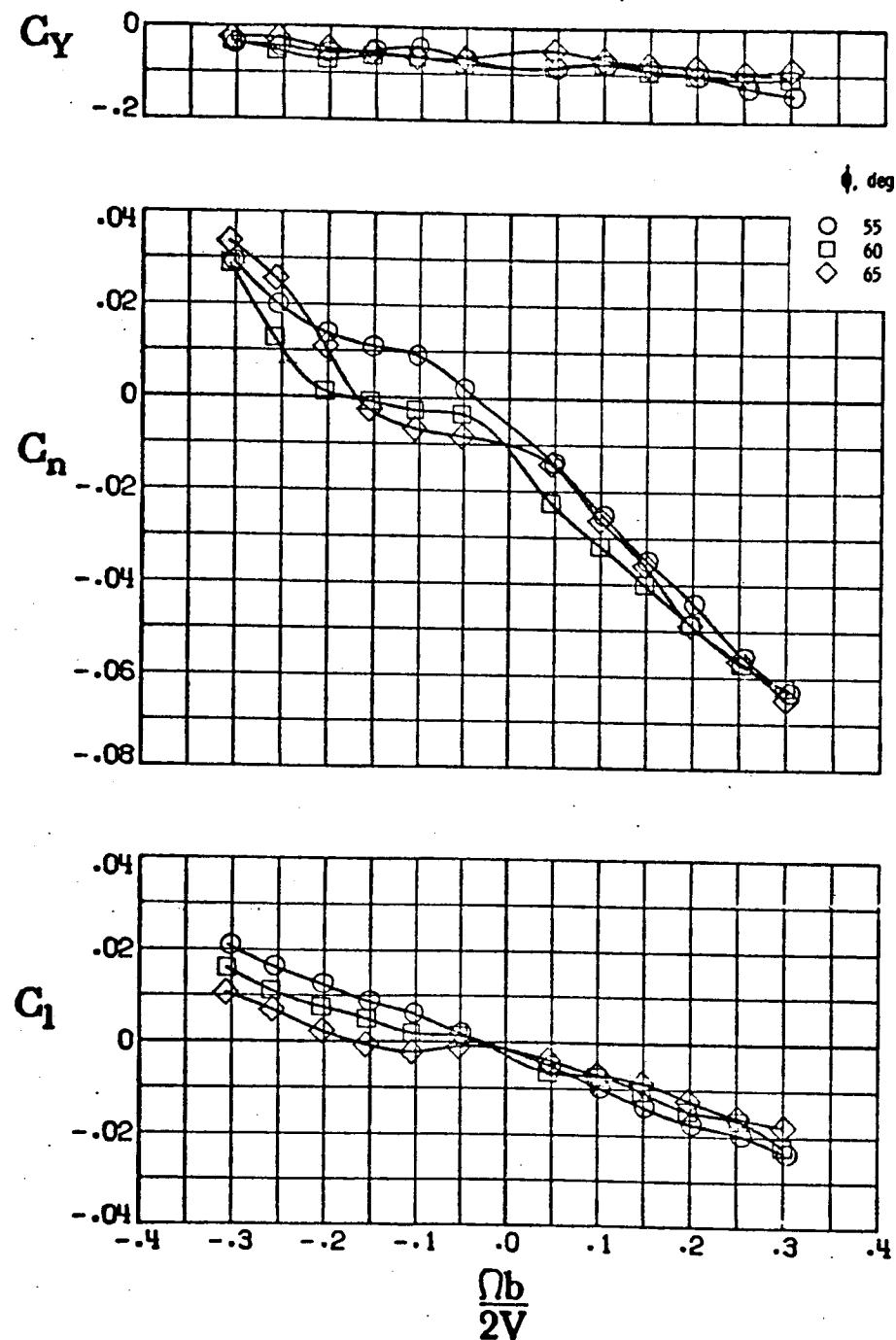
b) $\phi = 0^\circ$, $\theta = 70, 75$ and 80°

Figure C-30. - Continued.



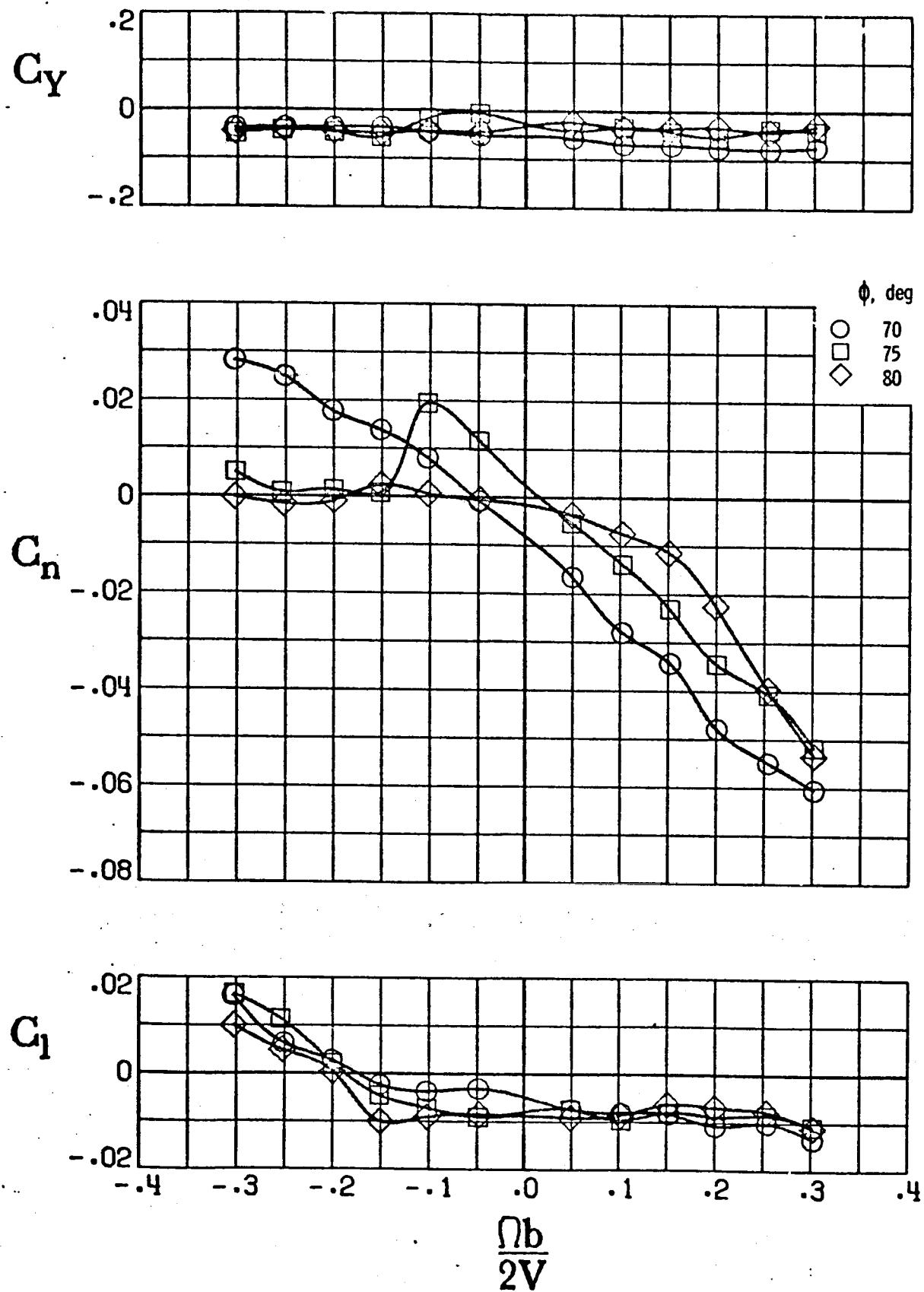
c) $\phi = 0^\circ$, $\theta = 85$ and 90°

Figure C-30. - Continued.



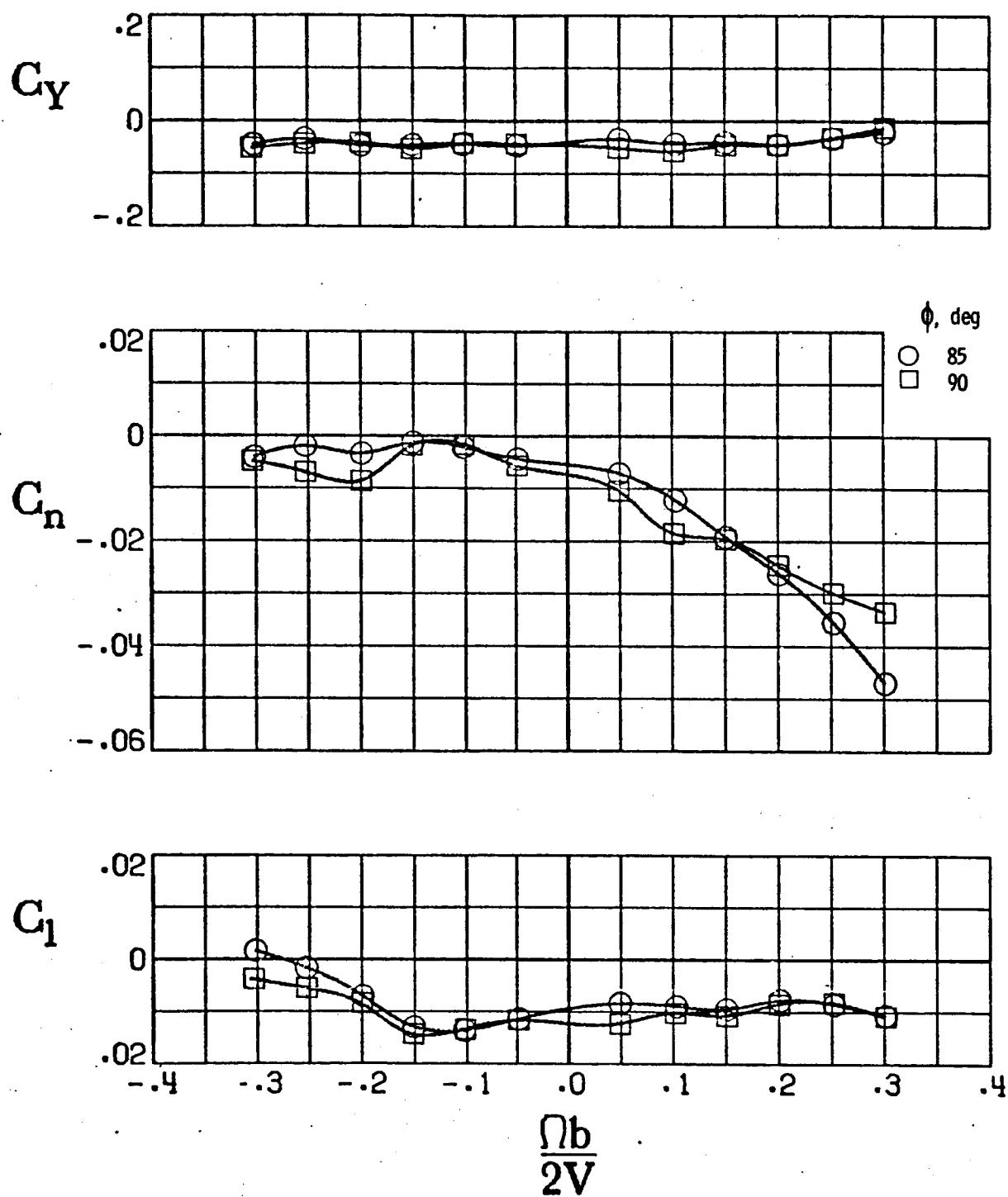
d) $\phi = 5^\circ$, $\theta = 55, 60$ and 65°

Figure C-30. - Continued.



e) $\phi = 5^\circ$, $\theta = 70, 75$ and 80°

Figure C-30. - Continued.



f) $\phi = 5^\circ$, $\alpha = 85^\circ, 90^\circ$

Figure C-30. - Concluded.